

Institut national de la recherche scientifique
Centre Eau Terre Environnement

Volcanology of two maar-diatremes: Round Butte and Twin Peaks, Hopi Buttes volcanic field, Navajo Nation, Arizona

Volcanologie de deux maars-diatrèmes, Round Butte et Twin Peaks, dans le champ
volcanique Hopi Buttes, Navajo Nation, Arizona

By
Benjamin Latutrie

Thesis submitted for the degree of
Philosophiae Doctor (Ph.D.)
In Earth Sciences

Evaluation jury

President of the jury and
internal examiner

Renaud Soucy La Roche
INRS-ETE, Canada

External examiner

Michael Higgins
Université du Québec à Chicoutimi, Canada

External examiner

Karoly Németh
Massey University, New Zealand

Research supervisor

Pierre-Simon Ross
INRS-ETE, Canada

ACKNOWLEDGEMENTS

I would like to express my gratefulness to my supervisor Pierre-Simon Ross for being present all along my PhD. I learnt a lot with Pierre-Simon both in the field and in the lab. When I started this PhD, I did not know much about maar-diatreme volcanoes. Pierre-Simon, who is a highly skilled field geologist, was very patient to explain in detail how to conduct field work and lab analyses and was always there for passionate discussions about these two fascinating volcanoes which are Round Butte and Twin Peaks. Writing papers was challenging but Pierre-Simon was always present to make constructive corrections and to give me advice. These permanent exchanges allowed me to increase my writing skills.

This PhD would not have been possible without the geological work permits delivered by the Navajo Nation Minerals Department. I also want to thank the Morris family that gave us permission to work at Round Butte and Twin Peaks. It is important to know that anyone wishing to conduct geological investigations within the Navajo Nation must first apply for, and receive, a permit from the Navajo Nation Minerals Department, P.O. Box 1910, Window Rock, Arizona 86515, USA, phone 1-928-871-6587.

The research was funded by the National sciences and engineering research council of Canada (NSERC) through a Discovery Grant and Accelerator Supplement to P-S Ross.

During these three years many people supported me in the field and in the lab. I first want to give all my gratitude to Pier Paolo Comida for his invaluable help and discussions in the field at Round Butte and at INRS. Then I also have a particular thought to Romain Jattiot who helped me in the field at Twin Peaks. George Billingsley is kindly thanked for taking time to discuss sedimentary rocks and for showing Pier and I the training car used by Neil Armstrong and Buzz Aldrin. Finally, I thank Marco Boutin, who helped me to develop a new method to make high definition scans of thin sections, and Philippe Girard who was present during the sawing of my samples.

All my friends of the 1309 and 1308 offices were very supportive during my project and I have a particular thought to Pier, Aurélie, Arnaud, Mirah, William, Alexandre and Caroline. We had many motivating discussions about our respective projects and it was all along helpful. I also

thank my friends at INRS in particular Simon with whom I had passionate discussions around coffees at “La Brulerie St Joseph”.

My parents, my brother and my friends in France were also very present and supportive during these past three years. I had the chance to visit them on many occasions and it was very precious to revitalize myself. I send my affection to Claire who was part of my life during this last year.

I give big hugs to my roommates Mariella (and Quinoa meow), Aurélie and Pier-Luc with whom I shared many good moments partying, eating or hiking in the mountains!!

The Heiseikan Dojo was a great part of my life during my PhD and I would like to tell how happy I was to study Aikibudo with Sensei Benoit and Sensei Sam. I have a particular thought to Isabelle and Christine who became sensei last December. It’s been an honor to participate to their black belt exam as their Uke. I’m going to miss training with all the members of the dojo, especially my friend Pier.

I have an emotional thought for Maria Isabel who will be missed.

For all the food lovers who supported me, here is the famous recipe of:

Baked apple and maple syrup

Quantity: 4 portions

Preparation time: 5 min

Cooking time: 25-30 min

Ingredients: 4 organic apples (not too big not too small) and maple syrup

Preparation: Remove the center of each apple, forming a small well (be careful to not cut the other side of the apple). You don’t have to remove the skin. Then fill the well with maple syrup up to the top and put it in the oven at 180°C during 25-30 mins (check the cooking with a knife) and enjoy!

ABSTRACT

Maar-diatremes are small, monogenetic, short-lived volcanoes that are mainly phreatomagmatic in origin. They display a funnel morphology and are composed, from top to bottom, by an ejecta ring, a maar crater, a typically bedded upper diatreme, a typically non-bedded lower diatreme, a root zone and a feeder intrusion. The Miocene Hopi Buttes volcanic field in northern Arizona comprises many maar-diatreme volcanoes, and provides excellent exposures of diatremes. The well-known stratigraphy of the sedimentary country rocks in the area allows the depth of current diatreme remnants relative to the pre-eruptive surface to be estimated. From north to south (younger to older), the main sedimentary formations are the Bidahochi Formation, the Moenave Formation, the Chinle Formation (Owl Rock Member, Petrified Forest Member and Shinarump Member) and the Moenkopi Formation. Two months of field work were carried out on the Round Butte diatreme and on the Twin Peaks volcanic complex. Round Butte is a small diatreme exposed ~190 m below the pre-eruptive surface and exposes the transition from upper diatreme to lower diatreme. Twin peaks is composed by two 'plug'-dominated volcanic remnants reaching up to the pre-eruptive surface, and a small satellite diatreme. Detailed mapping, componentry measurements and sampling were realised at both sites. In the laboratory, geochemistry of coherent lavas, dikes and juvenile fragments was characterized. Thin sections of coherent and pyroclastic rocks were described and a subset of the pyroclastic thin sections was point counted.

At **Round Butte**, three main groups of pyroclastic lithofacies were highlighted with undisturbed bedded rocks, disturbed bedded rocks and non-bedded rocks, as well as two minor groups comprising megablocks (blocks over 2 m in long axis) and debris avalanche deposits. Undisturbed bedded pyroclastic rocks were deposited on the floor of the syn-eruptive crater by fallback and pyroclastic surges. They are now part of the upper diatreme and sit on an unconformity. This unconformity formed during the eruption as a consequence of crater excavation, without requiring a significant pause in volcanic activity. Below this unconformity is the association of disturbed bedded and non-bedded pyroclastic rocks. The former are crater floor pyroclastic deposits in which the bedding has been progressively disturbed, whereas the latter form invasive columns created by passing debris jets. This association is interpreted as a transition zone toward the lower diatreme at depth. The transition zone has been integrated into the general model for maar-diatreme volcanoes, and was the missing link between upper diatreme rocks which are clearly phreatomagmatic at many sites, and the more enigmatic lower

diatreme rocks. Both are shown to form at the same time, by the same suite of phreatomagmatic processes.

Lithic fragment proportions measured with field componentry at Round Butte are compared with country rock fragmentation models based on the stratigraphy of surrounding country rocks and the size of the diatreme. The best models have a root zone within the Moenkopi Formation, up to 440 m below the pre-eruptive surface. Competent sedimentary formations/members (Moenave Formation, Owl Rock Member and Moenkopi Formation) are found in higher proportions in the field componentry than in the models because they are resistant to disaggregation. On the other hand, the less competent stratigraphic formations/members (Bidahochi Formation, Petrified Forest Member, Shinarump Member) show a depletion because they disaggregate easily; they are possibly included within the matrix of the pyroclastic rocks. In addition, Bidahochi clasts were preferentially expelled toward the ejecta ring during early maar formation. Sedimentary megablocks originate from the Bidahochi Formation, Moenave Formation and Owl Rock Member. These megablocks, and debris avalanche deposits, formed from slumps related to the destabilization of the crater walls.

Not all maar-diatremes are purely phreatomagmatic. At **Twin Peaks**, this work describes 'plug'-dominated volcanic remnants composed by two main peaks (North and South) and a satellite diatreme forming a SE-NW line. The two main peaks are maar-diatreme volcanoes because they display a round shape, gentle to steep contacts with the country rocks and contain some phreatomagmatic deposits. Detailed mapping highlights four stratigraphic units. Unit 1 is composed by grey to brown juvenile clasts with the highest proportion of lithic clasts of the massif; it is interpreted as phreatomagmatic. Unit 2 is less rich in lithic and brown juvenile clasts, but displays a higher proportion of moderately to highly vesiculated juvenile clasts; it is interpreted as phreato-strombolian. Unit 3a is characterized by non-welded spatter within a fine pyroclastic matrix and is interpreted as phreato-hawaiian. Unit 3b is composed by welded spatter to clastogenic lavas; the eruptive style was fire fountaining. Finally, Unit 4 is composed of black jointed coherent basanite and is interpreted as a lava lake. The lava-filled maar crater could have overflowed, forming lava flows, and this is an under-recognized hazard associated with maar-diatremes.

Keywords: transition zone, upper diatreme, lower diatreme, phreatomagmatism, magmatism, lithic clasts, lithic-rich lithologies, non-bedded rocks, disturbed beds, undisturbed beds

RÉSUMÉ ÉTENDU

Ce travail de doctorat porte sur la description et l'interprétation de deux volcans ou complexes de volcans de type maar-diatrème du champ volcanique Hopi Buttes en Arizona : Round Butte et Twin Peaks. Ils ont eu une activité principalement phréatomagmatique à cause de l'interaction entre le magma et l'eau souterraine, bien qu'à Twin Peaks il y ait eu un changement d'activité éruptive de phréatomagmatique vers magmatique. L'étude de Round Butte permet notamment de mieux comprendre les processus éruptifs formant le diatrème inférieur. Pour Twin Peaks, l'intérêt principal est plutôt de mieux définir ce qui a entraîné le passage de l'activité purement phréatomagmatique à purement magmatique.

Cette partie de la thèse résume rapidement l'état des connaissances sur les maar-diatrèmes, puis présente le champ volcanique Hopi Buttes, la problématique et les objectifs. Il y aura aussi une synthèse des résultats principaux obtenus à Round Butte et Twin Peaks et enfin une synthèse générale.

Les volcans de type maar-diatrème

Les maar-diatrèmes sont des volcans de petite taille ayant une durée de vie courte (principalement jours à semaines). Ils sont particuliers du fait de leur morphologie en forme d'entonnoir recoupant la surface pré-éruptive (Lorenz 1986, 2007; White et Ross 2011; Valentine et White 2012). Ils se regroupent dans des champs volcaniques monogénétiques et ont des compositions chimiques allant d'ultramafiques (p. ex. Hopi Buttes, Vazquez 1998; Hooten 1999) à felsiques (p. ex. Sugarloaf Mountain, Sheridan et Updike 1975; Tepexitl, Austin-Erickson et al. 2011). La formation de ces volcans résulte principalement d'une activité explosive phréatomagmatique bien qu'ils peuvent aussi avoir des phases magmatiques plus ou moins importantes.

Du haut vers le bas, les maar-diatrèmes se décomposent en trois grandes parties : l'anneau d'éjectas, le cratère du maar et le diatrème (Fig. 1.1; White et Ross 2011). Le diatrème lui se sépare en un diatrème supérieur lité (Gernon et al. 2013; Delpit et al. 2014; Bélanger et Ross 2018), un diatrème inférieur non-lité (White 1991; Lefebvre et al 2013), une zone racine (Lorenz et Kurszlaukis 2007; Haller et al. 2017) et une intrusion nourricière (Re et al. 2015, 2016; Muirhead et al. 2016). Il est très rare de pouvoir observer un maar-diatrème dans son ensemble

car dans le cas des maars quaternaires, on ne voit pas le diatrème, alors que pour les volcans plus anciens, la partie supérieure est habituellement érodée.

Le champ volcanique Hopi Buttes (HBVF)

Le champ volcanique Hopi Buttes est situé dans la partie centre-sud du Plateau du Colorado qui est une zone géologiquement stable (Fig. 1.4, Gilbert et al. 2007). Le champ volcanique est daté du Miocène et recouvre une aire approximative de 2300 km² avec environ 300 édifices volcaniques, principalement des maar-diatrèmes, mais aussi des cônes de scories, des coulées de laves et des intrusions (dykes, sills; Fig. 1.5). Les diatrèmes sont exposés de manière exceptionnelle dans le champ Hopi Buttes car ils n'ont pas subi de déformation ou de métamorphisme, et aussi car la végétation est très peu développée. Les dykes sont généralement de faible épaisseur (autour de 40 cm) et se regroupent dans des complexes de dykes et de sills (Re et al. 2015; 2016; Muirhead et al. 2016). Le style éruptif majoritairement phréatomagmatique des volcans dans les Hopi Buttes est lié à l'environnement qui régnait au Miocène. En effet, pendant le volcanisme, cette région était riche en eau avec des étangs entourés de vastes plaines arides (White 1989) ce qui a favorisé l'interaction eau-magma.

Dans les Hopi Buttes, l'âge, l'épaisseur, et l'attitude des roches sédimentaires encaissantes des diatrèmes sont bien caractérisées (Billingsley et al. 2013). En effet, en identifiant les roches sédimentaires présentes autour des restes volcaniques, il est possible de se placer précisément dans la stratigraphie régionale et donc de retrouver la profondeur actuelle de ces restes volcaniques. Du nord vers le sud du champ volcanique, nous descendons en profondeur dans la stratigraphie et par conséquent dans la structure des maar-diatrèmes exposés. Dans les Hopi Buttes, les édifices volcaniques à l'affleurement permettent d'étudier ces volcans de l'anneau d'éjectas (ex. Teshim maar, White 1991) au diatrème inférieur (ex. West Standing Rocks, Lefebvre et al. 2013).

Problématique

De grandes villes sont parfois localisés près de champs volcaniques monogénétiques dominés par des volcans de type maar-diatrème (Németh et al. 2012; Boivin et Thouret 2014; Poppe et al. 2016). Leurs éruptions peuvent être dangereuses à cause des déferlantes pyroclastiques ou encore des retombées de cendres (Moore et al. 1966; Nairn 1979; Self et al. 1980; Poppe et al. 2016). Aussi, les diatrèmes kimberlitiques peuvent être riches en diamants (Kjarsgaard 2007).

Les processus éruptifs des maar-diatrèmes ne sont toujours pas complètement compris, principalement car la majeure partie de l'activité est localisée dans le diatrème (White 1991; White et Ross 2011; Lefebvre et al. 2013, 2016). L'anneau d'éjectas qui est facilement accessible dans les jeunes champs volcaniques renseigne sur les processus d'excavation du cratère du maar et sur ce qui se passe dans l'atmosphère. Les expériences en laboratoire quant à elles définissent mieux les processus de fragmentation des magmas lors des interactions avec l'eau souterraine (Zimanowski et al. 1997; Büttner et al. 2002; Austin-Erickson et al. 2008). Les expériences analogiques de formation des cratères nous donnent des informations sur l'importance des cratères préexistants et de la profondeur de l'explosion sur la morphologie finale du cratère obtenu (Valentine et al. 2012, 2014; Ross et al. 2013; Taddeucci et al. 2013; Graettinger et al. 2014). La géophysique avec la gravimétrie et la magnéto­métrie est intéressante pour définir la taille d'un diatrème ou d'un complexe de diatrème (Blaikie et al. 2012; Nunns et al. 2019). Mais pour mieux comprendre les processus éruptifs dans le diatrème, la stratégie principale demeure de réaliser des études détaillées de terrain sur les diatrèmes.

La principale étude antérieure de ce type dans les Hopi Buttes est celle de Lefebvre (2013), qui porte sur trois volcans. Pendant son doctorat, Lefebvre (2013) a principalement détaillé le diatrème inférieur à West Standing Rocks (Lefebvre et al. 2013), une fissure se remplissant de spatter à Castle Butte Trading Post (Lefebvre et al. 2012) et a conclu que East Standing Rocks n'était pas une zone racine mais un diatrème qui a arrêté sa croissance brutalement (Lefebvre et al. 2016). Néanmoins, il reste encore beaucoup de questions à résoudre dans les Hopi Buttes pour mieux comprendre le fonctionnement des maar-diatrèmes.

Objectifs

Ce doctorat propose une étude détaillée des volcans et complexes volcaniques de Round Butte et Twin Peaks. Ils ont été mentionnés plusieurs fois dans des publications (White 1991; White et Ross 2011) et ont fait l'objet de visites de terrain (White et al. 2008, 2012a, 2012b) mais n'ont jamais été décrits dans le détail. Le *but principal* de ce projet est de décrire précisément et d'interpréter les processus éruptifs de ces deux sites.

Pour le diatrème de Round Butte, ce travail essaiera de comprendre l'importance d'une zone de transition entre le diatrème supérieur et inférieur, avec des implications pour la mise en place du diatrème inférieur (*Chapitre 2*). Le second but sera d'éclaircir l'importance de l'étude des clastes lithiques et des lithologies riches en lithiques pour la compréhension des processus internes au diatrème (*Chapitre 3*). Pour le complexe volcanique de Twin Peaks, l'intérêt principal sera de

mieux comprendre les causes du changement d'activité éruptive de purement phréatomagmatique à purement magmatique (Chapitre 4).

Méthodes

Un mois de travail de terrain a été effectué sur chaque volcan, Round Butte et Twin Peaks. Des cartes géologiques en plan et des cartes des falaises composant les massifs ont été réalisées. Les lithofaciès pyroclastiques ont été définis à partir des structures, de la granulométrie et de l'estimation visuelle de la composition des roches. Des mesures quantitatives de composition ont été réalisées sur les lithofaciès à l'aide des méthodes de « *line count* » et « *clast count* ». Pour finir, un échantillon a été collecté sur tous les lithofaciès définis lors de la cartographie de terrain.

Au laboratoire, des observations sur la taille, la morphologie, la composition des différents clastes ont été faites sur des tranches de roches et sur des lames minces. Certaines lames minces pyroclastiques ont fait l'objet de comptages de points pétrographiques. Enfin, plusieurs échantillons cohérents (dykes, laves, fragments juvéniles) ont fait l'objet d'analyses géochimiques.

Résultats et interprétations : Round Butte

La cartographie détaillée à Round Butte a mis en évidence trois groupes de facies pyroclastiques principaux qui sont les roches litées non-perturbées, les roches litées perturbées et les roches non-litées. Il y a aussi deux groupes de facies mineurs, les mégablocs et les avalanches de débris. L'architecture complexe de Round Butte est interprétée comme résultant de deux cycles d'excavation et de remplissage du cratère (Fig. 2.12). En effet, pendant le premier cycle, un cratère relativement profond a été formé et rempli, formant le remplissage 1 qui correspond maintenant aux roches pyroclastiques litées perturbées. La phase d'excavation du second cycle a creusé un nouveau cratère dans le remplissage 1, laissant une importante discontinuité, avant d'être rempli par le remplissage 2, correspondant aux roches litées non-perturbées interprétées comme étant le diatrème supérieur à Round Butte.

En dessous de la discontinuité se trouve une association de colonnes invasives (roches pyroclastiques non-litées) avec des colonnes résiduelles (roches litées perturbées) qui ne semble pas correspondre à la définition des dépôts pyroclastiques typiques du diatrème inférieur. Cette association est plutôt interprétée comme étant une zone de transition entre les roches typiquement litées du diatrème supérieur et celles typiquement non-litées du diatrème

inférieur. A Round Butte, le diatrème supérieur et inférieur semble donc intimement lié et s'être mis en place simultanément. Les roches typiquement non-litées se sont formés à partir de jets de débris qui se déplacent vers le haut en recoupant les roches litées perturbées, pour former des colonnes invasives. Ces jets de débris ont perturbé le litage des dépôts encaissants, mais des processus de liquéfaction et de subsidence ont aussi pu contribuer à la perturbation du litage.

L'étude des clastes lithiques et des lithologies riches en lithiques a permis de mieux comprendre les processus d'élargissement du cratère pendant l'activité éruptive. En effet, les avalanches de débris et les mégablocs sédimentaires et pyroclastiques résultent d'effondrements locaux des roches sédimentaires encaissantes pouvant entraîner des morceaux d'anneau d'éjectas. Ces effondrements sont les mécanismes principaux de l'élargissement du cratère syn-éruptif. À Round Butte, aucun mégabloc ne montre un mouvement net vers le haut et ils sont donc toujours retrouvés soit au même niveau ou plus bas que leur profondeur d'origine.

La création d'un modèle de fragmentation des roches sédimentaires de Round Butte a permis d'estimer les proportions de chaque formation sédimentaire fragmentée (Fig. 3.8). Une comparaison a été faite entre les proportions estimées par le modèle de fragmentation et les proportions recalculées à partir des *line counts* et *clast counts*. Cette comparaison a permis de mieux comprendre le devenir des différents clastes lithiques dans le diatrème. En effet, les unités sédimentaires compétentes sont surreprésentées, alors que celles qui sont friables sont sous-représentées. La raison est que les roches compétentes sont difficiles à désagréger alors que les plus friables se désagrègent facilement et sont donc « cachées » dans la matrice des roches pyroclastiques. De plus, l'appauvrissement en fragments de la Formation de Bidahochi, située au sommet de la stratigraphie, est aussi expliqué par l'excavation et l'expulsion préférentielle de cette formation vers l'anneau d'éjecta.

Résultats et interprétations : Twin Peaks

Le complexe volcanique de Twin Peaks se compose de deux principaux pics (le nord et le sud) avec une masse de lave noire au sommet. Il existe aussi un diatrème satellite et le tout s'oriente sur une ligne SE-NO (Figs. 4.2, 4.3). Ces restes volcaniques sont interprétés comme étant trois maar-diatrèmes. De la base au sommet, quatre unités stratigraphiques ont été définies pour les deux pics avec les unités 1, 2 et 3 qui sont pyroclastiques et l'unité 4 qui est composée de laves cohérentes. Ces unités stratigraphiques montrent un changement de régime éruptif de

phréatomagmatique à magmatique (Fig. 4.11). En effet, l'unité 1 (purement phréatomagmatique) est surmontée par l'unité 2 (phréato-strombolienne) puis l'unité 3a (phréato-hawaiienne) et l'unité 3b (fontaine de lave). L'unité 4, au sommet, est quant à elle purement magmatique et effusive : c'est un lac de lave qui a fini de remplir le cratère du maar. Ce changement progressif de régime éruptif semble être le résultat soit de l'augmentation du flux éruptif et/ou de l'appauvrissement de l'apport en eau.

Twin Peaks est une localité parfaite pour passer en revue les critères traditionnels permettant de distinguer les styles phréatomagmatiques et magmatiques dans les maar-diatrèmes ultramafiques à mafiques. Ces critères sont toujours très pertinents dans l'ensemble. Seule la nature du verre volcanique (tachylite vs sideromelane) se formant dans les clastes juvéniles semblent être un critère ambigu.

Synthèse

Ce travail introduit de nouvelles informations sur les processus éruptifs et les structures internes des volcans de type maar-diatrème. A Round Butte, une importante zone de transition a été identifiée entre le diatrème supérieur et le diatrème inférieur. Le modèle général des maar-diatrèmes a donc été modifié pour y ajouter cette zone de transition (Fig. 2.13). Cette zone de transition est le lien manquant pour prouver que le diatrème supérieur et le diatrème inférieur se mettent en place simultanément, et que le diatrème inférieur est typiquement phréatomagmatique.

A Round Butte, il a aussi été mis en évidence que les phases éruptives formant les maar-diatrème sont soit dominées par des processus d'excavation, soit par ceux de remplissage. Les maar-diatrèmes ne sont pas simplement le résultat d'une seule phase d'excavation profonde du cratère syn-éruptif puis de son remplissage qui forme le diatrème. Deux cycles d'excavation/remplissage ont été documentés, résultant probablement de variations dans l'intensité de l'activité phréatomagmatique. Les phases intenses favorisent les processus d'excavation alors que les phases plus calmes sont dominées par les processus de remplissage. Pendant l'éruption, les mégablocs et les avalanches de débris élargissent et remplissent le cratère. Certains volcans kimberlitiques sont aussi des maar-diatrèmes, mais typiquement moins bien exposés et préservés que Round Butte. La meilleure compréhension du fonctionnement interne des diatrèmes obtenue à Round Butte pourrait informer sur les processus éruptifs des kimberlites et aider l'exploration pour les diamants au Canada.

Ce travail met aussi en évidence que les maar-diatrèmes ne sont pas uniquement des volcans phréatomagmatiques. A Twin Peaks, un changement d'activité éruptive de phréatomagmatique à magmatique a probablement été lié à une augmentation du flux éruptif et/ou une diminution de l'apport en eau (Fig. 4.11). D'autres volcans dans les Hopi Buttes montrent des phases magmatiques plus fluctuantes comme à Hoskietso Claim (White 1991; White et Ross 2011) ou allant jusqu'à un lac de lave qui déborde à Triplets maar (Graettinger et Valentine 2017).

Dans la littérature, les risques volcaniques les plus destructeurs associés aux maar-diatrèmes sont les déferlantes pyroclastiques pouvant voyager jusqu'à 5 km de l'événement (Moore et al. 1966; Moore 1967; Vazquez et Ort 2006; Poppe et al. 2016), mais aussi les retombées pyroclastiques qui peuvent causer des dommages sur les bâtiments alentour. Ce travail montre un aspect moins connu des risques volcaniques associés aux phases magmatiques des maar-diatrèmes : les coulées de laves. Ces coulées sont moins dangereuses que les déferlantes latérales car elles se déplacent lentement, mais peuvent être très destructrices même à bonne distance de l'événement. Après avoir débordé du cratère du maar, les coulées de lave peuvent former des chenaux et atteindre de longues distances (Robert et al. 2014; Harris et Rowland 2015; Latutrie et al. 2015) pour toucher des villes qui ne seraient pas affectées par des déferlantes ou des retombées pyroclastiques. Il semble donc important de considérer ces coulées de lave dans les plans de prévention des risques dans des zones urbaines densément peuplées associées à des maar-diatrèmes. Ce genre de travail semble devoir se faire en amont, avant le début d'une nouvelle crise volcanique, pour permettre la modélisation précise des coulées de lave éventuelles et prévoir des zones d'évacuation sûres pour la population.

TABLE OF CONTENTS

ACKNOWLEDGEMENTS	II
ABSTRACT	V
RÉSUMÉ ÉTENDU	VII
TABLE OF CONTENTS	XV
LIST OF FIGURES	XXI
LIST OF TABLES	XXIII
1 INTRODUCTION	1
1.1 MAAR-DIATREME VOLCANOES	1
1.1.1 <i>Ejecta ring</i>	3
1.1.2 <i>Maar crater</i>	4
1.1.3 <i>Upper diatreme</i>	5
1.1.4 <i>Lower diatreme</i>	6
1.1.5 <i>Root zone and feeder intrusion</i>	7
1.2 EXPLOSIVE MAGMA/WATER INTERACTIONS	7
1.3 HISTORICAL ERUPTIONS AND VOLCANIC HAZARDS.....	8
1.4 GEOLOGICAL SETTING.....	9
1.4.1 <i>The Colorado Plateau</i>	9
1.4.2 <i>Hopi Buttes volcanic field (HBVF)</i>	11
1.5 PROBLEMS AND AIMS	13
1.6 METHODOLOGY	15
1.6.1 <i>Field work overview and terminology</i>	15
1.6.2 <i>Laboratory work</i>	20
1.7 THESIS ORGANIZATION.....	21
1.8 CONTRIBUTIONS OF EACH AUTHOR AND PARTICIPANT IN MULTI-AUTHOR PUBLICATIONS.....	21
2 FIRST ARTICLE: TRANSITION ZONE AT ROUND BUTTE DIATREME	23
2.1 ABSTRACT.....	25
2.2 INTRODUCTION	25
2.3 GEOLOGICAL SETTING.....	26
2.4 METHODS	28
2.5 RESULTS.....	28
2.5.1 <i>Undisturbed bedded pyroclastic rocks</i>	32
2.5.2 <i>Disturbed bedded pyroclastic rocks</i>	35
2.5.3 <i>Non-bedded pyroclastic rocks</i>	36

2.5.4	<i>Faults in pyroclastic rocks</i>	36
2.5.5	<i>Juvenile clasts</i>	40
2.6	INTERPRETATION: ORIGIN OF ROUND BUTTE ROCKS AND FEATURES	43
2.6.1	<i>A maar-diatreme volcano</i>	43
2.6.2	<i>Formation of juvenile clasts</i>	43
2.6.3	<i>Syn-eruptive faults and subsidence</i>	44
2.6.4	<i>Undisturbed bedded pyroclastic rocks</i>	44
2.6.5	<i>Disturbed bedded pyroclastic rocks</i>	46
2.6.6	<i>Non-bedded pyroclastic rocks</i>	47
2.6.7	<i>The unconformity: morphology and origin</i>	48
2.7	ROUND BUTTE EVOLUTION MODEL	48
2.7.1	<i>Initial crater and proto-diatreme</i>	50
2.7.2	<i>First cycle of excavation and infilling</i>	50
2.7.3	<i>Second cycle of excavation and infilling</i>	51
2.7.4	<i>Post-eruptive events</i>	52
2.8	THE UPPER/LOWER TRANSITION ZONE AT ROUND BUTTE	52
2.9	CONCLUSIONS	53
2.10	ACKNOWLEDGEMENTS	55
2.11	ONLINE RESOURCE 2.1: PANORAMAS	55
2.12	ONLINE RESOURCE 2.2: GEOCHEMISTRY AND PETROGRAPHY OF COHERENT SAMPLES FROM ROUND BUTTE DIATREME	60
2.12.1	<i>Methods</i>	60
2.12.2	<i>Petrographic observations</i>	60
2.12.3	<i>Major elements geochemistry</i>	61
2.12.4	<i>Trace element geochemistry</i>	64
3	SECOND ARTICLE: LITHICS AND LITHIC-RICH LITHOLOGIES AT ROUND BUTTE DIATREME	67
3.1	ABSTRACT	69
3.2	INTRODUCTION	70
3.3	REGIONAL SETTING	71
3.3.1	<i>Hopi Buttes volcanic field (HBVF)</i>	71
3.3.2	<i>Sedimentary formations of the HBVF area</i>	72
3.4	METHODS	74
3.4.1	<i>Mapping and facies groups at Round Butte</i>	76
3.4.2	<i>Componentry measurements</i>	76
3.5	ROUND BUTTE MASSIF OVERVIEW	79
3.5.1	<i>Summary of the three main pyroclastic facies groups</i>	79

3.5.2	<i>Megablocks</i>	79
3.5.3	<i>Debris avalanche deposits (DADs)</i>	79
3.6	COMPONENTRY	80
3.6.1	<i>Field line counts</i>	80
3.6.2	<i>Field clast counts</i>	86
3.6.3	<i>Petrographic point counts</i>	87
3.7	TYPES OF CLASTS.....	90
3.7.1	<i>Lithic clasts</i>	90
3.7.2	<i>Tuff clasts</i>	92
3.8	COUNTRY ROCK FRAGMENTATION MODEL OF ROUND BUTTE.....	92
3.8.1	<i>Model parameters</i>	92
3.8.2	<i>Origin and proportion of lithic clasts</i>	93
3.9	COMPARISON OF FIELD LINE COUNT AND FIELD CLAST COUNT METHODS	95
3.10	INTERPRETATION AND DISCUSSION	96
3.10.1	<i>Summary of the origin of the three main groups of facies</i>	96
3.10.2	<i>Megablocks</i>	97
3.10.3	<i>Debris avalanche deposits (DADs)</i>	99
3.10.4	<i>Implication on lithic transport within the diatreme</i>	100
3.10.5	<i>Lithic clasts in the ejecta ring versus the diatreme</i>	101
3.11	CONCLUSIONS.....	102
3.12	ACKNOWLEDGEMENTS.....	103
3.13	ONLINE RESOURCE 3.1: PANORAMAS.....	103
4	THIRD ARTICLE: TWIN PEAKS VOLCANIC COMPLEX.....	111
4.1	ABSTRACT.....	113
4.2	INTRODUCTION	113
4.3	GEOLOGICAL SETTING.....	115
4.4	TWIN PEAKS VOLCANIC COMPLEX	115
4.5	METHODS	122
4.6	UNIT DESCRIPTIONS.....	123
4.6.1	<i>Spatial organization of stratigraphic units</i>	123
4.6.2	<i>Unit 1</i>	123
4.6.3	<i>Unit 2</i>	124
4.6.4	<i>Unit 3</i>	126
4.6.5	<i>Unit 4</i>	126
4.6.6	<i>Intrusions</i>	130
4.7	COMPONENTRY MEASUREMENTS.....	130
4.7.1	<i>Field clast counts</i>	130

4.7.2	<i>Petrographic point counts</i>	130
4.7.3	<i>Integration of field clast counts and petrographic point counts</i>	132
4.8	ORIGIN OF TWIN PEAKS VOLCANIC ROCKS	134
4.8.1	<i>Volcano type</i>	134
4.8.2	<i>Provenance of lithic clasts</i>	134
4.8.3	<i>Interpretation of juvenile clasts</i>	135
4.8.4	<i>Unit 1</i>	135
4.8.5	<i>Unit 2</i>	136
4.8.6	<i>Unit 3</i>	137
4.8.7	<i>Unit 4</i>	138
4.8.8	<i>Simultaneously active craters?</i>	138
4.9	TWIN PEAKS EVOLUTION MODEL	139
4.9.1	<i>Onset of activity</i>	139
4.9.2	<i>Phreatomagmatic activity</i>	141
4.9.3	<i>Phreato-strombolian activity</i>	141
4.9.4	<i>Lava fountain activity</i>	141
4.9.5	<i>Lava lake filling the crater</i>	143
4.9.6	<i>Post-eruptive erosion</i>	143
4.10	PHREATOMAGMATIC VS MAGMATIC ERUPTIVE STYLES IN ULTRAMAFIC TO MAFIC MAAR-DIATREME SETTINGS	143
4.11	CONCLUSIONS.....	146
4.12	ACKNOWLEDGEMENTS	147
4.13	ONLINE RESOURCE 4.1: GEOCHEMISTRY AND PETROGRAPHY OF COHERENT SAMPLES FROM TWIN PEAKS VOLCANIC COMPLEX	147
4.13.1	<i>Methods</i>	147
4.13.2	<i>Petrographic observations</i>	148
4.13.3	<i>Major element geochemistry</i>	149
4.13.4	<i>Trace element geochemistry</i>	151
5	SYNTHESIS	157
5.1	MAIN CONCLUSIONS AND SCIENTIFIC CONTRIBUTIONS	157
5.1.1	<i>Cycles of excavation and infilling</i>	158
5.1.2	<i>A transition zone between the upper and lower diatreme</i>	158
5.1.3	<i>Lower diatreme eruptive processes</i>	159
5.1.4	<i>Crater enlargement processes</i>	160
5.1.5	<i>Movement and preservation of lithic clasts</i>	160
5.1.6	<i>'Plug'-like remnants are maar-diatremes with lava-filled craters</i>	161
5.1.7	<i>Magmatic versus phreatomagmatic fragmentation in maar-diatremes</i>	161

5.2	AN IMPROVED UNDERSTANDING OF MAAR-DIATREME VOLCANOES.....	162
5.2.1	<i>Phreatomagmatic activity in diatremes</i>	162
5.2.2	<i>Magmatic activity</i>	163
5.2.3	<i>Implications for natural hazards</i>	164
5.2.4	<i>Implications for kimberlites</i>	164
5.3	FUTURE WORK IN THE HBVF.....	166
6	REFERENCES.....	169
7	APPENDIX 1: CONFERENCE ABSTRACTS	189
7.1	Poster session at IAVCEI (2017), Portland, USA	189
7.2	Oral session at 7IMC (2018), Olot, Spain	191
7.3	Poster session at 7IMC (2018), Olot, Spain.....	195
7.4	Oral session at GAC-MAC-IAH (2019), Quebec City, Canada	201
7.5	Oral session at IUGG (2019), Montreal, Canada.....	203
7.6	Poster session at IUGG (2019), Montreal, Canada	205
7.7	Oral session planned for COV11 (2020), Heraklion, Greece.....	207

LIST OF FIGURES

Figure 1.1: Maar-diatreme model in cross-section, redrawn from White and Ross (2011).	2
Figure 1.2: Photo plate of the subaerial parts of maar-diatreme volcanoes.	4
Figure 1.3: Photo plate of the subterranean parts of maar-diatreme volcanoes.	6
Figure 1.4: Map of the southwestern part of the USA.....	10
Figure 1.5: Geological map of the Hopi Buttes volcanic field	12
Figure 1.6: Photo plate of the field work methods	17
Figure 1.7: The Fisher (1961) diagram after White and Houghton (2006)	19
Figure 2.1: Geological map showing a portion of the Hopi Buttes volcanic field	27
Figure 2.2: Round Butte geological map displaying the igneous remnants.....	29
Figure 2.3: Geological map of the cliffs in the south part of Round Butte	30
Figure 2.4: Geological map of the cliffs in the north part of Round Butte	31
Figure 2.5: Geological map of the cliffs in the southwest part of Round Butte	32
Figure 2.6: Geological map of the cliffs in the west part of Round Butte	33
Figure 2.7: Geological map of the cliffs in the west-northwest part of Round Butte	35
Figure 2.8: Photo plate of the principal facies of the undisturbed bedded pyroclastic rocks	39
Figure 2.9: Photo plate of the principal facies of the disturbed bedded pyroclastic rocks	40
Figure 2.10: Photo plate of the principal facies of the non-bedded pyroclastic rocks.....	41
Figure 2.11: Photo plate showing the diversity and the morphology of juvenile clasts	42
Figure 2.12: The six-step Round Butte evolution model.....	49
Figure 2.13: General maar-diatreme cross-sectional sketch introducing the transition zone.....	55
Figure 2.14: Geological map of the cliffs in the southeast part of Round Butte.....	56
Figure 2.15: Geological map of the cliffs in the southeast part of Round Butte.....	57
Figure 2.16: Geological map of the cliffs in the east part of Round Butte	58
Figure 2.17: Geological map of the cliffs in the north-northwest part of Round Butte	59
Figure 2.18: TAS diagram after Le Bas et al. (1986) and Le Maitre (1989).	62
Figure 2.19: Harker diagrams presenting the geochemistry of various major oxides.....	63
Figure 2.20: Immobile element diagram after Winchester and Floyd (1977).....	65
Figure 2.21: Extended trace elements normalized to the primitive mantle	66
Figure 3.1: Maps A) the Colorado Plateau, B) geology of the HBVF and C) Round Butte.	73
Figure 3.2: Photo plate of the main sedimentary formations in the HBVF area	75
Figure 3.3: Geological map of the cliffs in the southern part of Round Butte	77
Figure 3.4: Geological map of the cliffs in the southwest part of Round Butte	78

Figure 3.5: Photo plate of the megablocks.	81
Figure 3.6: Photo plate of the facies in the main DAD.....	82
Figure 3.7: Photo plate showing the diversity of lithic clasts, and a tuff clast.	91
Figure 3.8: Scenarios of country rock fragmentation at Round Butte.....	93
Figure 3.9: Geological map of the cliffs in the southeast part of Round Butte.....	104
Figure 3.10: Geological map of the cliffs in the southeast part of Round Butte.....	105
Figure 3.11: Geological map of the cliffs in the east part of Round Butte	106
Figure 3.12: Geological map of the cliffs in the north part of Round Butte	107
Figure 3.13: Geological map of the cliffs in the north-northwest part of Round Butte	108
Figure 3.14: Geological map of the cliffs in the northwest part of Round Butte.....	109
Figure 3.15: Geological map of the cliffs in the west part of Round Butte	110
Figure 4.1: Geological map of the HBVF	116
Figure 4.2: Geological map of the Twin Peaks volcanic complex.....	117
Figure 4.3: Detailed geological map of Twin Peaks.....	118
Figure 4.4: Geology of the north cliff of the North Peak.....	119
Figure 4.5: Geology of the south cliff of the North Peak	120
Figure 4.6: Geology of the south face of the South Peak	121
Figure 4.7: Photo plate of unit 1	125
Figure 4.8: Photo plate of unit 2	127
Figure 4.9: Photo plate of unit 3.....	128
Figure 4.10: Photo plate of unit 4	129
Figure 4.11: Twin Peaks evolution model.	140
Figure 4.12: Longitudinal cross-section of the Twin Peaks volcanic complex.....	142
Figure 4.13: TAS diagram after Le Bas et al. (1986) and Le Maitre (1989)	150
Figure 4.14: Harker diagrams. Twin Peaks coherent rocks.....	152
Figure 4.15: Immobile element diagram after Winchester and Floyd (1977).....	154
Figure 4.16: Extended trace elements normalized to the primitive mantle.	155

LIST OF TABLES

Table 2.1: Characteristics of undisturbed bedded pyroclastic rocks*	34
Table 2.2: Characteristics of disturbed bedded pyroclastic rocks	37
Table 2.3: Characteristics of non-bedded pyroclastic rocks (invasive columns)	38
Table 2.4: Major oxides (wt%) for Round Butte rocks	61
Table 2.5: Trace elements (ppm) for Round Butte rocks	64
Table 3.1: Characteristics of megablocks and the debris avalanche deposits (DADs)	83
Table 3.2: Results of field line counts	84
Table 3.3 Mann-Witney U Test ¹ on componentry data	86
Table 3.4: Results of field clast counts	88
Table 3.5: Results of petrographic point counts	89
Table 3.6: Comparison of the country rock fragmentation model with lithic proportions	94
Table 3.7: Compilation of mean value of line and clast count methods acquired at the 15 sites	98
Table 4.1: Results of field clast counts	131
Table 4.2: Results of petrographic point counts	133
Table 4.3: Integration of point counts measurements in clast counts data	134
Table 4.4 Traditional criteria used to distinguish phreatomagmatic from magmatic eruptive styles	144
Table 4.5: Major oxides (wt.%) for Twin Peaks volcanic complex rocks.	149
Table 4.6: Trace elements (ppm) for Twin Peaks volcanic complex rocks.	153

1 INTRODUCTION

This PhD thesis describes and interprets two well-exposed ultramafic maar-diatreme volcanoes, Round Butte and Twin Peaks, in the Hopi Buttes volcanic field (HBVF), Navajo Nation, Arizona. Their activity was mainly phreatomagmatic, due to interactions between the magma of the feeder intrusion and groundwater, although Twin Peaks switched to magmatic activity during the late stage of the eruption. Round Butte is easy to access and allows the study of the transition zone between bedded pyroclastic deposits of the upper diatreme and non-bedded pyroclastic deposits of the lower diatreme. Studying Round Butte can also help to constrain eruptive processes occurring in the lower diatreme, which are still debated in the literature. Twin Peaks is mainly of interest because it is composed of two main maar-diatremes displaying the same progression of eruptive style from phreatomagmatic to magmatic, and the causes of this evolution can be evaluated.

This chapter summarizes the state of the knowledge on maar-diatreme volcanoes, then presents the geological context of the study, the problems to be solved, the aims, the methods, and outlines the organization of the thesis.

1.1 Maar-diatreme volcanoes

After scoria cones, maar-diatreme volcanoes are the second-most common type of volcanoes on continents (Vespermann and Schmincke 1998). They are monogenetic, i.e. small, short-lived (days to years) volcanoes (Lorenz 1986a, 2007; White and Ross 2011; Kereszturi and Németh 2012; Valentine and White 2012; Lefebvre et al. 2013; Ross et al. 2017; Valentine et al. 2017). They have a funnel-shape morphology cut below the pre-eruptive surface, with the underground portion called the diatreme (Fig. 1.1). Maar-diatremes can be located in or near cities such as Auckland in New Zealand (Németh et al. 2012; Németh and Kereszturi 2015; Nunns and Hochstein 2019), Goma in the Democratic Republic of Congo (Poppe et al. 2016); or Clermont-Ferrand in France (Boivin and Thouret 2014). The involved magmas display various chemical compositions including ultramafic (e.g., HBVF, White 1991; Vazquez 1998; Hooten 1999; Hooten and Ort 2002; Lefebvre et al. 2012, 2013, 2016), mafic (e.g., Coombs Hills, McClintock and White 2006; Ross and White 2006; Auckland volcanic field, Németh et al. 2012; Nunns et al. 2019), intermediate (e.g., Lac Pavin, Leyrit et al. 2016) and felsic (e.g., Sugarloaf Mountain, Sheridan and Updike 1975; Tepexitl, Austin-Erickson et al. 2011).

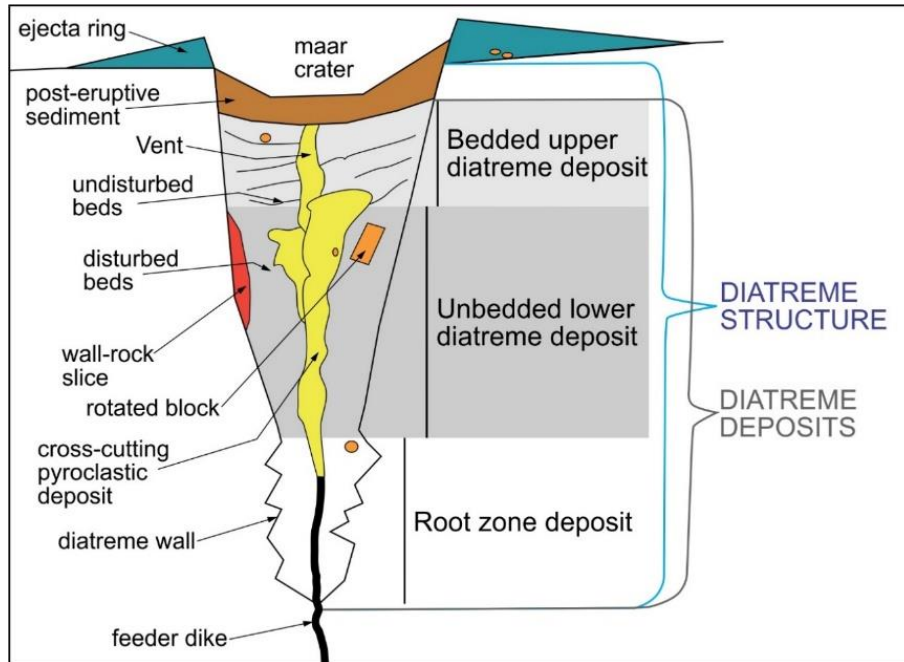


Figure 1.1: Maar-diatreme model in cross-section, redrawn from White and Ross (2011).

The formation of maar-diatreme volcanoes is mainly related to phreatomagmatism, i.e. explosive magma-water interaction (Lorenz 1986b; Zimanowski et al. 1997; Büttner and Zimanowski 1998). More specifically, they start to form when the feeder intrusion comes in contact with an aquifer (Re et al. 2015, 2016; Muirhead et al. 2016; Le Corvec et al. 2018). The aquifer can consist of water-filled fractures in a hard rock environment, or of water-saturated sediments (Lorenz 2003; Auer et al. 2007; Ross et al. 2011). Maar-diatremes can have subordinate magmatic explosive phases, as observed at Ukinrek in 1977 (Kienle et al. 1980; Self et al. 1980; Büchel and Lorenz 1993; Ort et al. 2018) or at Taal in 2020 (Smithsonian / USGS Weekly Volcanic Activity Report 8-14 January 2020). Many studies document intercalation of phreatomagmatic and magmatic beds within ejecta rings (Houghton and Schmincke 1986, 1989; Houghton et al. 1996; Ross et al. 2011; Ort et al. 2018). Transitional to magmatic units are also reported within diatreme deposits (White 1996a; Valentine and van Wyk de Vries 2014; Sonder et al. 2018). There is sometimes an overall evolution of eruptive activity from phreatomagmatic to magmatic (Lorenz 1986a; Tietz et al. 2018) or the opposite (Valentine and Cortés 2013; Geshi et al. 2019).

The upper part of maar-diatremes is the ejecta ring (Self et al. 1980; White 1991; Vazquez and Ort 2006; Valentine et al. 2015) and the maar crater (Lorenz 1973; White 1991; Graettinger 2018). The subterranean part is composed of a typically bedded upper diatreme (White 1991;

Gernon et al. 2013; Delpit et al. 2014), a typically non-bedded lower diatreme (White 1991; Lefebvre et al. 2013, 2016), a root zone (Clement 1982; Lorenz and Kurszlaukis 2007; Haller et al. 2017) and a feeder intrusion (Re et al. 2015, 2016; Muirhead et al. 2016; Le Corvec et al. 2018). It is very rare to observe an entire section across a maar-diatreme, mainly because Quaternary examples display the ejecta ring and the maar crater, whereas older, partially eroded ones display only the diatreme or the root zone. Only the Suoana crater, exposed in the Miyakejima caldera (Japan), is an example showing the entire structure of a small maar-diatreme volcano from the feeder dike to the ejecta ring (Geshi et al. 2011).

1.1.1 Ejecta ring

Ejecta rings consist of pyroclastic deposits around maar craters. They are up to 50 m thick and extend radially up to 5 km (Lorenz 2008; White and Ross 2011). They are bedded deposits composed of a multitude of mm- to m-thick beds often rich in lithic clasts (Figs. 1.2a, 1.2b; Ollier 1967; Kienle et al. 1980; White 1991; White and Ross 2011; Lefebvre et al. 2013; Graettinger and Valentine 2017). Beds preserved in ejecta rings offer a partial record of the 'life' of the maar-diatreme and can be phreatomagmatic to magmatic in origin (Fig. 1.2b; Houghton and Schmincke 1986; Houghton et al. 1996; Ross et al. 2011), although phreatomagmatic deposits tend to dominate. Phreatomagmatic beds tend to be pale in color, thin on average and are mainly composed by ash and lapilli (Figs. 1.2a, 1.2b) whereas magmatic beds are usually black in color and composed of thick coarse beds (clast size range from lapilli to blocks and bombs, Fig.1.2b).

Phreatomagmatic beds display lateral variations from the proximal area, mostly composed of structureless beds, to the medial area, which is bedded and characterized by crossbedding, dunes and bomb sags, and the distal part, which is finely bedded and composed of planar beds (Sohn 1996). The numerous beds result mainly from base surges (Moore 1967; Crowe and Fisher 1973; Nairn 1979; Self et al. 1980) or from lesser fallout (White 1991; White and Ross 2011; Graettinger and Valentine 2017). Subordinate ballistic processes are recorded as bomb sags in the plastically deformable beds of the ejecta ring (Sohn and chough 1989; Vazquez and Ort 2006; White and Ross 2011). For their part magmatic beds tend to become finer and thinner with distance from the vent.

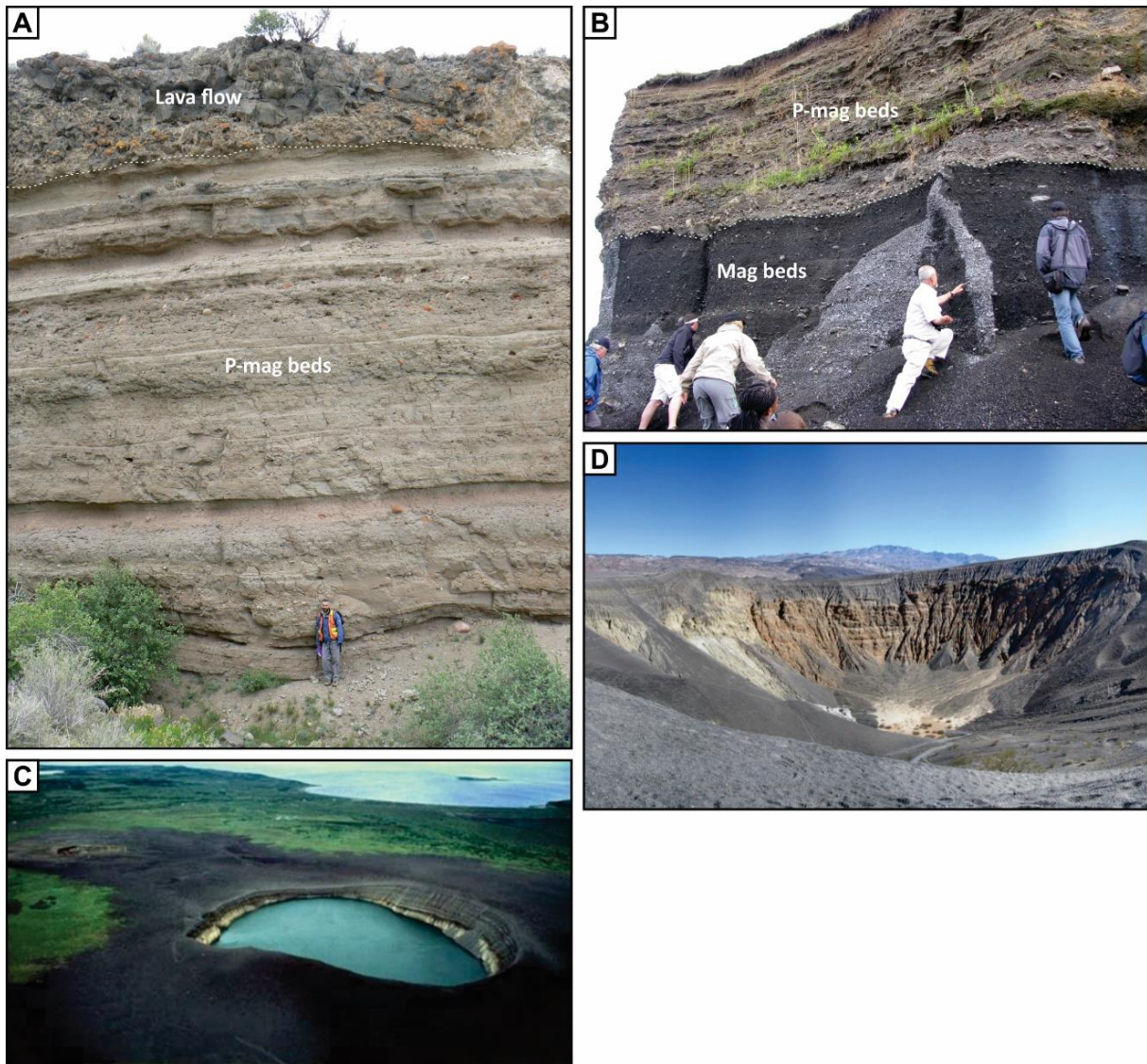


Figure 1.2: Photo plate of the subaerial parts of maar-diatreme volcanoes. A) Ejecta ring displaying phreatomagmatic beds (P-mag beds) at Teshim maar in the HBVF (photo by B. Latutrie, 2017), B) phreatomagmatic beds and magmatic beds (Mag beds) at Oberwinckel maar, West Eifel (photo by P.-S. Ross, 2008), C) the 320 m wide east maar at Ukinrek, Alaska (photo by C. Neal, 1993) and D) the 700 m wide main crater at Ubehebe crater complex, California (photo by L. Siebert, 1974).

1.1.2 Maar crater

Maar craters are formed during the eruptive activity because material is expelled toward the ejecta ring. A distinction is commonly made between the syn-eruptive crater, which is formed directly by the eruption, and the post-eruptive crater, which evolves over a longer period after the end of the eruption (White and Ross 2011). Post-eruptive craters are 69 to 5000 m wide (mostly 200-1400 m wide) and 5 to 400 m deep (Figs. 1.2c, 1.2d; Lorenz 1973; Ross et al. 2011; Graettinger 2018). The lateral growth of maar craters during and after the eruption is

mainly driven by collapse due to gravitational destabilization of the walls (Kienle et al. 1980; White 1991; White and Ross 2011). After the end of the eruptive activity, maar craters are commonly filled by lacustrine sediments (Sunflower Butte maar, HBVF; White 1992) or fluvial to aeolian sediments (Teshim maar, HBVF; White 1992). One of the main source of sediments is the remobilisation of the pyroclastic deposits of the ejecta ring (Pirrung et al. 2008). Examples of crater lakes include Pulvermaar, West Eifel, Germany (Ollier 1967; Lorenz and Zimanowski 2008), Albano maar, Italy (Giacco et al. 2007; Sottili et al. 2010) or Lac Pavin, France (Leyrit et al. 2016). The lacustrine sediments can be good archives to reconstruct the paleoclimate from the time of the eruption to the present if the lake still exists (Németh et al. 2008). Maar craters are underlain by a variably deep diatreme (Lorenz 1986a, 2007; White and Ross 2011; Valentine and White 2012).

1.1.3 Upper diatreme

Upper diatremes typically contain well-bedded to diffusely bedded pyroclastic deposits (White 1991; Gernon et al. 2013; Delpit et al. 2014; Bélanger and Ross 2018). White and Ross (2011) distinguish two varieties of upper diatreme deposits: Type I and Type II. Type I deposits subside along ring faults during eruptive activity, forming distinctive saucer shape beds as observed in the Missouri River Breaks volcanic field, Montana (Fig. 1.3a; Delpit et al. 2014).

Type II upper diatreme deposits are inferred to be deposited into deep craters without strong subsidence processes. They are typical of the HBVF and correspond to an infilling of the syn-eruptive crater with phreatomagmatic to magmatic deposits (White and Ross 2011). Examples of Type II diatremes are Hoskietso Claim (Fig. 1.3b; White 1991) or Round Butte (this study). During phreatomagmatic activity, Type II deposits form within the syn-eruptive crater from PDCs (surges), proximal fallout and fallback processes (Delpit et al. 2014; Bélanger and Ross 2018) whereas during magmatic activity they form from fallout from a strombolian vent or even from lava flows filling the crater (Martin and Németh 2002; Tietz et al. 2018). Megablocks that are defined to be blocks over 2 m in long axis (e.g., lithic megablocks, Brown et al. 2008; Delpit et al. 2014; Ross et al. 2017 or pyroclastic megablocks, Gernon et al. 2013) and landslides (Kurszlaukis et al. 2009; Borrero et al. 2017) can be included in upper diatreme deposits.

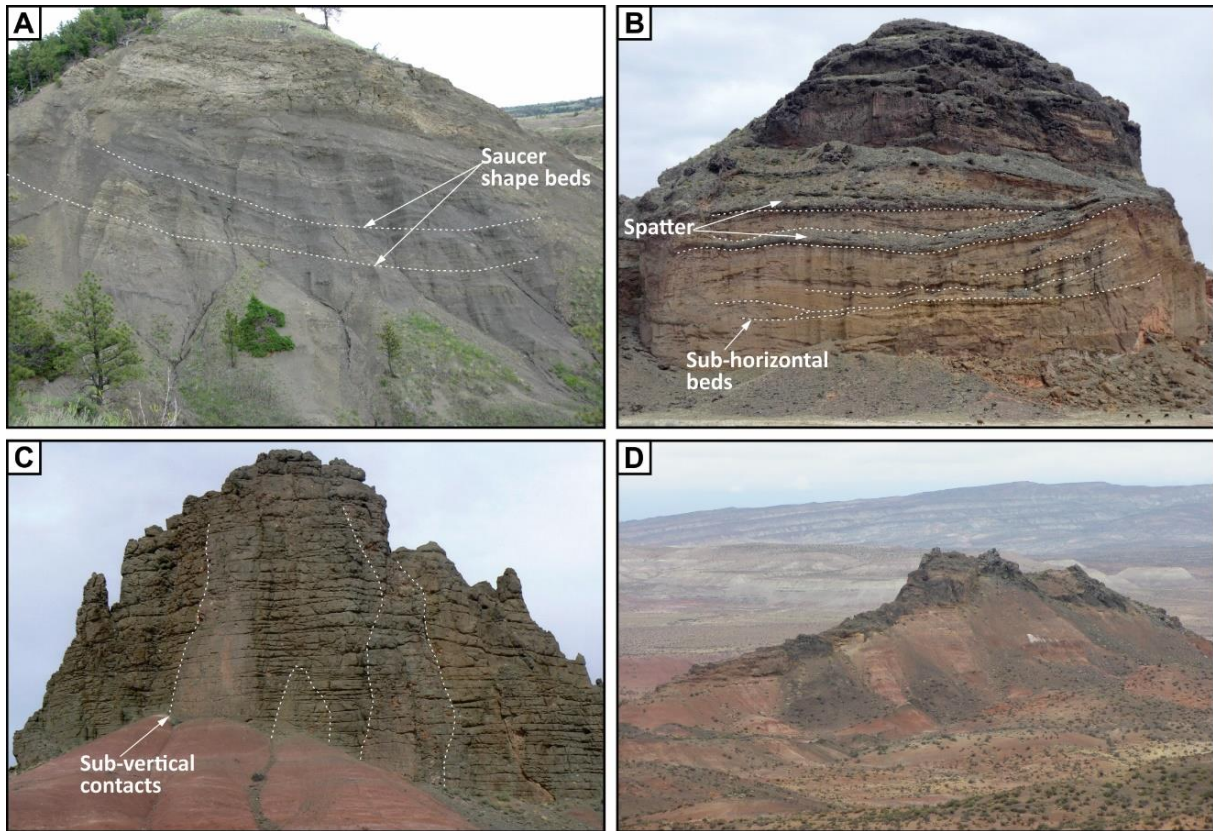


Figure 1.3: Photo plate of the subterranean parts of maar-diatreme volcanoes. A) Type I upper diatreme deposits displaying saucer shaped beds at Black Butte, Missouri River Breaks, Montana (photo by P-S. Ross, 2009), B) Type II upper diatreme deposits displaying phreatomagmatic beds intercalated with spatter deposits at Hoskietso Claim, HBVF (Photo by B. Latutrie, 2017), C) lower diatreme deposits with subvertical features at West Standing Rocks, HBVF (photo by P.P. Comida, 2017) and D) an elongated root zone extending over 900 m at Cerro 117, Cerro Chivo volcanic field, Argentina (photo by P-S. Ross, 2017).

1.1.4 Lower diatreme

The lower diatreme is typically filled by non-bedded pyroclastic deposits (Fig 1.3c; White and Ross 2011; Lefebvre et al. 2013; Ross et al. 2017), variably cut by coherent intrusions. The origin of the non-bedded pyroclastic deposits in the lower diatreme is debated in the literature (see discussion in Bélanger and Ross 2018) and three hypotheses are mainly discussed. Some workers, such as Porritt et al. (2008) or Gernon et al. (2008, 2013), consider a dissociated history for the emplacement of the upper and lower diatreme deposits. This means that the eruptive styles and processes of the two portions can be completely different. Porritt et al. (2008) proposed that the lower diatreme forms by the in-vent collapse of a subplinian to plinian plume. Gernon et al. (2008, 2013) instead favoured fluidization processes.

The third hypothesis is that the upper and lower diatreme deposits form simultaneously, mainly as a result of phreatomagmatic activity (e.g., White 1991; Ross and White 2006; Valentine and White 2012; Lefebvre et al. 2013; Valentine et al. 2014; Lorenz et al. 2017; Bélanger and Ross 2018). Proponents of this hypothesis note that non-bedded pyroclastic deposits of the lower diatreme often contain vertical structures called columns (White 1991; Ross and White 2006; Bélanger et al. 2018) and a well-known example of these is the West Standing Rocks diatreme in the HBVF (Fig. 1.3c; Lefebvre et al. 2013). The columns in the lower diatreme are thought to be related to the passage of debris jets, some of which rise all the way to the crater floor to become eruptive columns and jets, which generate the ejecta ring and upper diatreme deposits. The debris jets originate in the diatreme and root zone, where feeder intrusions such as dikes and sills interact explosively with groundwater (Valentine and White 2012). Debris jets not only push material upward, but also disturb and homogenise older bedded pyroclastic deposits, eventually destroying the bedding (Bélanger and Ross 2018).

1.1.5 Root zone and feeder intrusion

Root zones are considered to be the link between the lower diatreme and the unfragmented feeder intrusion, but they are still poorly documented and understood (Lorenz and Kurszlaukis 2007). Most of the root zone knowledge comes from the study of kimberlitic pipes (Clement 1982; Hubbard 1986) or carbonatite pipes (Lorenz and Kurszlaukis 1997). Root zones commonly display an elongate shape (Fig. 1.3d; Lorenz and Kurszlaukis 2007; Haller et al. 2017). They are composed of country rocks breccias, non-bedded pyroclastic rocks and numerous coherent dikes. Those coherent dikes propagate from the feeder intrusion through the root zone and reach the overlying diatreme. This part of maar-diatreme volcanoes is the location where numerous phreatomagmatic explosions start to fragment country rocks, allowing the deepening of the diatreme in some models (Lorenz 1986a; Lorenz and Kurszlaukis 2007). Root zones rarely crop out and none of them are described in the HBVF. Recently Haller et al. (2017) described the occurrence of basaltic root zones in the Cerro Chivo volcanic field, Patagonia, Argentina.

1.2 Explosive magma/water interactions

Phreatomagmatic explosions in maar-diatremes are caused by a violent interaction between the magma and the groundwater (Lorenz 1986b; Zimanowski 1998; Zimanowski et al. 1991, 1997). Two mechanisms for explosive magma/water interactions have been reproduced in the

laboratory and are thought to be possible in nature. In ultramafic to mafic experiments, water and magma are intimately mixed, forming a “premix”. During this stage, a vapor film provides an efficient insulation between the magma and the water. The destabilization of the vapor film, due to its condensation or to shockwaves from surrounding phreatomagmatic explosions, allows a rapid heat transfer from the magma to the water. This fragments the magma. The liquid water is nearly instantaneously transformed into vapor, triggering a sudden volume increase which expels the mixture from the crucible (Zimanowski et al. 1991; 1997) or in nature, creates a phreatomagmatic eruptive column or jet. By analogy with industrial accidents (Cho et al. 1976; Cronenberg 1980), this mechanism is called Molten-Fuel Coolant Interaction (MFCI) with magma acting as the “Molten Fuel” and the water as the “Coolant” (Büttner and Zimanowski 1998; Zimanowski 1998).

In intermediate to felsic eruptions (and experiments), a similar “premix” step is not reached because the magma viscosity is too high, in the 10^7 to 10^{12} Pa.s range for rhyolite (Spera 2000). However, cracks can open in the moving felsic magma, which allows liquid water to make direct contact and interact explosively (Austin-Erickson et al. 2008, 2011). This mechanism does not depend on the collapse of vapour films and has recently been called “Induced Fuel Coolant Interaction” (IFCI) (White et al. 2019).

1.3 Historical eruptions and volcanic hazards

Examples of historical maar-diatreme eruptions are relatively rare but give important information about eruptive phenomena and hazards. The four best known historical examples are the Rotomahana (New Zealand) eruption in 1886 (Thomas 1888; Nairn 1979), the Nilahue (Chile) eruption in 1956 (Muller and Veyl 1957), the Taal (Philippines) eruption of 1965 (Moore et al. 1966; Moore 1967) and the Ukinrek (Alaska) eruption in 1977 (Kienle et al. 1980; Self et al. 1980; Büchel and Lorenz 1993; Ort et al. 2018). These events highlighted the dangerousness of maar-diatreme volcanoes. Powerful phreatomagmatic explosions can occur during those eruptions, forming 20 km high plumes (Moore et al. 1966; Kienle et al. 1980; Self et al. 1980) and pyroclastic density currents (PDCs, Nairn 1979; Ort et al. 2018). Surges, also known as low-concentration or dilute PDCs, can travel radially 5 km or more from the vent and cause severe destruction (Moore 1967). Indeed, such PDCs and associated ballistic bombs are able to destroy the vegetation or human constructions in the surroundings of the volcano. At greater distance, ash and lapilli in the eruptive plume fall to form fallout deposits. Over time, during eruptions, fallout deposits can accumulate on roofs, leading to building collapse. Magmatic

phases are documented in historical maar-diatreme eruptions as scoria cones (Ukinrek, Ort et al. 2018 or Taal, Moore 1967) or lava fountains (Taal, Smithsonian / USGS Weekly Volcanic Activity Report 8-14 January 2020) but are commonly not taken into account in hazard maps and should be given more attention.

1.4 Geological setting

The HBVF, which hosts the two studied volcanoes, is located in the southern part of the Colorado Plateau. The geology of the Colorado Plateau is presented first, and then that of the HBVF.

1.4.1 The Colorado Plateau

The Colorado Plateau is an area of relatively tectonically stable continental crust since the Lower Permian (Billingsley et al. 2013). It is located in southwestern USA, between the Rocky Mountains and Rio Grande Rift to the east, and the Basin and Range Province to the west and south (Fig. 1.4; Thompson and Zoback 1979; Fitton et al. 1991; Kempton et al. 1991). The plateau crust is ~40 km thick (Frassetto et al. 2006; Gilbert et al. 2007).

During the Paleoproterozoic, two main terranes (Yavapai and Mazatzal; Karlstrom and Bowring 1988; Karlstrom and Humphreys 1998) were accreted along a NE-SW axis, forming the basement of the plateau. The boundary of these two terranes is still unclear (Gilbert et al. 2007). During the Precambrian, an orogenic phase formed large scale uplifts and subsidence (Davis 1978; Marshak et al. 2000; Davis and Bump 2009). The Sevier Thrust Belt and the Laramide subduction zone were active almost at the same time, from the lower Cretaceous to the Eocene (Fig. 1.4; Gilbert et al. 2007; Davis and Bump 2009). Finally, during the Pliocene, the region was affected by an extensive deformation phase generated by the convergence and the destruction of the Farallon plate (Atwater 1970). This formed the Basin and Range Province and the Rio Grande Rift. A 50-100 km wide Transition Zone is present between the Colorado Plateau and the Basin and Range Province. This Transition Zone is characterised by late Tertiary normal faults and Quaternary volcanism (Thompson and Zoback 1979).

The Colorado Plateau is capped by 3-5 km of Phanerozoic sedimentary rocks that were deposited on crystalline basement rocks (Cooley et al. 1969; Keller et al. 1998). Sedimentary rocks display a low dip of 1-2° northeastward and didn't experience strong tectonic deformation processes (Billingsley et al. 2013). In the HBVF area, the main formations are dated from the

Lower Triassic (Moenkopi Formation) to the Miocene (Bidahochi Formation) and are described in detail in Chapter 3.

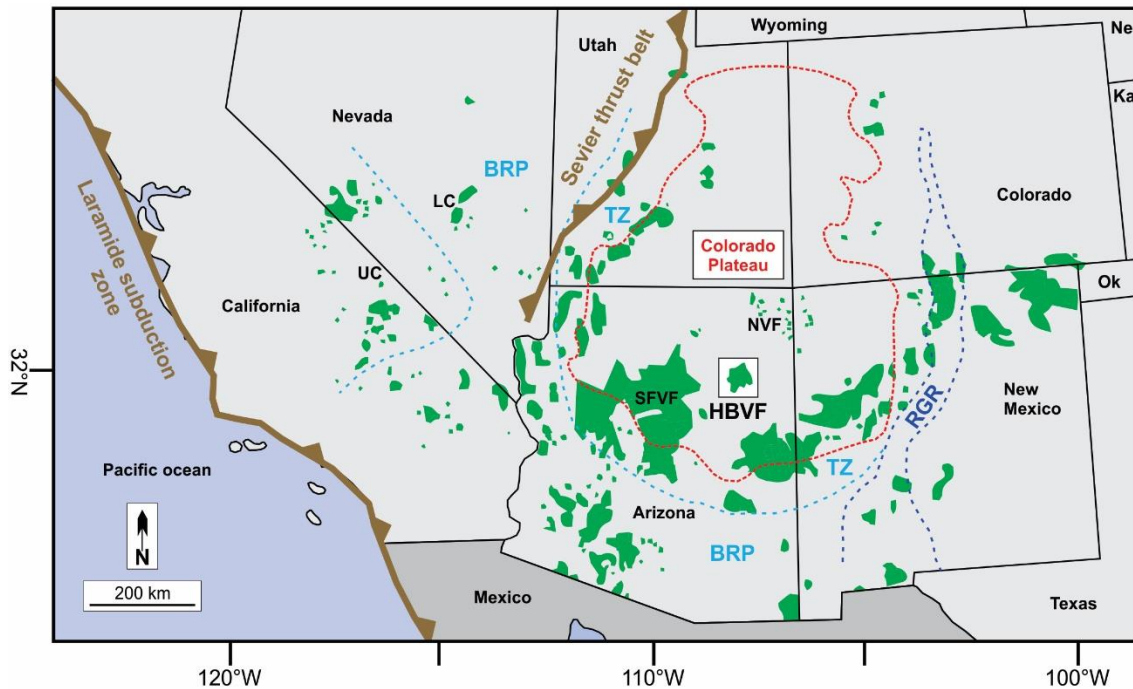


Figure 1.4: Map of the southwestern part of the USA showing the location of the Colorado Plateau with the recent volcanic fields (< 30 Ma) in green and the main tectonic structures that are the Sevier Thrust Belt, the Laramide subduction zone, the Basin and Range Province (BRP), the Rio Grande Rift (RGR) and the Transition Zone (TZ). Figure modified from Lefebvre (2013) who used the papers of Akers et al. (1971); Kempton et al. (1991); Delaney and Gartner (1997); Tingey et al. (1999); Davis and Bump (2009). Note: HBVF = Hopi Buttes volcanic field, NVF = Navajo volcanic field, SFVF = San Francisco volcanic field, LC = Lunar Crater volcanic field, UC = Ubehebe crater, Ne = Nebraska, Ka = Kansas, Ok = Oklahoma.

Two main phases of volcanism occurred during the Colorado Plateau history. A first phase occurred between the Lower Cretaceous and the Eocene. Intense magmatism occurred on the edge of the Colorado Plateau and low intensity magmatism toward the center (Lipman et al. 1972; Snyder et al. 1976). The second phase of magmatism, during the Pliocene, was generated because of the destruction of the Farallon plate and occurred on the margin of the plateau (Fitton et al. 1991). Notable volcanic fields on the Plateau (Fig. 1.4) include the HBVF (Miocene), described in the next section, as well as the San Francisco volcanic field (Miocene to Holocene, Ulrich et al. 1984; Ulrich 1987) and the Navajo volcanic field (Oligocene, Nybo et al. 2011). The Navajo volcanic field igneous remnants are mainly large maar-diatreme volcanoes and minette dikes (Semken 2003; Bélanger and Ross 2018) whereas basaltic volcanoes of the San Francisco volcanic field are mainly composed of scoria cones and lava flows (Riggs et al. 2019).

1.4.2 Hopi Buttes volcanic field (HBVF)

The HBVF is mainly composed by maar-diatreme volcanoes, intrusions, lava flows and scoria cones (Williams 1936; White 1991; Hooten 1999; Vazquez and Ort 2006; Lefebvre et al. 2013; Re et al. 2015, 2016). It contains about 300 Miocene (8-6.5 Ma) volcanic remnants distributed over an area of 2300 km² (Fig. 1.5).

The pioneering stage of HBVF exploration occurred in the first half of the 20th century. Gregory (1917) provided the first description of the volcanic remnants and observed mainly “volcanic necks”, lavas and dikes. Williams (1936) observed that most HBVF volcanoes were circular in shape and composed by coherent or pyroclastic rocks. He observed that volcano remnants are typically tuff breccia “shafts” in the Navajo volcanic field (e.g., Cathedral Cliff, Bélanger and Ross 2018; Ship Rock, Delaney 1987) whereas those of the HBVF are often ‘plug’-dominated, i.e. mostly consisting of thick jointed lavas, and referred as “Hopi necks”. More detailed studies on maar-diatreme volcanoes in the HBVF concluded that they form from magma-water interactions (Hack 1942).

Modern volcanological studies of the HBVF started with the work of White (1989, 1990, 1991). He described ejecta ring and diatreme deposits in detail, but also the environmental setting at the time of the volcanism (playa and pond setting). He obtained new insights on emplacement processes of maar-diatremes in the HBVF, and popularized the field as one the best places in the world to study such volcanoes (White and Ross 2011).

Vazquez (1998) and Hooten (1999) focused on the physical volcanology of several other HBVF volcanoes and documented the geochemistry of the field. They observed that most of the volcanic remnants are basanite/tephrite in composition. Hooten (1999) and Hooten and Ort (2002) highlighted peperite deposits formed by non-explosive fragmentation processes. Vazquez (1998) and Vazquez and Ort (2006) investigated an ejecta ring and demonstrated lateral facies changes in base surge deposits.

More recently, Lefebvre et al. (2012, 2013, 2016) returned to diatreme deposits. They introduced the concept of spatter dikes (fissures filled by spatter), detailed the architecture of the lower diatreme by describing vertical columns at West Standing rocks (Figs. 1.3c, 1.5) and gave an example of a diatreme that stopped early during its formation at East Standing Rocks. Re et al. (2015, 2016) and Muirhead et al. (2016) focused on feeder intrusions. They emphasized that sills or inclined sheets could also be the feeders of maar-diatreme volcanoes

(the typical model instead shows a vertical dike) and considered that many *en echelon* dikes in the HBVF could have fed scoria cones.

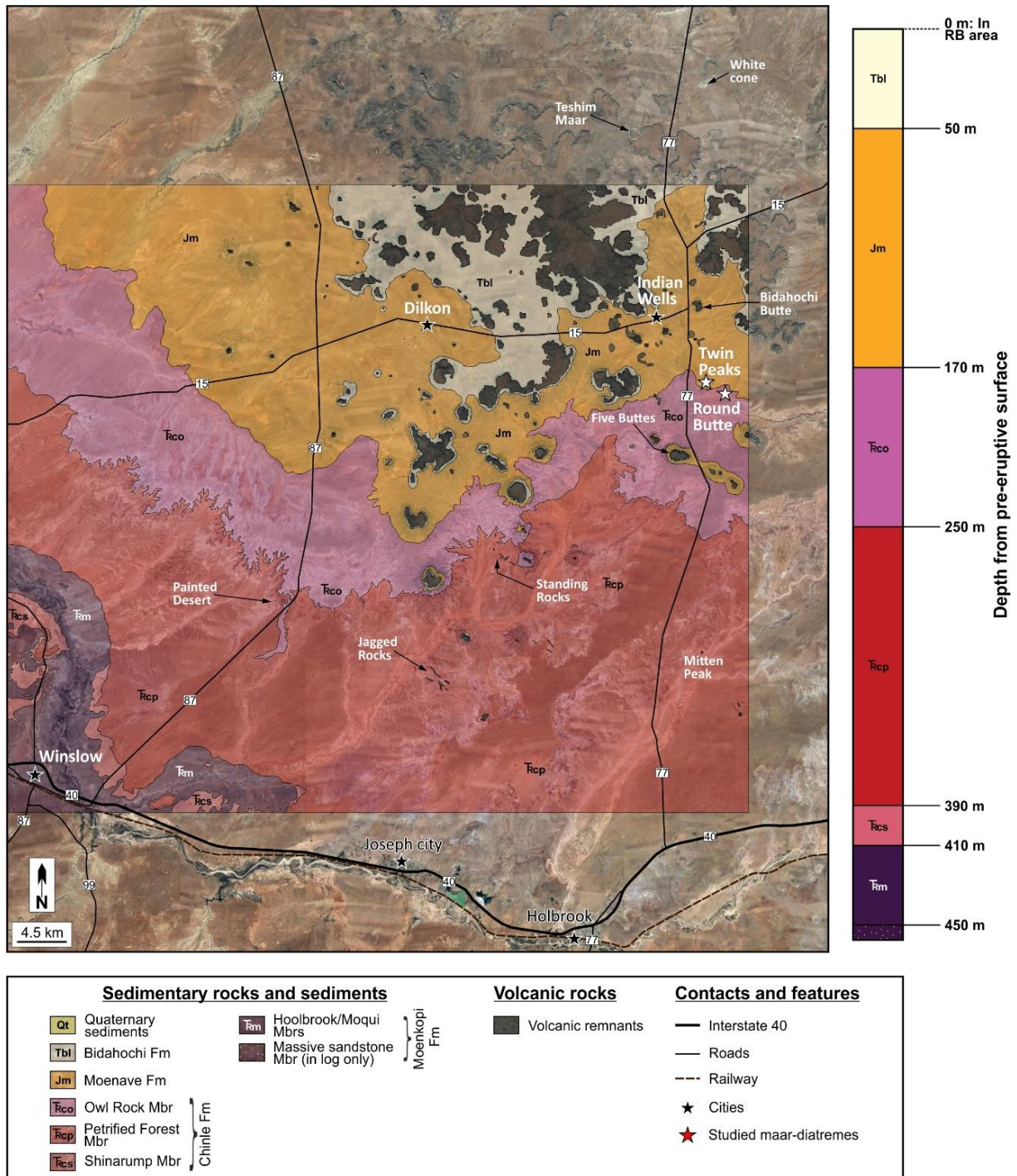


Figure 1.5: Geological map of the Hopi Buttes volcanic field (after Billingsley et al. 2013) superimposed on a Google Earth image (centre at UTM zone 12S, 572 410 m E, 3 916 058 m N). The location of the Round Butte diatreme and the Twin Peaks volcanic complex are indicated, along with the position of other notable features. A stratigraphic log of the country rocks for the Round Butte area has been constructed based on the literature (Billingsley et al. 2013).

1.5 Problems and aims

Maar-diatreme volcanoes can be located near cities. As noted above, the eruptive activity of maar-diatremes is characterised by violent phreatomagmatic explosions that produce plumes able to reach a height up to 20 km (e.g., Ukinrek, Kienle et al. 1980; Self et al. 1980). The eruption columns generate fallout. The main hazard though is the low-concentration PDCs (surges) that are able to travel up to 5 km radially and cause severe destruction (Moore 1967; Crowe and Fisher 1973; Nairn 1979; Self et al. 1980; Vazquez and Ort 2006; Lorenz 2007; White and Ross 2011; Poppe et al. 2016; Hayes et al. 2018). On the positive side, kimberlitic maar-diatreme volcanoes can host diamond deposits (Kjarsgaard 2007).

Despite this socio-economic importance, the eruptive processes of maar-diatremes are still not completely understood, mainly because most of the explosive activity takes place in the subterranean diatreme (White 1991, 1996a; White and Ross 2011; Lefebvre et al. 2013, 2016). Ejecta rings are easily accessible in young volcanic fields but their study only gives a partial understanding, because not all explosions in the diatreme or root zone send material all the way to the surface (Lorenz 1973, 2007; Houghton and Schmincke 1986; Houghton et al. 1996; Stoppa 1996; Valentine et al. 2015). Laboratory experiments on phreatomagmatic explosions provide information on how the magma and water interact (Zimanowski 1998; Zimanowski et al. 1991, 1997; Büttner et al. 2002; Austin-Erickson et al. 2008). Large-scale experiments with chemical explosives illustrate cratering processes and give insights on the relation between the depth of the explosion and the size of the crater, as well as on the importance of pre-existing craters on the morphology of the final one (Valentine et al. 2012, 2014; Ross et al. 2013; Taddeucci et al. 2013; Graettinger et al. 2014). Geophysical studies such as gravity or magnetic surveys are interesting to provide an estimation of the size of the diatreme or of a diatreme complex (Blaikie et al. 2012; Nunns et al. 2019) but do not provide details of the internal structure. Therefore, the main strategy to better understand the internal structure and eruptive processes of maar-diatremes is still to conduct detailed field studies on partly eroded volcanoes displaying the diatreme (Ross and White 2006; Delpit et al. 2014; Bélanger et al. 2018).

A few previous studies have utilized the HBVF diatremes for this purpose. Notably, Lefebvre (2013) examined three volcanoes in the HBVF. She worked on the lower diatreme composed by subvertical columns at West Standing Rocks (Lefebvre et al. 2013), reconstructed processes that form spatter dikes at Castle Butte Trading Post (Lefebvre et al. 2012) and concluded that East Standing Rocks is not a root zone as originally thought, but instead a diatreme

characterized by a brutal stop during its activity (Lefebvre et al. 2016). However, there are still many questions to answer about how maar-diatreme volcanoes work (see examples below), and studying other well-exposed HBVF diatremes is a good way to try to make progress in answering them.

This thesis contains a detailed study of the Round Butte and Twin Peaks volcanoes. Their emplacement processes and eruptive dynamics will be modeled. These volcanoes are cited in publications (White 1991; White and Ross 2011) and are commonly visited during field trips (White et al. 2008, 2012a, 2012b) but had never received focussed attention. At Round Butte, early workers observed both non-bedded and bedded pyroclastic deposits, suggesting that a transition zone between the upper and lower diatreme may be exposed there; this is very rare worldwide. Reconnaissance at Twin Peaks indicated that this is an example of a plug-type necks thought to be typical of the HBVF by Williams (1936), but never studied in detail in this field.

At Round Butte, this work will focus on the significance and the genetic importance of the transition zone between the upper and lower diatreme (Chapter 2). Another research axis at Round Butte will be the contribution of the study of lithic clasts and lithic-rich lithologies in our understanding of eruptive processes in the diatreme (Chapter 3). The main interest at Twin Peaks is to learn about processes leading to the change in eruptive regime from phreatomagmatic to magmatic to form plug-type necks (Chapter 4).

Specific questions at Round Butte include:

- How is the syn-eruptive crater filled?
 - What are the processes by which pyroclastic rocks are deposited in the upper diatreme?
 - Is there only one phase of crater excavation and infilling, or several?
- How are non-bedded deposits formed in the lower diatreme?
 - Are homogenisation processes responsible for the formation of the pyroclastic rocks in the lower diatreme?
 - If so, what are these homogenisation processes?
- What does the transition between the upper and lower diatreme look like, and how does it form?
 - Is the transition sharp or is it a thick/gradual zone?

- Are the upper and lower diatreme formed simultaneously?
- What can lithic clasts and lithic-rich lithologies tell us about diatreme processes?
 - Where are the lithics coming from; are they moving up or down?
 - What can country rock fragmentation models tell us on maar-diatreme geometry and formation?

Specific questions at Twin Peaks include:

- Is the explosive activity in maar-diatreme continuous or can there be breaks?
- What influences the change of eruptive regime from phreatomagmatic to magmatic?
- Is there only one active vent at the time?
- Can lava fill the maar crater and even potentially overflow?

These questions are not HBVF-specific, but instead are fundamental questions about how maar-diatreme volcanoes work. The transition zone is the missing link between bedded and non-bedded pyroclastic deposits in the diatreme and no study has yet focused on the timing of its formation. Studying the transition zone will provide details on the timing and processes of formation of the upper and lower diatreme, and clarify the ongoing debate on the phreatomagmatic origin of the lower diatreme. This has implications for kimberlitic maar-diatremes, because the internal architecture and emplacement processes of diatremes influences diamond distribution. Lithic clasts are interesting because unlike juvenile fragments, they have known depths origin when the country rock stratigraphy is well known. They can be used in other volcanic fields to reconstruct the net movement of clasts in the diatreme and provide information on geometric parameters of diatremes such as their sizes, wall angles or the depth of the root zone. Finally, the study of drivers of eruptive style change from phreatomagmatic to magmatic is important to better constrain volcanic hazards related to magmatic phases in maar-diatreme eruptions.

1.6 Methodology

1.6.1 Field work overview and terminology

One month of field work was completed at Round Butte and a second month at Twin Peaks. Geological mapping was performed and lithofacies were described. A lithofacies is “a body or interval of rock or sediment which has a unique definable character that distinguishes it from other facies” (Cas and Wright 1987). In this study, pyroclastic lithofacies were defined using

structures, grain size and a visual assessment of componentry. The componentry of each lithofacies was then quantified using field line counts and field clast counts.

At Round Butte, lithofacies with similar structures (e.g., bedded versus non-bedded) and a spatial association were combined into facies groups. Each lithofacies contains one or more depositional unit, i.e. a body of rock deposited by a single event. Beds and columns are examples of depositional units. This terminology allows both bedded and non-bedded lithofacies to be integrated into a consistent scheme.

At Twin Peaks, a slightly different terminology was used. Facies groups were defined, but instead of using only structures as the defining characteristic of facies groups (as done at Round Butte), a combination of structures, grain size, componentry and clast shapes was utilized. In the paper, the facies groups are called 'units' (labelled 1 to 4), with the implication that they are stratigraphic units and that were formed sequentially by different eruptive styles. Therefore, the term 'unit' has a different meaning depending on the chapter: depositional unit at Round Butte, and stratigraphic unit at Twin Peaks.

Finally, fist-sized samples were collected for all units and facies mapped.

1.6.1.1 Mapping the volcanic edifices

Two types of mapping were done at Round Butte and Twin Peaks. First, Google Earth images were printed (e.g., Fig. 1.6a) and plan view geological maps were drafted in the field. For Round Butte, because the top of the massif is not safely accessible, and the cliffs are subvertical, this map simply shows the contact between the country rocks and the pyroclastic rocks of the diatreme, some large sedimentary megablocks outside the massif, and the orientation of surrounding dikes (see Chapter 2). For Twin Peaks, most of the hill is accessible, so the plan view geological map shows the four different stratigraphic units of the two main peaks (see Chapter 4).

The second type of map relies on cliffs or very steep rock faces present at both sites, providing exposure akin to cross-sections through the interior of the volcanoes. High quality pictures of the cliffs were taken from the ground (9 at Round Butte and 3 at Twin Peaks) and printed using photo paper (e.g., Fig. 1.6b). Contacts were drawn directly on the photos in the field, often with the assistance of binoculars. At Round Butte, this allowed detailed mapping of pyroclastic lithofacies not visible on the plan view map. At Twin Peaks, it better showed the relations

between the four stratigraphic units and the internal variations within these units (the different facies).

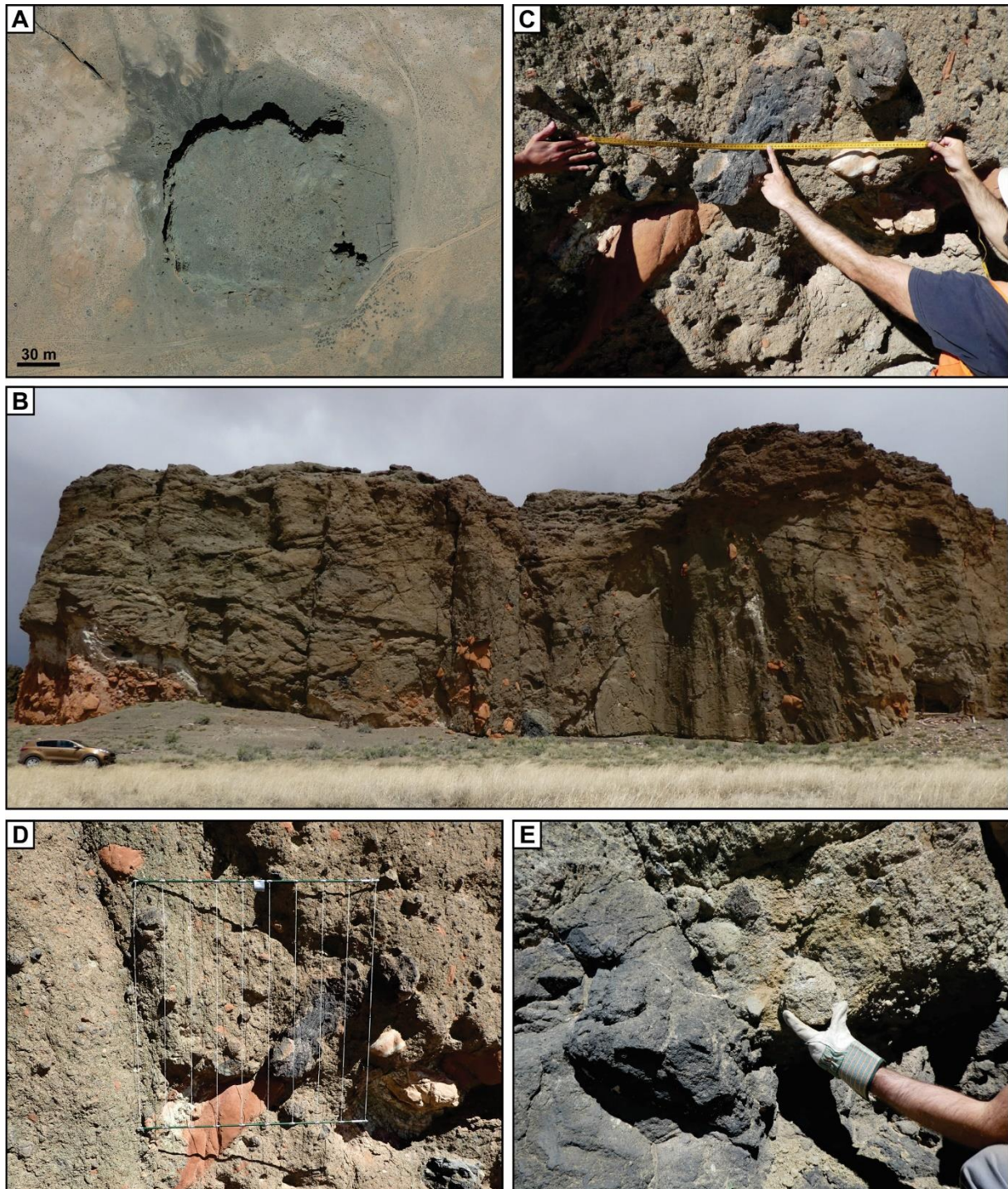


Figure 1.6: Photo plate of the field work methods. A) Google Earth image (centre near zone 12S, 588 158 m E, 3 910 326 m N) of Round Butte diatreme, B) high quality photograph of the south face of Round Butte diatreme, C) 1 m tape used for the line count method, D) 1 m² net for the clast count method, E) example of a hand sample of pyroclastic rock, taken at Round Butte diatreme.

1.6.1.2 Field componentry

Two field componentry methods were used at Round Butte and Twin Peaks: line counts and clast counts. These methods allow the quantification of the proportion of fragments found in pyroclastic rocks. The reason for using two methods is that line counts are more convenient on subvertical rock faces, but clast counts are more established, being a field version of point counting. At both volcanoes, clast counts were done on a subset of line count sites to enable a comparison between the methods.

The line count method shown in Fig. 1.6c was inspired by Lefebvre (2013) and the clast count method shown in Fig. 1.6d was modified from Ross and White (2006). Line count measurements were acquired using three horizontal 1 m-long lines, spaced vertically by 50 cm, to characterize fragments within an area of 1 m². Clast counts used a 1 m² net with a 10 cm mesh, yielding 100 points. For both methods, only clasts (juvenile, lithic and tuff) greater than or equal to 4 mm were measured because smaller ones were too difficult to identify in the field. In line counts, the length of the clast intersections with the measuring tape were quantified whereas for clast counts, points were counted using the net. During quantification, everything smaller than 4 mm was counted as matrix or as calcite-dominated cement. A total of 43 line count sites and 15 clast count sites were acquired at Round Butte and only five clast count sites were quantified at Twin Peaks.

1.6.1.3 Sampling strategies

One fist sized sample was taken in each major depositional unit at Round Butte, making sure that all pyroclastic lithofacies were represented, if accessible. A minimum of two samples were taken in each stratigraphic unit at Twin Peaks. These samples were used to make slabs and thin sections in the lab (Fig. 1.6e). Samples of coherent lava and dikes were also taken for geochemical analyses and petrography. A total of 44 samples (38 pyroclastic and 6 coherent) were collected at Round Butte and 28 samples (16 pyroclastic and 12 coherent) at Twin Peaks. Sample locations are shown in subsequent chapters.

1.6.1.4 Lithological description of pyroclastic rocks

After the componentry measurements and the sampling, a visual description of each major depositional unit mapped was performed in order to give a name to the lithofacies. Rocks were

named using structures, grain size and componentry. Bedding, or lack thereof, was described for each lithofacies.

To quantify the grain size of the rocks, the Fisher (1961) diagram modified by White and Houghton (2006) was used (Fig. 1.7). This implies visually estimating the proportion of blocks & bombs (size over 64 mm), lapilli (size 2-64 mm) and ash (size below 2 mm). Breccias (B) need to have over 75% blocks & bombs (B&B), tuff breccias (TB) have over 25% of blocks & bombs, lapilli tuffs (LT) have a proportion of lapilli over 25% and less than 25% blocks and bombs, and tuffs contain over 75% ash.

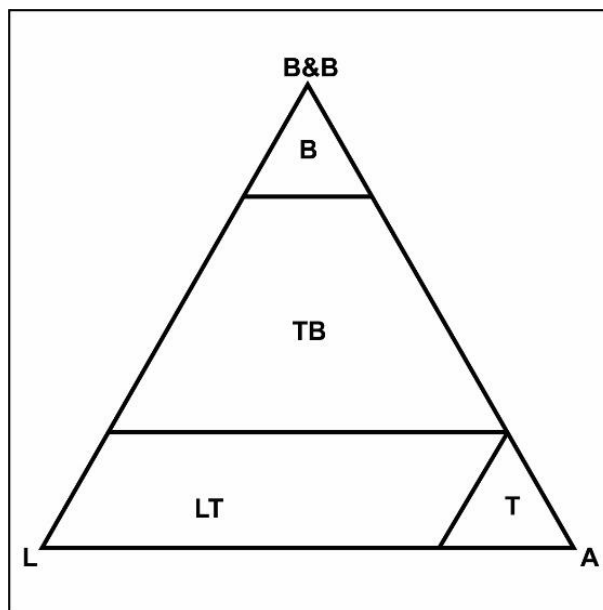


Figure 1.7: The Fisher (1961) diagram after White and Houghton (2006). On this diagram each peak of the triangle corresponds the 100% of the grain size associated. This means that in the lapilli (L) and Blocks and Bombs (B&B) axis the lapilli value vary from 100% at the L side to 0% at the B&B side. Note: B&B = Blocks and Bombs, L = Lapilli, A = Ash, B = Breccia, TB = Tuff Breccia, LT = Lapilli Tuff, T = Tuff. A lapillistone field can be added in the lower left corner of the diagram, with 75%+ lapilli in the rock.

Lithofacies were then separated, where relevant, into up to three componentry groups, namely juvenile-rich (typically rich in juvenile clasts), heterolithic (composed by a significant proportion of both lithic and juvenile clasts) and lithic-rich (typically rich in lithic clasts). Juvenile clasts were described in detail considering their shape (angular, round, irregular, amoeboid...), their color (black, grey or brown), their vesicularity, their mineralogy and their size. Lithic clasts, which come from the surrounding country rocks, were divided into their source sedimentary formations as much as possible.

At Round Butte, these descriptive steps allowed classification of each major depositional unit into the correct lithofacies, following which a final facies label was added to the cliff maps. At both volcanoes, this dataset also allows a better comparison between different lithofacies and lithofacies groups.

1.6.2 Laboratory work

1.6.2.1 Geochemical analyses of lavas

Coherent samples of Round Butte and Twin peaks (lavas and dikes) were cut with a diamond blade to remove the weathered crust and most calcite amygdules. Fresh parts of the coherent samples were sent to Activation Laboratories (Actlabs) in Ancaster, Ontario, Canada, to analyze major oxides and trace elements. Actlabs coarsely crushed the samples and then pulverized them in a mild steel shutter box following their “RX1” sample preparation protocol. The powders were mixed with a lithium metaborate and lithium tetraborate and fused by melting. The obtained melts were dissolved in a 5% nitric acid solution. Solutions containing the dissolved sample were then read on a ICP-OES for major oxides and some trace elements (Ba, Be, Sc, Sr, V and Zr) and on a ICP-MS for 39 trace elements following their “WRA+Trace 4 Lithoresearch” protocol. In total, 20 samples were analyzed (6 at Round Butte and 14 at Twin Peaks).

1.6.2.2 Petrography and point counting

During the sawing of the pyroclastic and lava samples, representative parts were taken in order to make thin sections, which were manufactured by Vancouver Petrographics (Langley, British Columbia, Canada). This yielded 38 thin sections at Round Butte and 16 at Twin Peaks. All thin sections were qualitatively described using a petrographic microscope. Then a subset were point counted to obtain the componentry of the clasts under 4 mm that were not taken into account during field line and clast counts. Fine ash was classed as ‘unresolvable’. The petrographic point count method utilized at INRS requires images. These images were first obtained by creating a mosaic of around 70 plane polarized light photomicrographs taken with a petrographic microscope at a magnification of 25x. Later this method was replaced by a single image of each thin section obtained with a “PowerSlide 5000” photographic slide scanner at an optical resolution of 5000 dpi. The point counting was then carried out using the point count tool and the recursive grid of the “JmicroVision 1.2.7” software (Roudit 2007; <https://jmicrovision.github.io/>). Several classes of clasts were defined and 450 points were

analyzed over the entire thin section. More detail about the Round Butte point counts is given in Chapters 3.

1.7 Thesis organization

This thesis is organized in five chapters corresponding to a general introduction (Chapter 1), three journal articles (Chapters 2, 3, and 4) and finally a general conclusion (Chapter 5). Chapters 2 and 4 are already published in Bulletin of Volcanology whereas Chapter 3 is ready to submit to Journal of Volcanology and Geothermal Research. Efforts were made to minimize repetition, but because all the journal articles must work independently, some parts such as the geological/regional setting and the methods are slightly repetitive between chapters. Each article has online resources due to space limitations in the journals, and these supplements are inserted at the end of the relevant chapters.

Round Butte is covered by two chapters. The general volcanology of the diatreme is first presented and the concept of the transition zone between the upper and lower diatreme is developed in Chapter 2. Then, Chapter 3 is focused on lithic clasts and lithic-rich lithologies preserved in the diatreme, and explains which diatreme emplacement processes can be reconstructed from these lithologies. At the Twin Peaks volcanic complex, presented in Chapter 4, the main interest was to understand processes that can generate a progressive change in the eruptive regime from phreatomagmatic to magmatic, in maar-diatreme settings. Finally, Chapter 5 summarizes the conclusions, makes links between the different articles and discusses the broader implications of this work on the understanding of maar-diatremes and phreatomagmatism.

1.8 Contributions of each author and participant in multi-author publications

Chapter 2 is published in Bulletin of Volcanology and is entitled “Transition zone between the upper diatreme and lower diatreme: origin and significance at Round Butte, Hopi Buttes volcanic field, Navajo Nation, Arizona”.

Chapter 3 is ready to submit to Journal of Volcanology and Geothermal Research and is entitled “What lithic clasts and lithic-rich lithofacies can tell us about diatreme processes: an example at Round Butte, Hopi Buttes volcanic field, Navajo Nation, Arizona”.

Chapter 4 is published in Bulletin of Volcanology and is entitled “Phreatomagmatic vs magmatic eruptive styles in maar-diatremes – a case study at Twin Peaks, Hopi Buttes volcanic field, Navajo Nation, Arizona”

Benjamin Latutrie (BL) and Pierre-Simon Ross (PSR) are the authors of these three research articles or chapters. BL carried out the field work with the help of Pier Paolo Comida and Romain Jattiot. BL also performed the sample preparation, the petrography and the point counting. BL compiled all relevant data and wrote several versions of the article (manuscript, figures and tables). PSR designed the study, supervised the field and lab work, and worked on several versions of the paper.

2 FIRST ARTICLE: Transition zone at Round Butte diatreme

Transition zone between the upper diatreme and lower diatreme: origin and significance at Round Butte, Hopi Buttes volcanic field, Navajo Nation, Arizona

Origine et importance de la zone de transition entre le diatrème supérieur et le diatrème inférieur à Round Butte, champ volcanique Hopi Buttes, Nation Navajo, Arizona

Authors:

Benjamin Latutrie and Pierre-Simon Ross

Institut national de la recherche scientifique, Centre Eau Terre Environnement, 490 rue de la Couronne, Québec (QC), G1K 9A9, Canada

Title of the journal:

Bulletin of volcanology

Published online: 19 March 2019

DOI: 10.1007/s00445-019-1285-x

This chapter is the preprint version of the research article:

Latutrie B, Ross P-S (2019) Transition zone between the upper diatreme and lower diatreme: origin and significance at Round Butte, Hopi Buttes volcanic field, Navajo Nation, Arizona. Bull Volcanol 81: article 26

2.1 Abstract

Round Butte is a small but complex Miocene diatreme that crops out ~190 m below the pre-eruptive surface, in the southeastern part of the Hopi Buttes volcanic field. Erosional remnants consist of a diatreme 170-190 m in diameter, of which the central 130-150 m is well-exposed in a massif featuring 20-30 m high subvertical cliffs, and a 50 cm-thick basanite dike. Field mapping allowed us to define three main groups of pyroclastic rocks in the diatreme: undisturbed beds, disturbed beds and non-bedded rocks. Pyroclastic rocks range in grain size from coarse tuff to tuff breccia and in componentry from juvenile-rich to lithic-rich, with a dominance of heterolithic lapilli tuffs. Rocks from the undisturbed bedded pyroclastic group are present above an unconformity found all around the massif, whereas the disturbed bedded and the non-bedded pyroclastic groups are always found below it. This unconformity was previously understood as the contact between the upper and the lower diatreme. The undisturbed beds above the unconformity indeed compose the upper diatreme, but the assemblage of non-bedded rocks (invasive columns) and disturbed beds (residual columns) below it is not typical of the lower diatreme. Instead, they represent a transition zone between the upper and lower diatreme. Such a transition zone also occurs in other diatremes, it is important genetically, and we propose to add it to the general model of maar-diatreme volcanoes.

2.2 Introduction

Maar-diatremes are small, dominantly phreatomagmatic volcanoes that fragment country rocks to form a funnel-shape structure called a diatreme (e.g., Lorenz 1986a; White and Ross 2011; Valentine and White 2012; Ross et al. 2017). Eruptive processes occurring in the diatreme and the underlying root zone have never been directly observed, being subterranean, but have been interpreted based on a combination of documentation of historical maar eruptions (Thomas 1888; Moore 1967; Kienle et al. 1980; Self et al. 1980; Ort et al. 2018), field work on maar ejecta ring and diatreme pyroclastic deposits and rocks (e.g., White 1991; Ross et al. 2008a; Lefebvre et al. 2013; Bélanger and Ross 2018), and experiments at various scales (Zimanowski et al. 1997; Kurszlaukis et al. 1998; Ross et al. 2008b, 2008c, 2013; Valentine et al. 2012, 2015; Taddeucci et al. 2013; Graettinger et al. 2015). Part of the complexity of diatremes comes from their formation from hundreds to thousands of explosions (Self et al. 1980; White 1991; Lorenz 2007; Valentine et al. 2014). Another complicating factor is that phreatomagmatic and magmatic vents can be active at the same time, as observed at Ukinrek east maar in 1977 (Kienle et al. 1980; Self et al. 1980; Ort et al. 2018).

Due to exposure constraints, most maar-diatreme studies focus on a specific part of the volcano, such as the ejecta ring and crater (e.g., Kienle et al. 1980; White 1991; Vazquez and Ort 2006; Ort and Carrasco-Núñez 2009; Austin-Erickson et al. 2011; Valentine et al. 2015; Graettinger 2018), the upper diatreme (e.g., White 1991; White and Ross 2011; Delpit et al. 2014), the lower diatreme (e.g., White 1991; Lefebvre et al. 2013, 2016; Bélanger and Ross 2018), or rarely, the root zone (Clement 1982; Lorenz and Kurszlaukis 2007) or the intrusive plumbing system (Re et al. 2015, 2016; Muirhead et al. 2016; Le Corvec et al. 2018). The origin of the lower diatreme is still strongly debated in the literature (see discussion in Bélanger and Ross 2018). The contact between the lower and upper diatreme is rarely exposed (Kurszlaukis et al. 2009) and has only been documented in detail at a few localities (e.g., Cathedral Cliff diatreme: Bélanger and Ross 2018). Some workers have emphasized a major contact in the diatremes they studied, with deposits above and below formed by different processes or eruptive styles, at different times, with the lower diatreme being older than the upper diatreme (e.g., Porritt et al. 2008; Gernon et al. 2008, 2013). The importance of studying the upper/lower diatreme transition, in particular its morphology, is to understand whether the upper and lower parts have a disconnected history, or if they formed simultaneously. If the upper and lower diatreme formed at least partly simultaneously, then bedded pyroclastic rocks within the upper diatreme – the origin of which is typically clearer – can be used to interpret non-bedded pyroclastic rocks of the lower diatreme.

This transition from upper to lower diatreme is exposed at Round Butte, a small Miocene diatreme in the Hopi Buttes volcanic field (HBVF), Navajo Nation, Arizona (USA). This locality has been known for several decades because of the quality of exposure and the complexity of its pyroclastic rocks (White 1991; White and Ross 2011), but no detailed study was previously conducted. In this paper, we present the results of detailed mapping of the cliffs at Round Butte. We provide new insights on the architecture of the diatreme deposits and discuss the following topics: crater excavation and infilling; the link between the upper and the lower diatreme; the formation processes of the lower diatreme; and the origin and significance of the upper/lower transition zone.

2.3 Geological setting

The HBVF is located in the south central portion of the Colorado Plateau (Williams 1936) and was active during the Miocene from 8 to 6.5 Ma (Vazquez and Ort 2006). At the time of the eruptive activity, playas and ponds occupied the region (White 1990). This water-rich

environment in the Miocene permitted magma-water interactions and produced numerous phreatomagmatic explosions (White 1991; Hooten and Ort 2002; Lefebvre et al. 2013). The four main sedimentary formations in the HBVF region are, from top to bottom, the Bidahochi Formation (Miocene), the Moenave Formation (Lower Jurassic), the Chinle Formation (Upper Triassic) and the Moenkopi Formation (Lower Triassic) (Billingsley et al. 2013). The Chinle Formation is the thickest and is divided into three members, namely the Owl Rock Member, the Petrified Forest Member and the Shinarump Member (Fig. 2.1).

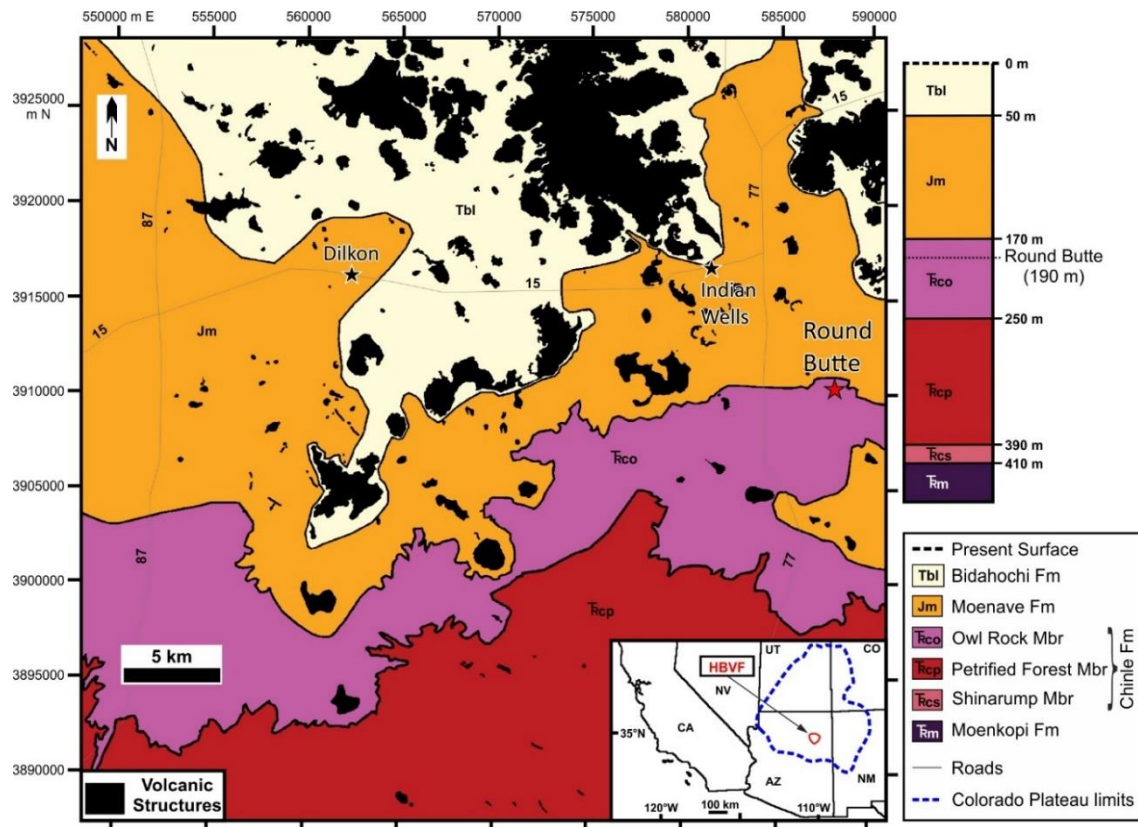


Figure 2.1: Geological map showing a portion of the Hopi Buttes volcanic field (HBVF, black) and the sedimentary formations that crop out in the region. Grid is UTM WGS 84 zone 12S. Stratigraphic column illustrates the position of the base of the cliff at Round Butte relative to the pre-eruptive surface. Inset map locates the HBVF in the SW United States. Modified from Lefebvre (2013).

The HBVF covers an area of about 2300 km² and contains more than 300 volcanic structures (Fig. 2.1, Hack 1942; White 1991). Igneous remnants are mainly maar-diatremes (e.g., Williams 1936; White 1989; 1991; Hooten 1999), dikes (Re et al. 2015; 2016; Muirhead et al. 2016; van Otterloo et al. 2018) and lava flows (Williams 1936, Vazquez 1998), but also scoria cones (Williams 1936; White 1990; Vazquez 1998). Maar-diatreme volcanoes in the HBVF are exceptionally preserved, without tectonic deformation and metamorphism (Gilbert et al. 2007). The erosion level increases from north to south, exposing progressively older Colorado Plateau

sedimentary rocks (Fig. 2.1, Billingsley et al. 2013). This corresponds to progressively deeper levels in maar-diatreme structures, making the HBVF an outstanding place for maar-diatreme studies from the ejecta ring (e.g., Teshim maar, White 1991) to the lower diatreme (e.g. Standing Rocks, Lefebvre et al. 2013; 2016). Round Butte is located in the southeastern part of the HBVF (Fig. 2.1).

2.4 Methods

One month of field work was carried out at Round Butte. We mapped the subvertical cliffs (20 to 30 m high) using nine high-resolution panoramic photographs. Their distribution is shown on the Round Butte geological map (Fig. 2.2) as figure numbers in the paper (Figs. 2.3 to 2.7) or in the Online Resource 2.1 (Figs. 2.14 to 2.17). The photographs were printed, then geological contacts were traced in the field, with the help of binoculars and cliff-base detailed observations. For each mapped unit, we obtained meter-scale observations, lithological descriptions, compositional measurements and a hand sample. Our visual descriptions took into account the semi-quantitative lithic vs juvenile clast proportions and their mean grain size (ash, fine to coarse lapilli and blocks and bombs). Pyroclastic rocks were named according to the White and Houghton (2006) nomenclature. This allowed us to associate the described unit to a facies (all facies codes in Tables 2.1, 2.2, 2.3). Based on the hand sample collection, 32 thin sections were prepared to characterize the matrix (particles smaller than 4 mm) of the pyroclastic rocks with a petrographic microscope.

Finally, for geochemical analyses, we collected five samples of juvenile blocks and bombs in different pyroclastic facies and one sample from the northwest dike. The geochemical methods and results are presented in Online Resource 2.2.

2.5 Results

The plain around Round Butte exposes Owl Rock Member sedimentary rocks ~190 m below the pre-eruptive surface (Billingsley et al. 2013). Round Butte is a diatreme 170 to 190 m in diameter at the current level of exposure, of which the central 130-150 m is well-exposed in a massif featuring 20-30 m high subvertical cliffs. The outer portion of the diatreme is very poorly to moderately well-exposed at the same elevation as the surrounding country rocks. Northwest of the diatreme is a ~90 m long coherent basanite dike, up to 50 cm thick, extending in the northwest direction (Fig. 2.2).

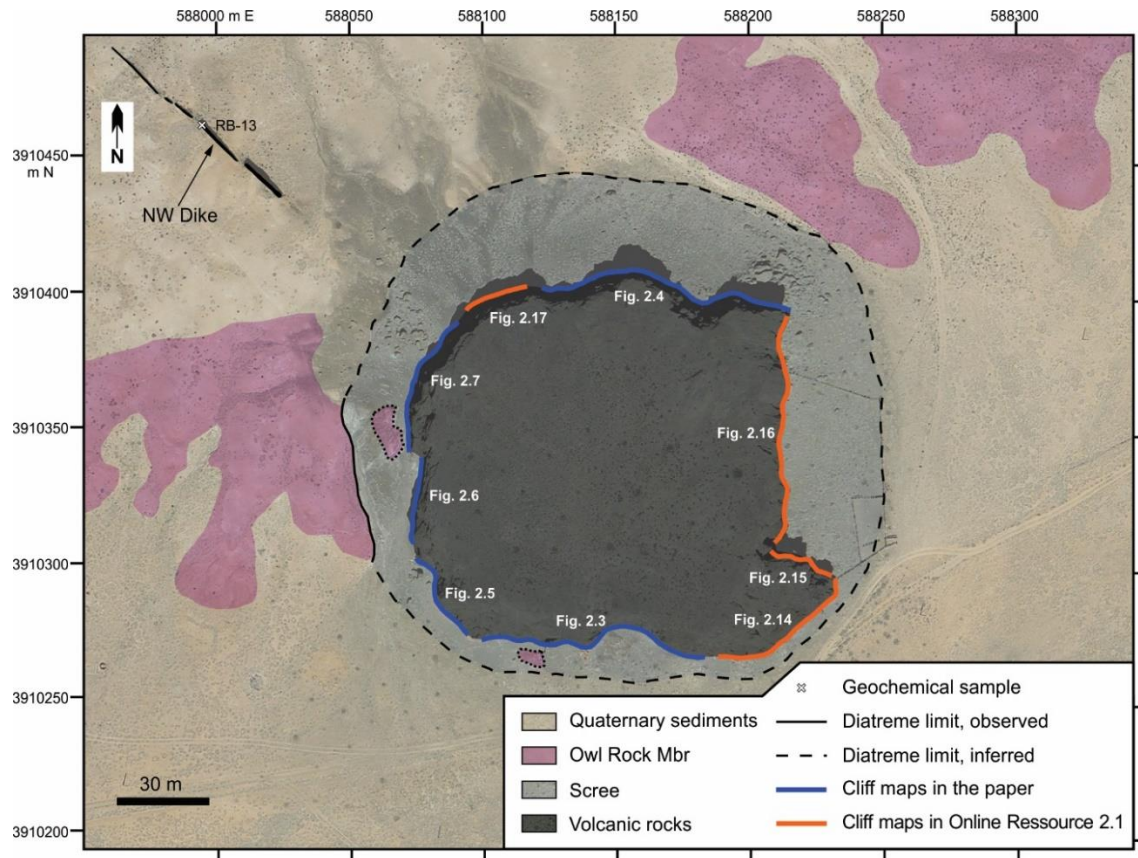


Figure 2.2: Round Butte geological map displaying the igneous remnants (diatreme and NW dike) and the location of the different panoramic photographs used for drawing cliff maps. Grid is UTM WGS 84, zone 12S.

Detailed mapping of the whole circumference of the massif is presented here (Figs. 2.3 to 2.7) and in Online Resource 2.1 (Figs. 2.14 to 2.17). Based on this mapping we have defined five groups of facies: (1) undisturbed bedded pyroclastic rocks (~25% of the total area of the panoramic photographs), (2) disturbed bedded pyroclastic rocks (~38%), (3) non-bedded pyroclastic rocks (~30%), (4) megablocks (~3%) and (5) debris avalanche deposits (~4%). The first three main facies groups make up the bulk of the exposure and we focus on those groups here; information on the megablocks and debris avalanche deposits are presented in [Chapter 3](#). An unconformity¹ clearly separates the undisturbed bedded pyroclastic group (above it) from the disturbed bedded pyroclastic group and the non-bedded pyroclastic group (below it). This unconformity can be followed all around the diatreme; it is mostly subhorizontal (Figs. 2.3, 2.4, 2.14, 2.16) but locally becomes irregular (Figs. 2.3, 2.6, 2.7).

¹ The term 'unconformity' is used here in a purely descriptive sense. There is no implication of a long pause in eruptive activity.

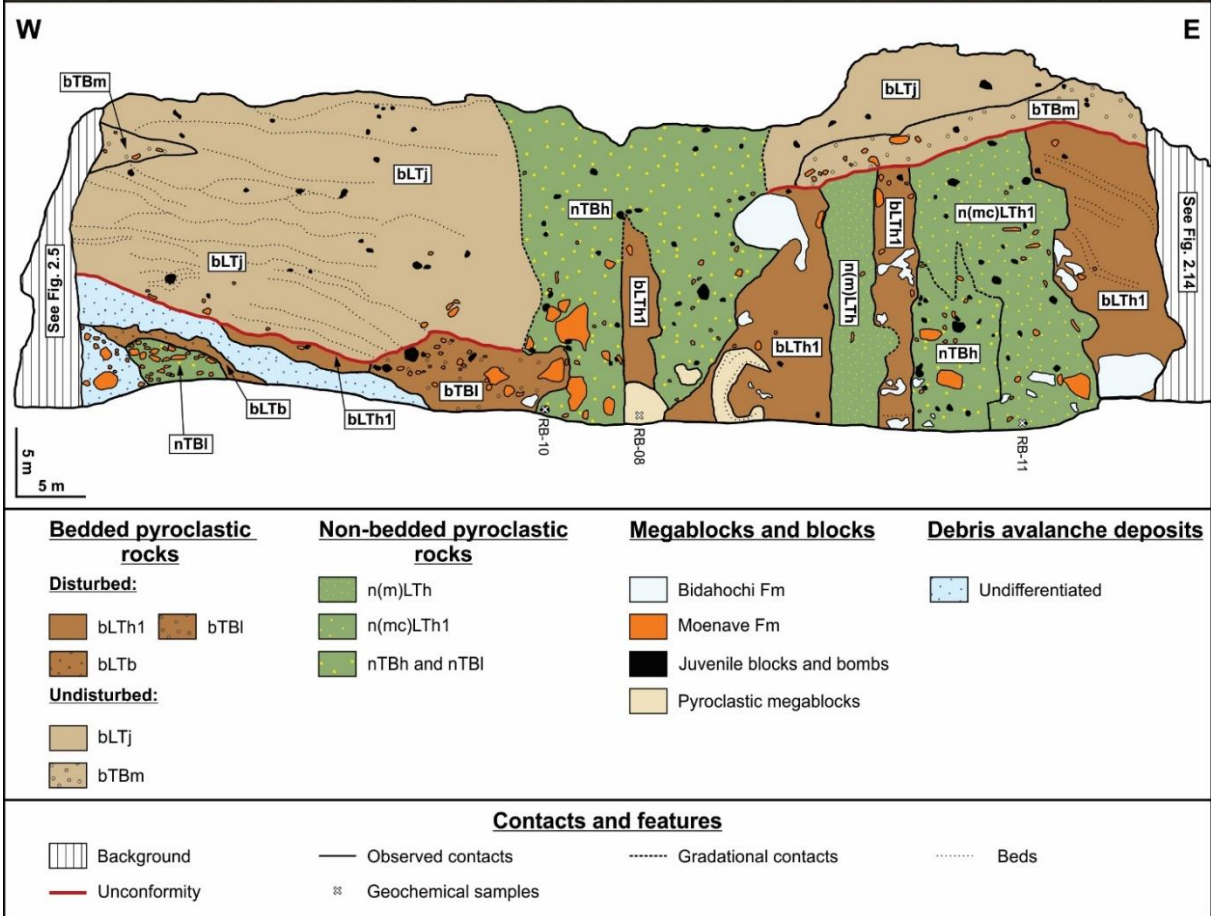


Figure 2.3: Geological map of the cliffs in the south part of Round Butte (location in Fig. 2.2) displaying the three main facies groups. Note the truncated invasive columns (non-bedded pyroclastic rocks), the unconformity, the discordant contact (onlap) between the undisturbed and the disturbed bedded group just above the bTBI facies. For facies codes, see Tables 2.1 to 2.3.

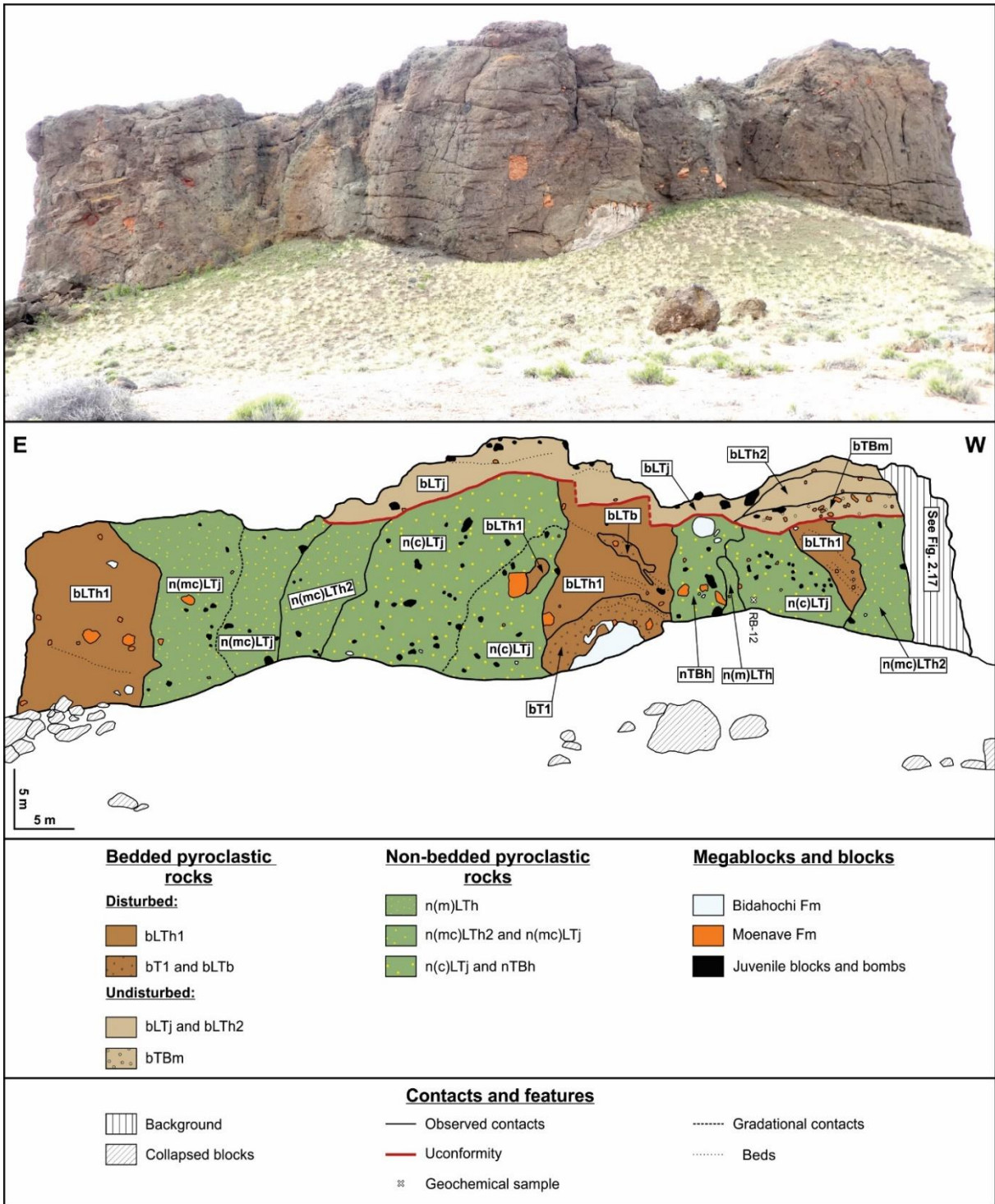


Figure 2.4: Geological map of the cliffs in the north part of Round Butte (location in Fig. 2.2) displaying the three main facies groups. Note the truncated invasive columns and the unconformity. For facies codes, see Tables 2.1 to 2.3.

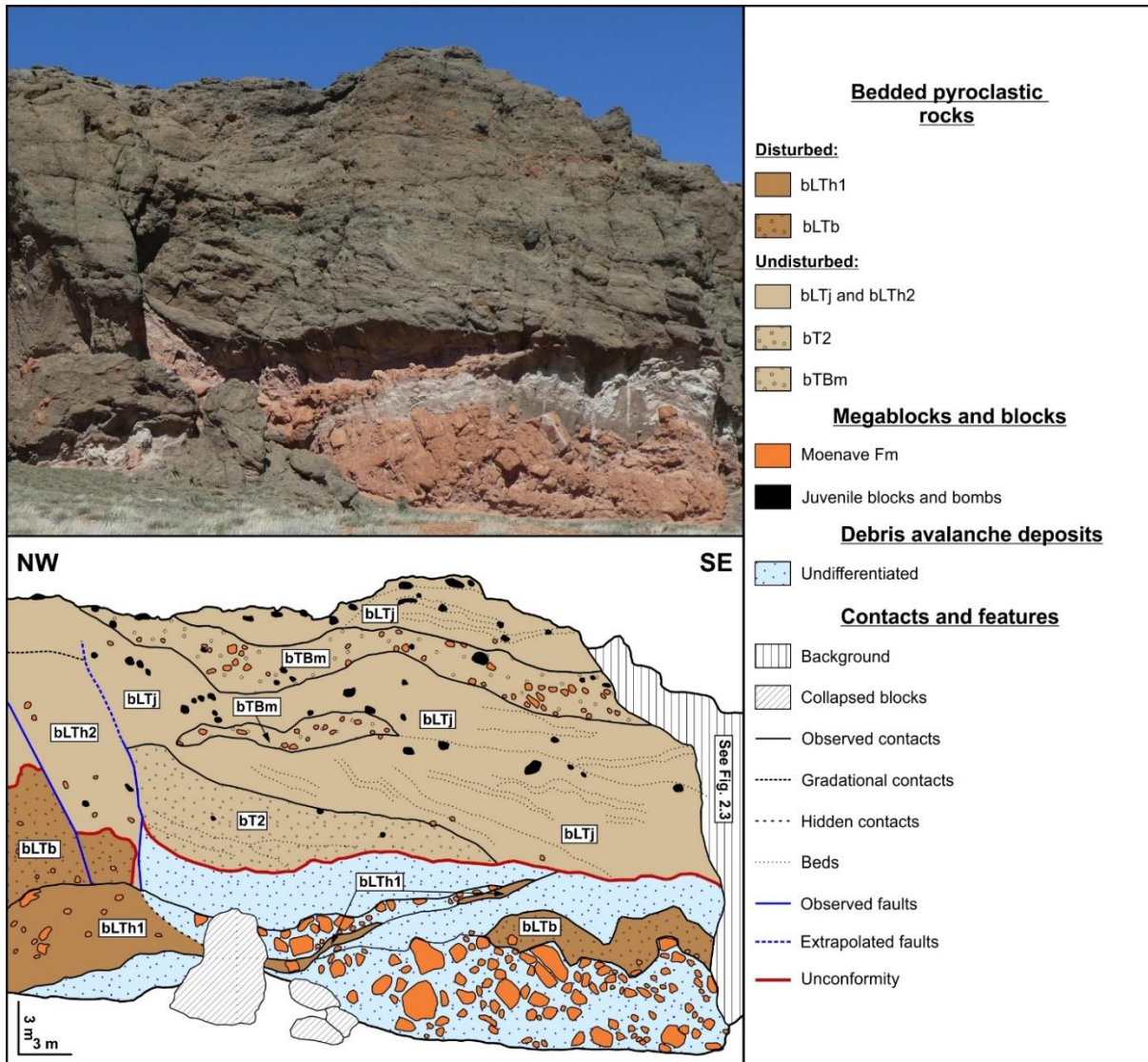


Figure 2.5: Geological map of the cliffs in the southwest part of Round Butte (location in Fig. 2.2) displaying two main facies groups. For facies codes, see Tables 2.1 and 2.2.

2.5.1 Undisturbed bedded pyroclastic rocks

The upper part of the massif typically exposes well-preserved, undisturbed bedded pyroclastic rocks. These rocks are discontinuous and display a mean thickness around 5 m (Figs. 2.3, 2.4, 2.16, 2.17). This facies group is thickest in the southwest part of the massif (10-20 m thick, Figs. 2.3, 2.5) and disappears in the northeast part (Figs. 2.4, 2.16). Five different undisturbed bedded pyroclastic facies are distinguished on the basis of their componentry, grain size and structures (facies codes in Table 2.1). All five facies form well-defined subhorizontal beds or lenses ranging in thickness from centimeters to several meters (Fig. 2.8). Grainsize is coarse tuff to tuff breccia and componentry ranges from lithic-rich to juvenile-rich.

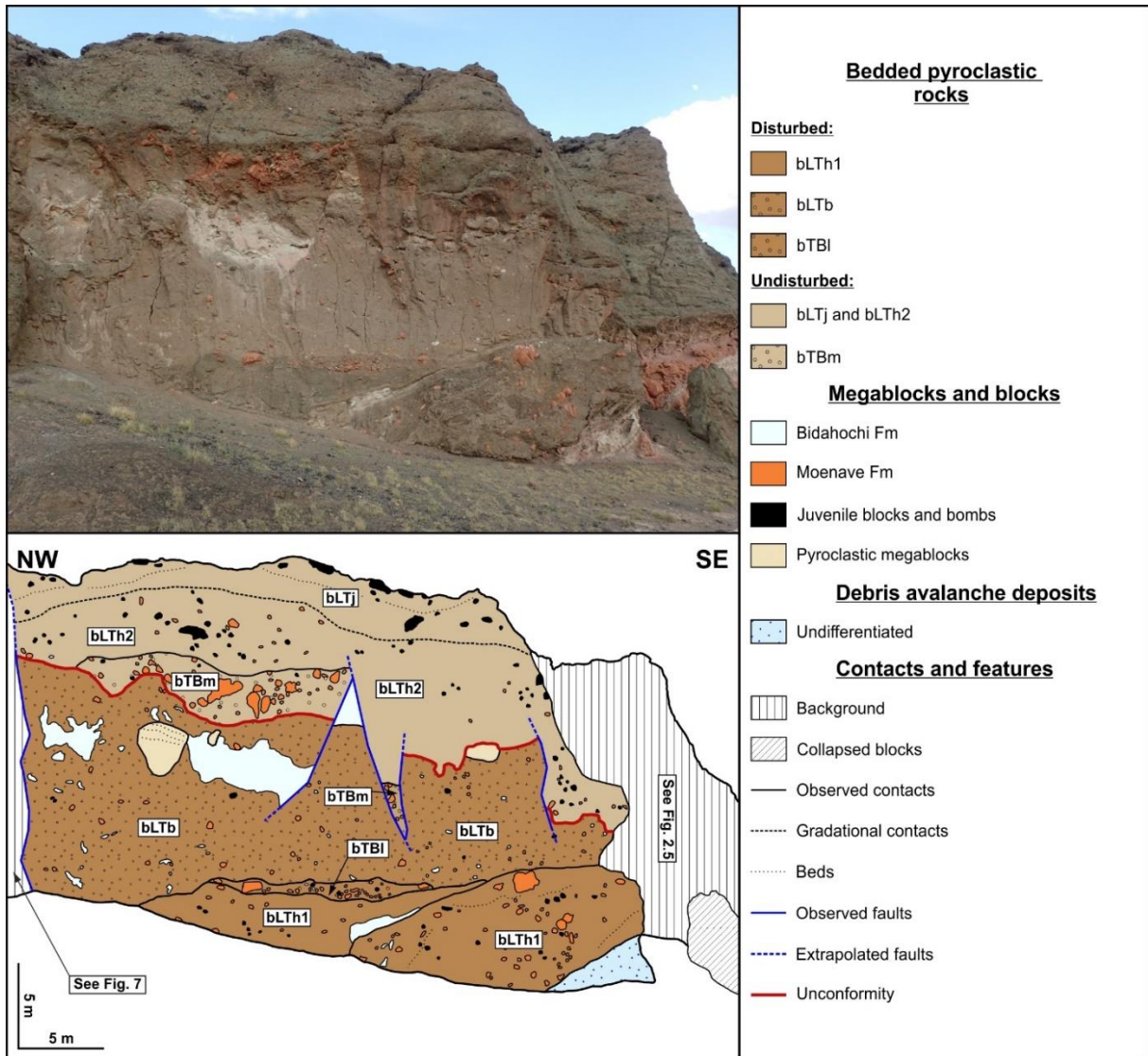


Table 2.1: Characteristics of undisturbed bedded pyroclastic rocks*

Facies code	Name	Bed thickness	Blocks and bombs	Lapilli	Ash	Cement	Comments	Panoramas (Fig. nb)
bT2	Bedded tuff to fine lapilli tuff, juvenile-rich, with thin beds	cm to dm	~0%, Juv >> Lith (Jm)	Unknown but >10%	<90%	?	Thin beds with cross-bedding, dunes and some bomb sags (Figs. 2.8a, 2.8c).	2.5, 2.7
bLTj	Bedded medium to coarse lapilli tuff, juvenile-rich	dm to m	<1%, Juv >> Lith (Jm)	Unknown but >25%	<75%	?	Contacts between beds are sometimes difficult to see. Bomb sags are locally observable. A few blocks of Moenave Fm are present (Figs. 2.8a, 2.8b).	2.3, 2.4, 2.5, 2.6, 2.7, 2.14 to 2.17
bLTh2	Bedded medium to coarse lapilli tuff, heterolithic	dm to m	3-5%, Juv > Lith (Jm > Tbl)	Unknown but >25%	<75%	?	Very diffusely bedded. Beds are mostly metric with gradational contacts and various amounts of lithics.	2.4, 2.5, 2.6, 2.7, 2.14, 2.17
bTBm	Bedded tuff breccia, Moenave-rich	m	25-35%, Lith (Jm >> Tbl) >> Juv	?	?	?	Structureless beds or lenses mainly composed of Moenave Fm blocks and some juvenile blocks/bombs. In some units, blocks of Bidahochi Fm are present (Fig. 2.8d).	2.3, 2.4, 2.5, 2.6, 2.7, 2.14, 2.17
bLS	Bedded lapillistone, juvenile-rich	m	<2%, Juv only	>75%	<25%	?	The best sorted facies in the massif, composed of coarse dark grey to black juvenile lapilli and blocks/bombs (Fig. 2.8e). Probably rich in scoria.	2.7

*Due to inaccessibility, the description of these units was done from a distance using binoculars

Juv = Juvenile clasts, Lith = Lithic clasts, Jm = Moenave Fm clasts, Tbl = Bidahochi Fm clasts

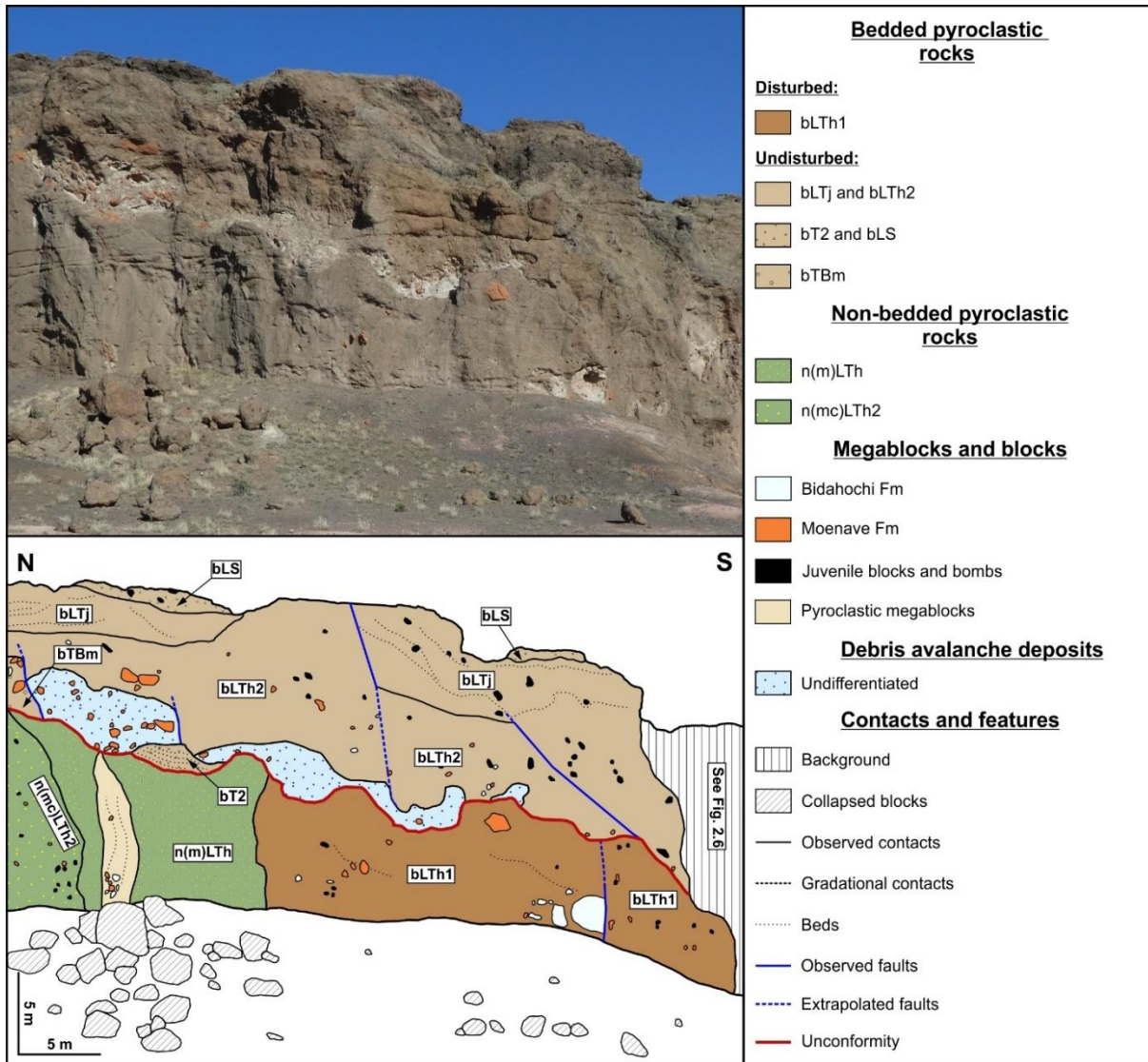


Figure 2.7: Geological map of the cliffs in the west-northwest part of Round Butte (location in Fig. 2.2) displaying the three main facies groups. Note the truncated invasive columns, the irregular unconformity, and the minor faults. For facies codes, see Tables 2.1 to 2.3.

2.5.2 Disturbed bedded pyroclastic rocks

One of the facies groups located below the unconformity consists of variably disturbed bedded pyroclastic rocks (Figs. 2.3 to 2.7 and 2.14 to 2.17). This group has a concordant contact with debris avalanche deposits (Figs. 2.3, 2.5, 2.7) and mostly subvertical contacts with non-bedded pyroclastic rocks (Figs. 2.3, 2.4, 2.7, 2.14, 2.16). Those subvertical contacts create an alternation of non-bedded pyroclastic rocks with disturbed bedded pyroclastic rocks that form column-like units. On the east side of the massif, disturbed pyroclastic rocks occupy most of the face (Fig. 2.16). In this facies group in general, the bedding is mostly diffuse to destroyed (Figs.

2.7, 2.16) but in some places it is better preserved (Figs. 2.3, 2.4, 2.6). Beds are subhorizontal (Figs. 2.3, 2.6, 2.9) to steeply dipping (Fig. 2.16), with thicknesses from centimeters to almost 10 m. The bedding is locally swirly in the pyroclastic rocks (Figs. 2.15, 2.16) and Bidahochi megablocks can also be highly deformed (Figs. 2.3, 2.9a). Flame structures are seen locally, at the bottom contact of a b(c)LTj unit (Fig. 2.14). Disturbed bedded pyroclastic rocks are composed of five different facies, ranging from lithic-rich to juvenile rich and from coarse tuff to tuff breccia (facies codes in Table 2.2).

2.5.3 Non-bedded pyroclastic rocks

Rocks of the non-bedded pyroclastic group are separated in seven different facies (facies codes in Table 2.3) and are mainly located in the bottom part of the cliffs (under the unconformity). However, in Fig. 2.3 the biggest non-bedded unit goes to the top of the outcrop. This group is mainly in contact with the disturbed bedded pyroclastic group (Figs. 2.3, 2.4, 2.7, 2.14, 2.16), and with debris avalanche deposits (Fig. 2.3, nTBI facies). The contacts between the non-bedded group and other facies are typically subvertical to steep, but locally flatten where the top of a column occurs (Fig. 2.3, nTBh column on the right side; two non-bedded columns in Fig. 2.16). The 1 to 20 m-wide, column-like units are composed by medium lapilli tuff to tuff breccia with a variable, but mainly heterolithic, componentry (Fig. 2.10).

2.5.4 Faults in pyroclastic rocks

Faults are present in the western part of the massif (Figs. 2.5, 2.6, 2.7) and are particularly visible in the undisturbed bedded group. Faults must continue below the unconformity in the disturbed bedded and non-bedded groups because those deposits are older, but we were not always able to follow them, due to a lack of clear marker beds to show offsets. These faults seem to have an arcuate 3D shape, steep dips and a normal slip component. Their orientation is difficult to evaluate, but the general impression is that the fault planes are sub-parallel to the cliffs. Most of the faults on the west side of the diatrema have a downward movement toward the southwest part of the diatrema (Figs 2.5, 2.6, 2.7). In the south face the unconformity is lower on the left side of the big nTBh column than on its right side. This could be explained by a fault with a downward movement toward the southwest part of the diatrema within this big nTBh column or within the rocks that were there before the column was emplaced (Fig. 2.3).

Table 2.2: Characteristics of disturbed bedded pyroclastic rocks

Facies code	Name	Bed thickness	Blocks and bombs	Lapilli	Ash	Cement	Comments	Panoramas (Fig. nb)
bT1	Bedded tuff to fine lapilli tuff, juvenile-rich, with thin beds	cm to dm	<1%, Lith (Jm) >> Juv	20-30%, Juv >> Lith (Jm > Tbl)	68-78%, mostly fine ash	0-1%, scattered	Thinly bedded units mostly composed of ash and fine lapilli. Juvenile bombs are more abundant than blocks. Brown juvenile clasts are difficult to distinguish from the matrix	2.4, 2.14
bLTb	Bedded fine to medium lapilli tuff, brown	dm to ~10 m	0-3%, Lith (Jm > Tbl > TRm > TRc) >> Juv	15-40%, Juv ≥ Lith (Jm ≥ Tbl > TRm > TRc)	55-85%, mostly fine ash	0-2%, scattered	Structureless, mostly composed of ash and fine to medium lapilli (Fig. 2.9a). Brown juvenile clasts are difficult to distinguish from the matrix. Presence of block-sized fragments of recycled tuff.	2.3, 2.4, 2.5, 2.6
bLTh1	Bedded medium to coarse lapilli tuff, heterolithic	m to tens of m	0-30%, Juv ≥ Lith (Jm > Tbl > TRm, TRc)	20-70%, Juv > Lith (Jm > Tbl > TRm, TRc)	20-80%, fine to coarse ash varying with beds	0-15%, scattered to patchy	Highly heterogeneous facies, mostly lapilli tuff, but local occurrence of coarse tuff and tuff breccia beds (Figs. 2.9c, 2.9d). Most of the units are richer in juvenile bombs than blocks. Brown juvenile clasts mostly in trace amounts. Presence of lapilli-sized fragments of recycled tuff.	2.3, 2.4, 2.5, 2.6, 2.7, 2.14 to 2.17
b(c)LTj	Bedded coarse lapilli tuff, juvenile-rich	m	10%, Juv >> Lith (Jm > Tbl)	60-70%, Juv >> Lith (Jm > Tbl)	19-29%, altered, mostly coarse ash	1%, scattered	Extremely altered unit with a greenish color. Rock is friable and fragments are sometime difficult to recognise. Rich in juvenile bombs.	2.14, 2.15
bTBI	Bedded tuff breccia, lithic-rich	dm to m	10-30%, Lith (Jm > Tbl > TRm, TRc) >> Juv	55-60%, Juv >> Lith (Jm > Tbl > TRm, TRc)	10-22%, mostly coarse ash	3-5%, patchy	Mostly composed of grey juvenile clasts (coarse ash to fine lapilli in size) (Fig. 2.9b). Rich in juvenile bombs. Contains traces of brown juvenile clasts.	2.3, 2.6, 2.14

Juv = Juvenile clasts, Lith = Lithic clasts, Jm = Moenave Fm clasts, Tbl = Bidahochi Fm clasts, TRc = Chinle Fm clasts, TRm = Moenkopi Fm clasts
Fine ash <250 µm, medium ash 250-500 µm and coarse ash >500 µm

Table 2.3: Characteristics of non-bedded pyroclastic rocks (invasive columns)

Facies code	Name	Column width	Blocks and bombs	Lapilli	Ash	Cement	Comments	Panoramas (Fig. n°)
n(m)LTh	Non-bedded medium lapilli tuff, heterolithic	1-10 m	0-5%, Lith > Juv to Juv > Lith (Jm ≥ Tbl > TRm)	40-55%, Juv > Lith (Jm > Tbl > TRm, TRc)	32-58%, mostly fine ash	0-10%, scattered to patchy	Mostly composed of ash and fine to medium lapilli (Fig. 2.10a). Juvenile bombs versus blocks in equal amounts. Traces of brown juvenile clasts, mainly of fine lapilli size. Some lapilli-sized recycled tuff fragments.	2.3, 2.4, 2.7
n(mc)LTh1	Non-bedded medium to coarse lapilli tuff, heterolithic	6-10 m	15-20%, Lith (Jm > Tbl) ≥ Juv	50-55%, Juv >> Lith (Jm > Tbl > TRm)	25-35%, mostly fine to medium ash	~1%, scattered	Mostly composed of medium to coarse lapilli-sized lithic and juvenile fragments. Rare recycled tuff fragments (Fig. 2.10b). Traces of brown juvenile clasts.	2.3, 2.14
n(mc)LTh2	Non-bedded medium to coarse lapilli tuff, heterolithic	4-20 m	5-10%, Juv > Lith (Jm >> Tbl, TRm, TRc)	50-70%, Juv >> Lith (Jm > Tbl, TRm, TRc)	17-40%, mostly medium to coarse ash	3-10%, scattered to patchy	Mostly composed of medium to coarse lapilli-sized lithic and juvenile fragments. Rare recycled tuff fragments (Fig. 2.10b). Traces of brown juvenile clasts. More juvenile bombs than juvenile and lithic blocks.	2.4, 2.7, 2.14, 2.16, 2.17
n(mc)LTj	Non-bedded medium to coarse lapilli tuff, juvenile-rich	3-6 m	5-10%, Juv >> Lith (Jm >> Tbl)	50-55%, Juv >> Lith (Jm > Tbl > TRm)	10-35%, mostly coarse ash	10-25%, scattered	In Fig. 2.4, unit is altered. In Fig. 2.16, unit crosscuts the entire outcrop like a vent would do it. More juvenile blocks than juvenile bombs. Traces of brown juvenile clasts.	2.4, 2.16
n(c)LTj	Non-bedded coarse lapilli tuff, juvenile-rich	5-11 m	10-20%, Juv >> Lith (Jm > Tbl > TRm)	50-70%, Juv >> Lith (Jm > Tbl > TRm, TRc)	10-30%, mostly coarse ash	10-15%, scattered	Mostly composed of dark grey to black coarse lapilli (Fig. 2.10c). More juvenile bombs than blocks; rare lithic blocks. Can be altered (e.g., Fig. 2.14). Traces of brown juvenile clasts.	2.4, 2.14, 2.17
nTBI	Non-bedded, tuff breccia, lithic-rich	~6 m	<50%, Lith (Jm >> TRc > TRm) >>> Juv	~30%, Juv = Lith (Jm > TRm > TRc)	~20%, reddish, Moenave-rich, mostly coarse ash	0%	Only one unit, extremely rich in Moenave Formation clasts (Fig. 2.10d). Chinle and Moenkopi clasts are represented whereas Bidahochi clasts are completely absent.	2.3
nTBh	Non-bedded, tuff breccia to coarse lapilli tuff, heterolithic	4-17 m	15-30%, Juv ≥ Lith (Jm > Tbl > TRm)	50-60%, Juv > Lith (Jm > Tbl > TRm > TRc)	8-28%, mostly coarse ash	5-10%, scattered to patchy	Mainly composed of coarse lapilli-sized lithic, juvenile and tuff fragments (Figs. 2.10e, 2.10f). More juvenile bombs than blocks. Great diversity of lithics and traces of brown juvenile clasts.	2.3, 2.4, 2.14

Juv = Juvenile clasts, Lith = Lithic clasts, Jm = Moenave Fm clasts, Tbl = Bidahochi Fm clasts, TRc = Chinle Fm clasts, TRm = Moenkopi Fm clasts
Fine ash <250 µm, medium ash 250-500 µm and coarse ash >500 µm

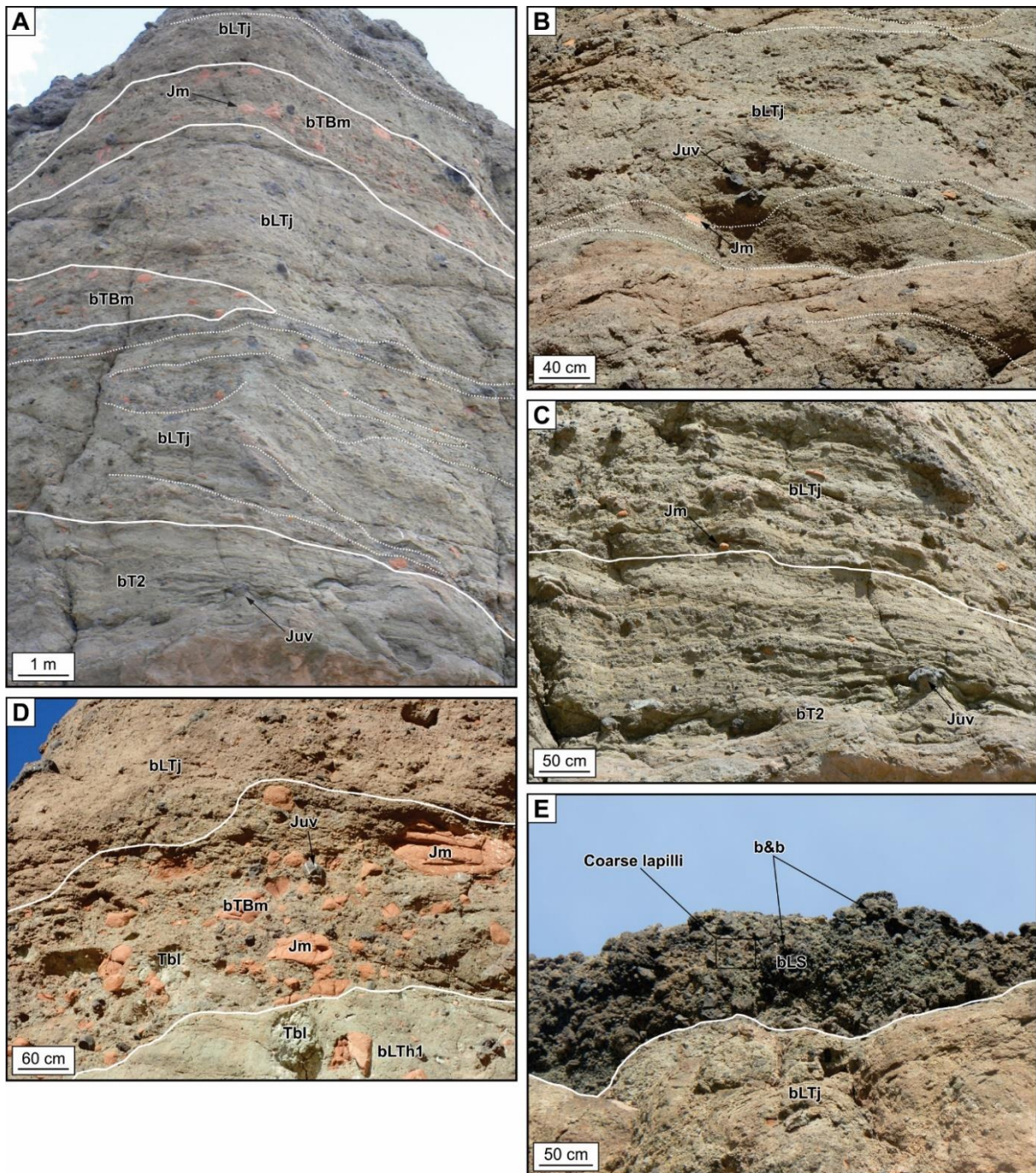


Figure 2.8: Photo plate of the principal facies of the undisturbed bedded pyroclastic rocks. A) General view of the thickest portion of the undisturbed bedded group in the southwest part of Round Butte diatreme, displaying organization of the bLTj, bT2 and bTBm facies. B) Close-up view of the diffusely bedded bLTj facies. C) Close up view of the thinly bedded bT2 facies, here overlain by bLTj. D) Close-up of a thick bed of bTBm facies displaying a high content of Moenave blocks. E) bLS facies mostly contains dark grey to black coarse lapilli. Abbreviations: Tbl=Bidahochi clasts, Jm=Moenave clasts, Juv=Juvenile clasts and b&b=blocks and bombs; facies codes see Tables 2.1 and 2.2.

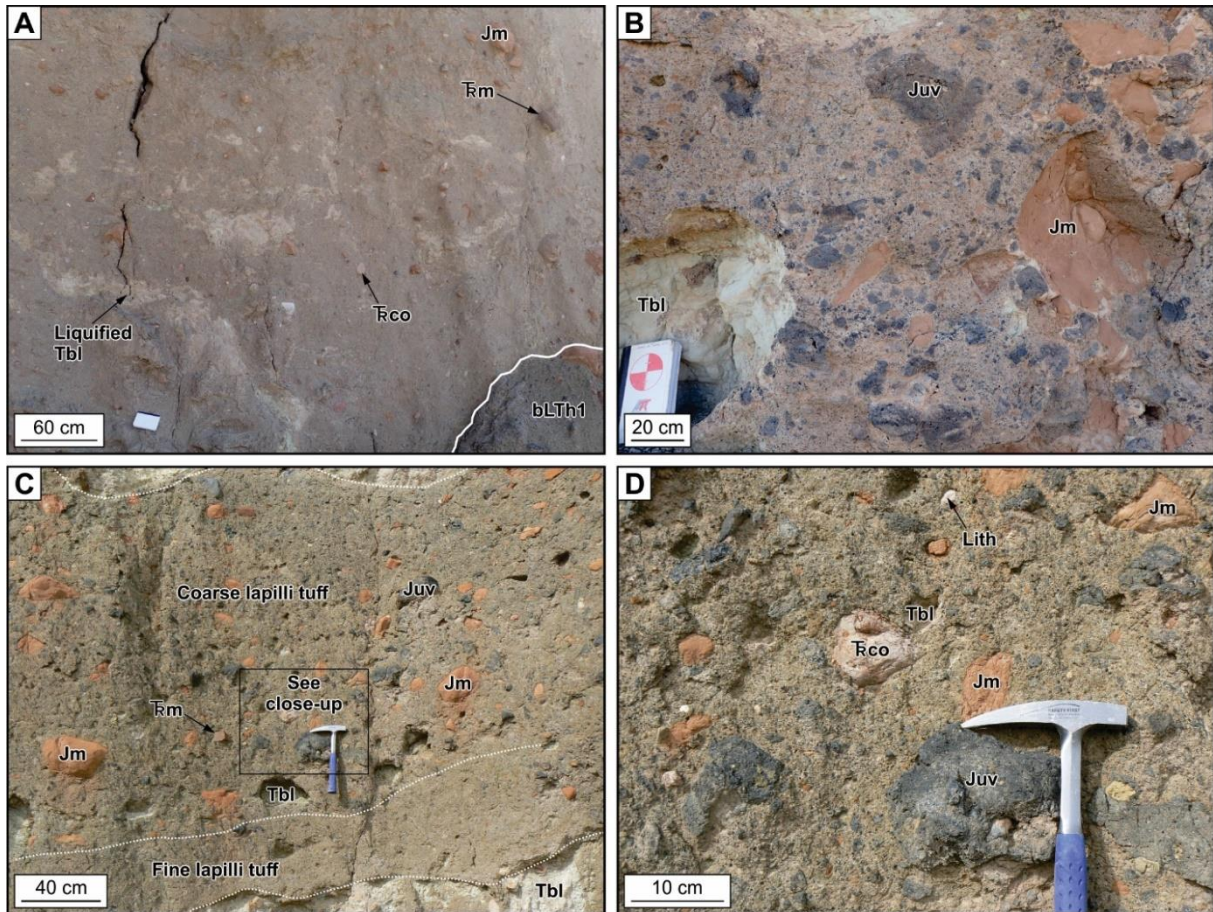


Figure 2.9: Photo plate of the principal facies of the disturbed bedded pyroclastic rocks. A) Structureless thick bed (~10 m thick) of the bLTb facies, displaying various lithic clasts including liquefied Bidahochi clasts, and a recycled tuff fragment. B) Lithic-rich bTbI facies, with Moenave and Bidahochi clasts and some juvenile blocks. C) Main disturbed facies bLTh1, with subhorizontal beds between to blocks of Bidahochi Formation. D) Close-up of bLTh1 facies with a great diversity of lithic clasts. Abbreviations: Tbl=Bidahochi clasts, Jm=Moenave clasts, Trco=Owl Rock clasts, Trm=Moenkopi clasts and Juv=Juvenile clasts; facies codes see Table 2.2.

2.5.5 Juvenile clasts

In the field, we defined three main families of juvenile clasts based on their color: (1) brown, (2) light grey, and (3) medium grey to black. Brown juvenile clasts are smaller on average (ash to <1 cm), appear less abundant than other types in the field, and have angular to sub-rounded shapes (Figs. 2.11a, 2.11b, 2.11c). Light grey juvenile clasts are slightly bigger than the brown ones, ranging in size from coarse ash to several cm and rarely to block/bomb sizes. They display angular to sub-round shapes and are often friable due to alteration. Medium grey to black juvenile fragments reach larger sizes (up to ~2 m) and have mainly sub-rounded to amoeboid, to locally angular, shapes (Figs. 2.11a, 2.11b, 2.11c).

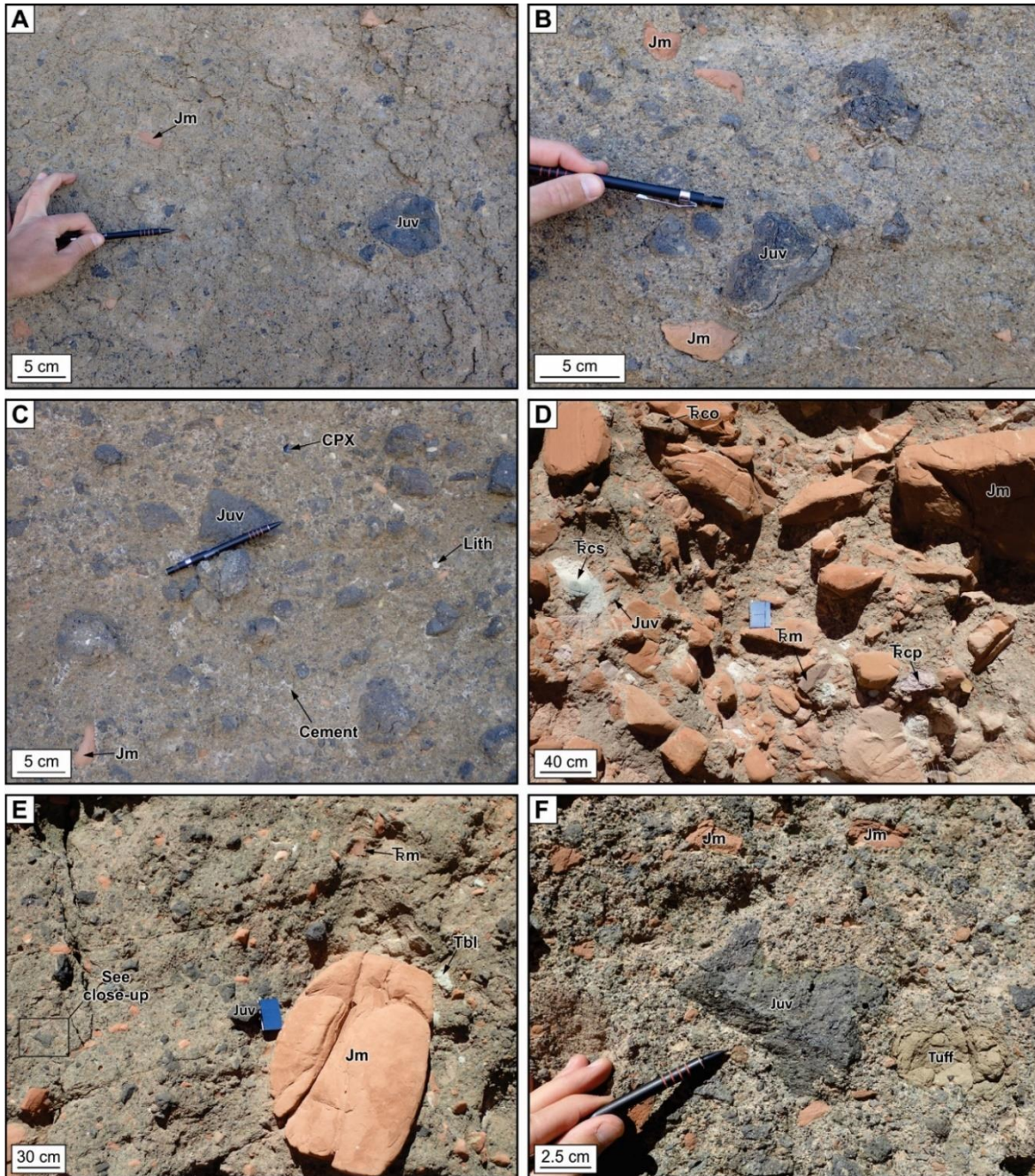


Figure 2.10: Photo plate of the principal facies of the non-bedded pyroclastic rocks. A) n(m)LTh corresponds to the finer non-bedded facies. B) Close-up view of n(mc)LTh2. C) The coarse facies n(c)LTj, rich in dark grey to black juvenile coarse lapilli. D) The coarser facies in the massif, nTBl, mainly composed of a great diversity of lithics principally represented by Moenave blocks. E) The coarse nTBh facies with a relatively high lithic content between juvenile clasts. F) Close-up of the nTBh facies. Abbreviations: Tbl=Bidahochi clasts, Jm=Moenave clasts, Trco=Owl Rock clasts, Trcp=Petrified Forest clasts, Trcs=Shinarump clasts, Trm=Moenkopi clasts, Juv=Juvenile clasts, Lith= undifferentiated lithic clasts and CPX=free clinopyroxene; facies codes see Table 2.3.

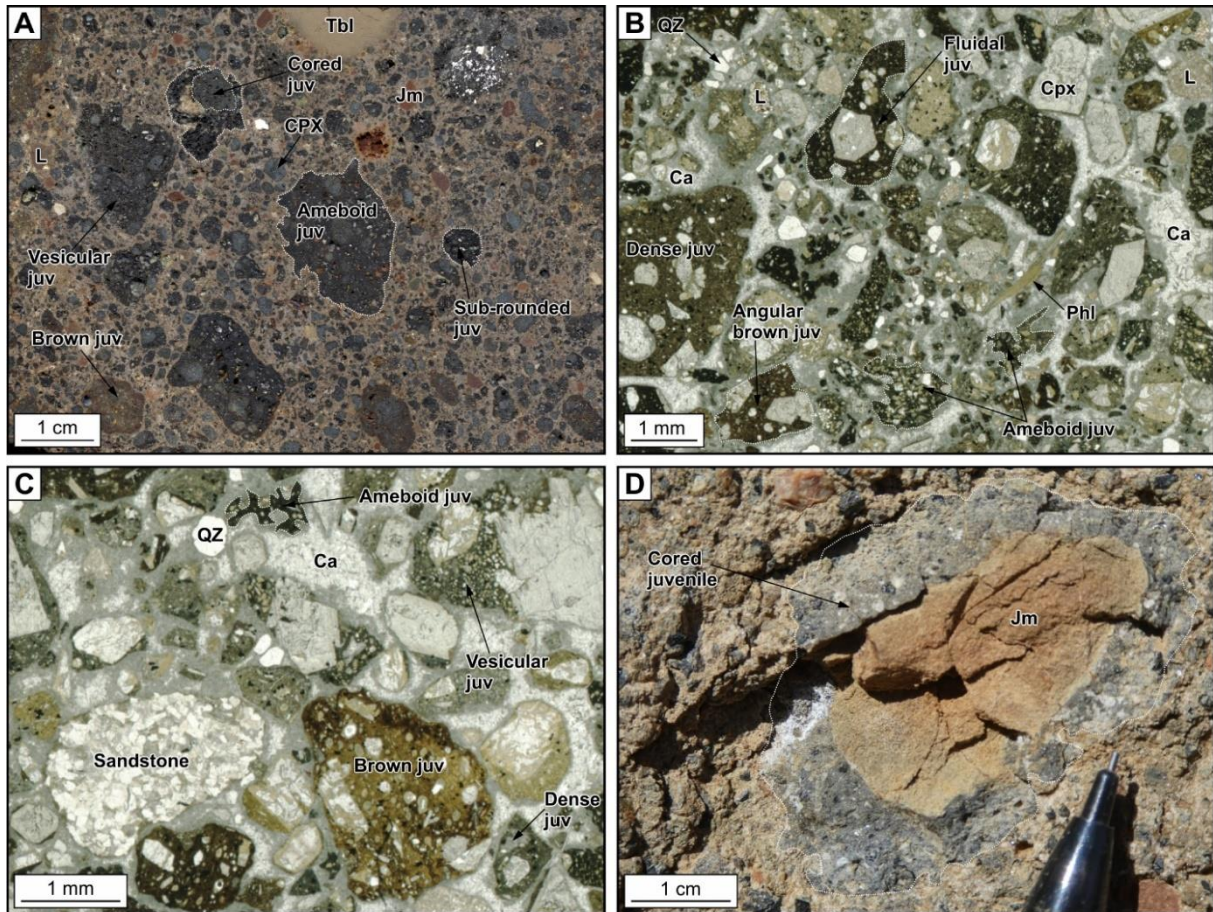


Figure 2.11: Photo plate showing the diversity and the morphology of juvenile clasts. A) Slab of bLTh1 facies highlighting the diversity of lithics and the morphology (amoeboid to sub-rounded) of juvenile clasts (brown and grey). The cored juvenile fragment evidences recycling processes in the diatreme. B) and C) thin section scans of facies bLTh1, highlighting the variability of the morphology of juvenile clasts in thin section. D) Moenave cored bomb. Abbreviations: Tbi=Bidahochi clasts, Jm=Moenave clasts, Trm=Moenkopi clasts, Juv=Juvenile clasts, L=Lithic clasts, CPX=free clinopyroxene, Phl = phlogopite and Ca=Calcite cement; facies codes see Tables 2.1.

Under the microscope, juvenile clasts of all families contain 10-15% of 0.5-5 mm phenocrysts of euhedral clinopyroxene, traces of euhedral to slightly resorbed phlogopite up to 1 cm across and traces of euhedral olivine, 0.5-3 mm across, now slightly to highly serpentinized. The groundmass is mainly composed of clinopyroxene microlites and microphenocrysts, plus “glass”. This “glass” component ranges from tachylite in the medium grey to black family to former sideromelane, now altered to palagonite and clays, in the brown family. Clasts of all families are non-vesicular to moderately vesicular according to the Houghton and Wilson (1989) scheme, with a vesicularity ranging from 0% to 60% overall, although most clasts have 15-25% vesicles (Figs. 2.11a, 2.11b, 2.11c). Vesicles are round to elongate and often filled with calcite or zeolites. Evidence of recycling is recorded in cored and loaded clasts (Figs. 2.11a, 2.11d; Lefebvre et al. 2013). Free fragmented crystals of clinopyroxene, phlogopite and rare

serpentinized olivine appear in the massif as juvenile components with the same size and morphology as described within the juvenile fragments (Figs. 2.11a, 2.11b).

2.6 Interpretation: origin of Round Butte Rocks and features

2.6.1 A maar-diatreme volcano

We interpret the Round Butte exposures as representing the diatreme portion of a small maar-diatreme volcano (Lorenz 1986a; White 1991; White and Ross 2011; Valentine and White 2012; Lefebvre et al. 2013, 2016) based on the following evidence:

- At the current level of exposure, the pyroclastic rocks are surrounded by older sedimentary country rocks (Owl Rock Member, ~190 m below the pre-eruptive surface);
- The mapped pyroclastic rocks form an elliptical body in map view (Fig. 2.2);
- The pyroclastic rocks have some features typical of phreatomagmatic diatremes elsewhere (e.g., White 1991; Lefebvre et al. 2013; Bélanger and Ross 2018): surge deposits (e.g., facies bT2), cross-cutting subvertical columns of non-bedded pyroclastic rocks, presence of megablocks from the host sedimentary rocks and megablocks of pyroclastic rocks, and for many pyroclastic rocks, poor sorting and a high lithic content;
- Several maar ejecta rings and maar crater infills are documented further north in the HBVF (White 1991; Lefebvre et al. 2013, 2016).

The current outcrop at Round Butte contains significant proportions of both bedded pyroclastic rocks (undisturbed + disturbed = 63%) and non-bedded pyroclastic rocks (30%) and has been previously interpreted as featuring the contact between the upper diatreme and the lower diatreme (White 1991; White and Ross 2011).

2.6.2 Formation of juvenile clasts

Juvenile clasts formed when a rising basanite intrusion was fragmented, both in the country rocks and in the evolving diatreme (Fig. 2.18). The NW dike (Fig. 2.2) may be an unfragmented expression of this feeder intrusion, based on geochemistry (Online Resource 2.2, Fig. 2.20). In the field and hand samples, we found three families of juvenile clasts in the diatreme, namely brown, light grey, and medium grey to black ones. Under the microscope, all three families share the same phenocrysts, microlites and range of vesicularities, strongly suggesting that they were derived from the same parental magma. Where they differ is in the character of their groundmass. The macroscopically brown clasts contain palagonitized sideromelane whereas

the macroscopically medium grey to black ones contain tachylite. The light grey juvenile clasts are also palagonitized, but may have consisted of material transitional between sideromelane and tachylite before alteration (e.g., Furnes 1975; Stroncik and Schmincke 2002). Brown and light grey juvenile fragments are less abundant overall, smaller on average, and more frequently have an angular shape, compared to the medium grey to black ones. Rapid magma cooling, probably in the presence of water, produced sideromelane, and slower cooling produced tachylite (Fisher and Schmincke 1984; White and Houghton 2015).

2.6.3 Syn-eruptive faults and subsidence

Faults have been observed within other diatremes and feature prominently in the Lorenz (1986a) model. These faults are restricted to the diatreme, i.e. they do not affect the country rocks outside the diatreme. The syn-eruptive timing of at least some of the faults at Round Butte is illustrated on Fig. 2.6, where the final bLTj unit is not affected, in contrast to the underlying beds which have sudden lateral thickness changes. Most of the faults have a downward movement toward the southwest part of the diatreme. This points to an area of maximum downward movement in the SW portion of the diatreme, where the infill of the undisturbed bedded group is also the thickest. Our preferred interpretation for these faults is that explosions in the southwest part of the diatreme sent material upwards. Some fell back into the crater, and some was expelled towards the ejecta ring. This removal of material from the diatreme allowed the remaining and newly deposited material to subside, by a few meters, in an asymmetric way. Some of these explosions would have formed the wide unit from the nTBh facies on the south face (Fig. 2.3).

The small syn-eruptive faults represent a minor form of subsidence. Beyond that, there is no evidence of a *large* amount of subsidence, such as saucer-shaped beds, in the undisturbed bedded group. However, the relatively coarse-grained nature of the lithofacies, and the large thickness of some beds, would make saucer-shaped bedding more difficult to identify compared to what is the case at some other diatremes (Delpit et al. 2014; Bélanger and Ross 2018).

2.6.4 Undisturbed bedded pyroclastic rocks

The undisturbed bedded pyroclastic group is composed of five facies and represents 25% of the exposure at Round Butte (Table 2.1). These rocks always occur *above* the unconformity and are thought to have been emplaced late in the eruptive history of the volcano. Depending on the facies, the subhorizontal beds are centimeters to several meters in thickness. Such bedded

deposits are typical of the upper diatreme (White 1991; White and Ross 2011). We consider that these rocks were emplaced more or less where we see them today, at a depth of <170 m below the pre-eruptive surface, because no strong evidence of subsidence is observable at Round Butte.

The numerous beds in the undisturbed bedded group imply multiple explosions. The main facies in terms of area exposed consist of lapilli tuff to tuff breccia (bLTj, bLTh2 and bTBm), interbedded with minor thin-bedded coarse tuff to fine lapilli tuff (bT2, Figs. 2.8a, 2.8c), and one unit of lapillistone (bLS, Fig. 2.8e). Componentry in the undisturbed bedded group is mainly juvenile-rich to heterolithic, with local Moenave-rich lenses or thick beds (bTBm, Figs. 2.5, 2.8a, 2.8d). We interpret all the facies in the undisturbed bedded group as phreatomagmatic, except for bLS.

The bT2 facies is thinly bedded and characterised by alternating finer and coarser layers with local low angle cross-bedding and dunes (Figs. 2.4, 2.8a, 2.8c). This facies is interpreted as pyroclastic surge deposits (Sohn and Chough 1989; White and Ross 2011). Deposits with bT2-like characteristics are typical of the medial parts of maar ejecta rings (e.g., White 1991; Sohn 1996; Vazquez and Ort 2006) but are also sometimes encountered in the upper parts of diatremes, where the crater is large enough to allow laterally moving currents (e.g., White and Ross 2011; Delpit et al. 2014; Bélanger and Ross 2018). Since the Round Butte crater was rather narrow (~180 m in diameter at ~190 m in depth), the bT2 facies in the SW corner of the massif may originate from explosions on the opposite side of the crater. Phreatomagmatic fallout deposits may also be present within this facies.

The main undisturbed bedded facies (bLTj) is coarser grained than bT2 and the beds are thicker, more diffuse and sometimes lenticular in shape (Figs. 2.3, 2.8a). Bomb sags are locally observed. These features suggest proximal deposits of pyroclastic density currents (PDCs), fallback (Ross et al. 2013) or proximal fallout. On the south face of Round Butte, bLTj has a gradational lateral transition into non-bedded rocks of the nTBh facies (Fig. 2.3), suggesting that the later unit may represent one of the vents for the bLTj facies.

The bLTh2 and bTBm facies are internally structureless to very diffusely bedded. They form lenses or thick beds. We interpret these two facies as very proximal deposits from PDCs or as fallback deposits. The bTBm facies presents an enrichment in Moenave blocks that fell from the crater walls during explosive activity.

The least abundant facies of this group (bLS) is preserved at the top of the massif in the western portion (Fig. 2.7). This facies is the best sorted of the massif, the least rich in ash (<25%) and is composed of lapilli and blocks/bombs of dark grey to black juvenile clasts. It seems to be rich in scoria but because of its high position in the outcrop, we were unable to quantify clast proportions. To produce coarse clasts and less ash, fragmentation needs to be less efficient than for the rest of the bedded facies. We infer a magmatic fragmentation similar to a strombolian style, or a very weak magma-water interaction, to produce this facies (Ripepe et al. 2008).

2.6.5 Disturbed bedded pyroclastic rocks

Rocks of the disturbed bedded pyroclastic group cover 38% of the exposure at Round Butte. They are similar to those of the undisturbed bedded group in terms of grain size and componentry, but they display various degrees of deformation and disturbance, and they occur *below* the unconformity. This group is composed of five different facies with one dominant facies (bLTh1) and four minor ones (Table 2.2). All of these facies are interpreted as phreatomagmatic.

Because bLTh1 deposits are still bedded, or were originally bedded, we interpret them as emplaced on the bottom of the syn-eruptive crater. Upon deposition, they were likely similar in aspect to those of the better-preserved bLTj (from the undisturbed bedded pyroclastic group). This suggests that the same volcanic processes (PDCs, fallout and fallback) were responsible for initial deposition of the bLTh1 facies. The bT1 facies found locally on the north side of the massif (Fig. 2.4) still presents primary features (bedding and grain size) that are comparable to those described for undisturbed bT2 facies, meaning they share a common origin.

The thickest bed of the massif (~10 m) is internally structureless and corresponds to the bLTb facies (Fig. 2.6). Its origin is not clear. The bTbI facies is the disturbed equivalent of bTBm facies (from the undisturbed bedded pyroclastic group). It forms small domains or lenses rich in Bidahochi and Moenave blocks that fell inside the crater during activity (Figs. 2.3, 2.14). Rare Owl Rock and Moenkopi blocks are present. The b(c)LTj facies is only found on the SE side of the massif, it forms a thick bed that grades laterally into a non-bedded column with the same componentry (Fig. 2.14, n(c)LTj facies). We assume that the bed is the erupted (fallback) equivalent to the column, which itself was formed by one or several juvenile-rich debris jet(s).

The bedding disturbance (in the disturbed bedded pyroclastic group) is likely due to a range of processes:

- syn-eruptive subsidence might have played a role (e.g., Delpit et al. 2014; Bélanger and Ross 2018), although there is no strong evidence for it, apart from the normal faults on the west side;
- liquefaction is manifested in the flame structures seen on the southeast side of the diatreme (bottom contact of b(c)LTj, Fig. 2.14), and perhaps in the swirly beds and Bidahochi megablocks seen in various places (Figs. 2.3, 2.9a, 2.16); such features are absent from the undisturbed bedded group, suggesting that liquefaction in the disturbed bedded pyroclastic group occurred during the eruption;
- debris jets due to phreatomagmatic explosions in the diatreme (White 1991; White and McClintock 2001; Ross and White 2006; Ross et al. 2008b, 2008c; Lefebvre et al. 2013) emplaced the non-bedded invasive columns and disturbed the surrounding host, forming residual columns.

Debris jets are thought to be the most important process to explain the bedding disturbance. With periodic injections of debris jets, the host bedded pyroclastic deposits got more and more disturbed until the bedding was largely destroyed within what became residual columns. The disturbed bedded pyroclastic rocks are genetically transitional between the undisturbed bedded pyroclastic rocks and the non-bedded pyroclastic rocks. They are conceptually analogous to the “broken beds” described at Cathedral Cliff by Bélanger and Ross (2018), although the coarser grained, perhaps less cohesive nature of the bedded pyroclastic rocks at Round Butte means that the “broken” aspect is much less visible (but see Fig. 2.16).

2.6.6 Non-bedded pyroclastic rocks

Non-bedded pyroclastic rocks are well represented at Round Butte, with 30% of the total exposed area of the massif. They are separated into seven facies (Table 2.3). Non-bedded facies are coarser on average than those of the undisturbed and disturbed bedded groups, with grain sizes ranging from medium lapilli tuff to tuff breccia. Componentry is mainly heterolithic and quite similar to the two other groups overall, with juvenile-rich to lithic-rich units. Non-bedded pyroclastic rocks seem richer in juvenile clasts than the other facies groups.

We consider that non-bedded pyroclastic columns are formed from the passage of debris jets, so we call the deposits “invasive columns”. The pulsating activity of maar-diatreme volcanoes is related to a multitude of subterranean phreatomagmatic explosions (e.g., White 1991; White and Ross 2011; Lefebvre et al. 2013; Bélanger and Ross 2018). Explosions can occur everywhere inside the diatreme (White and Ross 2011; Valentine et al. 2014) generating

upward moving jets composed of pyroclasts (juvenile and lithic), gas and perhaps liquid water (Ross and White 2006). Debris jets can reach the surface to generate a plume or eruptive jet that rises above the crater, but some debris jets remain confined inside the diatreme (Ross et al. 2008b, 2008c), meaning that the top of the invasive column will be visible (e.g., Fig. 2.3, nTBh invasive column on the right side; see also Fig. 2.16).

Very wide non-bedded units, from the nTBh facies (Fig. 2.3), the n(c)LTj facies (Fig. 2.4) and the n(mc)LTh2 facies (Fig. 2.17), are thought to be composite and formed by many debris jets of similar componentries, along with total destruction and homogenization of formerly bedded pyroclastic material. Some of the material involved in the debris jets would be newly generated fragments (mostly juvenile ones from the fragmenting intrusion), but a significant portion of each debris jet will consist of pre-existing diatreme infill. Therefore, debris jets are an efficient mechanism to disturb and homogenise bedded deposits to progressively form non-bedded deposits that compose the lower diatreme (Bélanger and Ross 2018).

2.6.7 The unconformity: morphology and origin

The unconformity seen all around the diatreme is an important component of its architecture. In some places, the unconformity truncates the top of invasive columns (Figs. 2.3, 2.7, 2.14), showing that it formed during a period of crater excavation, at a time when the diatreme was already filled by disturbed bedded pyroclastic deposits and non-bedded pyroclastic deposits. Therefore, this unconformity corresponds to one of the crater floor positions during Round Butte activity.

2.7 Round Butte evolution model

We present in Fig. 2.12 our model showing the evolution of the diatreme, drawn in such a way that the final cartoon looks like the south face of Round Butte (Fig. 2.3), since that face displays all five facies groups, including the three main facies groups which are the focus of this paper.

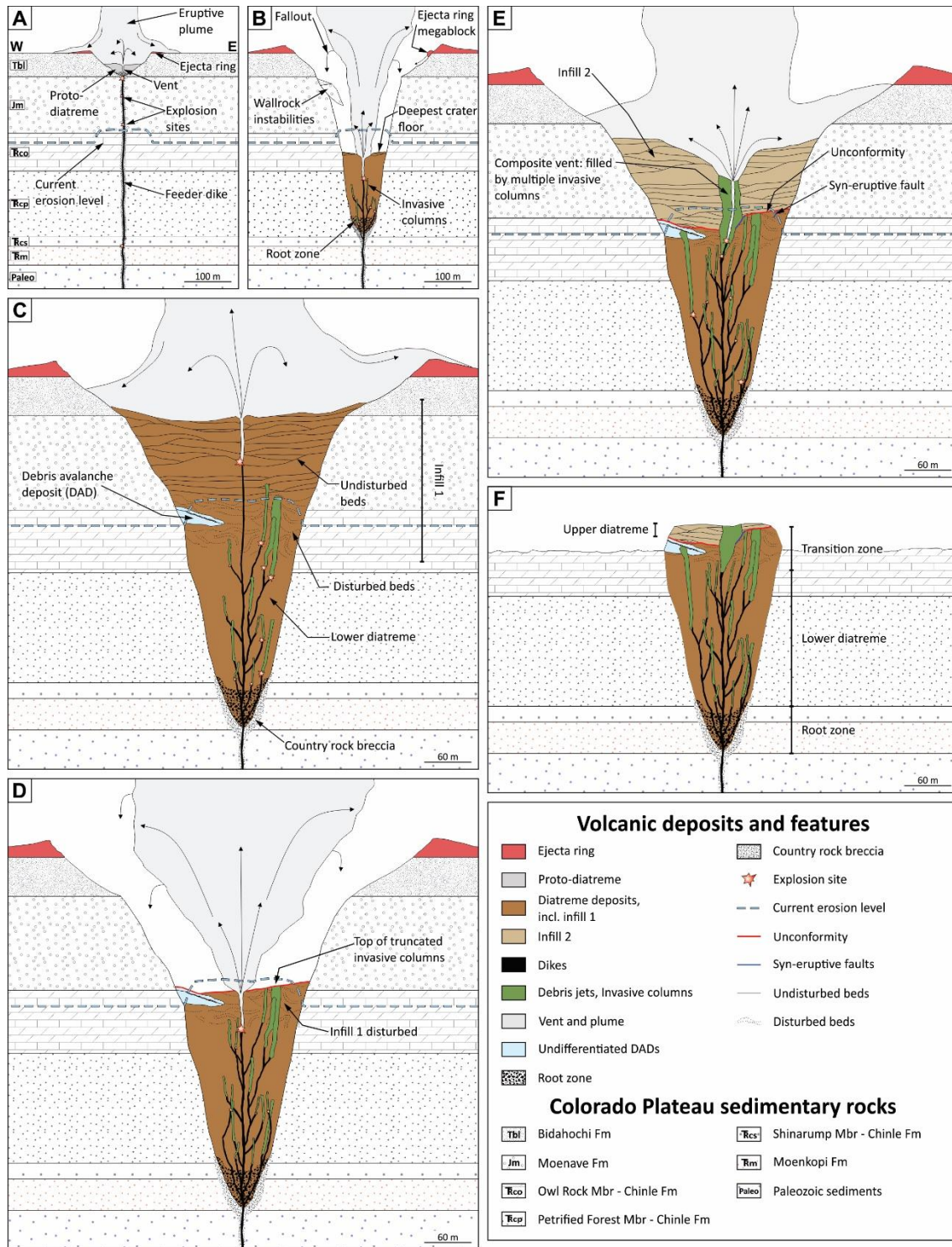


Figure 2.12: The six-step Round Butte evolution model. A) Onset of activity when a basanite dike rises through sedimentary rocks and forms the first crater in the Bidahochi Formation. B) First major excavation phase with the formation of the deepest crater. C) First phase of crater infill, forming the infill 1. D) Infill 1 is excavated during the second major phase of excavation. E) Formation of infill 2 and end of eruptive activity. F) Current erosion level at Round Butte. Note that during each cycle, crater excavation and infilling occurred partly simultaneously, i.e. initially excavation was stronger than deposition, and then deposition became stronger.

2.7.1 Initial crater and proto-diatreme

The recent literature mentions dikes, sills, sheets and plugs as possible feeders of maar-diatreme volcanoes (e.g. Re et al. 2015, 2016; Muirhead 2016; Le Corvec et al. 2018). In our model, for simplicity, we consider a dike, likely less than 1 m thick, as the feeder of the Round Butte diatreme. This is based on the 50 cm-thick basanite dike located NW of the massif (Fig. 2.2) and on measured dikes elsewhere in the HBVF (Re et al. 2015, 2016; Muirhead 2016). This feeder dike rose through the Colorado Plateau sedimentary rocks and interacted explosively to non-explosively with groundwater or wet sediments. In the region, aquifers were probably horizontal, following specific porous and permeable sedimentary layers such as the Moenave Formation, the Shinarump Member or the Moenkopi Formation (Hart et al. 2002). At the time of the eruptive activity, the Bidahochi Formation (mainly mudstone in the Round Butte area) was still being deposited regionally and was water-saturated (White 1990, 1991; Billingsley et al. 2013). Mudstones from the Bidahochi Formation likely had a low permeability, but incorporation of wet Bidahochi material within dikes and diatremes is a possible source of water for phreatomagmatic activity (e.g., White 1991, 1996a; Hooten and Ort 2002).

The initial crater at Round Butte was likely created by explosions close to the surface in the Bidahochi Formation (Fig. 2.12a; Valentine et al. 2014). Deposits that filled the initial crater are here called proto-diatreme and these deposits (as well as the initial ejecta ring) are inferred to have been Bidahochi-rich). At the same time, other explosions may have occurred at deeper levels (perhaps in the Moenave Formation, the Shinarump Member or the Moenkopi Formation) fragmenting country rocks around the dike at depth (Fig. 2.12a).

2.7.2 First cycle of excavation and infilling

An intense explosive phase widened and deepened the crater, as also proposed by Lefebvre et al. (2013) for West Standing Rocks in the HBVF. Eventually, the Round Butte crater floor reached its deepest level (Fig. 2.12b). The details of how this happened, and the nature of the diatreme infill at that stage, are unknown, since these deposits are located below the current ground level. A major excavation step is necessary in the model to have subsequently formed deposits (from the disturbed bedded pyroclastic group) filling a deep crater. One or many stages of crater excavation are also supported by the relatively low average lithic contents of the diatreme, in particular the low content of Bidahochi clasts.

This first excavation phase is inferred to have dug a relatively deep crater. At this stage, the root zone is inferred to have reached the Petrified Forest Member and the bottom of the crater was perhaps in the Owl Rock Member. We consider that the crater floor was deeper than the current plain (itself ~190 m below the pre-eruptive surface) because we found bedded pyroclastic rocks that seem to go below that (disturbed bedded group; Fig. 2.3).

During the major excavation phase and after it, pyroclastic material was deposited on the crater floor, the crater widened due to slumping of the walls (affecting the country rocks and the ejecta ring), and eventually the crater may have become filled to a high level (Fig. 2.12c). During this phase, bedded pyroclastic deposits now represented by the disturbed bedded group were formed (infill 1), as well as debris avalanches, many sedimentary and pyroclastic megablocks, and invasive columns in the lower diatreme and within infill 1 (Fig. 2.12c). This first cycle of crater excavation and infill (Figs. 2.12b, 2.12c) would have involved hundreds (or even thousands?) of phreatomagmatic explosions. At the end of this first cycle, we consider that the bottom part of infill 1 was already disturbed and crosscut by invasive columns (Fig. 2.12c). Then, a portion of infill 1 and associated invasive columns were both excavated back down to the unconformity during the second cycle of excavation and infilling (see below), forming truncated residual and invasive columns (Fig. 2.3).

At this stage, we consider that subterranean explosions, and the diatreme root zone, reached the Moenkopi Formation (Fig. 2.12c). This is demonstrated by Moenkopi clasts found in the disturbed bedded group and the non-bedded group.

2.7.3 Second cycle of excavation and infilling

A second cycle of crater excavation and infilling then followed (Figs. 2.12d, 2.12e). During this step, strong activity excavated some of the pyroclastic deposits of infill 1 and that material was partly transferred to the ejecta ring (Fig. 2.12d). This created a new crater floor that corresponds to the unconformity found all around Round Butte (Figs. 2.3 to 2.7 and 2.14 to 2.17). Excavation may have been strongest in the southwest part of the massif, leading to the development of a series of normal faults in this area.

A calmer period allowed renewed filling of the crater, to form infill 2, corresponding to the undisturbed pyroclastic group (Fig. 2.12e). These deposits were formed by fallback, fallout, as well as from dilute PDCs. Much of these pyroclastic deposits may have been fed from vents in the SW portion of the diatreme, including from what is now the nTBh column on the south face (Fig. 2.3).

Since the undisturbed bedded group (infill 2) contains fewer lithic clasts than the disturbed bedded group (infill 1) we consider that explosions probably occurred within the diatreme infill and that crater walls were mostly stable during this period. Minor widening of the crater is needed to explain the bTBm facies, which forms thick beds and lenses of Moenave-rich pyroclastic rocks. During this stage, the bottom part of infill 1 probably became homogenized to form at least some of the non-bedded pyroclastic deposits of the lower diatreme.

2.7.4 Post-eruptive events

After the end of the eruption, there would have been a crater left, as is typical of maar volcanoes (White and Ross 2011). This crater would likely have become filled by post-eruptive sediments, as seen in less deeply eroded volcanoes of the HBVF further north, such as Teshim maar (White 1991). Finally, erosion removed the post-eruptive crater infill, some of the upper diatreme (infill 2), and the surrounding Colorado Plateau sedimentary rocks (Bidahochi Formation, Moenave Formation, and the top of the Owl Rock Member), to form the current massif (Fig. 2.12f).

2.8 The upper/lower transition zone at Round Butte

Generalized models of maar-diatreme volcanoes draw the contact between the upper diatreme and the lower diatreme as a sharp subhorizontal surface (White 1991; White and Ross 2011), or a concave surface (Lorenz 1986a, 2003). Above the contact, pyroclastic deposits of the upper diatreme are bedded (although crossed by some non-bedded zones), and below the contact, deposits of the lower diatreme are non-bedded. The fact that the pyroclastic rocks below the unconformity at Round Butte also contain some bedding suggests a progressive, rather than abrupt, upper/lower transition between bedded and non-bedded rocks. The undisturbed bedded group, above the unconformity, formed during the second stage of crater infilling. Rocks below the unconformity include two types of columns: the invasive ones, formed by debris jets, and the residual ones, consisting of moderately to highly disturbed bedded pyroclastic rocks, emplaced during the first stage crater infilling. Bedding remnants within the residual columns only become apparent during close inspection of the base of the cliffs, or through the use of binoculars. The disturbed bedded material exposed below the unconformity does not resemble a classic lower, non-bedded diatreme. It is instead part of a transition zone toward the classic lower diatreme, i.e. at some depth below the current plain, all signs of bedding must disappear in the diatreme.

We therefore propose that the transition between the upper and lower diatreme is not an abrupt surface, but is a zone with a thickness of tens of meters at Round Butte, and perhaps hundreds of meters in larger diatremes. The transition zone is composed of a mixture of non-bedded and disturbed bedded deposits (Figs. 2.12f). At Round Butte, the upper contact of this transition zone corresponds to the unconformity formed by the second excavation phase. The lower contact of the transition zone is not exposed.

2.9 Conclusions

Round Butte is a small but complex Miocene diatreme, exposed 190 m below the pre-eruptive surface. Current outcrop includes bedded pyroclastic rocks (undisturbed and disturbed), non-bedded pyroclastic rocks, sedimentary and pyroclastic megablocks, and debris avalanche deposits. Detailed mapping of the cliffs allowed us to highlight relations between the different groups of facies in order to understand their emplacement dynamics and the evolution of the diatreme. Round Butte is a key site to understand:

1. how the cycles of crater excavation and infilling work;
2. the formation of non-bedded pyroclastic rocks that compose the lower diatreme;
3. the nature and significance of the transition between the upper and the lower diatreme.

Two main cycles of crater excavation and infilling are responsible for the current architecture of the Round Butte diatreme. During the first cycle, country rocks were excavated to the deepest crater floor, as a result of an explosive phase. Then the crater was filled by pyroclastic deposits (mapped as the disturbed bedded pyroclastic group), megablocks and undifferentiated DADs², which became part of the diatreme (infill 1). Explosions created debris jets, which left behind invasive columns cross-cutting the disturbed pyroclastic beds. It should be noted that crater excavation and infilling occurred partly simultaneously, i.e. initially excavation was stronger than deposition, and then deposition became stronger, completing the first cycle. During the second cycle, infill 1 was partly excavated, forming the major unconformity seen at Round Butte, and this new crater was partly filled again by pyroclastic deposits (mapped as the undisturbed bedded group) which became the new upper diatreme (infill 2). Because phreatomagmatic explosions in maar-diatreme systems are thought to be relatively small (Valentine et al. 2014), excavating a large portion of the diatreme to temporarily leave a relatively deep crater, like happened twice at Round Butte, only seems possible for a small maar-diatreme volcano, or

² Debris avalanche deposits

during the early stage of formation of a large one. For large mature diatremes, excavating the diatreme to depths over one kilometer seems very unlikely, especially in soft country rocks (Delpit et al. 2014).

At Round Butte, the bedded and non-bedded pyroclastic rocks in the diatreme formed simultaneously. We can therefore use the strong evidence for phreatomagmatism in the bedded pyroclastic rocks to interpret the origin of the non-bedded ones. Specifically, the disturbed bedded pyroclastic group and the non-bedded pyroclastic group are closely spatially associated and show similarities in componentry and grain size. Specific units within these groups display subvertical contacts and form column-like units (the residual and invasive columns, respectively). The disturbed bedded pyroclastic rocks are variably disturbed, and this is thought to be mostly due to injection of invasive columns as a result of explosion-related debris jets. Subsidence and liquefaction played lesser roles in the bedding disturbance. Over time, bedding would have completely disappeared at the bottom of infill 1. The lower non-bedded diatreme, therefore, results from progressive homogenization of bedded pyroclastic rocks mainly by injection of debris jets (Bélanger and Ross 2018).

Existing maar-diatreme models have two zones, the upper and the lower diatreme, separated by a sharp surface. We propose that a transition zone between the upper and lower diatreme, with a thickness in the meters to hundreds of meters range, should instead be included in maar-diatreme models (Fig. 2.13). This transition zone is another key to understand the formation of the lower diatreme. In volcanoes where the upper and lower diatreme are connected by this transition zone, it appears difficult to explain the formation of the upper and lower diatreme with completely different processes or eruption styles.

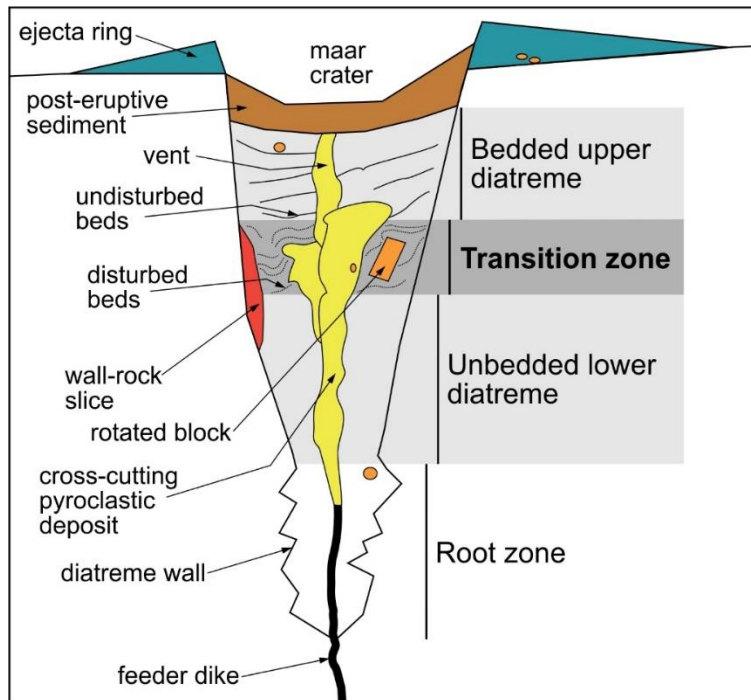


Figure 2.13: General maar-diatreme cross-sectional sketch introducing the concept of a transition zone between the upper and lower diatreme. Modified from White and Ross (2011).

2.10 Acknowledgements

James D.L. White did the early work on Round Butte, introduced Pierre-Simon Ross to this fascinating volcano and read a draft of the manuscript. Pier Paolo Comida helped us in the field. We thank the Morris family for allowing us to work at Round Butte. Any persons wishing to conduct geological investigations on the Navajo Nation must first apply for, and receive, a permit from the Navajo Nation Minerals Department, P.O. Box 1910, Window Rock, Arizona 86515, USA, telephone 1-928-871-6587. We thank Alison H. Graettinger and an anonymous reviewer for their constructive reviews, and editor Jacopo Taddeucci for his suggestions.

2.11 Online Resource 2.1: Panoramas

The Round Butte diatreme was mapped on nine high definition panoramic photographs of the subvertical cliffs (location, see Fig. 2.2). The most important and representative panoramas are included in the paper (Figs. 2.3 to 2.7), and the remaining four are included here for completeness (Figs. 2.14 to 2.17).

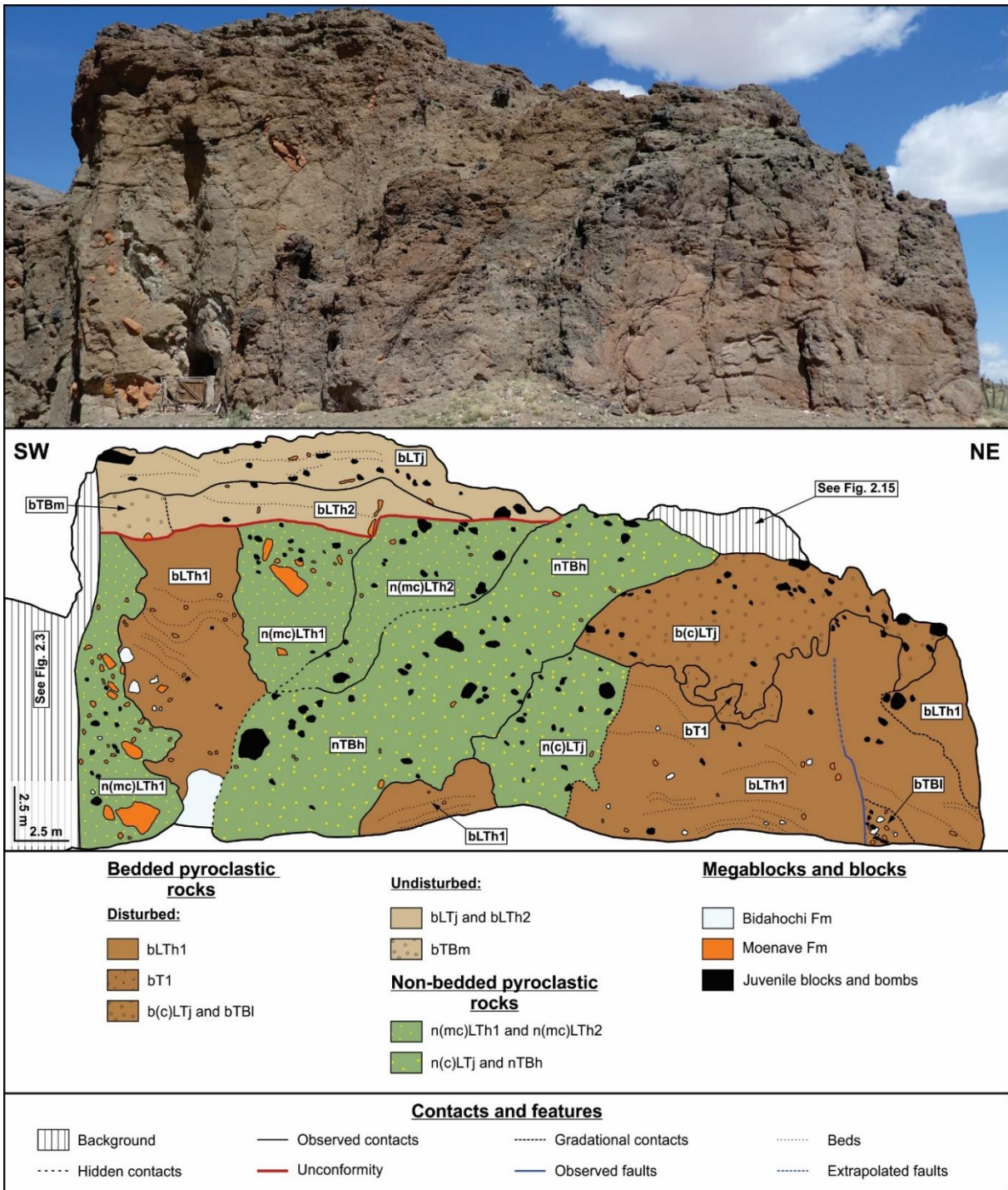


Figure 2.14: Geological map of the cliffs in the southeast part of Round Butte (location in Fig. 2.2) displaying the three main facies groups. Note the truncated invasive columns, the unconformity and flame features at the bottom of the b(c)LTj unit. For facies codes, see Tables 2.1 to 2.3.

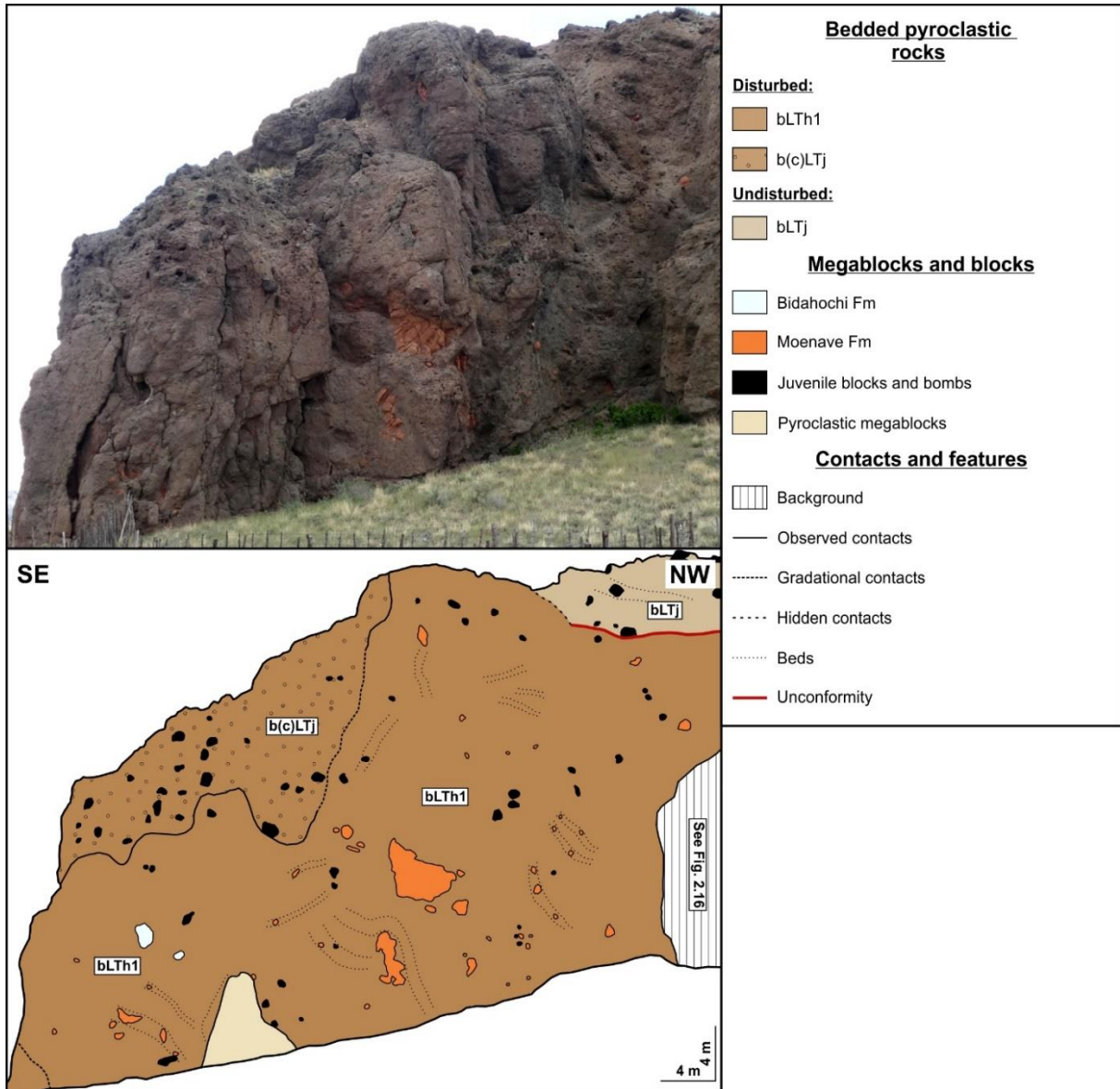


Figure 2.15: Geological map of the cliffs in the southeast part of Round Butte (location in Fig. 2.2) displaying two main facies groups. This face is dominated by disturbed bedded pyroclastic rocks overlain by undisturbed bedded pyroclastic rocks above the unconformity. Note the bedding planes with variable angles in the disturbed bedded group. For facies codes, see Tables 2.1 and 2.2.

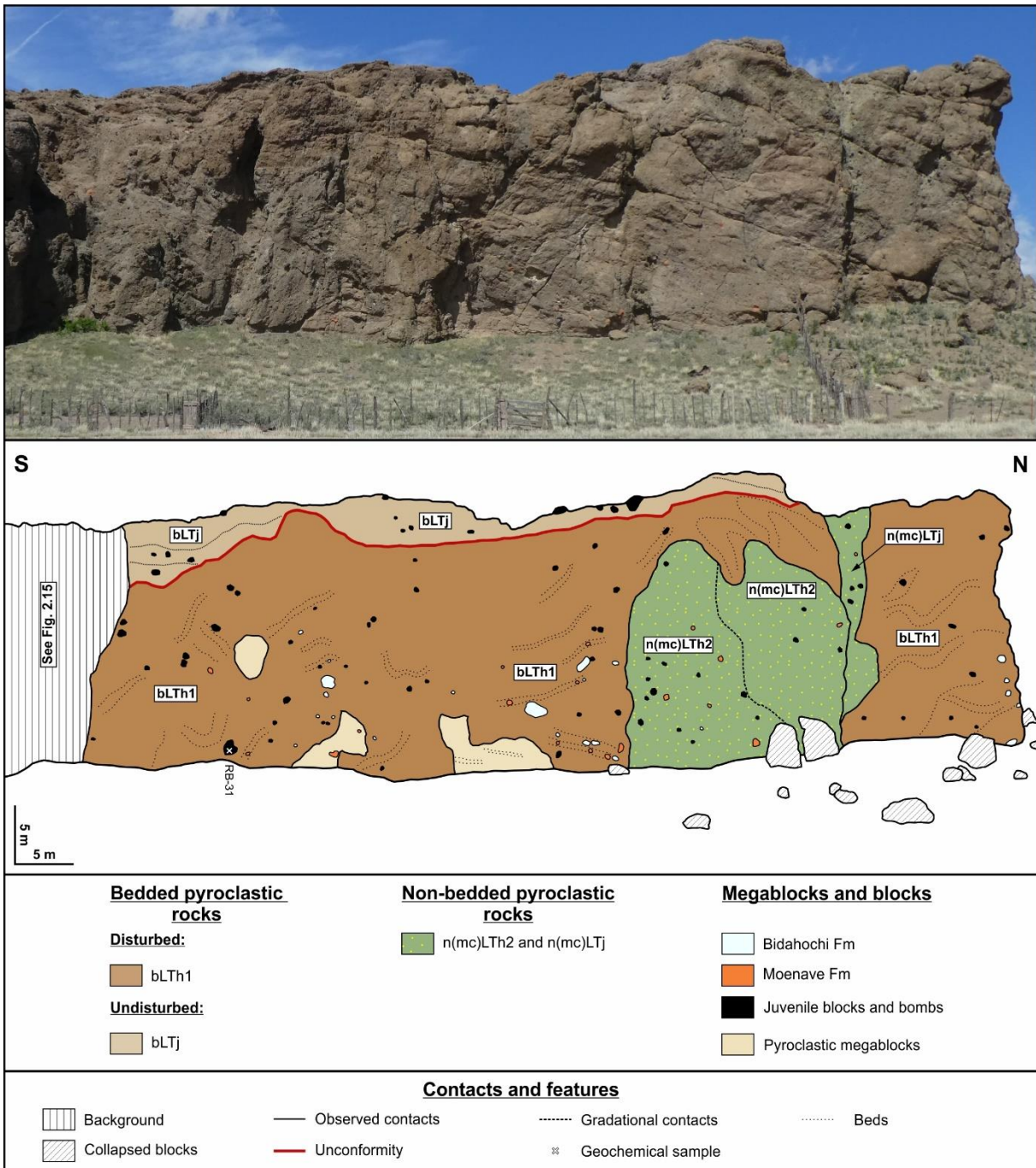


Figure 2.16: Geological map of the cliffs in the east part of Round Butte (location in Fig. 2.2) displaying the three main facies groups. This face features mostly disturbed bedded pyroclastic rocks (with subhorizontal to swirly bedding), containing pyroclastic megablocks. The disturbed bedded pyroclastic rocks are cut by invasive columns, and covered by undisturbed bedded pyroclastic rocks above the unconformity. The n(mc)LTj column on the right side of the figure appears to be one of the last emplaced units on this face, and *may* have cut the unconformity (and undisturbed pyroclastic beds), although erosion prevents visualizing that relationship. For facies codes, see Tables 2.1 to 2.3.

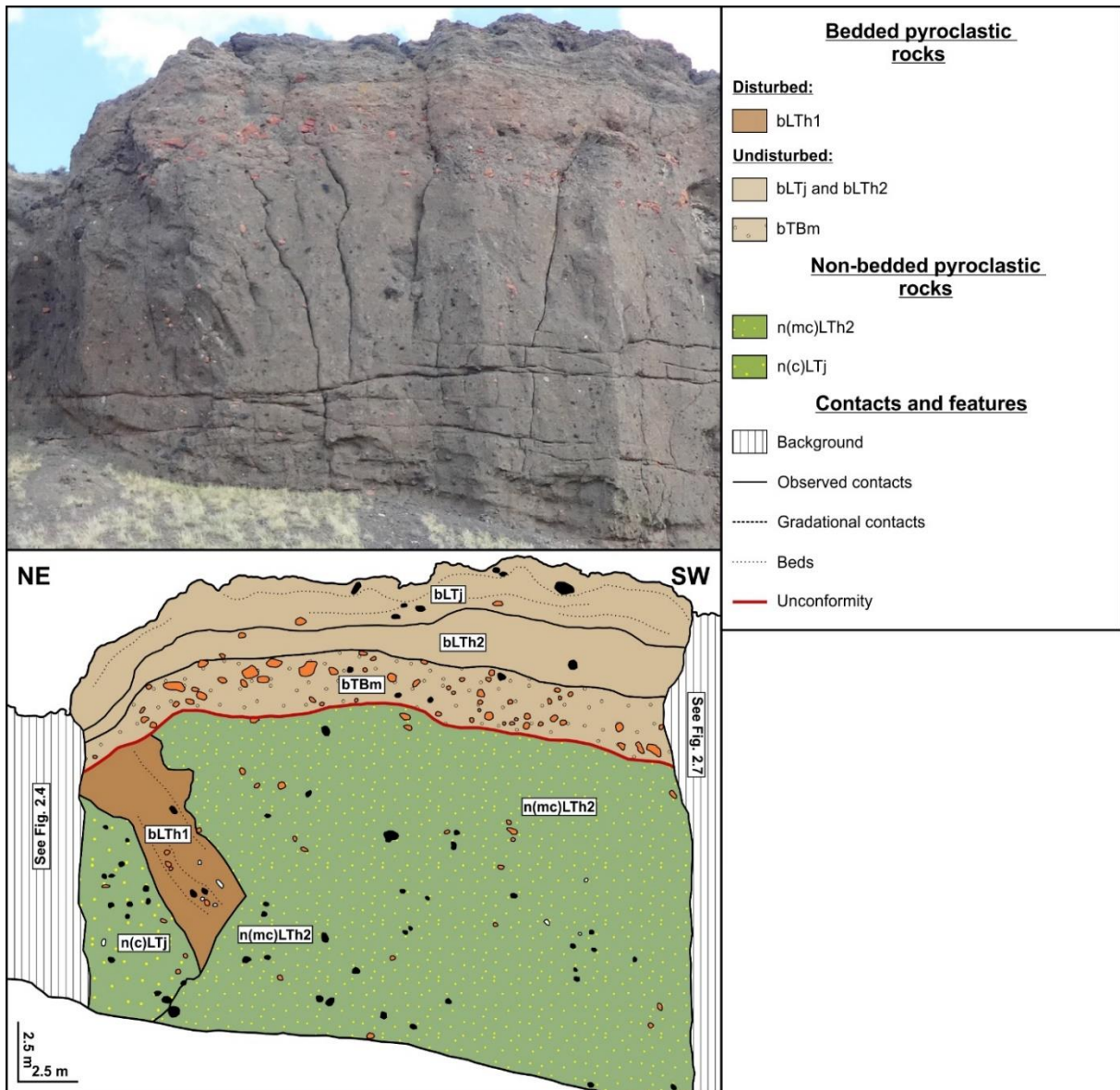


Figure 2.17: Geological map of the cliffs in the north-northwest part of Round Butte (location in Fig. 2.2) displaying the three main facies groups. Non-bedded pyroclastic rocks dominate this face and enclose a tilted domain of disturbed pyroclastic rocks. Above the unconformity are thick beds from the undisturbed group. For facies codes, see Tables 2.1 to 2.3.

2.12 Online Resource 2.2: Geochemistry and petrography of coherent samples from Round Butte diatreme

2.12.1 Methods

Six coherent samples from Round Butte were analyzed for geochemistry and petrography:

- five samples of juvenile blocks, bombs and a megablock, collected in different pyroclastic units of the massif (Figs. 2.3, 2.4, 2.16);
- one sample from the northwestern dike (Fig. 2.2).

Calcite amygdules were completely avoided when possible, although a few samples (RB-10 and RB-31) contain 10-15% of calcite amygdules. Weathered crusts were cut away with a diamond blade and discarded. Fist-size samples were sent to Activation Laboratories in Ancaster, Ontario, Canada, to analyze major oxides and trace elements. Samples were first coarsely crushed, then pulverized in a mild steel shutter box (Actlabs preparation code "RX1"). The powders were mixed with a lithium metaborate and lithium tetraborate flux and fused by melting. The melts were dissolved in a 5% nitric acid solution and read on a ICP-OES for major oxides and some trace elements (Ba, Be, Sc, Sr, V and Zr) and on a ICP-MS for 39 trace elements (Actlabs analysis code "WRA+Trace 4 Lithoresearch").

2.12.2 Petrographic observations

The mineral assemblage seen in polished slabs and thin sections of coherent rocks from Round Butte consists of:

- 15-20% of 0.5-5 mm phenocrysts of euhedral clinopyroxene (probably augite), slightly altered to fresh;
- 10-15% of 0.2-3 mm phenocrysts of euhedral olivine, extremely serpentinized;
- traces of euhedral phenocrysts of phlogopite sometimes slightly resorbed (xenocrysts), up to 1 cm across;
- a groundmass composed of microphenocrysts and microlites of euhedral oxides, clinopyroxenes and phlogopites.

Bombs contain 10-15% calcite amygdules, whereas other samples have 1-5%.

This mineral assemblage is typical of monchiquites, a type of lamprophyre (Williams 1936; Alibert et al. 1986; Hooten 1999; Rock 1991; Lefebvre 2013).

2.12.3 Major elements geochemistry

2.12.3.1 Geochemical data

Geochemical results for major elements are presented in Table 2.4.

Table 2.4: Major oxides (wt%) for Round Butte rocks

Sample name	RB-08	RB-10	RB-11	RB-12	RB-13	RB-31
Sample type	Megablock ¹	Bomb	Block	Block	NW dike	Bomb
Panorama (Fig. nb)	2.3	2.3	2.3	2.4	2.2	2.16
SiO ₂	40.76	39.8	41.89	41.07	39.15	33.93
TiO ₂	3.60	3.78	3.79	3.77	3.59	3.37
Al ₂ O ₃	9.52	10.01	10.27	10.01	9.54	8.61
Fe ₂ O ₃ ^(T)	12.15	10.85	12.33	12.59	11.98	9.87
MnO	0.16	0.21	0.16	0.17	0.16	0.14
MgO	12.48	7.91	8.86	11.01	8.30	6.11
CaO	11.15	15.69	12.68	11.89	15.41	20.80
Na ₂ O	3.56	4.09	3.99	3.46	2.97	3.31
K ₂ O	0.33	0.37	0.63	0.91	1.91	0.67
P ₂ O ₅	1.17	1.18	1.24	1.18	1.16	1.04
LOI	4.78	5.66	4.11	3.42	5.31	11.28
Sum	99.66	99.56	99.95	99.47	99.47	99.12

¹Coherent part of a pyroclastic megablock on Fig. 2.3 in the article.

2.12.3.2 TAS diagram

On the total alkali-silica (TAS) diagram, five of the Round Butte samples fall in the tephrite/basanite field (Fig. 2.18). Since their olivine contents are over 10%, they are basanites (Le Bas 1986). Data from the literature also shows a dominance of tephrites/basanites depending on the olivine content of batches of magma from one volcano to another in the Hopi Butte volcanic field (e.g., Vazquez 1998; Hooten 1999; Lefebvre 2013). In the HBVF, basanites and tephrites magmas are present in similar abundances, whereas foidites are rarer.

Sample RB-31 is a vesicular bomb with the highest content of calcite amygdules (15%) and the highest LOI. It falls in the foidite field because the high CaO content (23.7 wt%) dilutes other oxides including silica (38.6 wt%³ instead of around 42 wt% in other samples). This sample should not be used for major element interpretations.

³ Value of RB-31 sample recalculated to 100% without the LOI. This explains the difference with the SiO₂ value in Table 2.4.

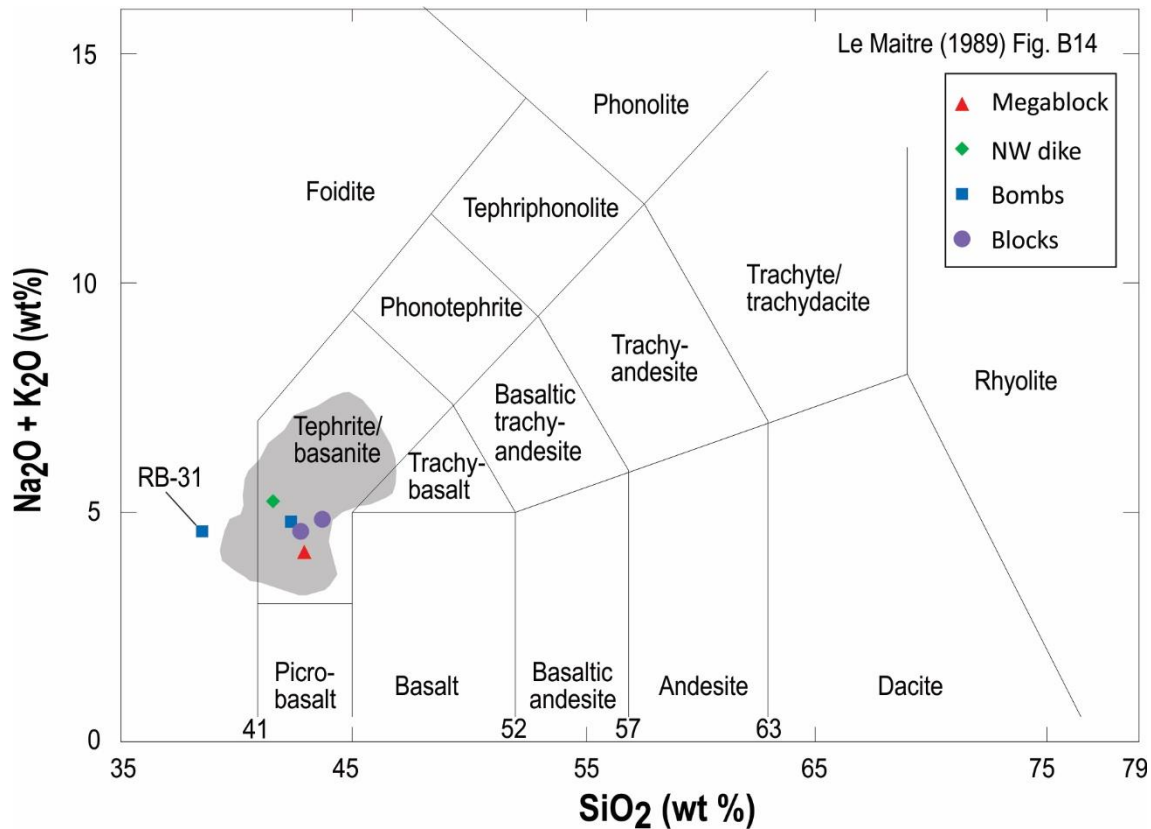


Figure 2.18: TAS diagram after Le Bas et al. (1986) and Le Maitre (1989). Round Butte rocks are shown by symbols, and the grey shaded area corresponds to data from the literature (Vazquez 1998; Hooten 1999; Lefebvre 2013).

2.12.3.3 Harker diagram

Round Butte samples are overlap with data from the literature on Harker diagrams (Fig. 2.19). The sample taken in the northwest dike plots separately from the Round Butte diatreme samples on a K_2O - SiO_2 diagram (Fig. 2.19, top right). On the other hand, K is a mobile element, so the dike versus diatreme difference on this diagram has to be verified using immobile element ratios (see below).

The MgO , $\text{Fe}_2\text{O}_3^{(T)}$ and CaO versus SiO_2 diagrams display weak negative trends. This must be related mostly to variable proportions of olivine and clinopyroxene in the rocks, although variations in CaO might also be due to various levels of calcite contamination of the samples.

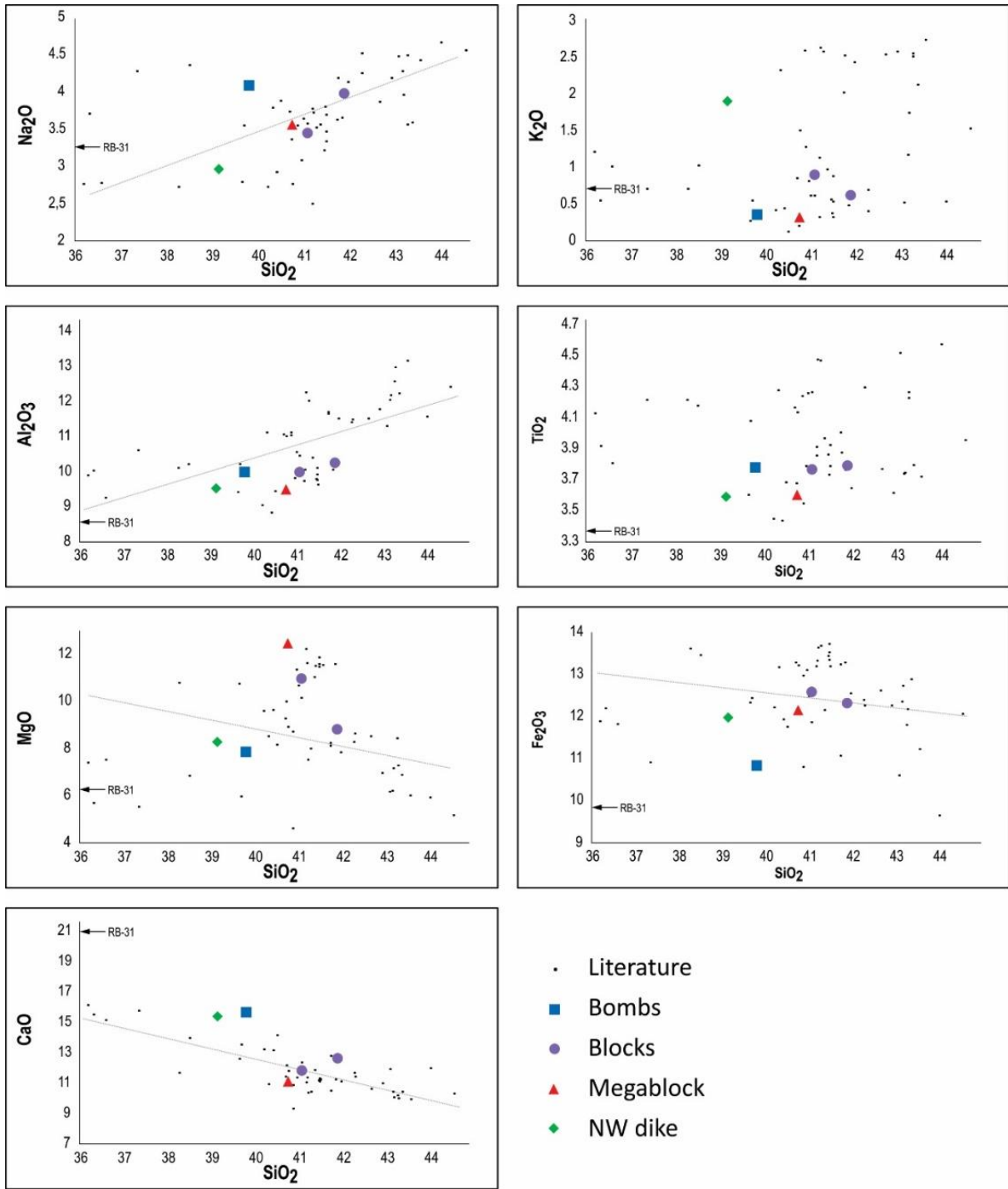


Figure 2.19: Harker diagrams presenting the geochemistry of various major oxides plotted against SiO_2 . Round Butte samples fall within the cluster of points from the literature (Vazquez 1998; Hooten 1999; Lefebvre 2013).

2.12.4 Trace element geochemistry

2.12.4.1 Geochemical data

Geochemical results for trace elements are presented in Table 2.5.

Table 2.5: Trace elements (ppm) for Round Butte rocks

Sample name	RB-08	RB-10	RB-11	RB-12	RB-13	RB-31
Sample type	Megablock ¹	Bomb	Block	Block	NW dike	Bomb
Panorama (Fig. nb)	2.3	2.3	2.3	2.4	2.2	2.16
LFSE						
Cs	3.4	4.0	4.0	2.9	0.5	2.0
Rb	4	6	8	8	33	8
Ba	958	599	871	866	919	676
Sr	1490	2205	1245	1390	1941	2768
HFSE						
Th	8.76	9.00	9.07	8.64	8.37	7.97
U	2.98	4.64	2.68	2.62	4.77	7.45
Nb	72.6	74.7	78.4	73.3	72.1	68.9
Ta	4.97	4.97	5.07	4.91	4.86	4.34
Pb	5	6	5	5	6	6
Zr	394	404	450	405	362	388
Hf	9.2	9.3	9.9	9.2	9.0	8.3
Y	28.9	29.4	30.6	29.2	28.5	26.6
REE						
La	76.8	79.1	82.2	77.2	76.1	71.4
Ce	163	167	171	164	162	149
Pr	19.7	20.1	20.3	19.9	19.5	18.0
Nd	79.5	80.6	82.4	77.9	78.0	72.0
Sm	14.6	14.7	14.8	14.3	14.3	13.2
Eu	4.35	4.43	4.57	4.34	4.33	3.93
Gd	11.4	11.3	11.4	10.9	11.0	10.1
Tb	1.30	1.37	1.40	1.32	1.36	1.24
Dy	6.74	7.19	7.18	6.95	6.75	6.00
Ho	1.04	1.09	1.14	1.11	1.04	0.96
Er	2.56	2.68	2.66	2.58	2.58	2.30
Tm	0.30	0.31	0.34	0.32	0.31	0.30
Yb	1.77	1.80	1.71	1.63	1.64	1.50
Lu	0.21	0.23	0.24	0.22	0.22	0.20

¹Coherent part of a pyroclastic megablock on Fig. 2.3 in the article.

2.12.4.2 Zr/TiO₂ vs Nb/Y diagram

In the classification diagram of Winchester and Floyd (1977), which uses immobile element ratios, Round Butte rocks form a cluster in the alkali basalt field (Fig. 2.20), not far from the basanite field. In this diagram, sample RB-31 plots together with the other samples because immobile elements ratios negate the effect of alteration. We also note that the NW dike clusters with the Round Butte diatreme samples. We consider that all our samples could have been

derived from one batch of magma and that the NW dike might have fed the Round Butte diatreme.

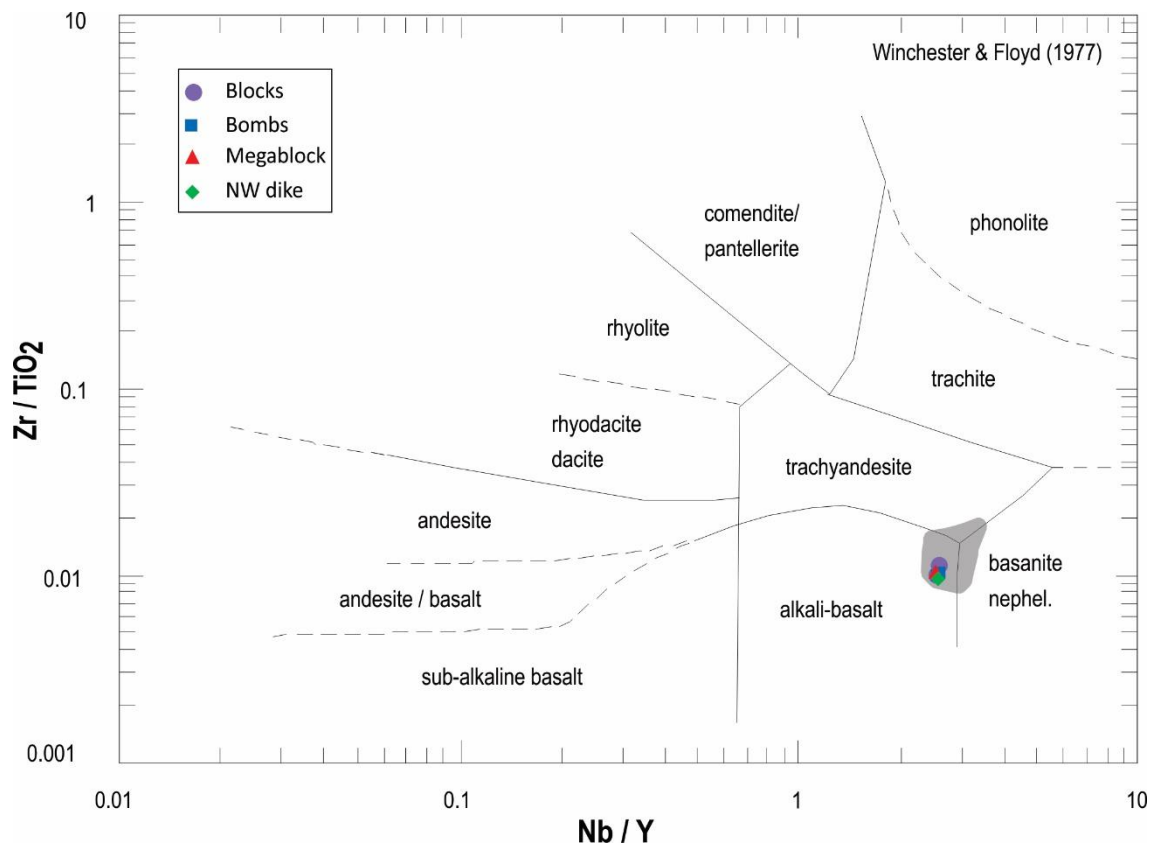


Figure 2.20: Immobility element diagram after Winchester and Floyd (1977) comparing Round Butte data (coloured symbols) with geochemical data from the literature (grey shaded area, Vazquez 1998; Hooten 1999; Lefebvre 2013).

2.12.4.3 Spider diagrams

Round Butte rocks are strongly enriched in incompatible elements in comparison to the primitive mantle of Sun and McDonough (1989). Compiled geochemical data of the HBVF shows a negative anomaly in Sm and Ti, whereas Round Butte samples display only a weak Sm anomaly (Fig. 2.21). The general trend of Round Butte samples is close to the Ocean Island Basalt (OIB) end-member even if the actual setting is continental intraplate volcanism. The Round Butte samples are nearly indistinguishable from each other on the spider diagram.

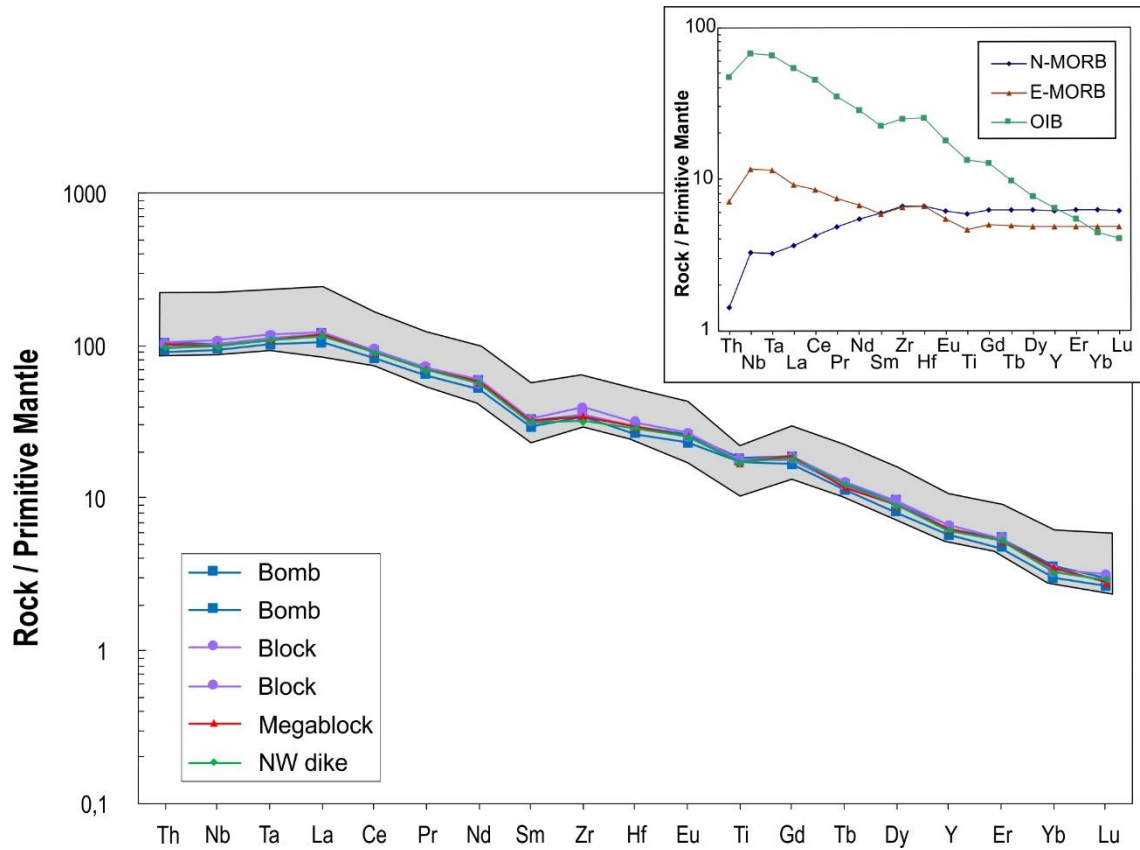


Figure 2.21: Extended trace elements normalized to the primitive mantle (Sun and McDonough 1989). Dark grey area corresponds to geochemical data from the literature (Vazquez 1998; Hooten 1999; Lefebvre 2013). Composition of N-MORB, E-MORB and OIB are from Sun and McDonough (1989).

3 SECOND ARTICLE: Lithics and lithic-rich lithologies at Round Butte diatreme

What lithic clasts and lithic-rich lithologies can tell us about diatreme processes: an example at Round Butte, Hopi Buttes volcanic field, Navajo Nation, Arizona

Que peuvent nous apprendre les clastes lithiques et les lithologies riches en lithiques sur les processus dans le diatrème : un exemple à Round Butte, champ volcanique Hopi Buttes, Nation Navajo, Arizona

Authors:

Benjamin Latutrie and Pierre-Simon Ross

Institut national de la recherche scientifique, Centre Eau Terre Environnement, 490 rue de la Couronne, Québec (QC), G1K 9A9, Canada

Title of the journal:

Journal of Volcanology and Geothermal Research

Ready to submit

3.1 Abstract

The Miocene Hopi Buttes volcanic field (HBVF) in northern Arizona comprises many maar-diatreme volcanoes, and provides excellent exposures of diatremes filled by phreatomagmatic deposits. Maar-diatreme deposits are variably rich in lithic clasts, specifically accidental fragments derived from surrounding country rocks. Within the HBVF, the country rock stratigraphy is well known, and the stratigraphic origin of the largest lithic fragments in diatremes can be identified. In the southeastern part of the HBVF, the Round Butte diatreme crops out ~190 m below the pre-eruptive surface and field observations of the current outcrops highlighted a diatreme 170-190 m in diameter. Its central part has a diameter of 130-150 m, forming a massif with 20-30 m high subvertical cliffs. One month of field mapping, componentry measurements and facies descriptions allowed us to define three main groups of pyroclastic rocks: undisturbed beds, disturbed beds and non-bedded rocks, which were described and interpreted in [Chapter 2](#). Two minor facies groups were also identified: pyroclastic and sedimentary megablocks (blocks over 2 m in long axis), and debris avalanche deposits. Pyroclastic megablocks are finer-grained, and richer in lithic clasts, than most diatreme rocks surrounding them. These pyroclastic megablocks are interpreted as subsided portions of the maar ejecta ring. Sedimentary megablocks originate either from above, or from the same level, relative to their current location, i.e. no megablock has a net upward displacement. Debris avalanche deposits result from slumping of the surrounding country rocks within the syn-eruptive crater. Slumps are related to gravitational destabilization of the crater walls driven by the phreatomagmatic explosions. Debris avalanches and individual megablock collapse are the main ways in which the crater grows in size laterally during the eruption.

We combine the componentry of the disturbed bedded lithofacies, the non-bedded lithofacies and pyroclastic megablocks with a series of conceptual country rock fragmentation models to show that lithic fragments at the current level of exposure come from elevations up to 190 m above (i.e., up to the pre-eruptive surface) and up to 220 m below their current locations. This exercise further allows us to estimate diatreme wall angles of 70° below the Bidahochi Formation to approximate the depth of the root zone. Pyroclastic units displaying the richest content of lithic clasts with a deep origin are typically the non-bedded columns interpreted to have formed from debris jets.

3.2 Introduction

Maar-diatremes are small, typically short lived, mainly phreatomagmatic monogenetic volcanoes (Lorenz 1986a, 2007; White and Ross 2011; Kereszturi and Németh 2012; Valentine and White 2012; Lefebvre et al. 2013; Ross et al. 2017) found in monogenetic volcanic fields around the world (e.g., Németh et al. 2012; Brown and Valentine 2013; Kereszturi et al. 2014; Poppe et al. 2016; Cas et al. 2017). They are, after scoria cones, the second most abundant type of volcanoes on continents (Vespermann and Schmincke 2000). From bottom to top, maar-diatreme volcanoes are composed of a feeder intrusion (Re et al. 2015, 2016; Muirhead et al. 2016; Le Corvec et al. 2018), a root zone (Clement 1982; Lorenz and Kurszlauskis 2007; Haller et al. 2017), a lower non-bedded diatreme (White 1991; Lefebvre et al. 2013, 2016), a transition zone (Bélanger and Ross 2018; [Chapter 2](#) or Latutrie and Ross 2019), an upper typically bedded diatreme (White 1991; Gernon et al. 2013; Delpit et al. 2014), a maar crater (Lorenz 1973; White 1991; Graettinger 2018) and an ejecta ring (Self et al. 1980; White 1991; Vazquez and Ort 2006; Valentine et al. 2015).

There are two main types of fragments in pyroclastic rocks: juvenile and lithic (White and Houghton 2006). Lithic fragments are defined as clasts generated by the fragmentation of pre-existing rocks and deposits (White and Houghton 2006). Typical lithic clasts in volcanic fields include sedimentary rocks, unconsolidated sediments, crystalline bedrocks, solidified lavas or pyroclastic rocks from older volcanoes. In a maar-diatreme volcano, existing pyroclastic rocks or deposits within the diatreme or ejecta ring can also be recycled as clasts during the eruption, and are considered lithic. However, individual juvenile fragments that are recycled during the eruption are still juvenile (White and Houghton 2006).

Pyroclastic rocks that compose the maar-diatreme often contain a high proportion of lithic clasts derived from the surrounding country rocks, especially in the ejecta ring (e.g., Németh et al. 2000; Raue 2004; Valentine 2012; Ort et al. 2018). In the literature, lithic clasts found in the ejecta ring have received greater attention (Ollier 1967; Lorenz 1973, 1975; Ross et al. 2011; Graettinger and Valentine 2017) than those found in diatreme (Lefebvre et al. 2013), even if the diatreme potentially preserves a more complete record of the eruption, since not all explosions expel material to the ejecta ring (Ross et al. 2008b, 2008c; Valentine et al. 2014, 2017).

In the area of the Hopi Buttes volcanic field (HBVF), Colorado Plateau sedimentary rocks are gently dipping to flat-lying and their stratigraphy is well known (Billingsley et al. 2013). Four main sedimentary formations crop out, namely from north to south, the Bidahochi Formation, the

Moenave Formation, the Chinle Formation and the Moenkopi Formation (Fig. 3.1, Billingsley et al. 2013). These are well described in the literature, and can be examined in situ for reference. This means that large lithic clasts in Hopi Buttes diatremes can often be assigned to a specific origin or source depth (Lefebvre et al. 2013). This makes the HBVF an excellent location to study the origin of the lithic clasts within diatreme pyroclastic deposits. Round Butte is a well exposed HBVF diatreme. Latutrie and Ross (2019) described the three main groups of pyroclastic facies there and provided a general model of its eruptive history.

In this paper, we document in detail two other facies groups of Round Butte diatreme, the megablocks and the debris avalanche deposits, that represent a volumetrically minor, but genetically important, part of the volcano's evolution. We provide a detailed study of lithic clasts and lithic-rich lithologies through a dataset of componentry measurements on pyroclastic rocks, acquired through the line count and clast count methods. The advantage of studying these lithic clasts in detail, along with lithic-rich lithologies such as debris avalanches and megablocks, is that since the ultimate source depth of the lithic material is known, the net upward or downward displacement of lithic clasts and megablocks can be reconstructed. This allows us to compare the measured lithic proportions with a series of conceptual country rock fragmentation models for the Round Butte diatreme. This exercise helps constrain the diatreme size and shape, and better understand eruptive processes within the maar crater and diatreme, including upward movements of fragments through debris jets related to phreatomagmatic explosions (Ross et al. 2008b, 2008c), and downward movements through crater wall collapse, mass wasting, and subsidence.

3.3 Regional setting

3.3.1 Hopi Buttes volcanic field (HBVF)

The HBVF covers 2300 km² in the south central part of the Colorado Plateau (Fig. 3.1a, Williams 1936; White 1991; Vazquez and Ort 2006; Lefebvre et al. 2012, 2013, 2016; Re et al. 2015, 2016; Latutrie and Ross 2019). Miocene volcanic remnants, representing over 300 edifices, are mainly maar-diatremes (White 1991; Lefebvre et al. 2013, 2016; Latutrie and Ross 2019), lava flows (Williams 1936), intrusions (Re et al. 2015, 2016; Muirhead et al. 2016) and rarely scoria cones (White 1991; Vazquez 1998). The abundant phreatomagmatic activity was related to the water-rich environments outlined at the surface by Miocene playas and ponds (White 1990; Dallegge et al. 2003) and underground by subhorizontal aquifers (for recent aquifers, see Hart et al. 2002). The current arid setting and the variable erosion level in the

HBVF provide excellent exposure of maar-diatremes from the ejecta ring (White 1991; Graettinger and Valentine 2017) to the lower diatreme (Lefebvre et al. 2013) and plumbing system (Re et al. 2015, 2016; Muirhead et al. 2016). Round Butte, the topic of this study, is a diatreme located in the eastern portion of the field (Figs. 3.1b, 3.1c).

3.3.2 Sedimentary formations of the HBVF area

The *Bidahochi Formation* (Pliocene and Miocene, Tbl) was named by Reagan (1924, 1932) and formerly divided into three informal members, namely the Upper fluvial Member, the Middle volcanic Member and the Lower mudstone and argillaceous sandstone Member (Repenning and Irving 1954; Shoemaker et al. 1962; Dallegge et al. 2003). Billingsley et al. (2013) redefined the Bidahochi Formation to include only the Upper fluvial Member (Pliocene) and the Lower mudstone/argillaceous sandstone Member (Miocene). The Middle volcanic Member was assigned by Billingsley et al. (2013) to the HBVF. In the Round Butte area, the Bidahochi Formation is inferred to have a thickness of about 50 m (see log in Fig. 3.1). The Bidahochi Formation sediments that are well exposed at Bidahochi Butte and White Cone (Figs. 3.1b, 3.2a) are lacustrine in origin and composed by white to greenish/yellowish-grey claystone, light-red to brown-red mudstone/siltstone and whitish-grey sandstone (Fig. 3.2b) with locally mixed levels displaying an enrichment of juvenile fragments and free pyroxene crystals derived of the HBVF volcanism. The Bidahochi Formation rests unconformably on the Moenave Formation.

The *Moenave Formation* (Lower Jurassic, Jm) is around 120 m thick at Twin Peaks, near Round Butte (Fig. 3.1). Rocks are bedded, jointed/fractured, orange red to light red, fine to coarse-grained, siltstone/sandstone, often displaying low angle cross-beds, and forming weathered slopes (Fig. 3.2c; Billingsley et al. 2013). White to greenish-white horizons, spots or stripes are commonly observed within these rocks. Because of the joints, Moenave Formation rocks were probably an aquifer at the time of the eruptions (White 1991; Lefebvre et al. 2012). The Moenave Formation rests unconformably on the Chinle Formation.

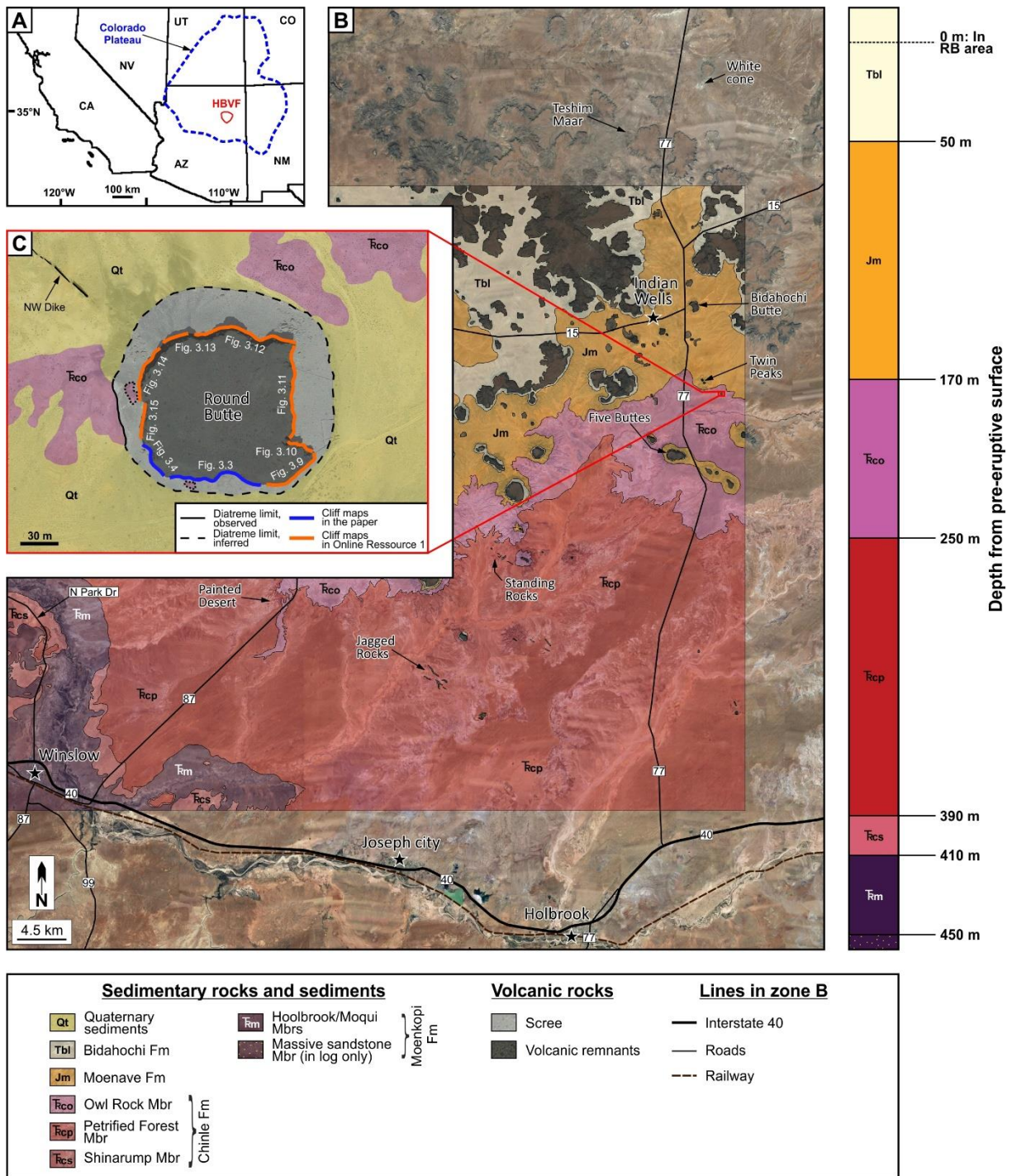


Figure 3.1: Maps displaying A) the location of the Colorado Plateau and the HBVF, B) geology of a portion of the HBVF (map centre at UTM zone 12S, 572 410 m E, 3 916 058 m N), simplified from Billingsley et al. (2013) and C) a close-up of the Round Butte diatreme (map centre at 588 158 m E, 3 910 326 m N). The sedimentary log displays the inferred thickness of the sedimentary formations.

The *Chinle Formation* (Upper Triassic) is composed by three members from top to bottom (Repenning et al. 1969; Billingsley et al. 2013): the Owl Rock Member (TRco, Figs. 3.1, 3.2d),

the Petrified Forest Member (TRcp, Figs. 3.1, 3.2e) and the Shinarump Member (TRcs, Figs. 3.1, 3.2f). The Owl Rock Member is mainly purple/pink in color and is 80 m thick in the Five Buttes to Round Butte area, where it crops out well (Figs. 3.1, 3.2d). It is composed of nodular limestone interbedded with slope-forming purple, light-blue/red calcareous claystone, siltstone and sandstone. The contact with the underlying Petrified Forest Member is marked by the last limestone bed of the Owl Rock member (Billingsley et al. 2013). The Petrified Forest Member is the thickest member of the Chinle Formation (140 m thick). This member is composed by multicolor mudstone/siltstone intercalated with lenses of yellow/white coarse-grained sandstone and fragments of logs of petrified wood. It forms badlands-type terrain, for example in the Painted Desert area north of Winslow (Figs. 3.1, 3.2e). At the bottom, the Shinarump Member is 20 m thick, composed of channelized coarse-grained sandstone to conglomerate rich in pebbles and intercalated with siltstone and mudstones (Fig. 3.2f). The Shinarump Member crops out along Interstate 40 and north of Winslow near N Park Dr road (Fig. 3.1b). The Chinle Formation rests unconformably on the Moenkopi Formation.

The Moenkopi Formation (Middle? to Lower Triassic) is composed of two members in the HBVF area, with the Holbrook/Moqui Member at the top and the Lower Sandstone Member at the bottom (McKee 1954; Billingsley et al. 2013). Holbrook/Moqui Member rocks are micaceous (mainly white micas) reddish/brown claystone, siltstone and sandstone displaying cross-bedding and cusp-type ripple marks (TRm, Figs. 3.1, 3.2g). This member is 40 m thick and crops out in Holbrook. The Lower Sandstone Member (up to 25 m thick) consists of light-red to light-brown, fine-grained calcareous siltstone/sandstone with crossbedding (Figs. 3.1, 3.2h). This member crops out south of Winslow near road 99 (Fig. 3.1b).

3.4 Methods

Several days were spent reconnoitering the regional sedimentary stratigraphy in the area of White cone, Bidahochi Butte, Twin Peaks, Five Buttes, Holbrook and Winslow as shown in Fig. 3.1b, to get familiar with the typical structures and textures of each formation and member. Most of the remaining time in the field was then spent on Round Butte, where lithic fragments could be identified in the diatrema, and the different facies groups mapped, characterized and sampled.

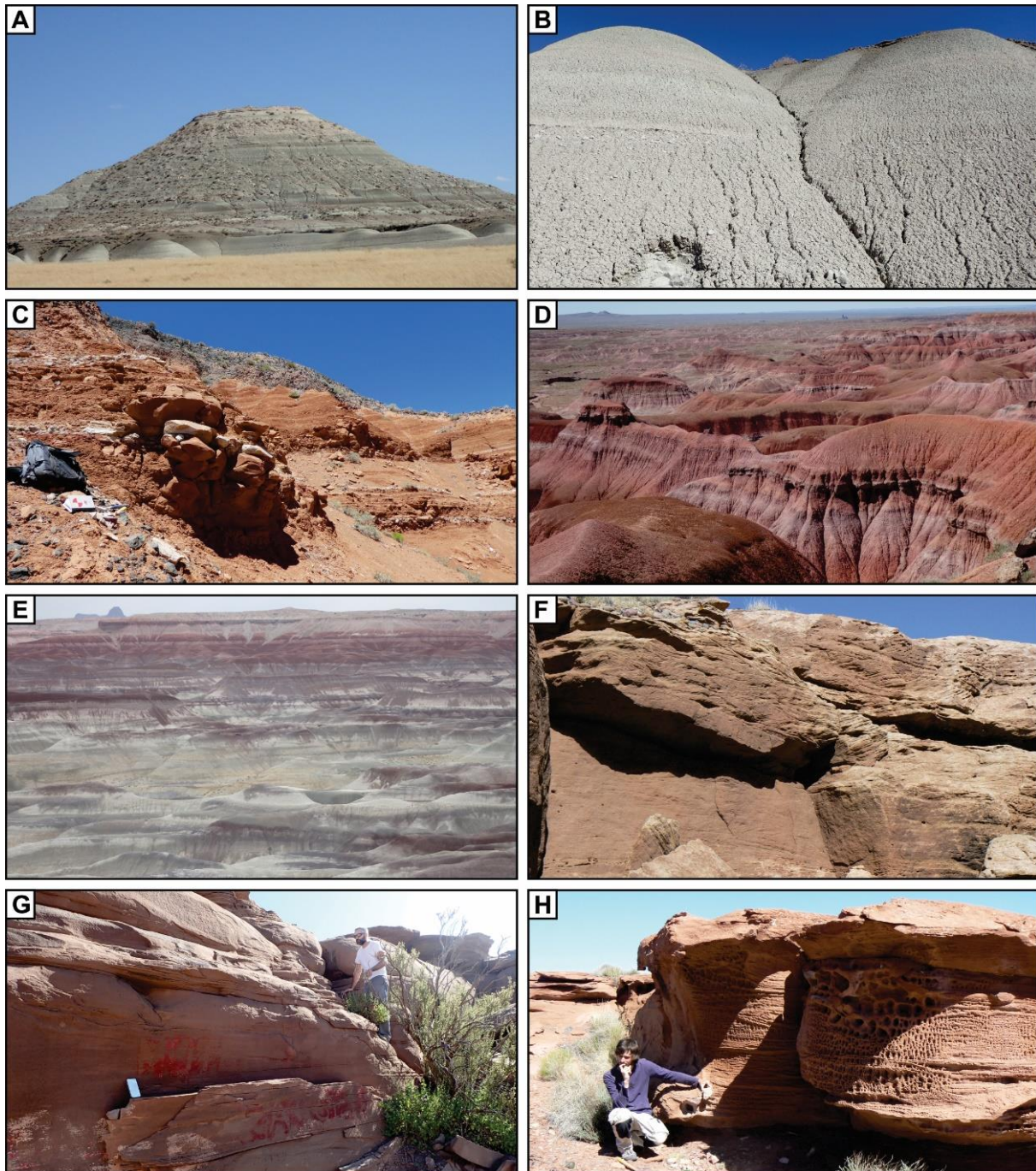


Figure 3.2: Photo plate of the main sedimentary formations in the HBVF area. A) General view of the Bidahochi formation at White cone, B) close-up on mudstone/siltstone and argillaceous sandstone of the Bidahochi Formation at White cone, C) Moenave Formation at Twin Peaks, D) Owl Rock Member of the Chinle Formation south of Five Buttes, E) Petrified Forest Member of the Chinle Formation in the Painted Desert area north of Winslow, F) Shinarump Member of the Chinle Formation close to the N park Dr road, north of Winslow, G) Holbrook/Moqui Member of the Moenkopi Formation in Holbrook city and H) Lower sandstone Member of the Moenkopi Formation close to road 99, south of Winslow.

3.4.1 Mapping and facies groups at Round Butte

Field work at Round Butte is described by Latutrie and Ross (2019). A geological map of Round Butte (Fig. 3.1c) and nine detailed cliff maps of 20-30 m high subvertical cliffs surrounding the massif were produced (Figs. 3.3, 3.4, Online Resource 3.1). Five groups of facies were defined: the undisturbed bedded pyroclastic group, the disturbed bedded pyroclastic group, the non-bedded pyroclastic group, the megablocks group and the debris avalanche deposits (DADs) group. The first three groups were described and interpreted by Latutrie and Ross (2019) whereas the last two are addressed here, along with the componentry for all facies groups that could be characterized.

3.4.2 Componentry measurements

In the field, two componentry methods were used to quantify the relative proportions of various types of fragments greater than or equal to 4 mm found in pyroclastic lithofacies: line counts (modified from Lefebvre 2013) and clast counts (modified from Ross and White 2006). The reason for using these two methods is that line counts are easier on subvertical rock faces, but clast counts, a field version of point counting, are more established. Clast counts were done on a subset of line count sites to enable a comparison between the methods. In addition, we used point counts on selected thin sections during lab work.

Field line counts were performed at 43 sites. At each site, we used three horizontal 1 m-long lines, spaced vertically by 50 cm, to cover an area of 1 m². The lines were manifested by a measuring tape, along which fragment intersection lengths were determined, for all particles (juvenile, lithic and tuff) greater than or equal to 4 mm. The rest of the material was classified as undifferentiated matrix/cement. The proportion of a certain component was defined as the sum of the intersection lengths, divided by the total length of the tape.

Field clast counts were obtained at 15 sites already covered by line counts. We used a 1 m² square net with a 10 cm mesh, allowing us to quantify 100 points per site. During these measurements, fragments greater or equal to 4 mm were classified into different componentry bins (juvenile, lithic and tuff), and we counted the rest as either matrix or cement.

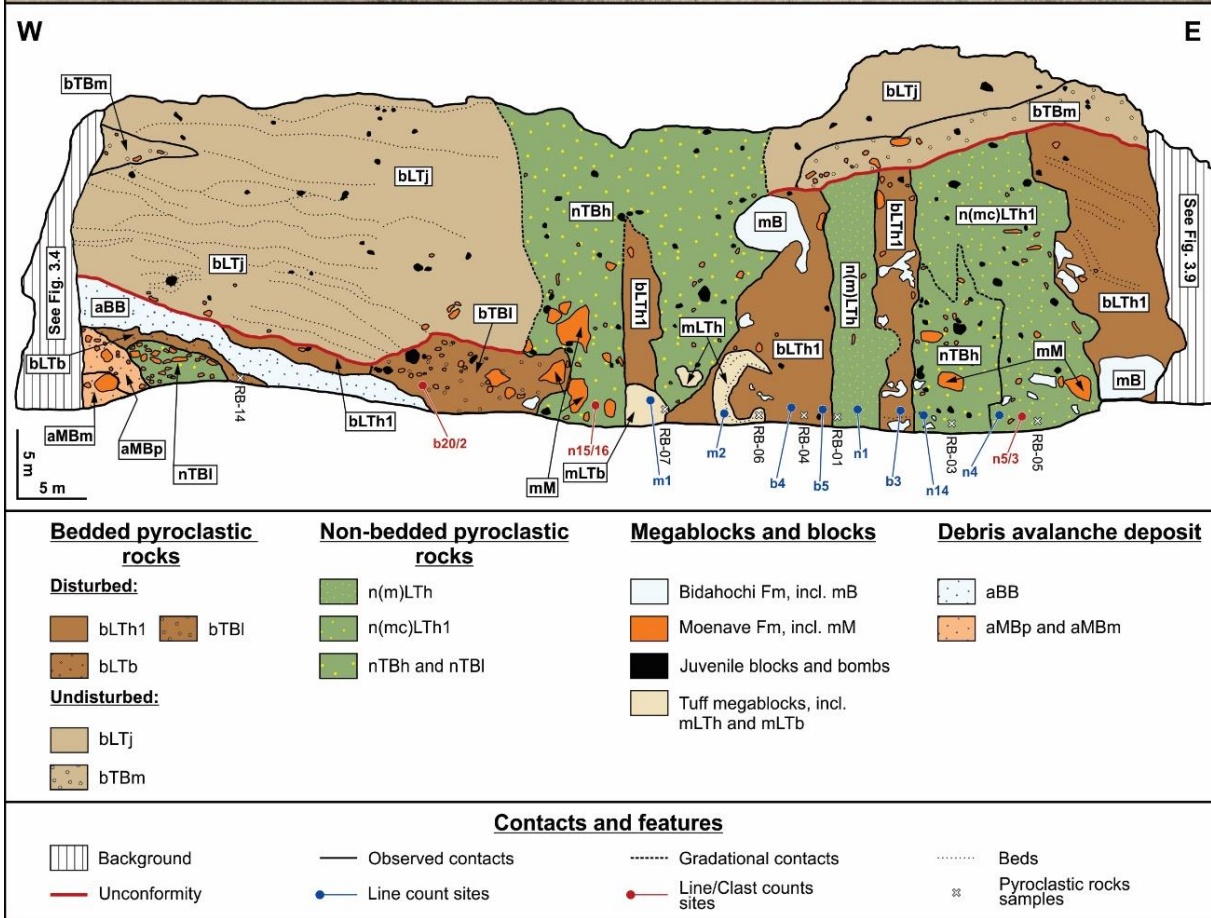


Figure 3.3: Geological map of the cliffs in the southern part of Round Butte (location in Fig. 3.1c) displaying three main groups of pyroclastic facies detailed in Latutrie and Ross (2019), the megablocks, and the debris avalanche deposits (DADs). For facies codes, see Latutrie and Ross (2019) and Table 3.1.

Thirty-two thin sections of pyroclastic rocks were prepared from hand samples taken in the field to characterize the matrix (particles smaller than 4 mm in this paper). Eighteen of these thin sections were point counted for componentry using the “JmicroVision 1.2.7” software (Roduit

2007; <https://jmicrovision.github.io/>). To obtain the necessary images, we used two different methods. Ten thin sections were initially imaged using a mosaic of plane polarized light photomicrographs taken with a petrographic microscope at a magnification of 25x. The remaining eight thin sections were imaged with a “PowerSlide 5000” photographic slide scanner at an optical resolution of 5000 dpi. We counted 450 points on each thin section and used the recursive grid setting of JmicroVision.

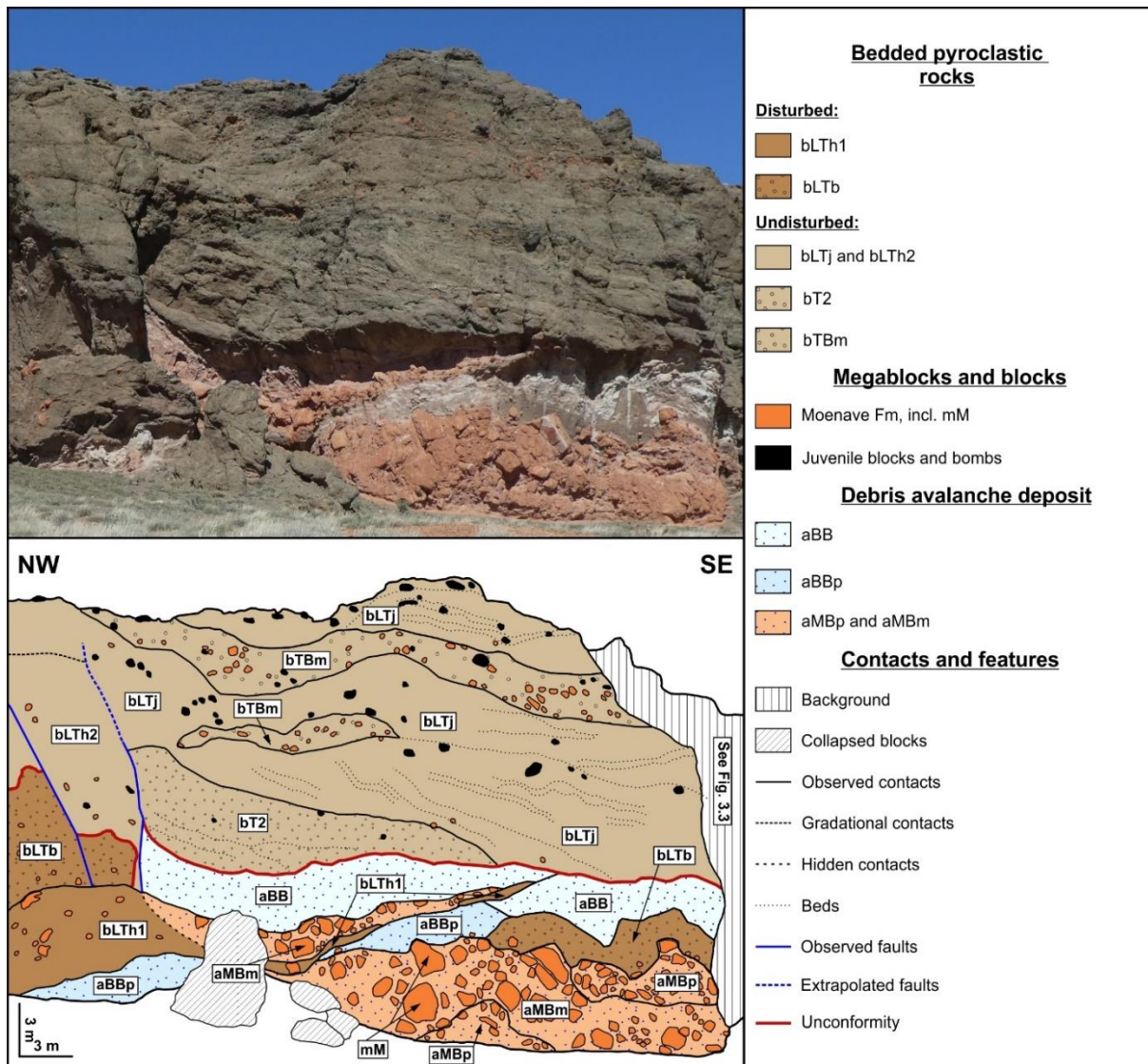


Figure 3.4: Geological map of the cliffs in the southwest part of Round Butte (location in Fig. 3.1c) displaying two main groups of facies detailed in Latutrie and Ross (2019), the megablocks, and the debris avalanche deposits (DADs). For facies codes, see Latutrie and Ross (2019) and Table 3.1.

3.5 Round Butte massif overview

3.5.1 Summary of the three main pyroclastic facies groups

Round Butte is a small (170-190 m diameter) but surprisingly complex maar-diatreme volcano. The erosion level of the surrounding plain is about 190 m below the pre-eruptive surface, and the 20-30 m high cliffs expose the transition zone between the upper diatreme and the lower diatreme (Latutrie and Ross 2019). The 130-150 m diameter massif in the central part of the diatreme displays three main pyroclastic groups. These are the undisturbed bedded pyroclastic group, the disturbed bedded pyroclastic group and the non-bedded pyroclastic group (Latutrie and Ross 2019). The disturbed bedded and non-bedded pyroclastic groups have subvertical contacts with each other, forming an alternation of non-bedded “invasive” columns and disturbed bedded “residual” columns (Figs. 3.3, 3.12, Latutrie and Ross 2019) whereas the undisturbed bedded group mainly sits on the top of the two other pyroclastic groups, above an unconformity (Figs. 3.3, 3.4, 3.9 to 3.15).

3.5.2 Megablocks

Round Butte massif includes three types of megablocks (blocks over 2 m in long axis), described in Table 3.1: (i) sedimentary (Bidahochi, Moenave and Chinle) megablocks, (ii) pyroclastic megablocks and (iii) juvenile megablocks (Fig. 3.5). They are mainly present in the disturbed bedded pyroclastic group and in the non-bedded pyroclastic group (Figs. 3.3, 3.12, 3.14, 3.15). Rare Moenave Formation megablocks occur in the undisturbed bedded pyroclastic group (e.g., Fig. 3.15). The sedimentary megablocks that occur within the DADs group are treated as part of this group (Figs. 3.3, 3.4).

3.5.3 Debris avalanche deposits (DADs)

The five facies interpreted as formed by DADs are described in Table 3.1 and Fig. 3.6. Four of the five facies (aMBm, aMBp, aBB and aBBp) constitute the main DAD in the southwest side of the massif (Figs. 3.3, 3.4, 3.15) whereas the last facies (aTBh) forms multiple small DADs on the west side (Fig. 3.14). The main DAD displays an inward dip of around 35° (towards the centre of the diatreme) and forms a 10 m thick package of sedimentary-dominated DAD facies with intercalations of disturbed bedded pyroclastic rocks (bLTb and bLTh1, Figs. 3.3, 3.4). The sedimentary-dominated facies consist of lapilli- to megablock-sized Moenave or Bidahochi fragments, in a matrix of fragmented sedimentary or pyroclastic material (Figs. 3.4, 3.6). The

main DAD has a concordant upper contact with the disturbed bedded pyroclastic group (Figs. 3.3, 3.4) and is crosscut by a unit of non-bedded pyroclastic rocks (nTBI, Fig. 3). The multiple smaller DADs (aTBh facies, Fig. 3.14) have a discordant lower contact with disturbed bedded pyroclastic rocks and the non-bedded pyroclastic rocks, and are conformably overlain by rocks of the undisturbed bedded pyroclastic group.

3.6 Componentry

3.6.1 Field line counts

Field line counts were carried out at 20 sites in disturbed bedded pyroclastic rocks, 17 sites in non-bedded pyroclastic rocks and six sites in pyroclastic megablocks. No line counts were done in the undisturbed bedded pyroclastic rocks because this group was inaccessible. Table 3.2 presents the raw data and gives the location of the different sites on figures. The proportion of undifferentiated matrix + cement is smallest in the non-bedded pyroclastic rocks (68%), intermediate in the disturbed bedded rocks (74%), and largest in the pyroclastic megablocks (83%). In other words, the non-bedded pyroclastic rocks are the coarsest-grained, and the pyroclastic megablocks are the finest-grained of the studied facies groups. The Mann-Witney U test (Davis 2002), a non-parametric statistical test, confirms that the difference of the distribution between the pyroclastic megablocks and the other facies groups is statistically significant at the 95% level (Table 3.3). However, given the relatively low number of measured sites, there is not enough information to confirm statistically that the non-bedded pyroclastic rocks are indeed coarser than the disturbed bedded rocks on average (Table 3.3).

We also recalculated to 100% the proportions of juvenile versus lithic fragments among clasts larger than or equal to 4 mm, to better compare the componentry of different groups of facies. This highlighted that on average, rocks from the disturbed bedded pyroclastic group contain 75% juvenile clasts (25% lithics) whereas rocks from the non-bedded pyroclastic group contain 84% juvenile clasts (16% lithics). Pyroclastic megablocks contain fewer juvenile clasts, 73% on average (27% lithics) within the counted fragments. Most of these differences are not statistically significant, except the lithic enrichment in the disturbed bedded group relative to the non-bedded group (Table 3.3). No significant differences were found in the relative proportion of lithics ($L/(L+J)$) between pyroclastic megablocks and the two other group of facies (Table 3.3). Lithic clasts originate mainly from the Bidahochi and Moenave Formations, whereas Chinle and Moenkopi Formations clasts are found in trace proportions (Table 3.2); this is discussed in more detailed below.

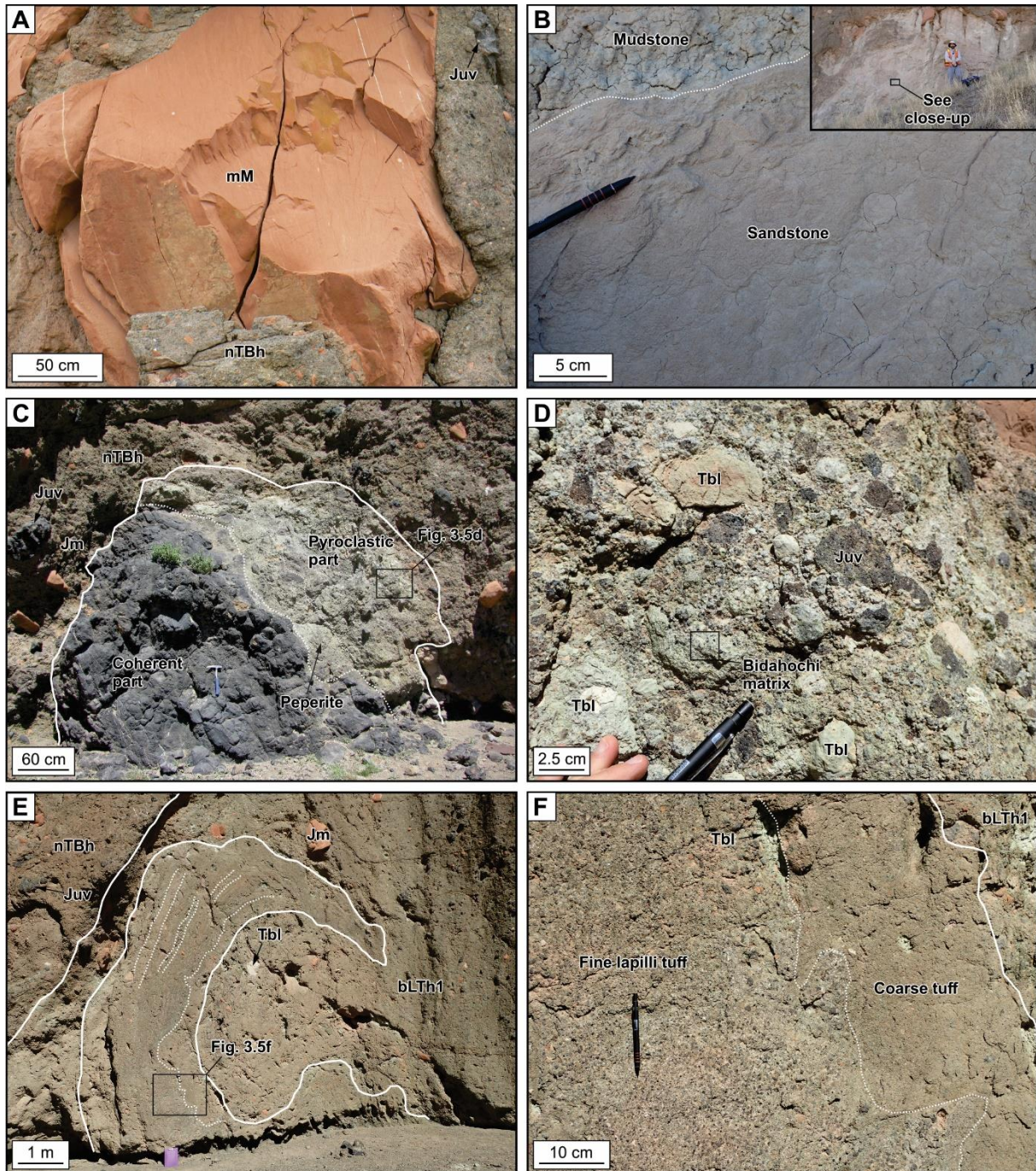


Figure 3.5: Photo plate of the megablocks. A) Red sandstone to siltstone from Moenave Formation (mM). B) Close-up of whitish sandstone to greenish mudstone from Bidahochi Formation. Inset shows the entire megablock (mB, Fig. 3.12). C) Composite mLTb megablock displaying a coherent basanite part and a pyroclastic part separated by a peperitic zone. D) Close-up of the pyroclastic rock in the mLTb megablock, displaying a high content of Bidahochi clasts and brown to grey juvenile clasts, within a whitish matrix rich in disaggregated Bidahochi sediment. E) C-shape mLTh megablock composed of thin beds of coarse tuff to fine lapilli tuff. F) Close-up on the irregular contact of two beds in a mLTh megablock. For facies codes, see Latutrie and Ross (2019) and Table 3.1. Abbreviations: Tbl=Bidahochi clasts, Jm=Moenave clasts and Juv=Juvenile clasts.

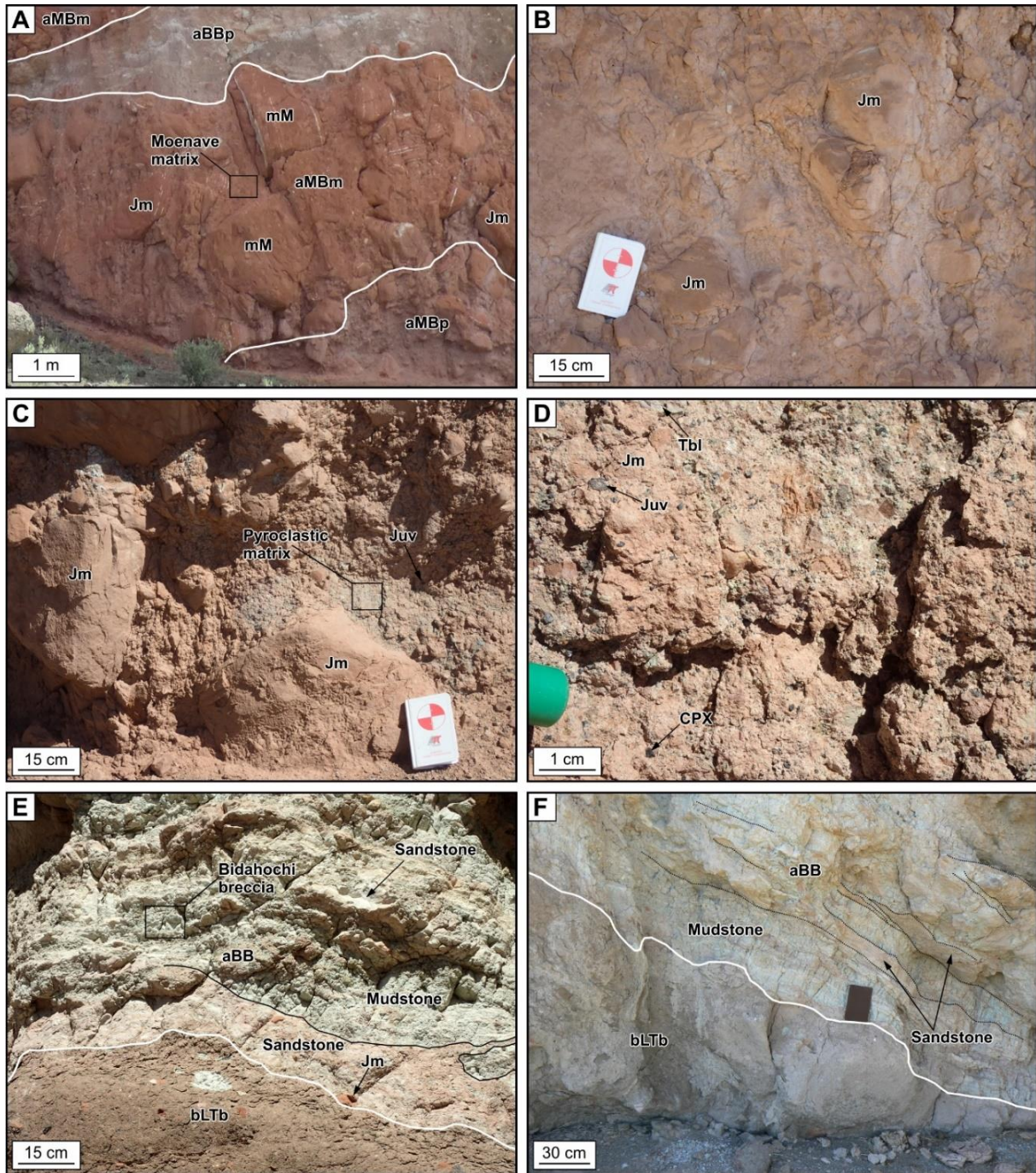


Figure 3.6: Photo plate of the facies in the main DAD. A) aMBm facies composed of Moenave megablocks and blocks, located between aMBp and aBBp facies. B) Close-up on the Moenave matrix of the aMBm facies. C) aMBp facies displaying a pyroclastic matrix between big blocks of Moenave Formation. D) Close-up on the pyroclastic matrix of the aMBp facies. E) More brecciated aBB facies just above a bLTb bed. F) Bedding in the aBB facies with remnants of beds of sandstone surrounded by mudstone. For facies codes, see Latutrie and Ross (2019) and Table 3.1. Abbreviations: Tbl=Bidahochi clasts, Jm=Moenave clasts, Juv=Juvenile clasts, CPX=free clinopyroxene.

Table 3.1: Characteristics of megablocks and the debris avalanche deposits (DADs)

Facies code	Name	Description	Panoramas (Fig. nb)
<i>Megablocks</i>			
mM	Megablocks of Moenave Formation	Sub-rounded to angular, 5 m maximum size, homogeneous megablocks composed of orange fine sandstone to siltstone (Fig. 3.5a) sometimes with white spots or white lines.	3.3, 3.4, 3.9, 3.10, 3.12, 3.14, 3.15
mB	Megablocks of Bidahochi Formation (Lower and Middle)	Sub-rounded to irregular (liquefied) megablocks up to 7 m across. Mainly heterogeneous, composed of whitish to purplish fine sandstone to whitish to greenish mudstone (Fig. 3.5b). External parts are sometimes intruded by small tuff dikes (~cm to dm thick). Some megablocks display thin bands (cm thick) rich in free pyroxenes and juvenile clasts.	3.3, 3.9 to 3.12, 3.14, 3.15
mC	Megablocks of Chinle Formation	Two megablocks (tens of meters) are preserved in pyroclastic rocks cropping out on floor around the Round Butte cliffs (Fig. 3.1c). They are not well exposed, are purplish in color and probably composed of sediments from the Owl Rock Member.	-
mJ	Juvenile megablocks	Sub-round to irregular very large juvenile bombs of basanite, vesicles are often filled by calcite or zeolites.	3.9
mLTb	Megablock composed of two parts, lapilli tuff (Bidahochi-rich) and coherent basanite	Sub-rounded composite megablock ~3 m in diameter <u>Coherent basanite part (Fig. 3.5c)</u> : 10-15% serpentinized olivine, ~20% clinopyroxene, traces of phlogopite, 20-60% vesicles. At the contact with the pyroclastic part, diffuse jointing occurs. <u>Pyroclastic part (Fig. 3.5d)</u> : 5% b&b (Juv ≈ Tbl), 50% lapilli (50-80% Juv and 20-50% Tbl), 43% ash (rich in Bidahochi mud and brown juvenile ash), 2% scattered cement. 50% of juvenile clasts are brown.	3.3
mLTh	Megablocks of lapilli tuff, heterolithic, bedded to non-bedded	Megablocks of 10 m maximum size, overall shape is elongated, sub-round, irregular or in 'c' (Figs. 3.5e, 3.5f). Within megablocks: 0-3% b&b (Tbl ≥ Jm > Juv), 15-60% lapilli (Juv ≥ Tbl, Jm, TRc, TRm), 54-80% ash (Juv and Lith), 0-15% cement. Traces of brown juvenile clasts. Local beds of coarse tuff, bed thickness from cm to m.	3.3, 3.10, 3.11, 3.14, 3.15
<i>Debris avalanche deposits (DADs)</i>			
aMBm	Moenave breccia with a Moenave matrix	Moenave Formation brecciated into clasts mm to several meters across (Figs. 3.6a, 3.6b).	3.3, 3.4
aMBp	Moenave breccia with a pyroclastic matrix	Moenave Formation fragments (block- to lapilli-sized) with a pyroclastic matrix composed of grey juvenile clasts, free clinopyroxenes and Bidahochi clasts (Figs. 3.6c, 3.6d).	3.3, 3.4
aBB	Bidahochi breccia (bedded to remobilized)	Facies only composed of Bidahochi Formation clasts (block- to ash-sized) with brecciated to bedded parts (Figs. 3.6e, 3.6f). Beds are few cm to m thick, comprising greenish-white mudstone and purplish fine sandstone.	3.3, 3.4
aBBp	Bidahochi breccia with a pyroclastic matrix	Facies mainly composed of Bidahochi Formation clasts (block- to ash-sized) with an ash-rich pyroclastic matrix composed of Moenave and juvenile clasts.	3.3, 3.15
aTBh	Tuff breccia, heterolithic, with blocks of Moenave Fm and Bidahochi Fm	Facies that fills channels above the unconformity, composed of a mixture of Moenave, Bidahochi and juvenile clasts in a pyroclastic matrix.	3.14

Juv = Juvenile clasts, Lith = Lithic clasts, Jm = Moenave Fm clasts, Tbl = Bidahochi Fm clasts, TRc = Chinle Fm clasts, TRm = Moenkopi Fm clasts, b&b = blocks and bombs

Table 3.2: Results of field line counts, expressed as percentages of clasts larger than, or equal to, 4 mm

Facies code*	Site number	Panorama (Fig. nb)	Line count numbers	Juvenile clasts								Lithic clasts						Tuff clasts	Matrix (< 4 mm) + cement
				Brown	Light grey	Medium grey	Dark grey	Black	Undiff.	CPX and phlogopite	Total	Bidahochi Fm	Moenave Fm	Chinle Fm	Moenkopi Fm	Undiff.	Total		
<i>Disturbed bedded pyroclastic rocks</i>																			
bLTb	b1	3.15	35:36:37	1.5	0.0	1.7	0.2	0.0	0.0	0.2	3.6	0.8	3.2	0.1	0.0	0.1	4.3	1.4	90.7
bLTb	b2	3.15	38:39:40	0.0	0.9	0.0	0.6	1.1	1.0	0.3	3.9	2.6	7.7	0.0	0.0	0.0	10.3	0.0	85.8
bLTh1	b3	3.3	04:07:08	0.7	1.9	3.4	6.1	2.0	0.5	0.3	14.9	6.3	9.1	0.0	1.3	0.2	16.9	0.0	68.2
bLTh1	b4	3.3	10:11:12	0.2	4.2	5.7	11.8	2.1	0.0	0.2	24.2	1.1	2.3	0.0	0.8	1.9	6.1	0.8	68.9
bLTh1	b5	3.3	13:14:15	0.2	1.4	3.7	6.7	0.9	0.0	0.1	13.0	0.8	2.5	0.0	0.9	1.1	5.3	3.9	77.8
bLTh1	b6	3.12	124:125:126	0.5	8.1	4.5	10.3	0.6	0.0	0.3	24.3	7.2	3.6	0.5	0.0	0.5	11.8	0.0	63.9
bLTh1	b7	3.15	32:33:34	2.5	2.8	1.9	17.6	3.0	0.4	0.3	28.5	0.0	3.8	0.0	0.1	2.5	6.4	0.0	65.1
bLTh1	b8	3.15	41:42:43	0.6	0.5	1.1	11.2	7.1	0.5	0.0	21.0	0.0	7.5	1.0	0.1	0.3	8.9	0.0	70.1
bLTh1	b9	3.14	44:45:46	0.3	1.3	7.1	5.5	0.0	0.0	0.0	14.2	0.4	1.3	0.0	0.0	0.2	1.9	0.0	83.9
bLTh1	b10	3.14	58:59:60	0.0	2.8	4.2	5.8	0.0	0.8	0.1	13.7	0.3	0.7	0.0	0.0	0.9	1.9	0.0	84.4
bLTh1	b11	3.9	47:48:49	0.3	1.3	4.6	11.2	2.1	0.0	0.7	20.2	0.0	4.8	0.0	0.0	0.0	4.8	0.0	75.0
bLTh1	b12	3.9	50:51:52	0.0	1.7	5.9	14.6	1.6	0.0	0.0	23.8	3.8	1.2	0.4	0.0	0.2	5.6	0.0	70.6
bLTh1	b13	3.10	67:68:69	0.2	1.2	3.1	16.2	3.5	0.0	0.1	24.3	0.2	6.2	0.0	0.0	0.3	6.7	0.0	69.0
bLTh1	b14	3.10	73:74:75	0.0	2.1	6.7	8.5	2.6	0.0	0.3	20.2	0.4	3.0	0.0	1.0	0.0	4.4	0.0	75.4
bLTh1	b15	3.10	76:77:78	1.0	8.5	5.0	4.2	0.3	3.6	0.5	23.1	0.0	7.5	0.0	0.0	0.2	7.7	0.0	69.2
bLTh1	b16	3.11	88:89:90	1.6	1.7	4.2	13.8	0.4	1.4	1.3	24.4	0.6	1.8	0.0	0.0	0.4	2.8	0.0	72.8
bLTh1	b17	3.11	94:95:96	0.1	2.8	8.3	16.5	1.4	0.0	0.0	29.1	0.7	3.8	0.0	0.0	0.1	4.6	0.0	66.3
bLTh1	b18	3.11	79:80:81	0.0	0.5	1.8	12.9	8.4	0.6	0.3	24.5	0.0	1.4	0.0	0.3	0.8	2.5	0.0	73.0
bLTh1	b19	3.11	82:83:84	0.4	3.5	10.8	12.5	1.3	0.2	0.8	29.5	0.1	2.1	0.2	0.0	0.0	2.4	0.0	68.1
bTBI	b20	3.3	30:31:32	0.0	1.6	6.9	10.5	2.2	0.0	0.0	21.2	0.0	3.9	0.8	0.0	0.0	4.7	0.0	74.1
Mean	-	-	-	0.5	2.4	4.5	9.8	2.0	0.5	0.3	20.1	1.3	3.9	0.2	0.2	0.5	6.0	0.3	73.6
<i>Non-bedded pyroclastic rocks</i>																			
n(m)LTh	n1	3.3	01:02:03	0.2	1.2	1.5	3.4	1.3	0.0	0.0	7.6	3.7	2.2	0.0	1.5	0.0	7.4	0.0	85.0
n(m)LTh	n2	3.12	109:110:111	0.3	1.6	3.5	5.7	0.9	0.1	1.1	13.2	1.6	0.5	0.0	0.0	0.3	2.4	0.0	84.4
n(m)LTh	n3	3.14	127:128:129	0.0	2.7	1.6	6.2	0.0	0.3	0.0	10.8	0.0	0.3	0.0	0.0	0.0	0.3	0.0	88.9
n(mc)LTh1	n4	3.3	16:17:18	0.0	1.2	10.4	10.7	5.9	0.0	0.4	28.6	2.0	2.8	0.0	0.2	0.0	5.0	1.3	65.1
n(mc)LTh1	n5	3.3	19:20:21	0.9	1.3	4.8	15.5	1.2	0.0	0.1	23.8	11.7	9.5	0.0	0.0	0.0	21.2	1.3	53.7
n(mc)LTh2	n6	3.12	121:122:123	1.2	5.1	3.7	13.6	0.5	0.0	0.3	24.4	0.1	4.5	0.0	0.0	0.3	4.9	0.0	70.7
n(mc)LTh2	n7	3.14	64:65:66	0.0	3.5	8.9	9.2	0.2	0.0	0.0	21.8	0.0	6.6	0.4	0.0	0.3	7.3	0.8	70.1
n(mc)LTh2	n8	3.11	97:98:99	1.2	5.7	6.5	17.0	2.9	0.2	0.8	34.3	0.6	0.4	0.0	0.0	0.2	1.2	0.0	64.5

n(mc)LTh2	n9	3.11	100:101:102	0.7	5.9	6.3	11.3	0.6	0.1	0.3	25.2	1.1	0.0	0.0	0.8	0.0	1.9	0.0	72.9
n(mc)LTh2	n10	3.13	103:104:105	1.2	1.4	4.4	30.3	2.1	0.0	0.5	39.9	0.2	1.0	0.0	0.0	0.5	1.7	0.0	58.4
n(c)LTj	n11	3.12	106:107:108	1.7	2.5	5.8	22.1	4.4	0.0	0.7	37.2	0.7	1.4	0.0	0.0	0.2	2.3	0.0	60.5
n(c)LTj	n12	3.12	115:116:117	0.3	4.2	4.7	18.2	0.7	0.0	0.2	28.3	0.0	0.4	0.0	0.0	0.1	0.5	0.5	70.7
n(c)LTj	n13	3.12	118:119:120	0.4	3.9	4.6	22.9	0.7	0.3	1.1	33.9	0.7	0.3	0.2	0.0	0.0	1.2	0.0	64.9
nTBh	n14	3.3	5:6:9	0.4	1.6	8.1	6.2	8.0	0.7	0.1	25.1	0.6	13.5	0.0	4.6	0.3	19.0	0.0	55.9
nTBh	n15	3.3	27:28:29	0.9	8.0	11.5	11.3	0.0	0.0	0.0	31.7	0.6	6.3	0.6	0.0	0.3	7.8	0.7	59.8
nTBh	n16	3.12	112:113:114	0.6	2.8	6.8	31.6	1.2	0.2	0.6	43.8	0.5	2.0	0.0	0.0	0.0	2.5	0.0	53.7
nTBh	n17	3.9	53:54:55	0.3	1.8	4.3	13.7	4.0	0.6	0.5	25.2	0.0	2.6	0.0	0.2	0.5	3.3	0.0	71.5
Mean	-	-	-	0.6	3.2	5.7	14.6	2.0	0.1	0.4	26.8	1.4	3.2	0.1	0.4	0.2	5.3	0.3	67.7
<i>Pyroclastic megablocks</i>																			
mLTb	m1	3.3	25:26	3.3	1.2	2.2	8.2	0.6	5.0	0.6	21.1	2.5	0.0	0.0	0.0	0.0	2.5	0.0	76.4
mLTh	m2	3.3	22:23:24	2.2	0.7	2.0	4.4	2.4	0.0	0.3	12.0	2.8	0.4	0.7	0.2	0.1	4.2	0.0	83.8
mLTh	m3	3.14	61:62:63	0.0	0.6	1.4	8.3	1.8	0.2	0.6	12.9	0.2	0.8	0.6	0.0	0.2	1.8	0.0	85.3
mLTh	m4	3.10	70:71:72	0.1	0.1	0.6	4.2	4.7	0.5	0.3	10.5	0.0	2.2	0.0	0.2	0.9	3.3	0.0	86.2
mLTh	m5	3.11	85:86:87	0.0	4.3	5.4	1.2	0.0	0.0	0.2	11.1	4.4	2.7	0.0	0.0	0.0	7.1	0.0	81.8
mLTh	m6	3.11	91:92:93	0.0	3.7	3.4	0.8	0.1	0.1	0.2	8.3	2.9	4.2	0.0	0.0	0.7	7.8	1.2	82.7
Mean	-	-	-	0.9	1.8	2.5	4.5	1.6	1.0	0.4	12.7	2.1	1.7	0.2	0.1	0.3	4.5	0.2	82.7

*Facies codes of the disturbed bedded pyroclastic rocks and the non-bedded pyroclastic rocks are detailed in Latutrie and Ross (2019)

3.6.2 Field clast counts

Field clast counts were carried out at five sites in disturbed bedded pyroclastic rocks, seven sites in non-bedded pyroclastic rocks and three sites in pyroclastic megablocks. No clast counts were done in the undisturbed bedded pyroclastic rocks because this group was unreachable. Table 3.4 provides the raw data, the location of the clast counts sites on figures and the name of the line count site used for comparison. The matrix + cement proportion is the highest in the pyroclastic megablocks (80%), intermediate in the disturbed bedded rocks (63%) and the lowest in the non-bedded pyroclastic rocks (60%). Again, the pyroclastic megablocks are the finest-grained of the studied facies groups at Round Butte and the non-bedded pyroclastic rocks are the coarsest-grained.

Table 3.3 Mann-Witney U Test¹ on componentry data for different facies groups

	<i>Matrix + cement</i> ²			<i>L/(L+J)</i> ³		
	Disturbed bedded rocks	Non-bedded rocks	Pyroclastic megablocks	Disturbed bedded rocks	Non-bedded rocks	Pyroclastic megablocks
Line counts						
Disturbed bedded rocks	-	-	-	-	-	-
Non-bedded rocks	N ⁴	-	-	Y ⁴	-	-
Pyroclastic megablocks	Y	Y	-	N	N	-
Clast counts						
Disturbed bedded rocks	-	-	-	-	-	-
Non-bedded rocks	N	-	-	N	-	-
Pyroclastic megablocks	N	N	-	N	N	-
Petrographic point counts						
Disturbed bedded rocks	-	-	-	-	-	-
Non-bedded rocks	-	-	-	N	-	-
Pyroclastic megablocks	-	-	-	N	N	-

¹ Null hypothesis for the statistical test: the two “groups” (here componentry datasets for different facies groups) come from populations with equal distributions (i.e., the difference in group distributions could be due to random sampling variability alone). Alternative hypothesis: the populations have different distributions.

² Matrix + cement is the proportion of material not consisting of clasts 4 mm or larger in the field componentry. Not applicable to petrographic point counts.

³ $L/(L+J)$ is the relative proportion of lithic (L) fragments, relative to the sum of lithics and juvenile (J) fragments.

⁴ Y = Yes, there is a significant difference in distributions (we reject the null hypothesis and accept the alternative, i.e., the populations are different); N = there is not a significant difference in distributions (we fail to reject the null hypothesis). Note that ‘N’ does not mean that the populations are *proven* to be the same. They could still be different, but there is not enough data to show it, given the large standard deviations.

The proportion of juvenile versus lithic clasts among clasts larger than or equal to 4 mm was recalculated to 100% for the different groups of facies. On average, the non-bedded pyroclastic

rocks are the richest in juvenile clasts with 82% (18% lithics) whereas rocks of the disturbed bedded group display an intermediate value of 71% (29% lithics) and the pyroclastic megablocks are the poorest in juvenile clasts with 66% (34% lithics). These averages are not directly comparable to those of the line count method because there are more line counts than clast counts, but we compare the data acquired by both methods at the same 15 sites below.

The Mann-Witney U test was not able to confirm significant differences in the distribution of matrix + cement or the relative proportion of lithic versus juvenile clasts ($L/(L+J)$) between the disturbed bedded rocks, non-bedded rocks and pyroclastic megablocks (Table 3.3). This is probably due to small sample sizes and internal variability within the facies groups.

3.6.3 Petrographic point counts

Whereas the field componentry methods focused on large clasts (≥ 4 mm), the petrographic point counts provide componentry information on the matrix (clasts < 4 mm). We point counted six regularly-sized thin sections of bedded pyroclastic rocks, nine of non-bedded pyroclastic rocks and three of pyroclastic megablocks. No data is available for the undisturbed bedded pyroclastic group because we were unable to sample it. Table 3.5 presents the results of the petrographic point counts and the location of the samples on figures. The “unresolved” column, ranging from 6% to 50%, represents very fine-grained material that could not be assigned to a specific category based on petrography: it probably consists of a mixture of altered juvenile ash and sedimentary mud. This abundance of very fine components in most samples confirms the poorly sorted nature of the rocks.

When only the known juvenile and lithic clasts are considered and the total is recalculated to 100%, juvenile fragments represent 87% of the counted clasts in the disturbed bedded group, on average (13% lithics), 90% of the non-bedded group (10% lithics), and 79% of pyroclastic megablocks (21% lithics). Table 3.3 highlights results of the Mann-Witney U test only on the relative proportion of lithics ($L/(L+J)$) because the category matrix + cement is not applicable to the petrographic point counts. The Mann-Witney U test did not confirm that these differences are statistically significant. A calcite-rich cement is present with the mean modal proportion at 8% and a range from near 0% to 23%.

Table 3.4: Results of field clast counts, expressed as percentages of clasts larger than, or equal to, 4 mm

Facies code*	Line count sites	Panorama (Fig. nb)	Clast count sites	Juvenile clasts							Lithic clasts					Tuff clasts	Cement	Matrix (< 4 mm)		
				Brown	Light grey	Medium grey	Dark grey	Black	Undiff.	CPX and phlogopite	Total	Bidahochi Fm	Moenave Fm	Chinle Fm	Moenkopi Fm				Undiff.	Total
<i>Disturbed bedded pyroclastic rocks</i>																				
bLTh1	b7	3.15	14	3.3	1.1	12.1	5.5	5.5	0.0	0.0	27.5	0.0	2.2	0.0	1.1	0.0	3.3	0.0	3.3	65.9
bLTh1	b8	3.15	15	0.0	0.0	8.9	6.9	0.0	0.0	0.0	15.8	0.0	17.8	1.0	1.0	1.0	20.8	0.0	6.9	56.4
bLTh1	b17	3.11	8	3.5	2.4	20.0	5.9	2.4	0.0	2.4	36.5	4.7	3.5	0.0	0.0	0.0	8.2	0.0	2.4	52.9
bLTh1	b19	3.11	5	1.2	4.7	12.8	10.5	0.0	0.0	1.2	30.2	1.2	8.1	0.0	0.0	1.2	10.5	0.0	12.8	46.5
bTBI	b20	3.3	2	1.0	7.1	7.1	7.1	0.0	0.0	0.0	22.4	0.0	10.2	0.0	0.0	0.0	10.2	1.0	0.0	66.3
Mean	-	-	-	1.8	3.0	12.2	7.2	1.6	0.0	0.7	26.5	1.2	8.4	0.2	0.4	0.4	10.6	0.2	5.1	57.6
<i>Non-bedded pyroclastic rocks</i>																				
n(mc)LTh1	n5	3.3	3	0.0	8.0	3.0	2.0	16.0	0.0	0.0	29.0	3.0	9.0	1.0	0.0	0.0	13.0	0.0	0.0	58.0
n(mc)LTh2	n7	3.14	12	7.4	1.1	12.8	12.8	8.5	0.0	0.0	42.6	1.1	5.3	0.0	0.0	1.1	7.4	0.0	2.1	47.9
n(mc)LTh2	n8	3.11	9	2.0	11.2	9.2	12.2	3.1	0.0	0.0	37.8	0.0	7.1	0.0	0.0	0.0	7.1	0.0	17.3	37.8
n(c)LTj	n11	3.12	11	0.0	5.0	6.0	5.0	1.0	0.0	0.0	17.0	0.0	2.0	0.0	0.0	1.0	3.0	0.0	4.0	76.0
n(c)LTj	n12	3.12	10	5.7	11.4	2.3	10.2	17.0	0.0	0.0	46.6	1.1	3.4	0.0	0.0	0.0	4.5	0.0	8.0	40.9
nTBh	n15	3.3	16	0.0	8.9	11.1	16.7	3.3	0.0	0.0	40.0	1.1	6.7	0.0	0.0	1.1	8.9	2.2	2.2	46.7
nTBh	n17	3.9	4	0.0	1.0	4.0	5.1	3.0	0.0	0.0	13.1	2.0	3.0	0.0	0.0	0.0	5.1	0.0	0.0	81.8
Mean	-	-	-	2.2	6.7	6.9	9.1	7.4	0.0	0.0	32.3	1.2	5.2	0.1	0.0	0.5	7.0	0.3	4.8	55.6
<i>Pyroclastic megablocks</i>																				
mLTh	m3	3.14	13	0.0	4.0	4.0	2.0	3.0	0.0	0.0	13.1	0.0	2.0	0.0	0.0	0.0	2.0	0.0	0.0	84.8
mLTh	m5	3.11	6	0.0	5.9	8.9	1.0	0.0	0.0	1.0	16.8	0.0	4.0	1.0	0.0	1.0	5.9	0.0	0.0	77.2
mLTh	m6	3.11	7	0.0	3.0	1.0	3.0	0.0	0.0	1.0	8.0	6.0	5.0	1.0	0.0	0.0	12.0	2.0	0.0	78.0
Mean	-	-	-	0.0	4.3	4.7	2.0	1.0	0.0	0.7	12.7	2.0	3.7	0.7	0.0	0.3	6.7	0.7	0.0	80.0

*Facies codes of the disturbed bedded pyroclastic rocks and the non-bedded pyroclastic rocks are detailed in Latutrie and Ross (2019)

Table 3.5: Results of petrographic point counts measurements, expressed as modal percentages

Facies code*	Sample	Panorama (Fig. nb)	Juvenile clasts							Lithic clasts					Tuff clasts	Calcite cement	Void ²	Unresolved
			Brown	Light grey ¹	Grey (medium to dark)	Black	Undiff.	CPX and phlogopite	Total	Sandstone	Siltstone	Mudstone	Quartz	Total				
<i>Disturbed bedded pyroclastic rocks</i>																		
bT1	RB-40	3.12	9.3	25.3	6.4	0.4	7.3	5.3	54.2	0.0	4.7	3.8	2.0	10.5	0.0	1.1	0.7	33.6
bLTb	RB-14	3.3	6.0	9.6	16.4	2.4	4.7	2.7	41.8	0.7	2.4	0.0	2.4	5.6	0.0	0.0	2.7	50.0
bLTb	RB-18	3.15	0.7	22.7	6.4	4.4	0.4	2.7	37.3	0.0	4.4	3.8	6.4	14.7	0.0	1.3	1.3	45.4
bLTh1	RB-04	3.3	1.3	15.8	37.6	4.7	2.7	2.7	64.7	0.0	1.3	2.0	1.1	4.4	0.0	11.8	0.4	18.7
bLTh1	RB-33	3.11	5.3	14.2	23.3	8.0	1.6	7.6	60.0	0.0	0.4	0.2	0.4	1.1	0.0	14.0	2.4	22.5
bLTh1	RB-16	3.15	4.9	14.9	22.9	8.0	3.8	1.8	56.2	0.9	5.8	1.6	1.3	9.6	0.0	8.7	0.0	25.6
Mean	-	-	3.6	17.1	18.9	4.7	3.4	3.8	52.4	0.3	3.2	1.9	2.3	7.6	0.0	6.1	1.3	32.6
<i>Non-bedded pyroclastic rocks</i>																		
n(m)LTh	RB-01	3.3	9.3	27.8	17.1	0.4	8.7	3.1	66.4	0.0	2.4	1.1	0.7	4.2	0.0	23.3	0.4	5.6
n(m)LTh	RB-38	3.12	2.7	9.1	25.6	7.1	3.6	3.6	51.6	0.0	2.7	1.6	2.9	7.1	0.0	1.3	2.9	37.1
n(mc)LTh1	RB-05	3.3	5.1	14.7	22.2	1.1	5.3	5.6	54.0	0.0	8.9	0.7	0.9	10.5	0.0	4.7	0.7	30.2
n(mc)LTh2	RB-43	3.12	13.6	16.2	11.3	0.2	3.6	7.6	52.5	0.0	3.6	1.1	2.0	6.7	0.0	0.2	0.4	40.2
n(mc)LTh2	RB-26	3.13	5.1	16.9	26.9	6.4	2.0	3.1	60.4	0.0	2.7	1.3	2.4	6.4	0.0	20.7	0.2	12.2
n(c)LTj	RB-37	3.12	11.1	20.4	20.7	2.2	1.8	7.1	63.3	0.0	1.1	0.4	0.4	2.0	0.0	9.8	0.2	24.7
n(c)LTj	RB-42	3.12	7.1	5.6	23.8	16.0	2.9	4.7	60.0	0.0	0.9	1.3	0.4	2.7	0.0	15.1	0.4	21.8
nTBh	RB-03	3.3	2.4	31.8	13.1	5.8	3.6	2.7	59.3	0.0	6.2	2.2	1.3	9.8	0.0	10.9	0.0	20.0
nTBh	RB-39	3.12	2.7	14.9	35.6	3.1	0.7	2.4	59.3	1.8	2.9	2.7	1.8	9.1	0.0	10.2	0.2	21.1
Mean	-	-	6.6	17.5	21.8	4.7	3.6	4.4	58.5	0.2	3.5	1.4	1.4	6.5	0.0	10.7	0.6	23.7
<i>Pyroclastic megablocks</i>																		
mLTb	RB-07	3.3	35.8	3.1	19.0	1.1	2.9	3.3	65.2	0.0	3.6	1.3	0.2	5.1	0.0	15.8	2.0	11.9
mLTh	RB-06	3.3	12.9	13.3	20.0	1.3	3.8	4.4	55.8	0.0	1.8	1.8	5.6	9.1	0.0	1.8	0.0	33.3
mLTh	RB-34	3.11	4.4	8.9	6.9	1.6	3.8	3.6	29.1	1.1	7.3	6.7	5.3	20.4	1.8	0.9	1.8	46.0
Mean	-	-	17.7	8.4	15.3	1.3	3.5	3.8	50.0	0.4	4.2	3.3	3.7	11.6	0.6	6.2	1.3	30.4

*Facies codes of the disturbed bedded pyroclastic rocks and the non-bedded pyroclastic rocks are detailed in Latutrie and Ross (2019)

¹ Clasts that are “light grey” in the field or in polished slabs are dark brown petrographically.

² The void category is composed the porosity of the rock, some of which might be related to the thin section-making process

3.7 Types of clasts

3.7.1 Lithic clasts

The most commonly identified clasts within the Round Butte massif are from the Bidahochi and Moenave Formations, i.e. from stratigraphic levels equal to, or higher than, the current elevation of the fragments in the diatreme. Chinle and Moenkopi clasts are much less common, and travelled mostly upward to their current locations (Fig. 3.1). Some of the lithic clasts could not be assigned to a specific formation and some unassigned clasts may have a deeper origin (Billingsley et al. 2013).

Some Bidahochi clasts consist of finely bedded sandstone composed of juvenile clasts in a fine whitish matrix (Fig. 3.7a). However, most are whitish to purplish fine sandstone as well as whitish, reddish or greenish mudstone (Figs. 3.5b, 3.5d, 3.6e, 3.6f, 3.7b), without obvious juvenile constituents. The size of Bidahochi fragments ranges from ash (disaggregated sedimentary particles within the matrix of pyroclastic rocks) to megablocks (Fig. 3.3). Sandstone fragments are angular in shape whereas the liquefied to brecciated mudstone clasts are sub-rounded to amoeboid (Figs. 3.3, 3.5d, 3.6e, 3.6f, 3.7a, 3.7b).

Moenave clasts are angular to sub-rounded with a size from coarse ash to megablocks. They are orange with occasional white spots or lines and are composed of competent fine sandstone to siltstone (Figs. 3.3, 3.5a, 3.6a, 3.7c).

Chinle clasts are present in the diatreme with sizes ranging from ash to megablocks. Owl Rock Member clasts are the most obvious in the massif and Owl Rock megablocks are observable in the diatreme margins (Fig. 3.1c). Identifiable Owl Rock clasts in the massif are mostly from competent interbeds of light-purple limestone with a sub-rounded to angular shape (Fig. 3.7d). Siltstone clasts within the massif can originate from the Owl Rock or the Petrified Forest Members. Petrified Forest clasts are mostly multicolor siltstones (Fig. 3.7e). Shinarump Member fragments are white to yellowish, medium to coarse sandstone (Fig. 3.7f).

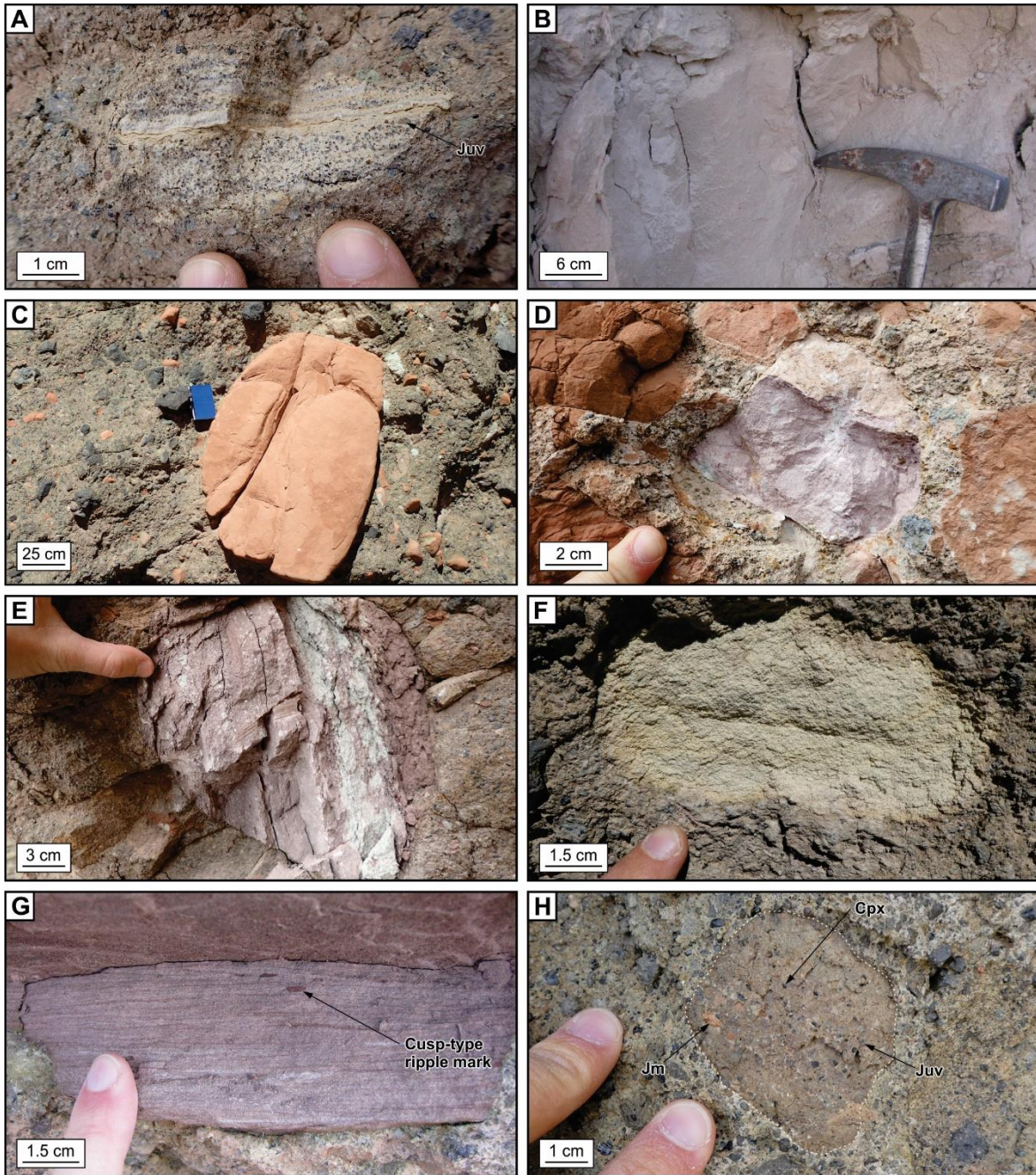


Figure 3.7: Photo plate showing the diversity of lithic clasts, and a tuff clast, in the pyroclastic rocks of Round Butte. A) Finely bedded, juvenile-bearing clast from the Bidahochi Formation, B) whitish fine argillaceous sandstone of the Bidahochi Formation, C) reddish fine sandstone to siltstone of the Moenave Formation, D) purplish limestone of the Owl Rock member of the Chinle Formation, E) purplish to whitish bedded siltstones of the Petrified Forest member of the Chinle Formation, F) yellowish coarse sandstone of the Shinarump Member of the Chinle Formation, G) purplish-brown siltstone to sandstone of the Holbrook/Moqui Member of the Moenkopi Formation and H) sub-round tuff clast rich in juvenile and lithic (Moenave Formation) fragments. Abbreviations: Jm=Moenave clasts, Juv=Juvenile clasts, CPX=free clinopyroxene.

Angular clasts from the Holbrook Member of the Moenkopi Formation are present (Tables 3.2, 3.4). They are purplish-brown to greenish-grey fine sandstone to siltstone, mainly composed of

quartz and mostly white micas (Fig. 3.7g). Clasts of the massive sandstone Member of the Moenkopi Formation are not identifiable either because they are absent or because they look like the Moenave Formation clasts.

3.7.2 Tuff clasts

Rare clasts of tuff have been found within coarser pyroclastic rocks in the diatreme. They are light brown to purplish-beige and are mainly sub-rounded to rarely angular in shape. These recycled tuff clasts are composed of juvenile and lithic fragments, often including Moenave clasts (Fig. 3.7h), and are classified as lithic clasts in the White and Houghton (2006) scheme but were not considered in field componentry measurements. The distinction between these tuff clasts and the Bidahochi Formation clasts rich in juvenile fragments is based on the proportion of juvenile clasts (more abundant in the tuff fragments) versus pale sediment (more abundant in the Bidahochi Formation clasts). Also, Moenave clasts are only typically found within the tuff fragments.

3.8 Country rock fragmentation model of Round Butte

In this section we present a conceptual model of country rock fragmentation during crater and diatreme formation at Round Butte. We calculate the 'theoretical' proportions of lithic fragments expected in the diatreme and compare those with actual componentry measurements. This is a forward modeling approach where we vary the model parameters and compare the results with the componentry data obtained in the field to constrain the approximate shape and volume of the diatreme, including for the unexposed and eroded portions.

3.8.1 Model parameters

Using a model similar to that of Lefebvre et al. (2013) for West Standing Rocks, we calculated the 'theoretical' volumes and proportions of each sedimentary formation fragmented during the creation of the syn-eruptive crater and diatreme at Round Butte. Thicknesses of the different sedimentary formations were derived from our observations around Round Butte and from regional observations of Billingsley et al. (2013), as compiled in the stratigraphic log (Fig. 3.1). The modeled fragmentation volume is a cone representing the crater and diatreme at the end of the eruption. Field observations show that the diatreme is 180 m in diameter at 190 m below the pre-eruptive surface and this is incorporated into the models (green dashed lines in Fig. 3.8). We explored a range of scenarios for diatreme wall angles in the Bidahochi and in the

underlying formations. Four of the most relevant scenarios are presented in Table 3.6 and Fig. 3.8. Wall angles in the Bidahochi Formation are either 20° (observed at Twin Peaks, Fig. 4.3.b) or 60° (used by Lefebvre et al. 2013) to cover a wide range of possibilities but still reflect the idea that the Bidahochi Formation was unconsolidated and easily excavated at the time of volcanism. Lefebvre et al. (2013) used 80° for wall angles in the underlying formations but more plausible angles are considered to be 70° or 75° even if observations at Twin Peaks range from 70° to 88° (Chapter 4, Fig. 4.3b). Smaller angle creates a cone that reaches more plausible stratigraphic depths based on lithic componentry data for Round Butte, as discussed below. The Moenave and Moenkopi Formations were consolidated and competent at the time of volcanism, forming steep diatreme walls, whereas the Chinle Formation is variably consolidated, but for simplicity we assumed the same relatively steep walls as in the Moenave and Moenkopi formations.

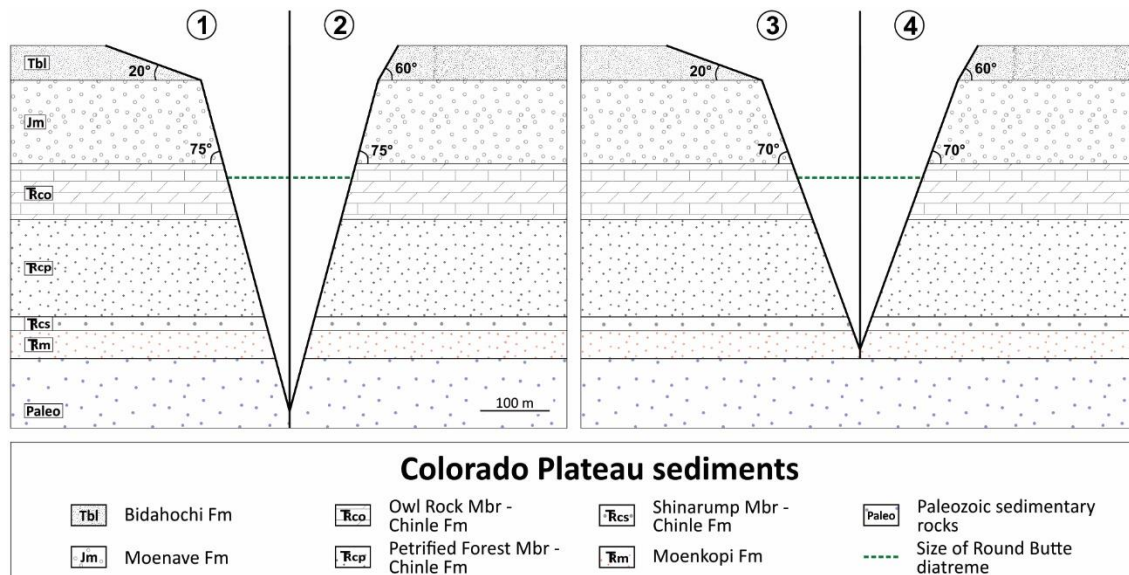


Figure 3.8: Scenarios of country rock fragmentation at Round Butte. Numbers 1 to 4 refer to different scenarios shown in Table 3.6. Although the diatreme is drawn as empty for simplicity, it is always occupied by pyroclastic material during the eruption, at least in part.

3.8.2 Origin and proportion of lithic clasts

In model scenarios 1 and 2, the root zone reaches down into the Paleozoic sedimentary rocks, due to slopes of 75° below the Bidahochi Formation (Fig. 3.8). We consider that these two scenarios are less probable because we do not have evidence of lithic clasts coming from below the Moenkopi Formation, although such clasts might appear in the diatreme at levels deeper than the current exposures. Scenarios 3 and 4 are more realistic for Round Butte: the root zone

probably ends in the Moenkopi Formation (up to 440 m below the pre-eruptive surface), which is the deepest identified source of lithics. Table 3.6 compares scenarios 3 and 4 with the line and clast count results, recalculated to 100% lithics, without considering the undifferentiated clasts. Relative to our best estimate of the ‘theoretical’ proportions within the fragmented domain, the diatreme is depleted in Bidahochi and Chinle clasts, but enriched in Moenave and Moenkopi clasts.

Table 3.6: Comparison of the country rock fragmentation model with lithic proportions in field line and clast counts¹

	Bidahochi Fm	Moenave Fm	Chinle Fm	Moenkopi Fm	Paleozoic sedcs. ²	Total
<i>Volume fragmented (x10⁶ m³)</i>						
Model scenarios (Fig. 3.8)						
1	6.2	4.6	3.2	0.08	0.03	14.1
2	3.2	4.6	3.2	0.08	0.03	11.0
3	7.1	5.3	2.6	0.002	0.00	14.9
4	3.8	5.3	2.6	0.002	0.00	11.7
<i>‘Theoretical’ proportion of fragmented formations (lithic clast %)</i>						
Model scenarios (Fig. 3.8)						
1	44	33	22	0.5	0.2	100
2	29	42	29	0.7	0.3	100
3	47	36	17	0.01	0.0	100
4	33	45	22	0.02	0.0	100
Mean (3 & 4)	40	40	19	0.02	0.0	100
<i>Field line counts at 43 sites (Table 3.2; lithic clast %)</i>						
Facies groups ³						
Disturbed bedded group	23	70	4	4	0	100
Non-bedded group	28	63	2	8	0	100
Pyroclastic megablocks	51	42	5	2	0	100
<i>Field clast counts at 15 sites (Table 3.4; lithic clast %)</i>						
Facies groups ³						
Disturbed bedded group	12	82	2	4	0	100
Non-bedded group	19	80	2	0	0	100
Pyroclastic megablocks	31	58	11	0	0	100

¹All percentages are recalculated on a 100% lithics basis

²Paleozoic sedimentary rocks (Billingsley et al. 2013)

³Facies groups are described in Latutrie and Ross (2019) and Table 3.1

The scenarios predict that the Bidahochi Formation should account for 33-47% of lithic clasts, depending on the slope angles. Yet much of diatreme is poorer in Bidahochi clasts. Only the pyroclastic megablocks have high proportions of Bidahochi fragments in the line counts, up to 51%. Our interpretation is that pyroclastic megablocks at Round Butte are parts of the ejecta ring recycled into the diatreme. The depletion in Bidahochi clasts within the diatreme is largely explained by excavation of the early crater within the Bidahochi Formation and expulsion of this material towards the ejecta ring. At Round Butte, the ejecta ring has been eroded after the

eruption, but preserved ejecta rings in the HBVF are known to be especially rich in Bidahochi material (e.g. Teshim maar, White 1991; Lefebvre et al. 2013 or Triplets, Graettinger and Valentine 2017), so we expect the diatremes to be commensurably depleted in Bidahochi clasts. Another factor explaining the Bidahochi depletion of the diatreme is that the Bidahochi Formation was poorly consolidated and prone to disaggregation, meaning that some loose grains are hidden into the matrix of the pyroclastic rocks (Graettinger and Valentine 2017).

For the Moenave Formation, the model scenarios predict a 36-45% contribution to the lithics in the diatreme. The line counts show much higher measured Moenave contents on a 100% lithics basis. The Moenave Formation is composed of competent sandstones to siltstones that are resistant to disaggregation after fragmentation, leading to the apparent enrichment in the diatreme.

The model scenarios predict that the Chinle Formation should account for 17-22% of lithic clasts. Line and clast counts show under 5% Chinle material among the lithic clasts. Most of the Chinle Formation is composed of poorly indurated sandstone, siltstone and mudstone, prone to disaggregation. We think that most of the Chinle clasts were completely destroyed and are hidden in the matrix as mineral grains or mud. The line count proportion of ~3% and the clast counts proportion of ~2% are largely explained by clasts derived from the rare competent limestone interbeds of the Owl Rock Member. These clasts are easy to identify and extremely resistant to disaggregation.

Finally, the Moenkopi Formation is only fragmented in a very narrow cone in the scenarios, yielding well under 1% of the lithic population. Yet, on average, line and clast counts show a much higher percentage in the diatreme, mainly because the root zone of diatreme is not as pointy as the cone shape illustrated in Fig. 3.8. The fact that the Moenkopi sandstones are well consolidated and resist transport is another factor explaining the discrepancy.

3.9 Comparison of field line count and field clast count methods

We acquired line counts and clast counts at the same 15 field sites in order to have a direct comparison of these two componentry methods (Table 3.7). Line counts are 1D measurements whereas clast counts are methodologically similar to petrographic point counts and give the volume or modal fraction of the components present within the pyroclastic deposits (Underwood 1970). Relative errors on point counting methods such as clast counts are theoretically predicted in a chart by van der Plas and Tobi (1965) whereas no chart addressing relative errors

of line counts is available. Therefore, the two methods are not necessarily expected to yield identical results.

At Round Butte, the proportions of matrix (clasts <4 mm) and cement are systematically overestimated in the line counts, relative to visual impressions and to the results of clast counts. On average, clast counts give a matrix + cement proportion of 60% in non-bedded rocks, 63% in disturbed bedded rocks, and 80% in pyroclastic megablocks whereas line counts average 64% in non-bedded rocks, 69% in disturbed bedded rocks, and 83% in pyroclastic megablocks. The overestimation of “matrix + cement” and the related underestimation of the proportion of clasts ≥ 4 mm arise because line counts rarely intersect particles exactly along their long axis.

When the percentage of juvenile clasts vs lithic clasts is recalculated to 100%, the proportions are similar by both methods, on average, for the non-bedded rocks (about 18% lithics) and pyroclastic megablocks (about 34-35% lithics). However, for the disturbed bedded group, line counts average 18% lithics (82% juvenile) whereas clast counts average 29% lithics (71% juvenile). A similar exercise for Twin Peaks, a nearby volcano ([Chapter 4](#); Latutrie and Ross 2020) showed instead that line counts tended to *overestimate* lithic proportions on average, relative to clast counts. We do not have a definite explanation for these discrepancies in lithic proportions (are they related to the grain size of the different components? to small numbers of sites being compared?), and more research seems warranted. Our current assessment is that although line counts are a good tool to quickly acquire a large amount of componentry measurements, clast counts seem more accurate and closer to visual estimates, especially with regards to matrix + cement proportions.

3.10 Interpretation and discussion

3.10.1 Summary of the origin of the three main groups of facies

The three main groups of facies that form the Round Butte diatreme are mainly phreatomagmatic in origin (Latutrie and Ross 2019). The undisturbed bedded pyroclastic group, at the top of the massif above the unconformity, is composed by numerous subhorizontal, centimeters to several meters thick beds of heterolithic to juvenile-rich coarse tuff to tuff breccia (Figs. 3.3, 3.4). Such bedded deposits were emplaced on the syn-eruptive crater floor by multiple explosions and are typical of the upper diatreme (White 1991; White and Ross 2011). Their characteristics suggest a deposition from proximal fallout, pyroclastic density currents (PDCs) or fallback (Ross et al. 2013). The disturbed bedded pyroclastic group is variably

deformed and disturbed but it displays similarities with the undisturbed bedded pyroclastic group in terms of componentry and grain size (coarse tuff to tuff breccia; Figs. 3.3, 3.4, 3.10, 3.11). Remnants of bedding are subhorizontal to swirly. Latutrie and Ross (2019) considered that the disturbed and the undisturbed bedded groups originally formed in the same way. The bedding disturbance resulted from syn-eruptive subsidence, liquefaction processes or the injection of debris jets. The non-bedded group of pyroclastic facies is coarser and richer in juvenile clasts than the other two, and is formed by subvertical columns (Figs. 3.3, 3.12) invading rocks of the disturbed bedded group, which therefore constitute residual columns (Figs. 3.3, 3.12). The non-bedded invasive columns were emplaced from debris jets (Latutrie and Ross 2019).

3.10.2 Megablocks

At Round Butte, sedimentary and pyroclastic megablocks together represent 4% of exposed rocks (Figs. 3.3, 3.5, 3.12). Sedimentary megablocks are pieces of sediments and sedimentary rocks from the Colorado Plateau (Moenave and Bidahochi Formations) that fell down into the crater during the eruption (Figs. 3.5a, 3.5b). Crater enlargement would have been due to gravitational instability and perhaps some large explosions (White 1991; White and Ross 2011; Latutrie and Ross 2019).

The composite mLTb megablock has a coherent basanite part and a pyroclastic part (Figs. 3.3, 3.5c, 3.5d). The coherent part is inferred to represent a piece of a dike (or other sheet-like intrusion) that has a peperitic transition with the pyroclastic rock on its right side. The lithic clasts in the pyroclastic part come exclusively from the Bidahochi Formation and are mixed with juvenile fragments. It is likely that the first crater-forming phreatomagmatic explosions occurred at shallow depth (Valentine et al. 2014) and formed the initial crater within Bidahochi sediments. This would have produced the required pyroclastic mixture of Bidahochi and juvenile clasts now found in the mLTb megablock (Table 3.1). Therefore, the pyroclastic rocks in this megablock are inferred to be a remnant of some of the first deposits that filled the crater at Round Butte, i.e. the proto-diatreme.

Table 3.7: Compilation of mean value of line and clast count methods acquired at the 15 sites, expressed as percentages of clasts larger than, or equal to, 4 mm

Methods	Nb of sites	Juvenile clasts								Lithic clasts					Tuff clasts	Matrix (< 4 mm) + cement	
		Brown	Light grey	Medium grey	Dark grey	Black	Undiff.	CPX and phlogopite	Total	Bidahochi Fm	Moenave Fm	Chinle Fm	Moenkopi Fm	Undiff.			Total
<i>Disturbed bedded pyroclastic rocks</i>																	
Line count	5	0.7	2.2	5.8	13.7	3.0	0.2	0.2	25.9	0.2	4.2	0.4	0.0	0.6	5.4	0.0	68.7
Clast count	5	1.8	3.0	12.2	7.2	1.6	0.0	0.7	26.5	1.2	8.4	0.2	0.4	0.4	10.6	0.2	62.7
<i>Non-bedded pyroclastic rocks</i>																	
Line count	7	0.8	3.9	6.6	15.3	1.9	0.1	0.3	28.9	1.9	3.9	0.1	0.0	0.2	6.2	0.5	64.4
Clast count	7	2.2	6.7	6.9	9.1	7.4	0.0	0.0	32.3	1.2	5.2	0.1	0.0	0.5	7.0	0.3	60.4
<i>Pyroclastic megablocks</i>																	
Line count	3	0.0	2.9	3.4	3.4	0.6	0.1	0.3	10.8	2.5	2.6	0.2	0.0	0.3	5.6	0.4	83.3
Clast count	3	0.0	4.3	4.7	2.0	1.0	0.0	0.7	12.7	2.0	3.7	0.7	0.0	0.3	6.7	0.7	80.0

Pyroclastic megablocks from the mLTh facies are bedded to non-bedded (Table 3.1; Figs. 3.3, 3.12). Where bedding is preserved, it consists of centimeters to meters thick beds composed of coarse tuff to fine lapilli tuff (Figs. 3.5e, 3.5f). Bedded units are typically formed by processes that occur only within the atmosphere, such as PDCs or fallout. We interpret these pyroclastic megablocks as parts of the ejecta ring that collapsed during stages of crater widening. Preservation of bedding planes was likely favoured by high cohesion due to a high water content in the ejecta ring deposits (Sohn 1996; Vazquez and Ort 2006).

3.10.3 Debris avalanche deposits (DADs)

The small debris avalanches on the west side of the massif were emplaced at the level of the unconformity and fill at least three channels (aTBh, Table 3.1; Fig. 3.14). We propose that a slump in the crater wall sent a mix of Bidahochi and Moenave material, and perhaps some pyroclastic material from the ejecta ring, down the crater sides. The small debris avalanches partly eroded existing pyroclastic deposits, forming channels and mixing with them. The unconformity is interpreted as one of the crater floor positions during the volcano's evolution. The unconformity formed at the end of an eruptive phase during which excavation dominated over infilling (Latutrie and Ross 2019). This would have destabilized the crater walls and caused the small debris avalanches.

The main DAD consists of Bidahochi-rich and Moenave-rich facies with no evidence of mixing between them. This main avalanche deposit likely resulted from several distinct slumps that affected different parts of the crater wall, with deposition of pyroclastic rocks (bLTb and bLTh1) in between the slumping events (Figs. 3.3, 3.4, 3.6). Facies aMBm and aMBp from the Moenave-rich part of the main DAD are closely associated and probably formed during one event (Table 3.1). Indeed, aMBp is found at the bottom and top of aMBm, suggesting that this part of the DAD was emplaced with a pure Moenave core surrounded by mixed parts composed of Moenave and pyroclastic materials. During the flow, the interior of the moving Moenave mass was preserved from mixing, whereas the bottom part mixed with the pyroclastic deposits at the sides and bottom of the crater. It is less clear how the aMBp found at the top formed. During the DAD emplacement, the front of the Moenave flow may have mixed with pyroclastic deposits in the diatreme and a small part of this mixture was able to overbank on the top.

The Bidahochi-rich part of the main DAD is composed of a main facies, aBB, at the top and a minor one, aBBp, at the bottom (Table 3.1). The main facies is bedded and is formed by many

small Bidahochi mudflows that piled up to form aBB. Locally, mudflows mixed with the bLTb facies to form the aBBp facies (Figs. 3.3, 3.4).

3.10.4 Implication on lithic transport within the diatreme

At Round Butte, lithic clasts range from single mineral grains within the matrix of pyroclastic rocks to megablocks. The lithics found at the current level of exposure originate from the Bidahochi, Moenave, Chinle (Owl Rock, Petrified Forest and Shinarump Members) and Moenkopi Formations. Fragments from the Bidahochi and Moenave Formations, and from the Owl Rock Member – including all sedimentary megablocks – have collectively moved down by 0-190 m from their sources, due to gravity and an occasionally deep crater. Fragments from the Petrified Forest Member, the Shinarump Member and the Moenkopi Formation are up to 20-30 cm across (no megablocks) and have a net upwards displacement of up to 220 m relative to their sources. The upward movement of these fragments is explained by debris jets resulting from phreatomagmatic explosions at various levels in the diatreme. One of the clearest manifestation of deeply sourced debris jets at Round Butte is the nTBI domain on Fig. 3.3. No clast or line count was obtained for this location, but the rocks are extremely rich in clasts from the Chinle and Moenkopi Formations. Since we explain the net upward movement of fragments from deeper formations with debris jets, and since no megablock has a net upward movement (at the current level of exposure), we conclude that debris jets can't permanently move megablocks upward. This could be related to the large mass of individual megablocks and the low density of debris jets. Megablocks of deep sedimentary formations may be preserved at deeper levels at Round Butte.

Lefebvre et al. (2013) built a conceptual country rock fragmentation model for West Standing Rocks (WSR), another diatreme in the HBVF (Fig. 3.1). Their model is generally similar to ours and can be compared with what we obtained for Round Butte. They considered diatreme wall angles of 60° in the Bidahochi Formation and 80° for the sedimentary rocks below. The WSR model suggests a diatreme around 700 m deep, i.e. 260 m deeper than for the Round Butte model. Within the WSR diatreme, at the current level of exposure, lithic clasts are mainly derived from the Moenave Formation and the Owl Rock Member. Only traces of the other sedimentary formations and members are represented. For the depletion in Bidahochi Formation material, Lefebvre et al. (2013) also proposed that most of the Bidahochi Formation was expelled toward the ejecta ring and/or that Bidahochi material is hidden within the matrix of WSR pyroclastic units. The main difference between the WSR and the Round Butte models is

the proportion of deep lithic clasts, derived from the Chinle Formation (Petrified Forest and Shinarump Members) and from the Moenkopi Formation. At WSR, despite the idea of a deeper diatreme overall, and despite the fact that the massif there crops out in the Petrified Forest Member – an estimated 110 m lower than the base of the Round Butte massif, relative to the pre-eruptive surface – deep lithic clasts are even less represented than at Round Butte. Lefebvre et al. (2013) proposed that those deep lithic clasts at WSR are likely preserved at a lower level within the country rock breccia. If the very steep wall angles assumed by Lefebvre et al. (2013) for WSR are correct, the difference in deep lithics relative to Round Butte could be the result of the variability of the intensity of the phreatomagmatic explosions, the location of the explosion sites or the size of the diatreme. Billingsley et al. (2013) highlighted that the Holbrook/Moqui Member of the Moenkopi Formation is formed by channels. This, could be another explanation for the very low concentration Moenkopi clasts because it was not highly present below WSR.

3.10.5 Lithic clasts in the ejecta ring versus the diatreme

Historically, more studies have focused on lithic clasts preserved in the maar ejecta ring (Ollier 1967; Lorenz 1973, 1975; White 1991; Ross et al. 2011; Valentine 2012; Graettinger and Valentine 2017) than in the diatreme (Lefebvre et al. 2013; Latutrie and Ross 2019). This is mainly due to the better worldwide availability and accessibility of maar ejecta rings, and the focus of many researchers on Quaternary, as opposed to older, volcanoes.

HBVF ejecta rings are rich in lithic clasts derived from the Bidahochi and Moenave Formations (White 1991; Lefebvre et al. 2013; Graettinger and Valentine 2017) but show little evidence of fragments derived from deep formations such as the Chinle or the Moenkopi. The Bidahochi Formation is particularly present at the bottom of some ejecta rings whereas the Moenave Formation starts to appear in the middle to upper parts (e.g., Teshim maar, White 1991). Studying the maar ejecta ring alone might lead to the idea of a shallow diatreme, perhaps with gentle wall angles. However, actual diatremes exposed in the HBVF, tell a different story. For example, at Round Butte, all formations are contained as clasts within the diatreme from the Bidahochi (up to the pre-eruptive surface) to the Moenkopi (up to 440 m below the pre-eruptive surface). Diatreme studies show that some lithic fragments have moved up while others have moved down, relative to their sources.

Deep phreatomagmatic explosions, i.e. 250 m deep or more, are typically not powerful enough to eject material to the atmosphere (Valentine et al. 2014; Sweeney and Valentine 2015). Some

debris jets remain constrained within the diatreme (when explosion sites are deeper than 120 m, Valentine et al. 2014), forming subterranean “invasive columns” (Latutrie and Ross 2019 and references therein). Lithic clasts with a deep origin will rarely reach the upper parts of the volcano (ejecta ring or upper diatreme), unless moved successively upwards by multiple debris jets (Valentine et al. 2014). In contrast, shallowly-sourced lithic clasts will probably be found in low concentrations in the lower diatreme and root zone because they are preferentially expelled toward the ejecta ring or sometimes disaggregated in fine fragments hiding in the matrix.

Studying lithic clasts in the diatreme directly, as opposed drawing inferences from the ejecta ring, reveals more of the full complexity of eruptive processes in the diatreme (Ross et al. 2008b, 2008c; Valentine et al. 2014, 2017).

3.11 Conclusions

We carried out a detailed study of lithic clasts and lithic-rich lithologies (debris avalanches, sedimentary megablocks) in the Round Butte diatreme to better constrain its overall evolution and eruptive processes. The layer cake stratigraphy of the country rocks in the HBVF area allowed us to build country rock fragmentation models for Round Butte and to quantify ‘theoretical’ volumes and proportions of each sedimentary formation fragmented. Those proportions were then compared to componentry measurements (line and clast counts) in the pyroclastic rocks. Componentry data highlighted that the diatreme extends to a depth of about 440 m below the pre-eruptive surface because no Paleozoic sedimentary rocks were found at Round Butte and lithics with the deepest origin derive from the Moenkopi Formation. This supports models 3 and 4 of Fig. 3.8, with diatreme walls sloping around 70°, except in the Bidahochi Formation where they were gentler. Competent sedimentary rocks (Moenave Formation, Owl Rock Member and Moenkopi Formation) are better preserved as recognizable lithic clasts in the diatreme than the less competent stratigraphic units (Bidahochi Formation, Petrified Forest Member and Shinarump Member), which must now be hiding as loose sedimentary grains in the matrix of the pyroclastic rocks. Additionally, the Bidahochi Formation was preferentially excavated during early crater development and expelled toward the ejecta ring. Fragments of deep formations travelled upwards within debris jets to the current exposure level inside the diatreme. Forward modeling exercises are useful tool to understand diatreme eruptive processes and to interpret componentry measurements, as long as the country rock stratigraphy is well known and distinctive, which unfortunately is not the case in all volcanic fields.

The main debris avalanche in the SW corner of Round Butte is the result of two crater wall slumps: one in the Moenave Formation and a second in the Bidahochi Formation. The smaller DADs on the west side of the massif were formed slightly later, at the time the uniformity was generated. Beyond these mass movements of material from the crater walls, individual megablocks from the country rocks and ejecta ring fell regularly into the crater due to gravitational instability. Slumps and individual megablock collapse are the main mechanisms which enlarged the crater laterally. We also highlighted that no megablocks show a net upward movement, suggesting that debris jets are not able to move them upwards.

3.12 Acknowledgements

James D.L. White introduced Pierre-Simon Ross to Round Butte and did the early work on this fascinating volcano. Pier Paolo Comida and Romain Jattiot helped us in the field. We thank the Morris family for allowing us to work at Round Butte. Any persons wishing to conduct geological investigations on the Navajo Nation must first apply for, and receive, a permit from the Navajo Nation Minerals Department, P.O. Box 1910, Window Rock, Arizona 86515, USA, telephone 1-928-871-6587.

3.13 Online Resource 3.1: Panoramas

The detail of the volcanology and the formation of Round Butte diatreme is available in Latutrie and Ross (2019). All the volcanic remnants were mapped on nine high definition panoramic photographs of the subvertical cliffs (location, see Fig. 3.1c). The most important and representative panoramas are included in the paper (Figs. 3.3, 3.4), and the remaining seven are included here to locate clast counts and line counts (Figs. 3.9 to 3.15).

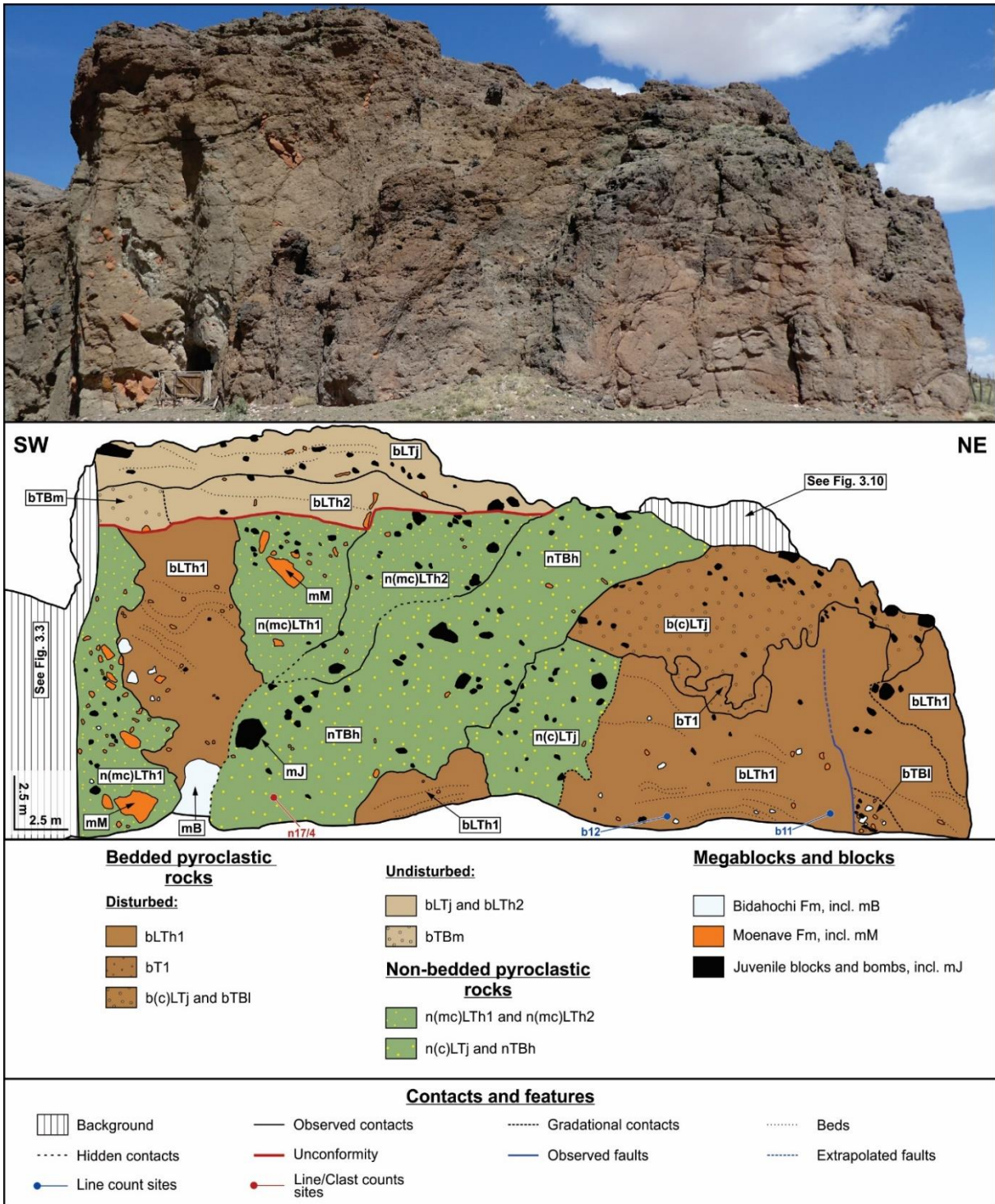


Figure 3.9: Geological map of the cliffs in the southeast part of Round Butte (location in Fig. 3.1c) displaying three main groups of facies detailed in Latutrie and Ross (2019) and the megablocks group of facies. For facies codes, see Latutrie and Ross (2019) and Table 3.1.

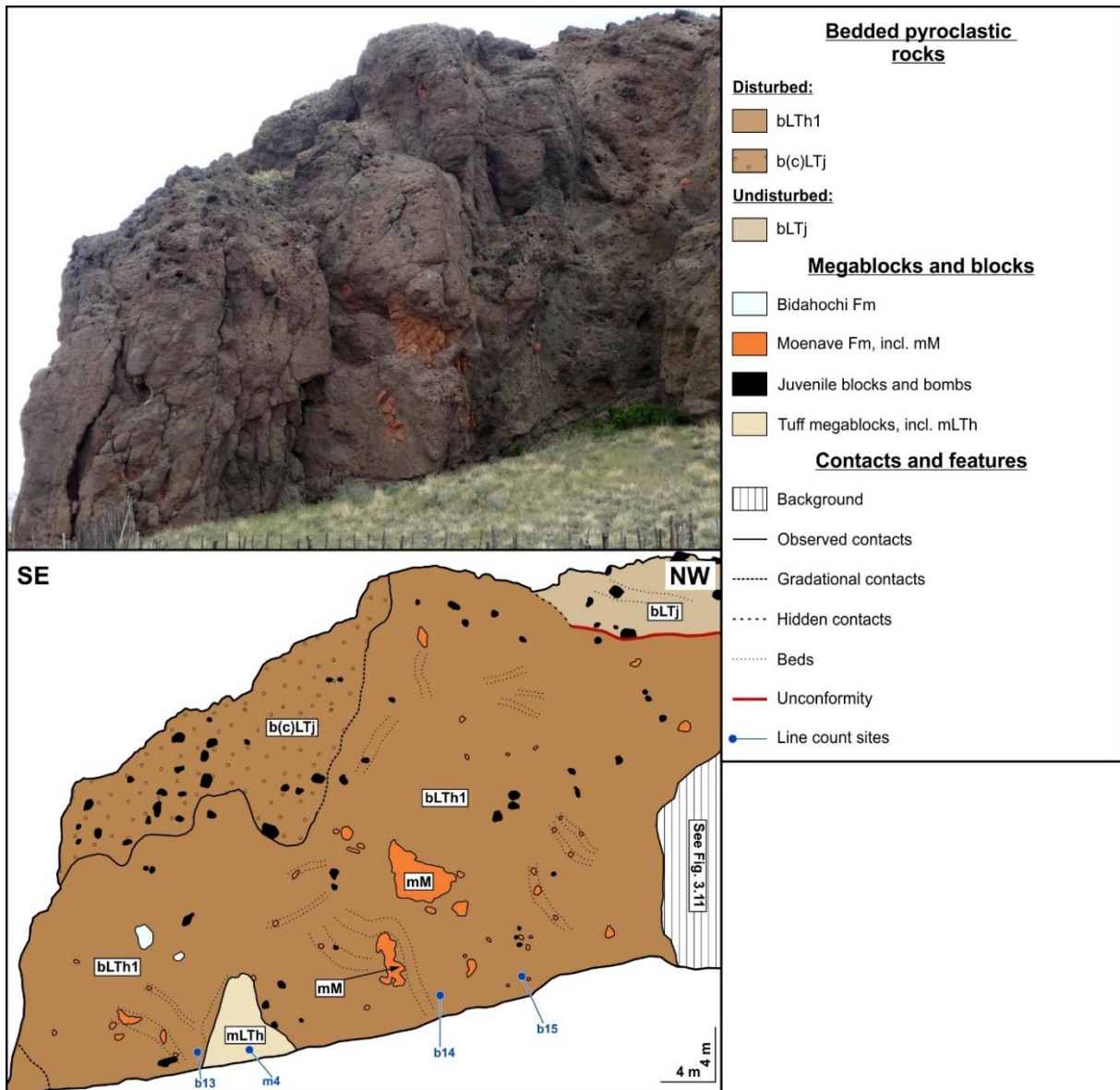


Figure 3.10: Geological map of the cliffs in the southeast part of Round Butte (location in Fig. 3.1c) displaying two main groups of facies detailed in Latutrie and Ross (2019) and the megablocks group of facies. For facies codes, see Latutrie and Ross (2019) and Table 3.1.

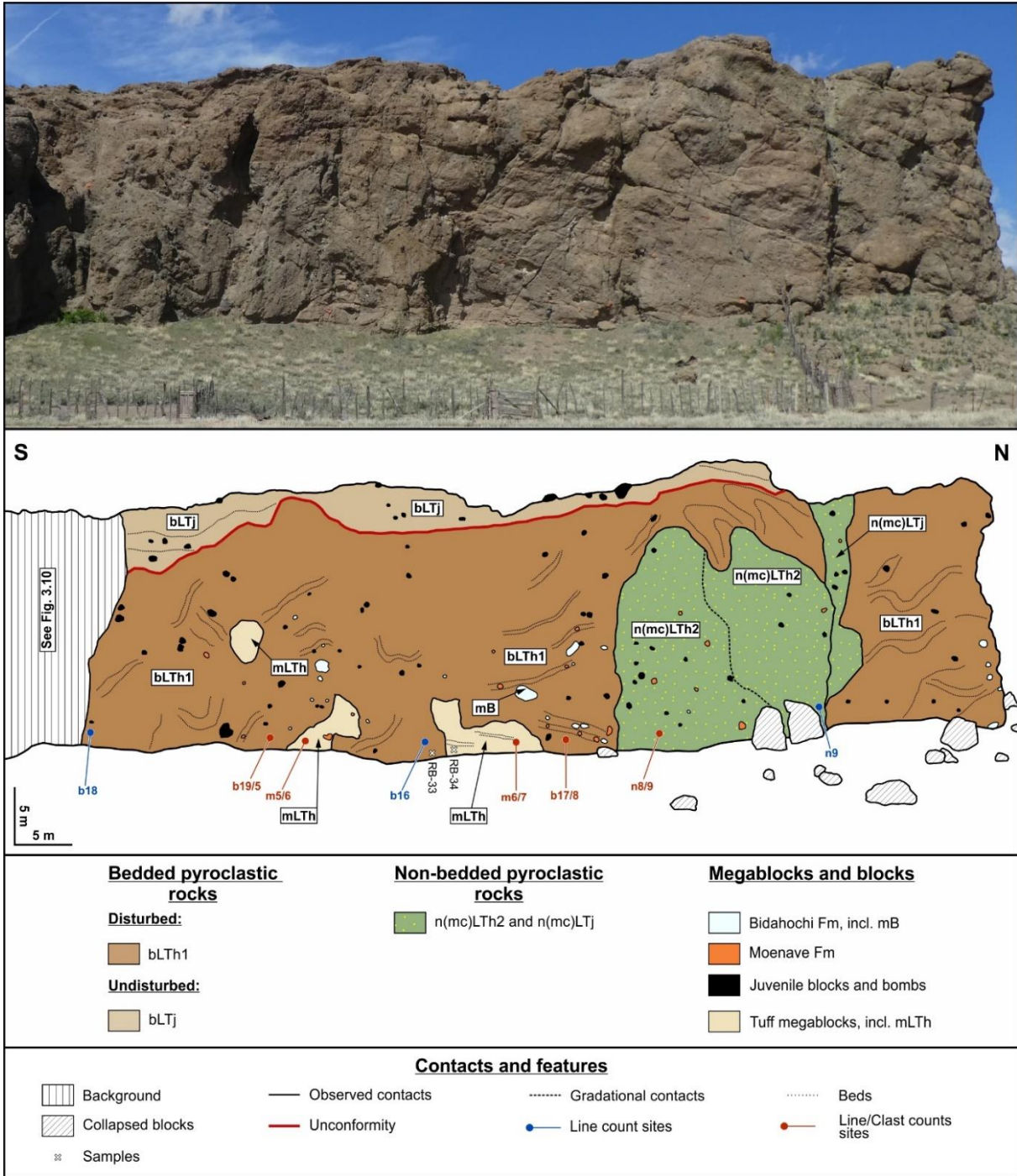


Figure 3.11: Geological map of the cliffs in the east part of Round Butte (location in Fig. 3.1c) displaying three main groups of facies detailed in Latutrie and Ross (2019) and the megablocks group of facies. For facies codes, see Latutrie and Ross (2019) and Table 3.1.

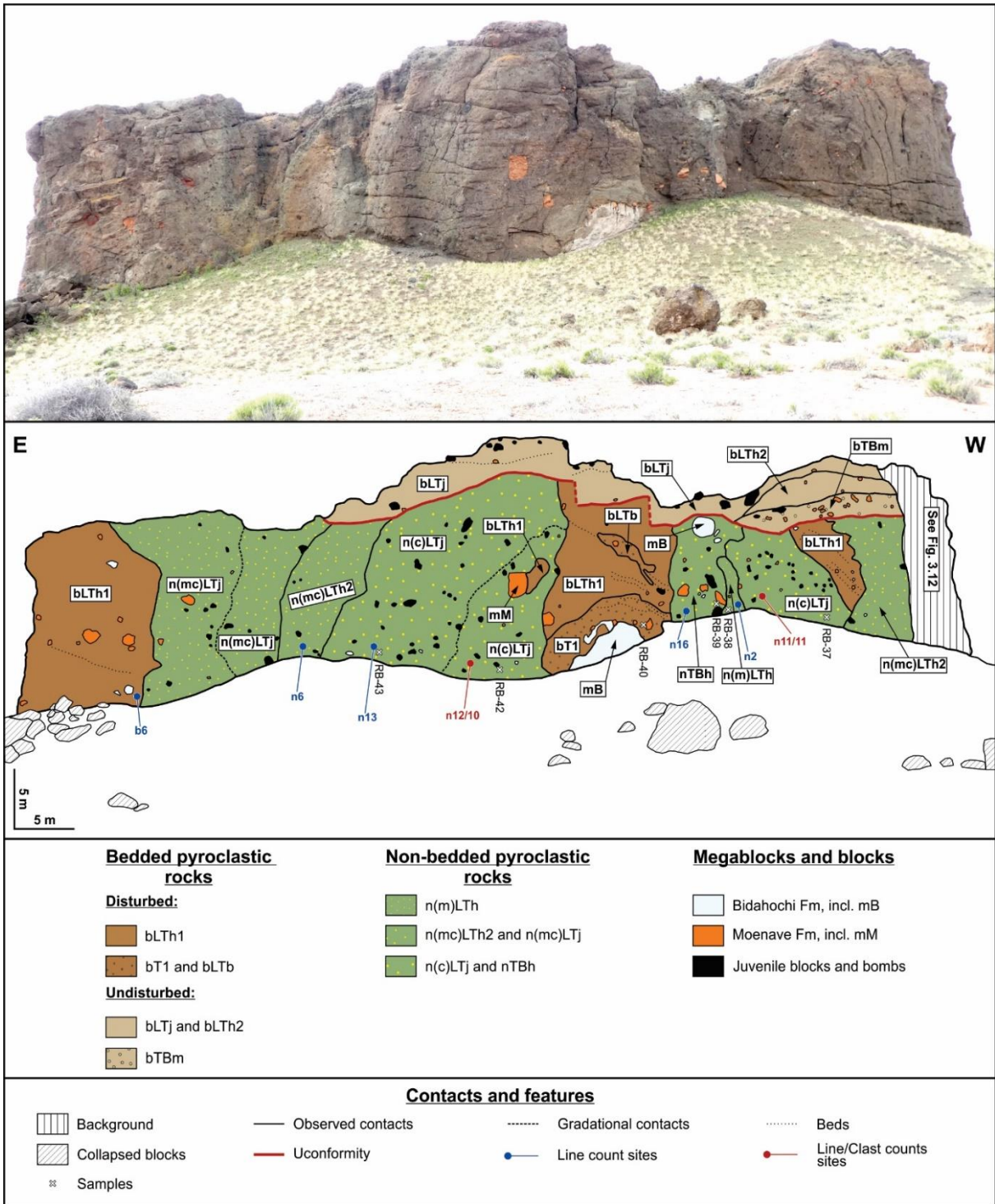


Figure 3.12: Geological map of the cliffs in the north part of Round Butte (location in Fig. 3.1c) displaying three main groups of facies detailed in Latutrie and Ross (2019) and the megablocks group of facies. For facies codes, see Latutrie and Ross (2019) and Table 3.1.

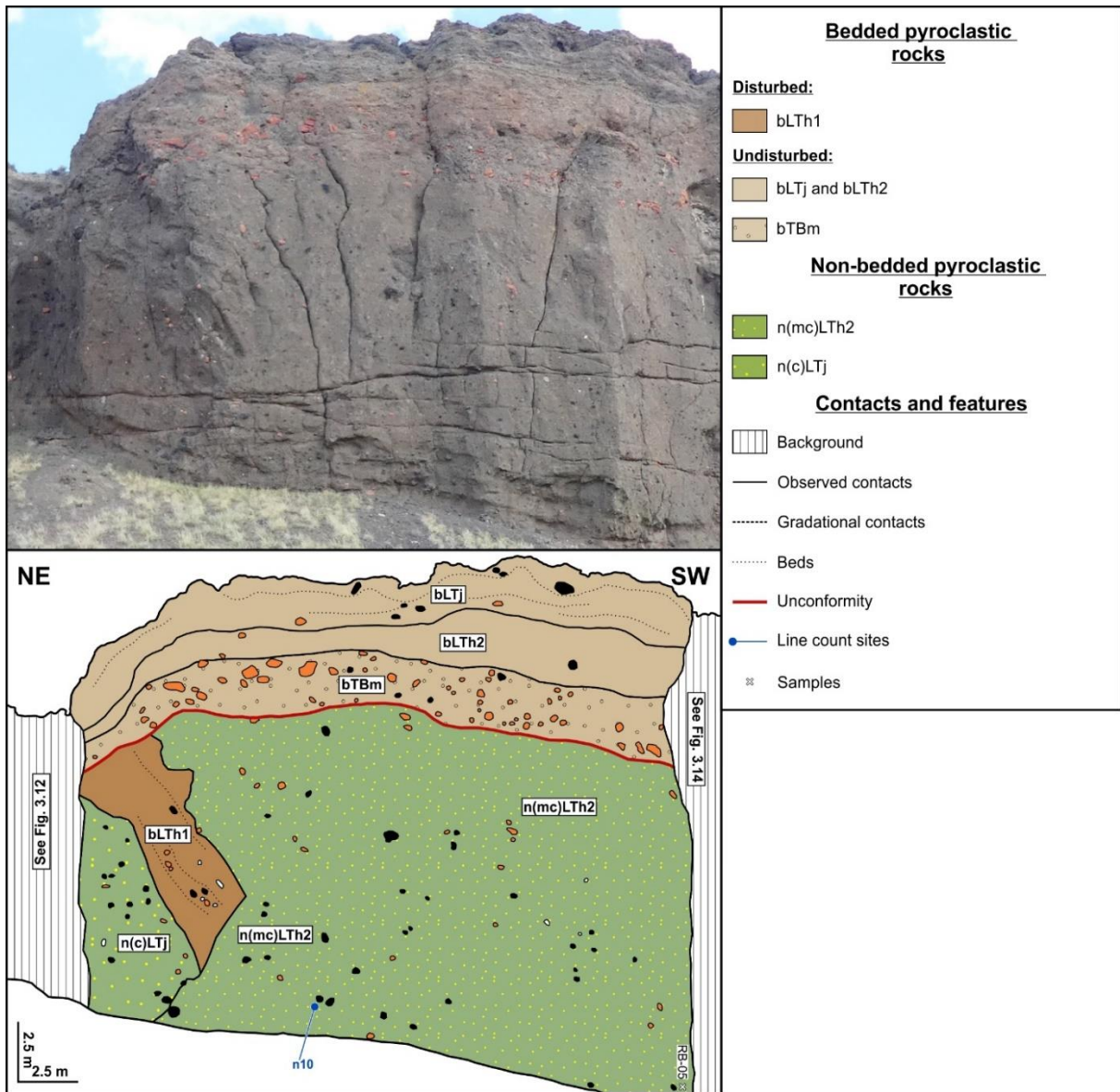


Figure 3.13: Geological map of the cliffs in the north-northwest part of Round Butte (location in Fig. 3.1c) displaying three main groups of facies detailed in Latutrie and Ross (2019). For facies codes, see Latutrie and Ross (2019).

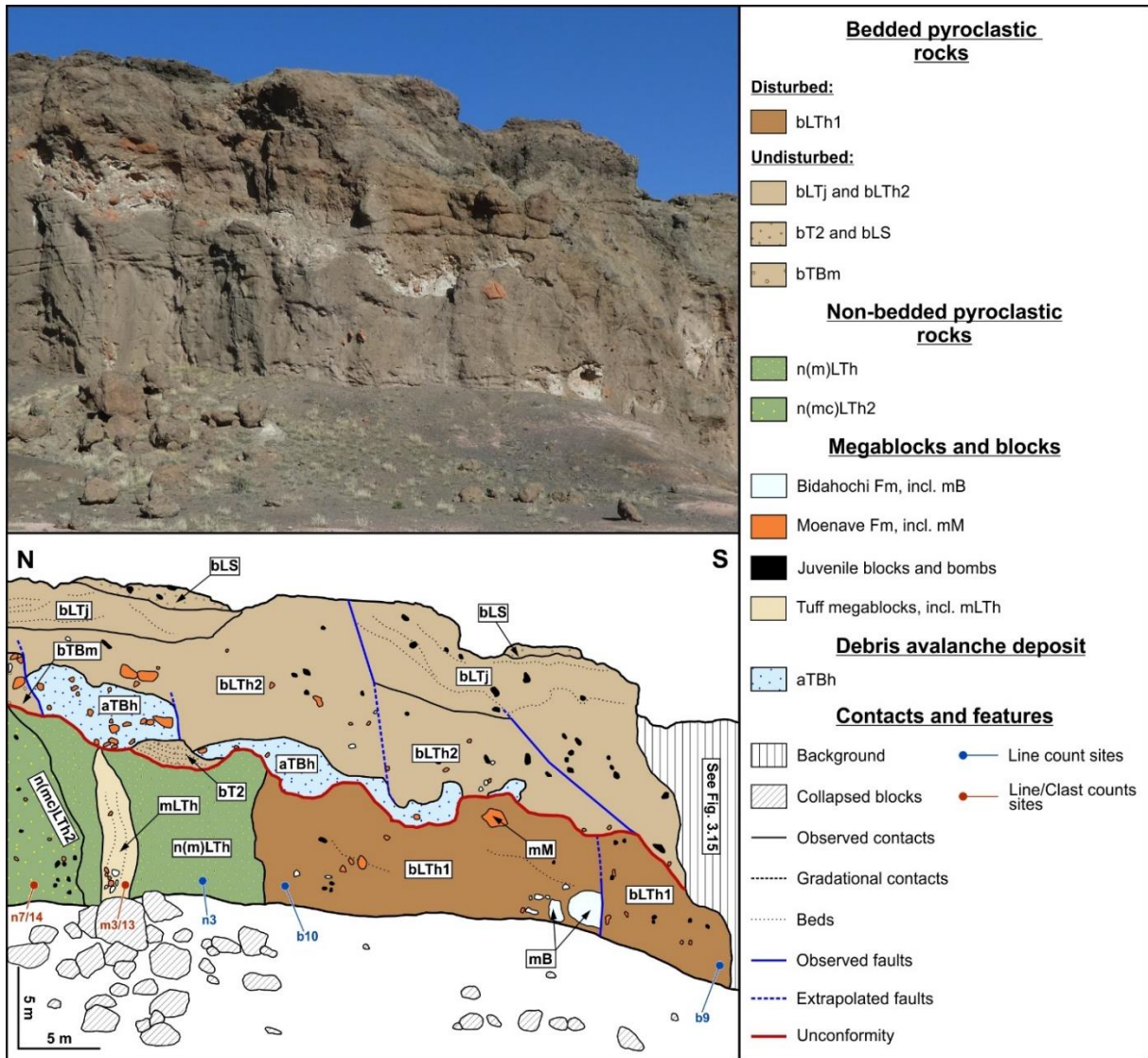


Figure 3.14: Geological map of the cliffs in the northwest part of Round Butte (location in Fig. 3.1c) displaying three main groups of facies detailed in Laturie and Ross (2019) and the megablocks and debris avalanche deposit (DADs) groups of facies. For facies codes, see Laturie and Ross (2019) and Table 3.1.

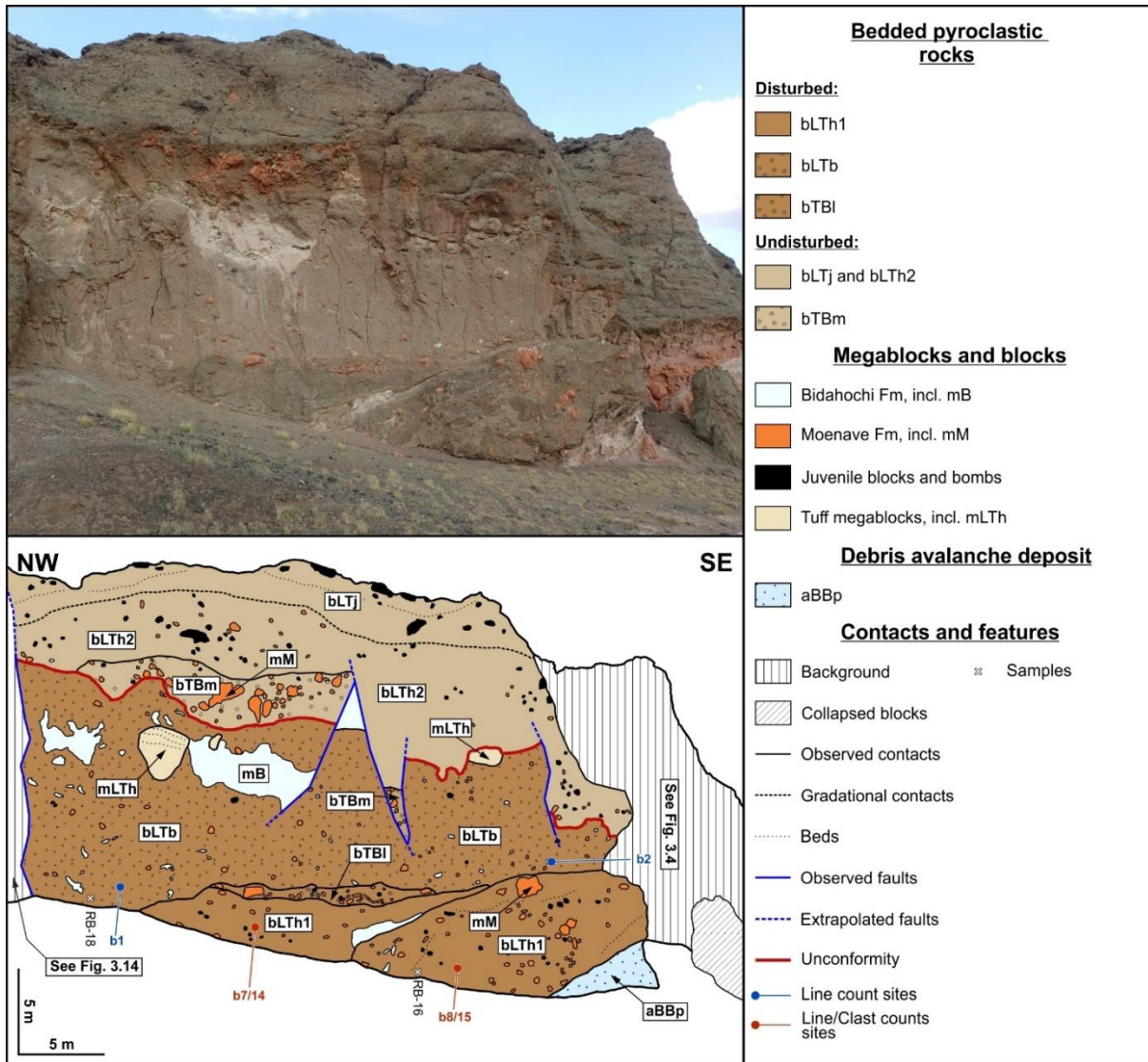


Figure 3.15: Geological map of the cliffs in the west part of Round Butte (location in Fig. 3.1c) displaying three groups of facies detailed in Latutrie and Ross (2019) and the megablocks and debris avalanche deposit (DADs) groups of facies. For facies codes, see Latutrie and Ross (2019) and Table 3.1.

4 THIRD ARTICLE: Twin Peaks volcanic complex

Phreatomagmatic vs magmatic eruptive styles in maar-diatremes – a case study at Twin Peaks, Hopi Buttes volcanic field, Navajo Nation, Arizona

Les styles éruptifs phréatomagmatique vs magmatique dans les maar-diatrèmes: une étude de cas à Twin Peaks, champ volcanique Hopi Buttes, Nation Navajo, Arizona

Authors:

Benjamin Latutrie and Pierre-Simon Ross

Institut national de la recherche scientifique, Centre Eau Terre Environnement, 490 rue de la Couronne, Québec (QC), G1K 9A9, Canada

Title of the journal:

Bulletin of volcanology

Published online: 24 February 2020

DOI: 10.1007/s00445-020-1365-y

This chapter is the preprint version of the research article:

Latutrie B, Ross P-S (2020) Phreatomagmatic vs magmatic eruptive styles in maar-diatremes: a case study at Twin Peaks, Hopi Buttes volcanic field, Navajo Nation, Arizona. Bull Volcanol 82: article 28

4.1 Abstract

The Hopi Buttes volcanic field (HBVF) is located on the Colorado Plateau, northern Arizona. In this Miocene volcanic field, the erosion level increases southward, allowing the study of maar-diatreme volcanoes from top (post-eruptive crater infill and ejecta ring) to bottom (lower diatreme). The Twin Peaks volcanic complex consists mostly of two hills (North Peak and South Peak) with thick lavas at their summits and pyroclastic rocks underneath. In the HBVF, such volcanic remnants have received little scientific attention so far, despite their relative abundance. Our field observations allow us to interpret the North and South Peaks as remnants of two maar-diatreme volcanoes which evolved into lava lakes filling the craters. Within the complex, we distinguish four volcanic units (from unit 1 at the bottom to unit 4 at the top). On the basis of the field description of the deposits and the componentry measurements, we suggest that Unit 1 is phreatomagmatic, Unit 2 is phreato-strombolian (with mixed phreatomagmatic and strombolian characteristics), Unit 3a is phreato-hawaiian (with mixed phreatomagmatic and hawaiian characteristics), Unit 3b is hawaiian (formed by lava fountains) and Unit 4 consists of lava lakes filling the maar craters. There is therefore a progressive evolution from a purely phreatomagmatic eruptive style, which excavated the craters and diatremes and partly filled them, to magmatic explosive to non-explosive eruptive styles, which filled the maar craters up to the pre-eruptive surface. We discuss traditional criteria used to distinguish phreatomagmatic from magmatic eruptive styles in ultramafic to mafic maar-diatreme volcanoes.

4.2 Introduction

Maar-diatreme volcanoes are, after scoria cones, the second most abundant type of volcanoes on continents (Vespermann and Schmincke 2000). They are small, complex, short lived, mainly phreatomagmatic volcanoes that are hazardous for the nearby population (Lorenz 1986a, 2007; White and Ross 2011; Valentine and White 2012). Around the world, maar-diatremes are found in active monogenetic volcanic fields, some of which are located near large cities such as Auckland, New Zealand (Németh et al. 2012; Németh and Kereszturi 2015; Nunns and Hochstein 2019) or Goma, Democratic Republic of Congo (Poppe et al. 2016). Maar-diatreme volcanoes comprise a subaerial part composed of an ejecta ring (Self et al. 1980; White 1991; Vazquez and Ort 2006; Valentine et al. 2015) and a maar crater (Lorenz 1973; White 1991; Graettinger 2018). Their subterranean part is composed of an upper typically bedded diatreme (White 1991; Gernon et al. 2013; Delpit et al. 2014), an upper/lower diatreme transition zone (Bélanger and Ross 2018; Latutrie and Ross 2019), a lower non-bedded diatreme (White 1991;

Lefebvre et al. 2013, 2016), a root zone (Clement 1982; Lorenz and Kurszlaukis 2007; Haller et al. 2017) and a feeder intrusion (Re et al. 2015, 2016; Muirhead et al. 2016; Le Corvec et al. 2018).

Upper diatreme deposits are bedded pyroclastic deposits emplaced onto the bottom of the syn-eruptive crater. White and Ross (2011) proposed to separate upper diatreme deposits into two types. Type I deposits progressively subside along ring faults during the eruption. Examples of type I deposits are found in the Missouri River Breaks volcanic field of Montana (Delpit et al. 2014). Type II deposits are deposited into deep craters, after an excavation-dominated phase, without strong subsidence. Examples of type II deposits comprise several cases in the Hopi Buttes volcanic field (HBVF) of Arizona, including the upper diatreme infill at Round Butte (Latutrie and Ross 2019). Type II upper diatreme deposits range from phreatomagmatic to magmatic in origin (White and Ross 2011), including in the HBVF. Phreatomagmatic and magmatic vents can be active simultaneously in a maar crater, as observed in 1977 at Ukinrek, Alaska (Kienle et al. 1980; Self et al. 1980; Büchel and Lorenz 1993; Ort et al. 2018). Another possibility is that the eruptive regime progressively switches from phreatomagmatic to magmatic. If a late magmatic phase of the eruption lasts long enough, the syn-eruptive maar crater could be filled (or over-filled) by a scoria cone (White 1991; Vazquez 1998) or a lava lake (e.g., Martin and Németh 2002; Kereszturi and Németh 2011; Hencz et al. 2017; Latutrie and Ross 2018; Tietz et al. 2018), so that the final landform at the end of the eruption would not necessarily be a maar, even if there is a diatreme under it.

Williams (1936) studied both the HBVF and the older Navajo volcanic field further north. In both fields, post-emplacment erosion has removed variable thicknesses of volcanic rocks and surrounding sedimentary rocks. Williams (1936) observed that volcano remnants in the Navajo volcanic field are typically tuff breccia “shafts” corresponding to pyroclastic rocks from diatremes (e.g., Cathedral Cliff, Bélanger and Ross 2018; Ship Rock, Delaney 1987). In the HBVF, many remnants are ‘plug’-dominated, i.e. mostly consisting of thick jointed lavas, and referred to as “Hopi necks” by Williams (1936). Most recent studies in the HBVF did not focus on these ‘plug’-dominated remnants, although HBVF workers know about them (e.g., White pers. commun. 2012; Ort pers. commun. 2017; authors’ observations). Instead, these recent studies documented plumbing systems (Re et al. 2015, 2016; Muirhead et al. 2016), as well as mostly phreatomagmatic pyroclastic rocks from the lower diatreme (Lefebvre et al. 2013, 2016), the upper/lower transition zone (Latutrie and Ross 2019), the upper diatreme (White 1991; Latutrie

and Ross 2019), and the ejecta ring (White 1991; Lefebvre et al. 2013; Graettinger and Valentine 2017).

In this paper, we present detailed mapping and interpretation of eruptive processes for a well exposed 'plug'-dominated remnant of the HBVF, the Twin Peaks volcanic complex. We describe four main volcanic units within the complex. Our interpretation is that the diatreme and crater excavation was phreatomagmatic as is typical of maar-diatreme volcanoes, but the crater infilling activity evolved from phreatomagmatic to magmatic. Therefore, Twin Peaks deposits display a continuous eruptive sequence from phreatomagmatic to magmatic, making it a great location to document in detail processes involved in this switching of eruptive styles in ultramafic to mafic maar-diatreme volcanoes. We take the opportunity to review and discuss the traditional criteria used to distinguish phreatomagmatic from magmatic eruptive styles in this setting.

4.3 Geological setting

The Miocene HBVF, located in the south central part of the Colorado Plateau, provides excellent exposures of maar-diatreme volcanoes (Fig. 4.1, Williams 1936; White 1991; Vazquez and Ort 2006; White and Ross 2011). Volcanic remnants are spread in an area of about 2300 km² (e.g., White 1991; Lefebvre et al. 2013; Latutrie and Ross 2019). Maar-diatremes are the main type of monogenetic volcanoes formed in the HBVF during volcanic activity (e.g., Williams 1936; White 1991; Vazquez 1998; Hooten 1999; Lefebvre et al. 2013, 2016; Latutrie and Ross 2019). This is related to the water-rich environments in the Miocene, characterised at the surface by playas and ponds (White 1990) and underground by subhorizontal aquifers (for current aquifers see Hart et al. 2002). Variable erosion levels in the HBVF allow the study of maar-diatremes from the ejecta ring (White 1991) to the lower diatreme (Lefebvre et al. 2013). The uppermost sedimentary formations in the HBVF region are, from top to bottom, the Miocene Bidahochi Formation, the Lower Jurassic Moenave Formation, and the Upper Triassic Chinle Formation (Fig. 4.1, Billingsley et al. 2013).

4.4 Twin Peaks volcanic complex

Twin Peaks volcanic complex forms the upper part of a 190 m-tall, ~1.3 km² hill in the southeastern part of the HBVF. The complex consists of two adjacent 'plug'-dominated volcanoes (North and South Peaks, Figs. 4.3a, 4.3b) and a small satellite diatreme (Figs. 4.2, 4.3c). The lower part of the hill, from ~1700 m above sea level (a.s.l.) in the south and from ~1720 m a.s.l. in the north, contains only Upper Triassic (Chinle Formation) to Lower Jurassic

(Moenave Formation) sedimentary rocks (Billingsley et al. 2013), often covered by Quaternary sediments (Fig. 4.2). The hill rises from a flat plain, the level of which approximates the contact between the Chinle and Moenave Formations (Figs. 4.1, 4.2). The lowest exposures of volcanic rocks of the main peaks are at around 1820 m a.s.l. (on the north flank of the North Peak), and reach ~1890 m a.s.l. Those of the satellite diatreme are preserved at ~1800 m a.s.l. within the sedimentary rocks of the Moenave Formation and form a ~20 m high outcrop (Fig. 4.3c). The total surface area occupied by volcanic rocks is 36 860 m² (~14 320 m² for the North Peak, ~22 210 m² for the South Peak, and ~330 m² for the satellite diatreme). The two main peaks display a sequence of pyroclastic rocks capped by thick jointed masses of black lava (Figs. 4.4, 4.5, 4.6). Sedimentary rocks from the Moenave Formation surround the volcanic remnants of each peak, whereas those of the Bidahochi Formation are eroded and not preserved in situ.

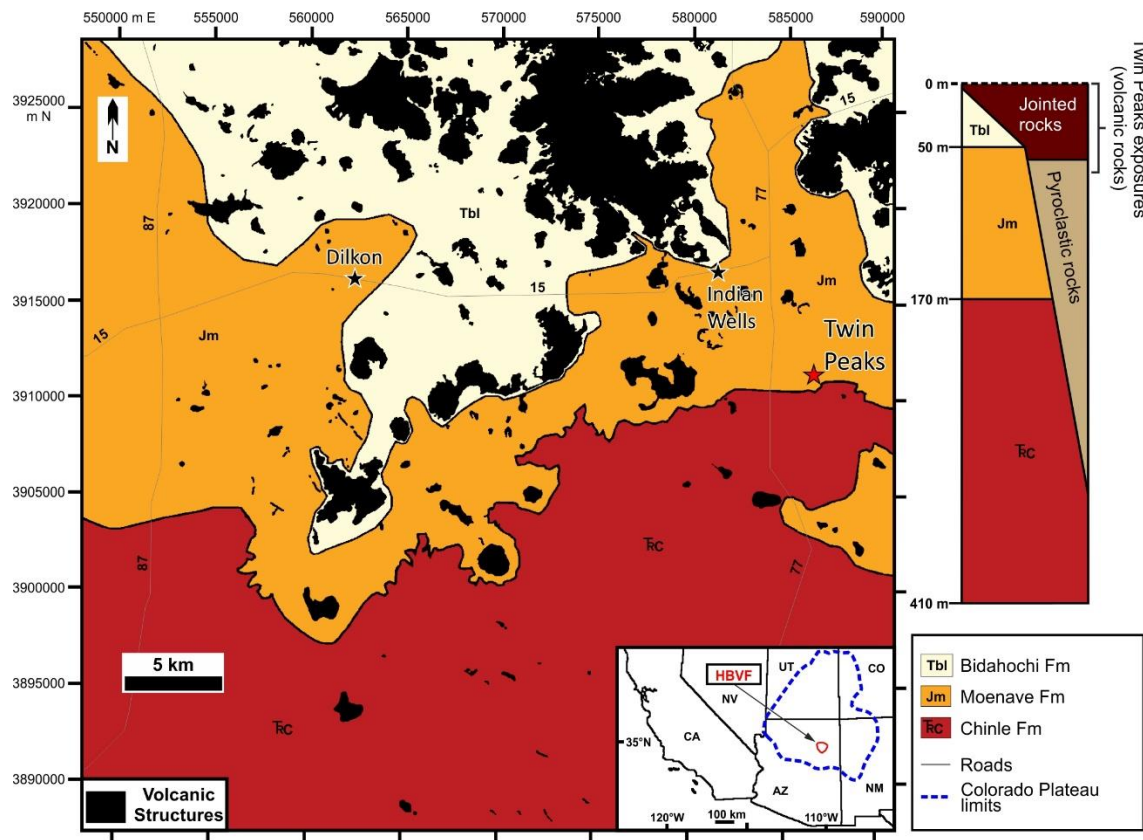


Figure 4.1: Geological map of the HBVF showing igneous remnants (black) and the main sedimentary formations. Grid is UTM WGS 84 zone 12S. Inset map locates the HBVF within the Colorado Plateau. Stratigraphic log illustrates the thickness of the main sedimentary formations and the exposure of Twin Peaks volcanic rocks (jointed lava and pyroclastic rocks). Black stars locate the main villages of the area. Modified from Lefebvre (2013).

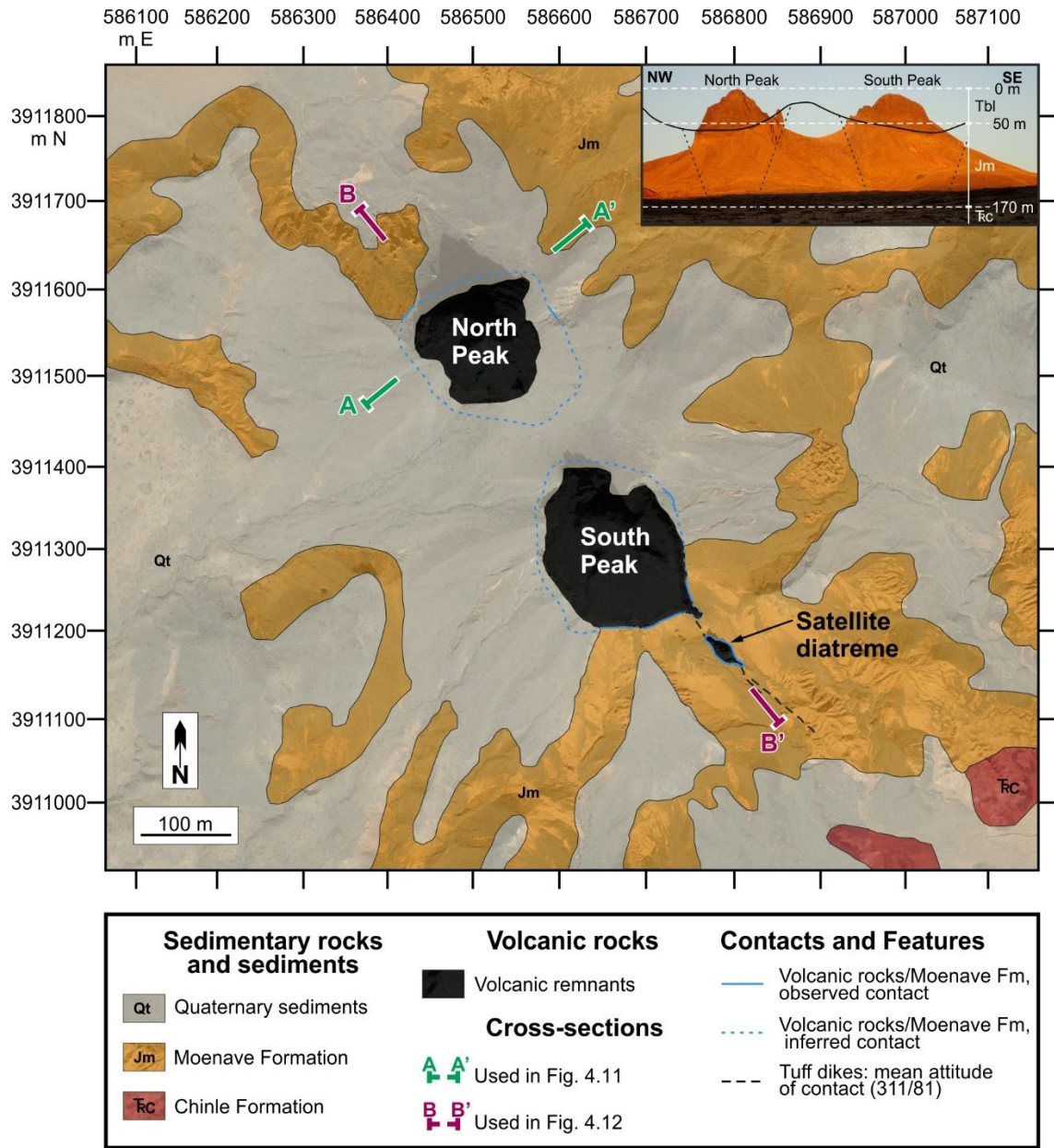


Figure 4.2: Geological map of the Twin Peaks volcanic complex showing the two main peaks (North and South) and the satellite diatreme. Grid is UTM WGS 84 zone 12S. Inset photograph show the current morphology of the two main peaks, looking NE. The satellite diatreme is hidden on the other side of the south slope of the South Peak. Dashed line represents the slopes of the inferred diatreme below the two main peaks on the B-B' cross-section whereas the black line corresponds to the crater floors as seen on the photograph.

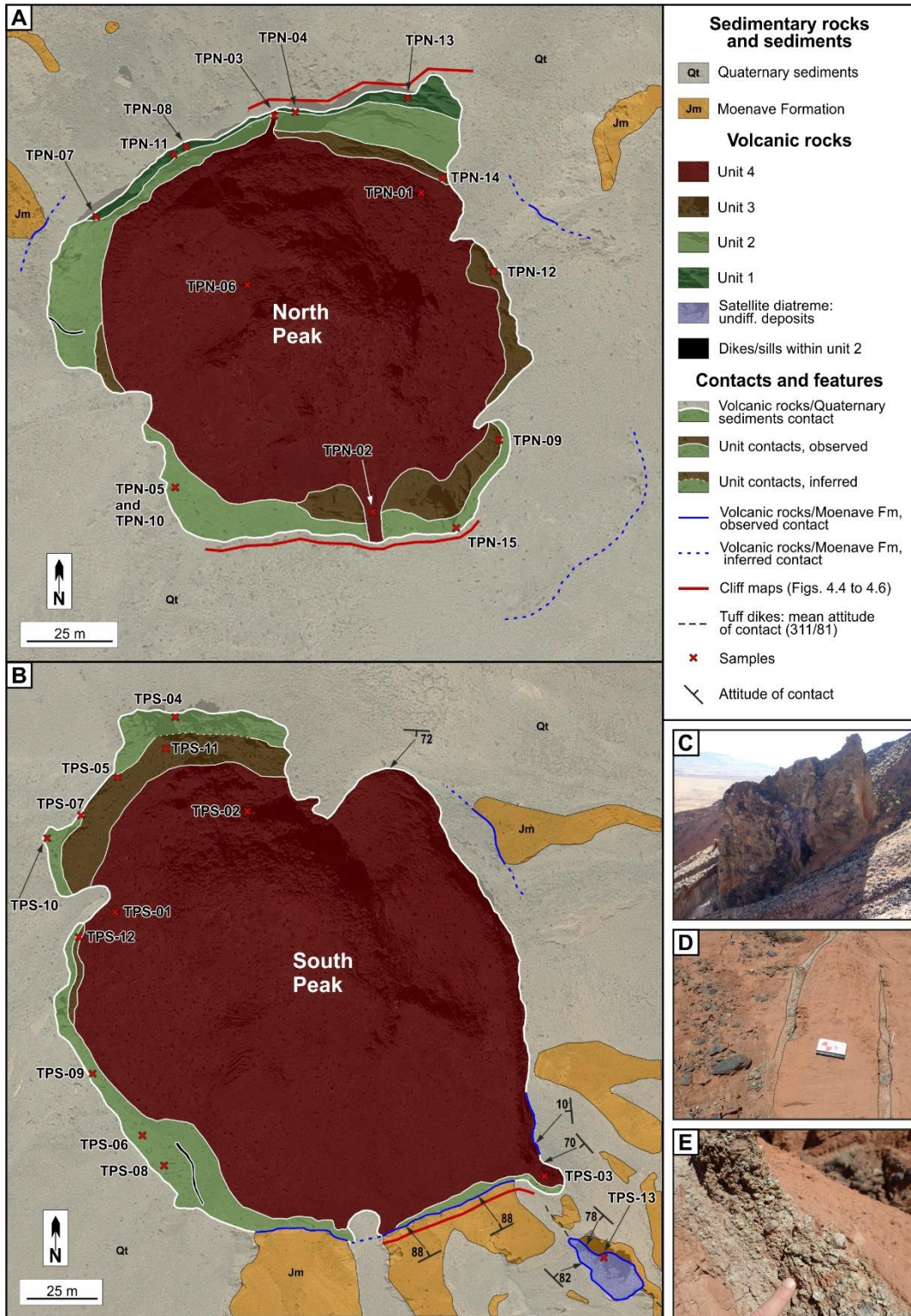


Figure 4.3: Detailed geological map of Twin Peaks. A) Zoom on the geology of the North Peak, B) zoom on geology of the South Peak, C) photo showing the vertical extension of the undifferentiated satellite diatreme, D) tuff to lapilli tuff dikes in the south of the satellite diatreme and E) close-up on the componentry of the tuff to lapilli tuff dikes.

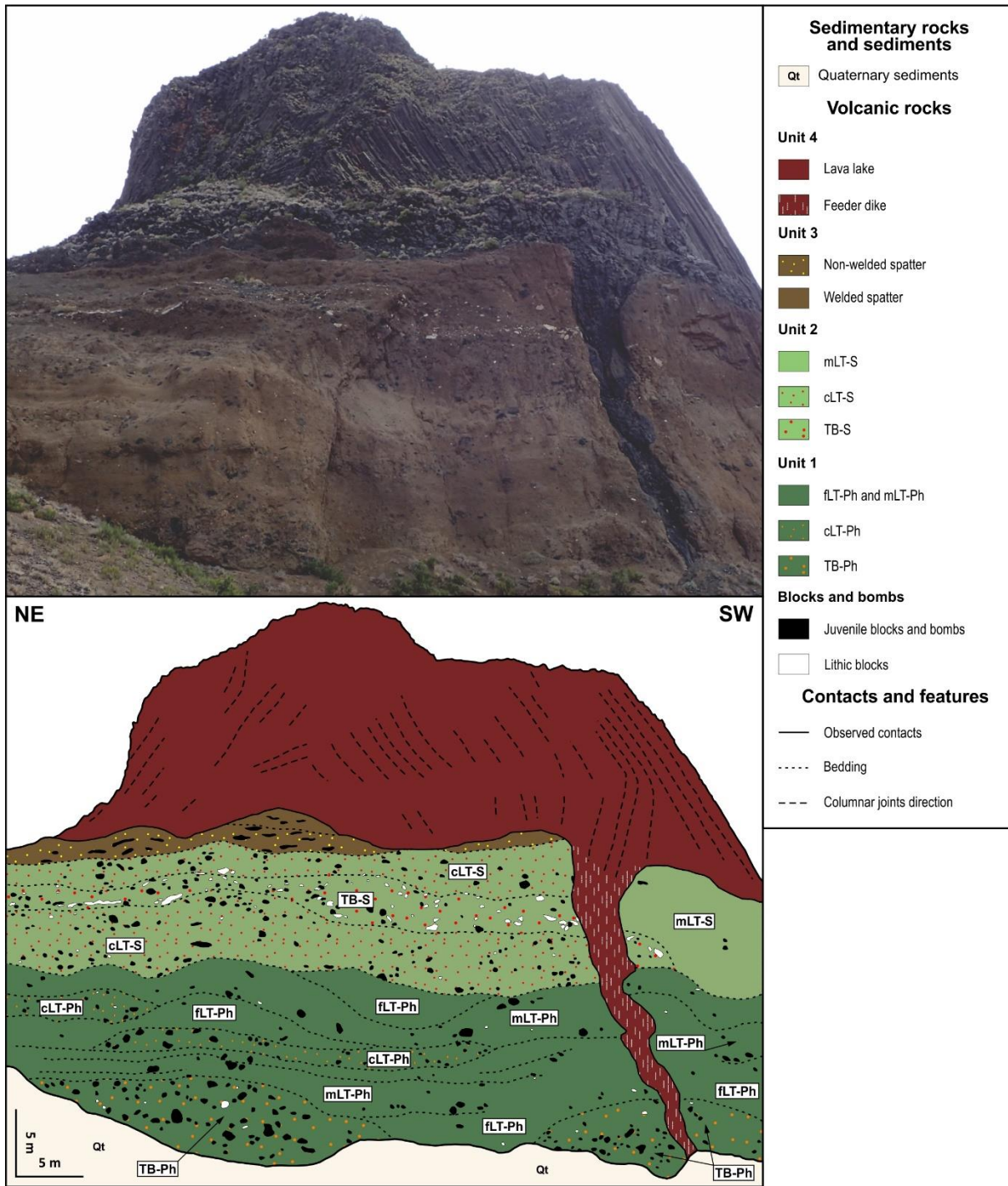


Figure 4.4: Geology of the north cliff of the North Peak. fLT-Ph = phreatomagmatic fine lapilli tuff, mLT-Ph = phreatomagmatic medium lapilli tuff, cLT-Ph = phreatomagmatic coarse lapilli tuff, TB-Ph = phreatomagmatic tuff breccia, mLT-S = phreato-strombolian medium lapilli tuff, cLT-S = phreato-strombolian coarse lapilli tuff and TB-S = phreato-strombolian tuff breccia.

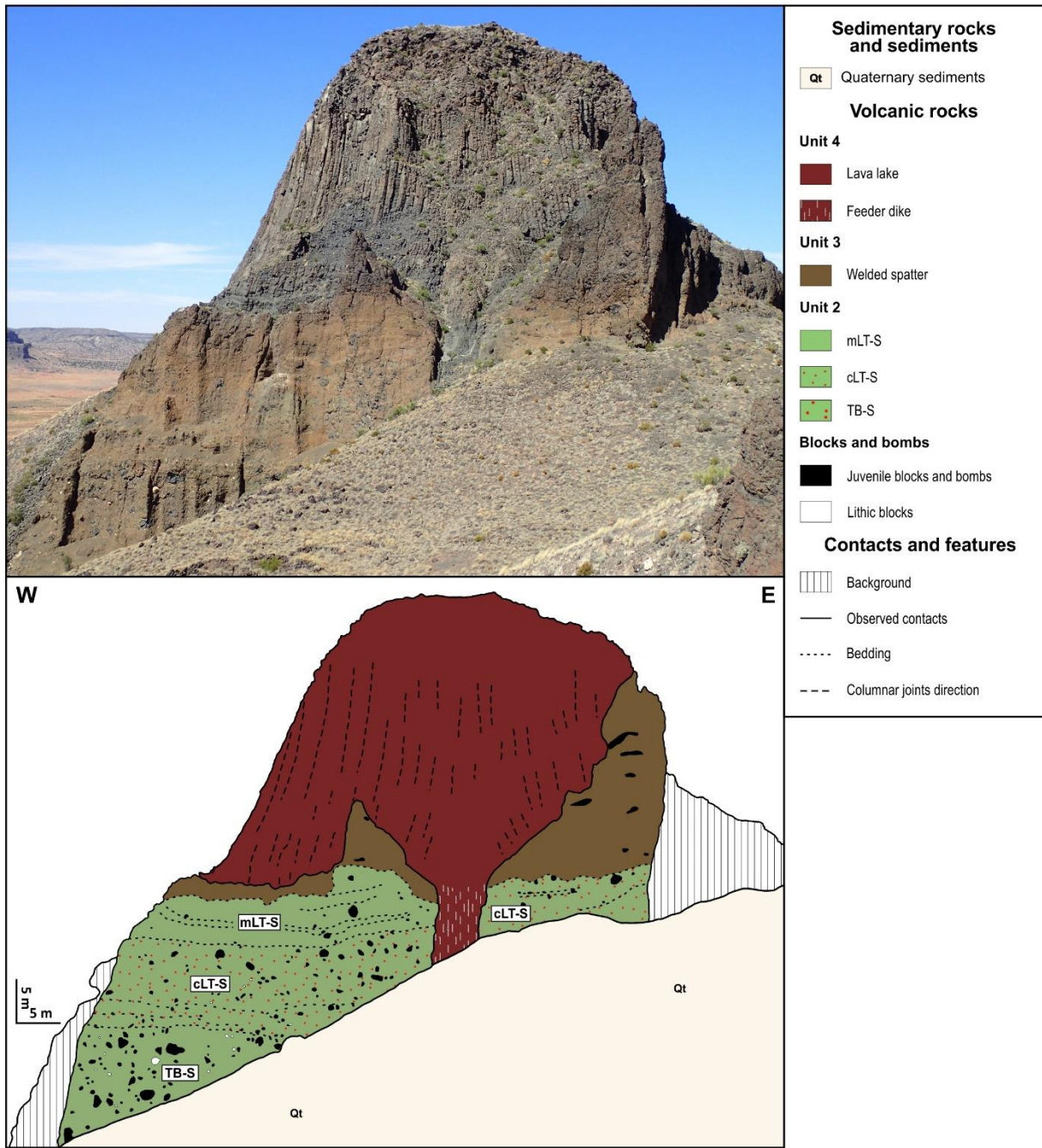


Figure 4.5: Geology of the south cliff of the North Peak. mLT-S = phreato-strombolian medium lapilli tuff, cLT-S = phreato-strombolian coarse lapilli tuff and TB-S = phreato-strombolian tuff breccia.

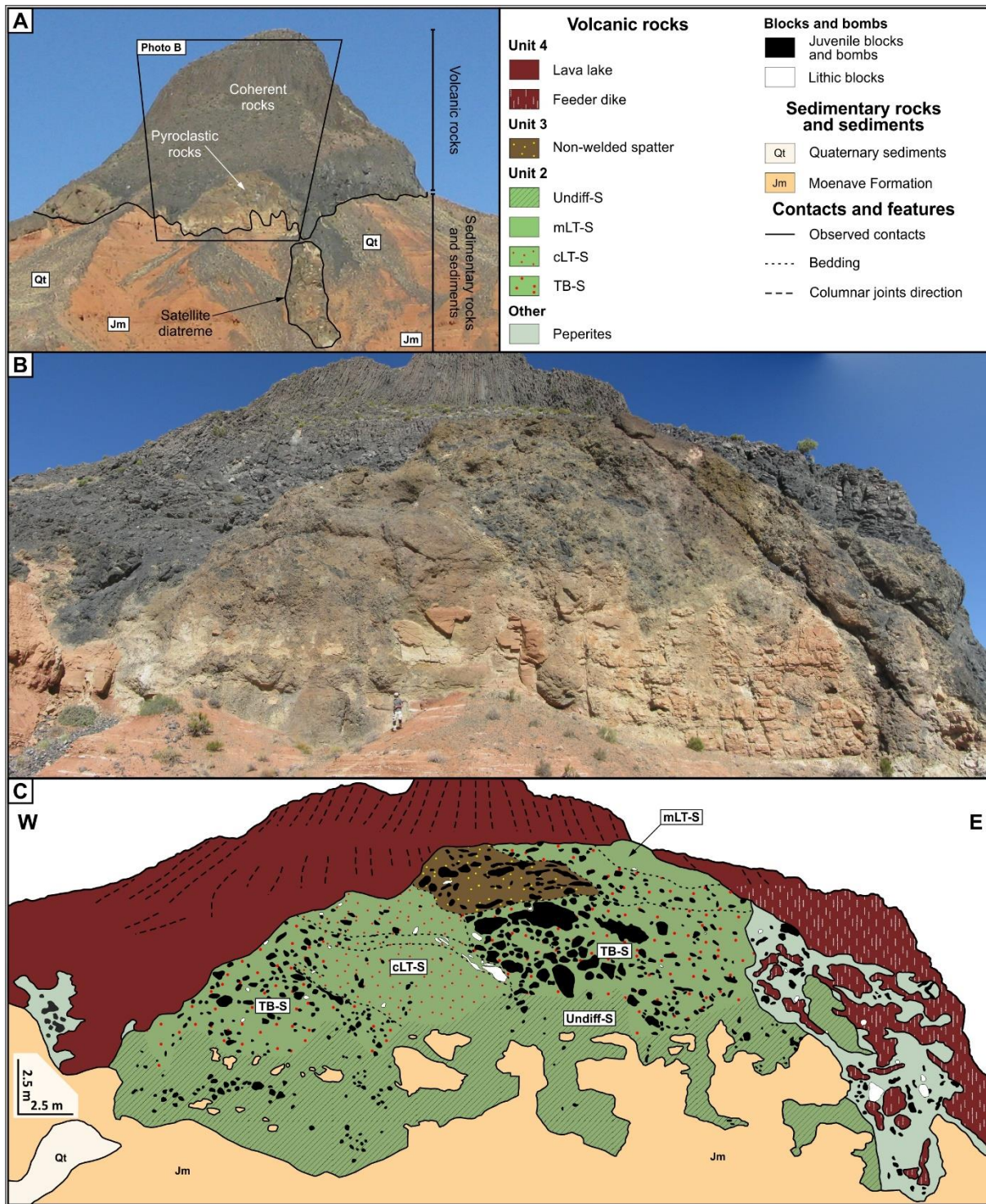


Figure 4.6: Geology of the south face of the South Peak. A) General view of the south face of the South Peak showing the perspective distortion of the photograph in B and C, B) Photograph of the south cliff, C) Geological map of the deposits highlighting the architecture of unit 2 to 4. Undiff-S = phreato-strombolian, undifferentiated, mLT-S = phreato-strombolian medium lapilli tuff, cLT-S = phreato-strombolian coarse lapilli tuff and TB-S = phreato-strombolian tuff breccia.

Pyroclastic deposits in the satellite diatreme are rich in lithic clasts and brown to black juvenile clasts; they are crosscut by numerous basanite dikes. Around the satellite diatreme, we observed tuff and lapilli tuff dikes that are few centimeters to ten centimeters thick (Fig. 4.3d) with a maximum extension in the south of ~150 m. These dikes are aligned NW-SE and are composed of lithic fragments and brown to black juvenile clasts within a whitish matrix (Fig. 4.3e). The satellite diatreme and tuff to lapilli tuff dikes are not considered further in this paper.

4.5 Methods

One month of field work was carried out at the Twin Peaks volcanic complex. We first mapped the entire complex, drawing limits of volcanic remnants, sedimentary rocks (Moenave and Chinle Formations, Billingsley et al. 2013) and Quaternary sediments on a geological map, using a satellite image as a background (Fig. 4.2). Then we mapped volcanic facies on each main peak, but not on the satellite diatreme, which remains undifferentiated (Fig. 4.3). We defined four volcanic units on the main peaks based on meter-scale observations and lithological descriptions of the rocks. They were named following the stratigraphic order with unit 1 at the bottom and unit 4 at the top. Units 1 to 3a are pyroclastic and non-welded, unit 3b is welded and unit 4 is a lava. Pyroclastic rock nomenclature follows White and Houghton (2006). Welding terms for spatter-bearing rocks are after Wolff and Sumner (2000) and Sumner et al. (2005). Vesicularity terms are taken from Houghton and Wilson (1989). Three subvertical cliffs (two on the North Peak, Fig. 4.3a and one on the South Peak, Fig. 4.3b), which provide cross-section-like exposures, were chosen to highlight relationships between the four units. The geology was drawn on high-resolution panoramic photographs of the cliffs (Figs. 4.4, 4.5, 4.6).

Componentry was quantified in the field using clast counts (Ross and White 2006) in units 1 and 2. Field clast counts are analogous to petrographic point counts and yield the volume fraction of components measured. Clast counts were obtained using a 1 m² net with a 10 cm mesh allowing us to quantify 100 points. During these measurements we classified only fragments greater or equal to 4 mm into different componentry bins, and put the rest as undifferentiated matrix (clasts <4 mm) and cement. We did not attempt to distinguish between true juvenile and recycled juvenile fragments during componentry measurements, since this distinction is very tricky. Loaded and cored juvenile clasts (Lefebvre et al. 2013) occur but were not counted separately. No clast counts were done on unit 3 because these rocks are extremely poor in sedimentary lithic clasts. Note that field *clast* counts are different from the field *line* counts

mentioned for Round Butte by Latutrie and Ross (2019). We are planning to compare the two methods elsewhere.

A total of 28 samples were taken: 14 are pyroclastic rocks, from unit 1 to 3, and 14 are non-fragmental rocks: lavas from unit 4, dikes, and blocks and bombs in unit 1 and unit 2 (Fig. 4.3). Each sample was sliced with a diamond blade, and the interior examined. This led to a selection of 16 representative samples in which thin sections were made. This includes 11 pyroclastic samples (four from unit 1, four from unit 2, and three from unit 3), and five non-fragmental rocks samples (two lavas in unit 4, one block and one bomb from unit 2 of the South Peak and one dike). All thin sections were petrographically described.

Matrix componentry was quantified by point counting on the thin sections of pyroclastic rocks. We first took images of entire thin sections using a “PowerSlide 5000” slide scanner at an optical resolution of 5000 dpi. Then we point counted the images using the “JMicroVision 1.2.7” free software (Roduit 2007; <https://jmicrovision.github.io/>; Németh and Kereszturi 2013), with 450 points per thin section and the recursive grid setting.

Finally, geochemical analyses were obtained on all 14 non-fragmental rock samples, distributed in Unit 3 (two samples of welded spatter), in Unit 4 (four samples of lava), in dikes from the main peaks (three samples), in juvenile blocks and bombs from pyroclastic units (four samples from units 1 and 2) and in a dike crossing the satellite diatreme (one sample). Geochemical methods and results are presented in the Online Resource 4.1.

4.6 Unit descriptions

4.6.1 Spatial organization of stratigraphic units

Unit 1 is the oldest and unit 4 is the youngest (Fig. 4.4). Due to post-volcanic erosion, this forms a concentric pattern in map view (Fig. 4.3). The north cliff map of the North Peak is the only location displaying the full eruptive sequence (Fig. 4.4). The other two cliff maps (south faces of both peaks, Figs. 4.5, 4.6) show unit 2 to unit 4.

4.6.2 Unit 1

Unit 1 forms the bottom 15-20 m of the north cliff map of the North Peak (Figs. 4.4, 4.7) and occurs over ~2 m² in the South Peak (e.g., sample TPS-7 on Fig. 4.3b). These pyroclastic rocks are medium brown in color and typically bedded, with subhorizontal beds or lenses tens of centimeters to several meters thick. The rocks are poorly sorted (visual assessment) and grain

size ranges from fine lapilli tuff to tuff breccia. Visual estimates yield 0-30% blocks and bombs, 40-60% lapilli, 20-45% ash and 0-10% calcite cement (Fig. 4.7). Beds from unit 1 are juvenile-rich to heterolithic in composition (75-95% juvenile clasts versus 5-25% lithics, in the lapilli and block/bomb fractions, see componentry below) but on average they display the highest lithic content of the whole complex.

In the field, juvenile clasts can be grey, black or brown in colour, the latter due to palagonite alteration. The brown clasts comprise 10 to 75% of all juvenile fragments (Fig. 4.7). Finer-grained beds (fine to medium lapilli tuff) tend to have a higher content in brown juvenile clasts (Figs. 4.7b, 4.7d). Independently of colour variations, juvenile clasts in unit 1 are mainly non-vesicular to incipiently vesicular (0-20% vesicles) to moderately vesicular (40-60% vesicles) and rarely highly vesicular (>60% vesicles). Moderately to highly vesicular clasts (scoria) are rare within beds and lenses of unit 1 (Fig. 4.7d). Juvenile fragments of all colours display similar shapes, from angular to amoeboid, but are mainly irregular to sub-round (Figs. 4.7c, 4.7d, 4.7e, 4.7f). Grey and black juvenile are larger on average than the brown ones, reaching block/bomb sizes (Figs. 4.7a, 4.7b, 4.7c). The brown ones range up to coarse lapilli (Figs. 4.7b, 4.7d).

Lithics fragments are scattered within the entire unit and derived mainly from the Bidahochi and Moenave Formations. Some lithic clasts originate from the Chinle Formation, perhaps up to ~200-250 m below their current location. Undifferentiated lithics with an inferred deeper origin are also present in traces. The proportion of lithics within the ash fraction is variable (Figs. 4.7e, 4.7f). In thin section, lithic clasts consist of greenish mudstone, greyish siltstone and fine sandstone (Figs. 4.7e, 4.7f).

4.6.3 Unit 2

In the north cliff map of the North Peak, unit 2 sits on top of unit 1 and on both peaks unit 2 is preserved below unit 3. This unit is dark brown, 7-20 m thick and pyroclastic. These rocks typically form subhorizontal beds several meters thick composed mostly of poorly sorted medium lapilli tuff to tuff breccia (Figs 4.4, 4.5, 4.6, 4.8). Visual estimates yield 10-30% blocks and bombs, 35-60% lapilli, 15-40% ash and 0-5% cement (Figs. 4.8a, 4.8b). Some parts of this unit are more thinly bedded, including well sorted medium lapilli tuff beds (Figs. 4.5, 4.6). On both peaks, this unit is juvenile-rich with 90-99% of juvenile clasts against 10-1% lithic clasts (in the lapilli and block/bomb fractions, see componentry below). Locally, beds with a higher lithic content occur (North Peak, see Figs. 4.4, 4.5, 4.8a; South Peak, see Fig. 4.8b). In the south cliff

map of the South Peak, we observed local peperite (Hooten and Ort 2002) at the contact between unit 2 and a feeder dike for unit 4 (Fig. 4.6).

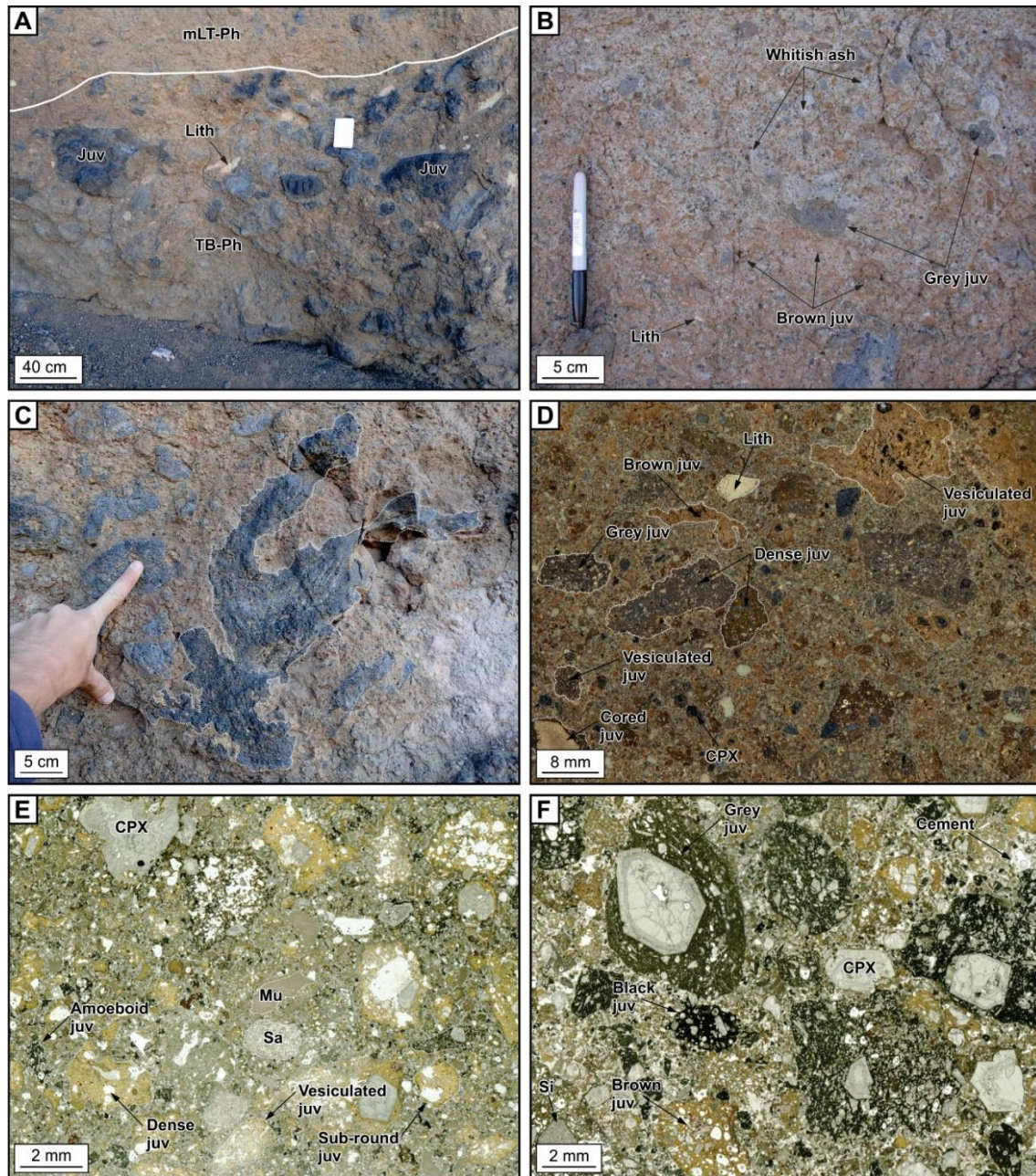


Figure 4.7: Photo plate of unit 1. A) TB-Ph bed overlain by a mLT-Ph bed, B) Close-up of the facies mLT-Ph rich in brown juvenile clasts, C) Amoeboid juvenile bomb, D) Slab of the facies mLT-Ph tuff (sample TPN-04 on Fig. 4.3a), E) High resolution scan of the mLT-Ph facies (sample TPN-04 on Fig. 4.3a) and F) High resolution scan of the mLT-Ph facies of the South Peak (sample TPS-07 on Fig. 4.3b). Juv = juvenile clasts, Dense juv = non-vesicular to incipiently vesicular juvenile clasts, Vesiculated clasts = moderately to highly vesicular clasts, Lith = lithic clasts, CPX = free clinopyroxene, Mu = mudstone clasts, Si = siltstone clasts and Sa = sandstone clasts.

In the field, juvenile fragments in unit 2 are mainly grey and black, and occasionally brown (0-15% of all juvenile clasts). Independently of the color, clasts are mainly irregular, sub-round to amoeboid, rarely sub-angular, and sometimes elongate like spatter, with a vesicularity ranging from <10 to 70% (Figs. 4.8c, 4.8d, 4.8e). Moderately to highly vesicular clasts (scoria) are present in higher proportion in this unit than in unit 1 (Figs. 4.8d, 4.8e) whereas non-vesicular to incipiently vesicular juvenile clasts are less abundant (Figs. 4.8c, 4.8d).

Lithic clasts are mainly whitish mudstone, siltstone to fine sandstone, ash to blocks and bombs in size. Some white lithic blocks/lapilli display radial cracks (Fig. 4.8f), with and a slight rim of alteration, suggesting that they were wet and unconsolidated when they were emplaced (Valentine and van Wyk de Vries 2014). They cooked and desiccated within the pyroclastic deposits and these particular clasts are likely derived from the Bidahochi Formation. Other lithic clasts display angular shapes and could be bleached Moenave Formation clasts (Jm, Fig. 4.8c). In thin sections or slabs, greenish mudstone from the Bidahochi Formation and reddish to whitish siltstone to fine sandstone from the Moenave Formation are present in these deposits as lapilli- or ash-sized clasts (Tbl, Fig. 4.8d and Jm, Fig. 4.8c).

4.6.4 Unit 3

The ~3-10 m-thick unit 3 consists of very dark brown to black tuff breccias (Figs. 4.4, 4.5, 4.9). These rocks are extremely juvenile-rich, with only traces of scattered white lithic blocks/lapilli, and are separated in two parts, namely unit 3a at the bottom and 3b at the top. In unit 3a, the spatter clasts are flattened but non-welded and occur in a matrix of fine/medium lapilli tuff, rich in ash (Fig. 4.9a). In unit 3b, the ash matrix is absent, spatter fragments are coarser than in unit 3a and are welded to strongly welded (Figs. 4.9b, 4.9c, 4.9d), grading locally into metric lenses of clastogenic lava (Fig. 4.9e). Lenses of clastogenic lavas record their pyroclastic origin by preserving ghosts of scoria, small spatter and non-vesicular clasts. Unit 3b is also better sorted than unit 3a with fragments from coarse lapilli to blocks and bombs in size. Rare spindle bombs are present in unit 3b. Spatter fragments in both subunits are generally flat, deformed and highly vesicular (up to 80%) with bigger vesicles in the middle (Fig. 4.9f, Stovall et al. 2011, 2012).

4.6.5 Unit 4

On each peak, unit 4 is composed of a 50-70 m thick black lava mass (Fig. 4.10a) that was fed by subvertical dikes (Figs. 4.4, 4.5, 4.6, 4.10b). Unit 4 is entirely jointed from bottom to top. Joints are spaced by 40-50 cm, diffuse to chaotic in the bottom and top parts, and well

developed in the middle part (Figs. 4.4, 4.5, 4.6, 4.10a). In general, within the thick columnar jointed portion, the joint orientation is vertical, but joints become less steep when the lateral margins of unit 4 are approached (Figs. 4.5, 4.6).

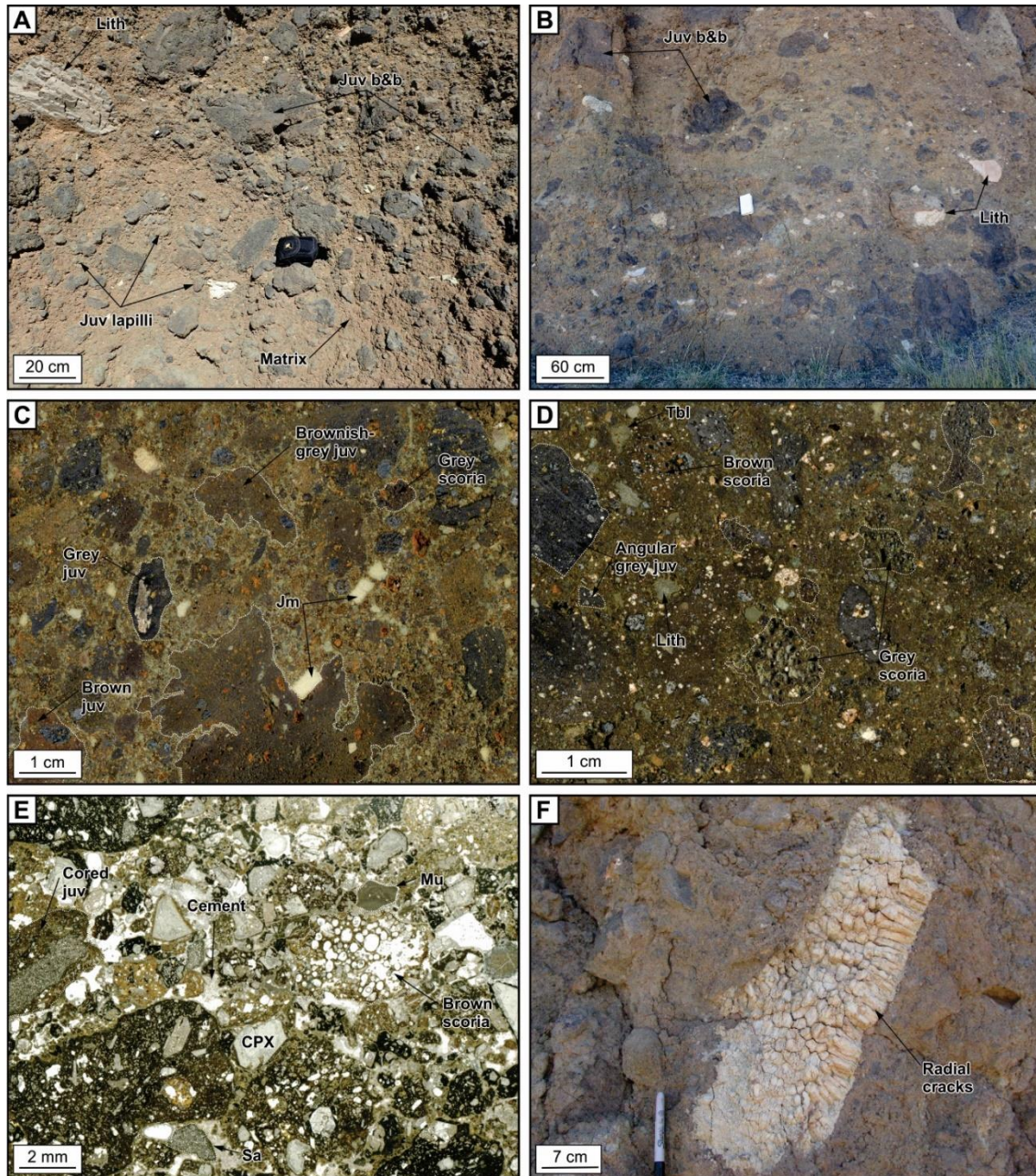


Figure 4.8: Photo plate of unit 2. A) Thick bed of TB-S facies on the North Peak, B) Bedded part displaying a lithic-rich TB-S facies at the bottom overlain by beds of mLT-S and TB-S rich in juvenile fragments on the South Peak, C) Slab of the lithic-rich TB-S facies of the North Peak (sample TPN-05 on Fig. 4.3a), D) Slab of the facies TB-S of the South Peak (sample TPS-04 on Fig. 4.3b), E) High resolution scan of the TB-S facies (sample TPN-15 on Fig. 4.3a) and F) Cooked Bidahochi block displaying radial cracks. Juv = juvenile clasts, Scoria = moderately to highly vesicular clasts, Lith = lithic clasts, b&b = blocks and bombs, CPX = free clinopyroxene, Tbl = Bidahochi Fm clast, Jm = Moenave Fm clast, Mu = mudstone clasts, Si = siltstone clasts and Sa = sandstone clasts.

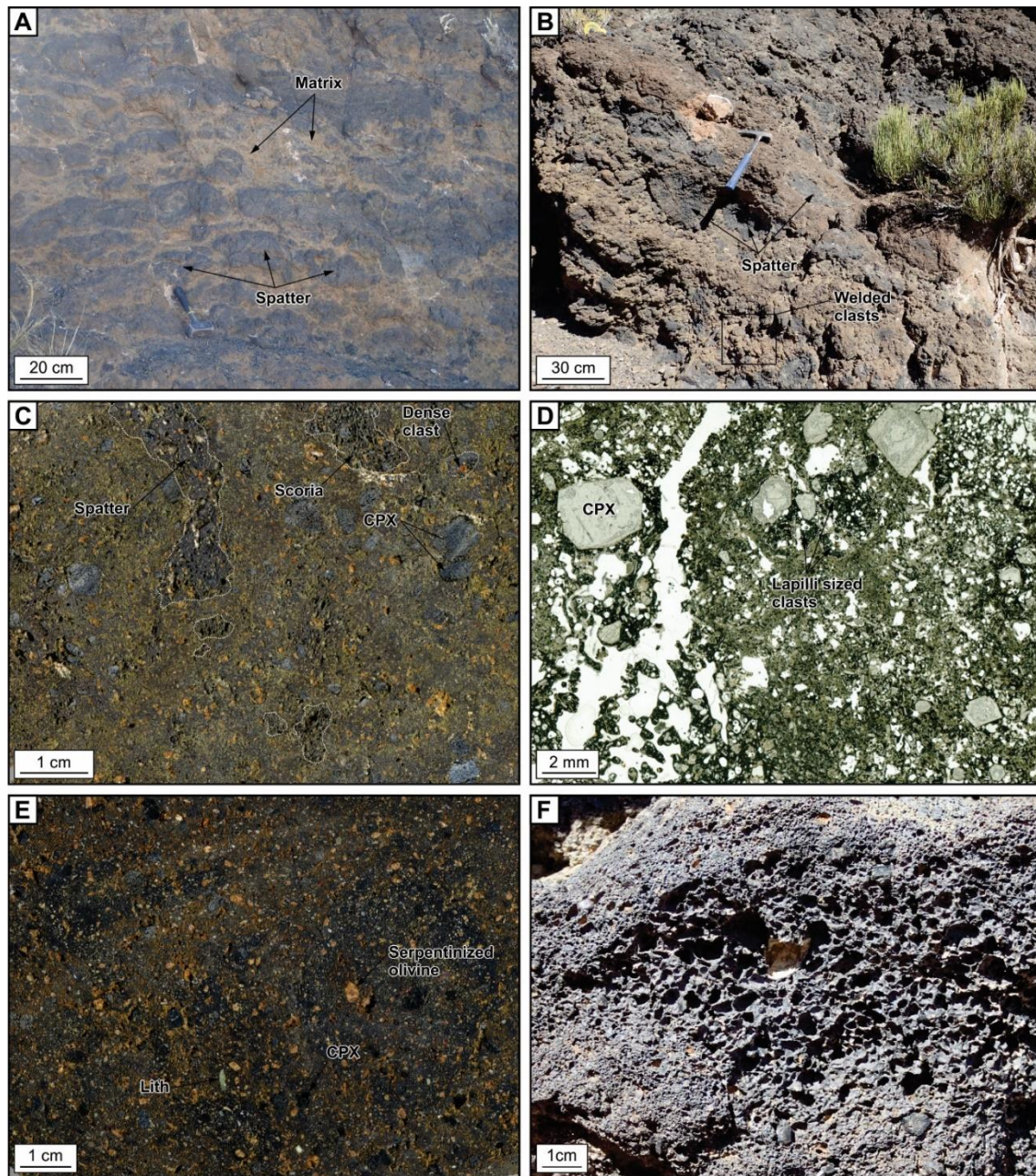


Figure 4.9: Photo plate of unit 3. A) Non-welded spatter deposit rich in matrix, B) Welded spatter deposits without matrix, C) Slab of a welded spatter deposit displaying various fragments (sample TPN-14 on Fig. 4.3a), D) High resolution scan of a welded spatter deposit (sample TPN-14 on Fig. 4.3a), E) Slab of a lens of a clastogenic lava displaying an homogeneous aspect and F) Spatter bomb with small vesicles at the edge and large vesicles in the center. Lith = lithic clasts, CPX = free clinopyroxene.

Samples from unit 4 and from feeder dikes (four samples from unit 4 and three from dikes) are all petrographically similar. These porphyritic rocks are composed of 5-10%, 0.2-5 mm, slightly to extremely serpentinized olivine; 10-15%, 0.2-10 mm, euhedral clinopyroxene; and 0-1%

vesicles (>1 mm, Figs. 4.10c, 4.10d). The microcrystalline groundmass contains serpentinized olivine, euhedral clinopyroxene and euhedral oxides (Fig. 4.10d).

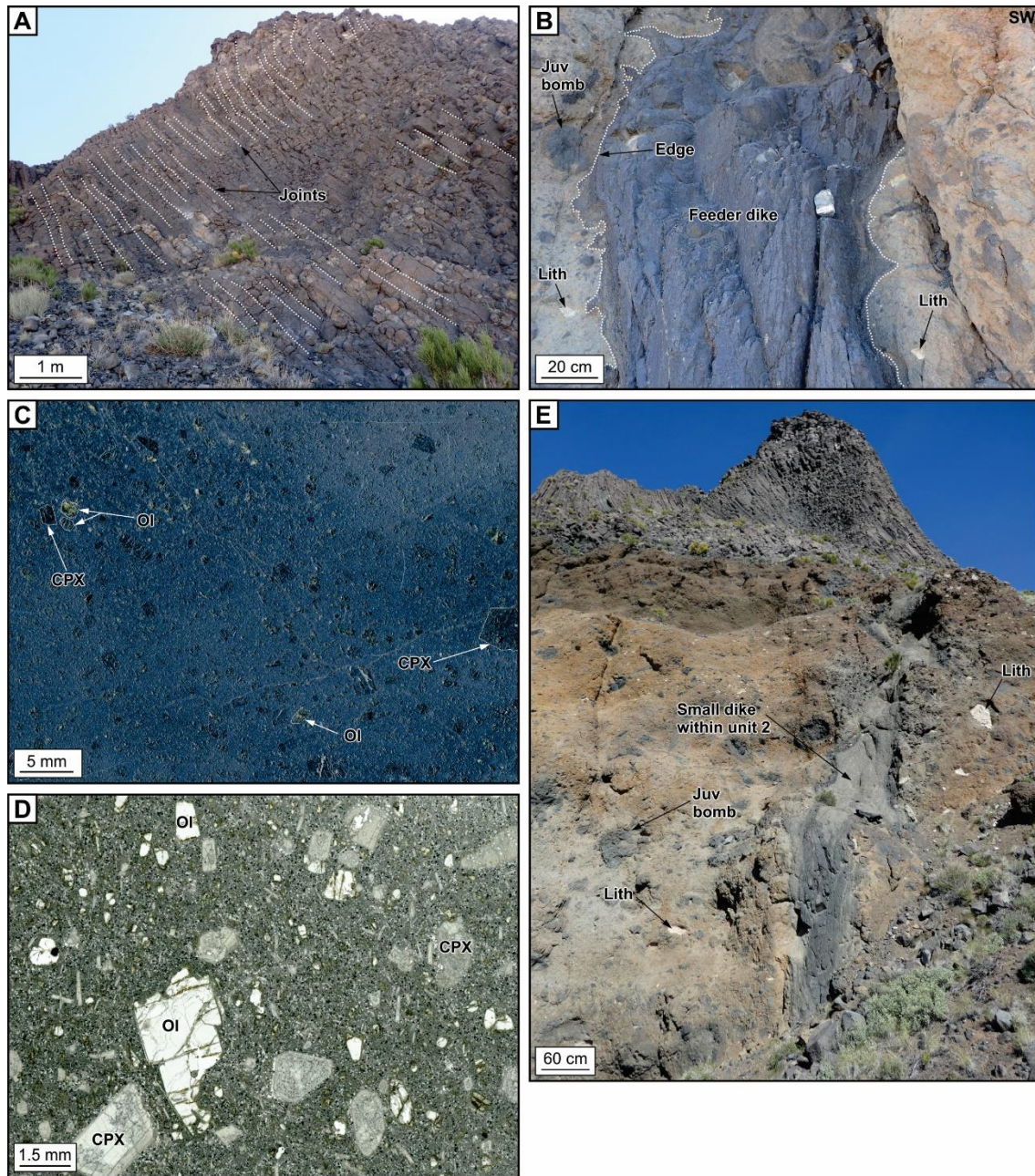


Figure 4.10: Photo plate of unit 4. A) Joints within unit 4 of the North Peak, B) Feeder dike displaying amoeboid edges, on the north cliff of the North Peak (Fig. 4.4), C) Slab of the lava that composes the feeder dike of the North Peak (sample TPN-02 on Fig. 4.3a), D) High resolution scan of the lava that composes unit 4 (sample TPS-02 on Fig. 4.3b), E) Small dike with amoeboid edges within unit 2. Juv = juvenile clasts, Dense juv = non-vesicular to incipiently vesicular juvenile clasts, Scoria = moderately to highly vesicular clasts, Lith = lithic clasts, CPX = clinopyroxene, OI = olivine.

4.6.6 Intrusions

Dikes that feed unit 4 are mapped on the three cliff maps. These subvertical dikes are oriented in a SE-NW direction, are 1-8 m thick and crosscut pyroclastic units 1 to 3 to feed unit 4 (Figs. 4.4, 4.5, 4.6, 4.10b). They display amoeboid margins implying an emplacement within unconsolidated pyroclastic sediments of units 1 and 2 (Fig. 4.10b). The dike that crops out in the south part of the South Peak probably crosscuts the Moenave sedimentary rocks at depth (Figs. 4.2, 4.3b), but most dikes at Twin Peaks do not seem to extend into the country rocks at the present level of exposure. We also mapped smaller intrusions that crop out in unit 2 (Figs. 4.3a, 4.3b, 4.10e). These are less than a meter thick, crosscut pyroclastic rocks and can be typically followed laterally (sills) or vertically (dikes) over several meters, locally up to 10 m (Fig. 4.10e).

4.7 Componentry measurements

4.7.1 Field clast counts

Field clast counts were carried out on seven sites corresponding to sample names on Fig. 4.3. They are distributed in unit 1 (three sites on the North Peak) and unit 2 (two sites on the North Peak and two sites on the South Peak) in order to quantify clasts ≥ 4 mm in long axis, versus 'matrix' (clasts < 4 mm) and cement. On average, unit 1 contains 46% "matrix + cement" whereas unit 2 has 40% for the South Peak and 30% for the North Peak (Table 4.1). In other words, unit 2 is coarser grained than unit 1. When the proportions of juvenile versus lithic clasts are recalculated to 100%, unit 1 is richer in lithic clasts, with 11% on average (range from 2% to 24%) against averages of 1% to 4% for unit 2 (range from 0-6%). We also recalculated to 100% the proportions of the different categories of juvenile clasts and found that on average, unit 1 is the richest in brown juvenile fragments with 20% (range from 0-34%), with other juvenile clasts being grey or black. Brown juvenile clasts are absent from unit 2 of the South Peak and comprise 17% of one clast count site of unit 2 of the North Peak. Note that most brown juvenile clasts are smaller than 4 mm, so are counted as 'matrix' in the field clast counts.

4.7.2 Petrographic point counts

For the componentry quantification of the < 4 mm clasts, we selected eight samples distributed in unit 1 (three samples from the North Peak and one from the South Peak) and unit 2 (two samples from the North Peak and two samples from the South Peak). Sample location is given in Fig. 4.3. Petrographic point counts show that unit 1 of the North Peak is the richest in

interstitial material (Table 4.2). This represents very fine-grained material that could not be assigned to a specific category based on our image resolution. Unit 2 is on average less rich in interstitial material than unit 1 of the North Peak (Table 4.2), again showing the poorly sorted nature of unit 1. One exception is unit 1 from the South Peak, which display the lowest value of interstitial material from all the petrographic point counts, based on only one sample.

Table 4.1: Results of field clast counts, expressed as percentages of clasts larger than, or equal to, 4 mm

Unit	Sample	Clast count number	Juvenile clasts						Lithic clasts				Matrix + Cement (<4 mm)
			Brown	Grey	Black	Undiff.	Free CPX/Olivine	Total	Bidahochi Fm	Moenave Fm	Undiff.	Total	
<i>South peak</i>													
2	TPS-04	2	0.0	38.0	2.0	22.0	0.0	62.0	0.0	0.0	1.0	1.0	37.0
2	TPS-06	1	0.0	56.1	1.0	0.0	0.0	57.1	0.0	0.0	0.0	0.0	42.9
Mean	-	-	0.0	47.1	1.5	11.0	0.0	59.6	0.0	0.0	0.5	0.5	39.9
<i>North peak</i>													
1	TPN-07	2	0.0	34.8	0.0	0.0	1.1	35.9	1.1	2.2	0.0	3.3	60.9
1	TPN-08	3	22.2	38.4	3.0	0.0	0.0	63.6	0.0	0.0	1.0	1.0	35.4
1	TPN-13	4	6.0	25.0	6.0	5.0	2.0	44.0	0.0	0.0	14.0	14.0	42.0
Mean	-	-	9.4	32.7	3.0	1.7	1.0	47.8	0.4	0.7	5.0	6.1	46.1
2	TPN-05	1	0.0	46.4	0.0	19.6	0.0	66.0	0.0	0.0	1.0	1.0	33.0
2	TPN-15	5	12.5	52.1	2.1	3.1	0.0	69.8	0.0	0.0	4.2	4.2	26.0
Mean	-	-	6.3	49.2	1.0	11.4	0.0	67.9	0.0	0.0	2.6	2.6	29.5

When the average proportion of juvenile versus lithic clasts is recalculated to 100% in the petrographic point counts, lithics clasts represent 12% of unit 1 of the North Peak. Unit 2 contains fewer lithic clasts with averages of 7% on the North Peak and 4% on the South Peak. We also recalculated to 100% the proportions of the different categories of juvenile clasts. This highlighted that on average, unit 1 of the North Peak has the highest proportion of brown juvenile clasts with 50% (range from 9-73%), whereas unit 2 has only 30% in the South Peak and 24% in the North Peak.

The juvenile clasts were counted into four vesicularity categories (Table 4.2). When recalculated to 100% juvenile clasts, unit 1 of the North Peak has the smallest abundance of clasts with a vesicularity higher than 40% (i.e. 17% clasts with a 40-60% vesicularity and 9% clasts with a >60% vesicularity). In contrast, unit 2 of the North and South Peaks comprises 34% and 31% clasts with 40-60% vesicles and 6% and 9% clasts with >60% vesicles, respectively. Non-vesicular to incipiently vesicular juvenile clasts are also more abundant within rocks of unit 1 of the North Peak ranging from 35% to 61% with an average value of 51%, whereas unit 2 of the

North Peak and South Peak has 45% and 36% respectively. In other words, juvenile clasts in unit 1 are less vesicular, on average, than those of unit 2 and vesicularity values in unit 1 are approaching the numbers reported by Ross and White (2012) for diatreme-like deposits at Coomb Hills, Antarctica.

4.7.3 Integration of field clast counts and petrographic point counts

Because the field clast counts and the petrographic point counts are similar methods applied at different scales, we integrated them to obtain an overall componentry estimate (Table 4.3). The “matrix + cement” value of the field clast counts represents the proportion of material to be accounted for using the petrographic point counts. On average, unit 1 is the richest in interstitial material with an average value of 21% whereas unit 2 has only low values (10% for the South Peak and 7% for the North Peak). Average values of juvenile versus lithic clasts recalculated to 100% highlight that unit 1 of the North Peak is richer in lithics (12-25%) than unit 2 of the North and South Peaks (5% and 1-3%, respectively). Considering only juvenile clasts recalculated to 100%, brown juvenile fragments have the highest abundance in unit 1 with 4-33%. These values do not reach 75% because we did not analyse the site richer in brown juvenile clasts with the two methods. Thanks to this integration we show that unit 2 of the South Peak contains about 10% of brown juvenile clasts instead of 0% as observed in field clast counts. Juvenile clasts are more abundant than lithics in all pyroclastic units. Finally, average values of the unit 2 of the North and South Peaks are extremely similar for all total juvenile and total lithic categories (Table 4.3).

Table 4.2: Results of petrographic point counts, expressed as a modal percentages

Unit	Sample	Juvenile clasts														Lithic clasts				Interstitial material	Cement						
		Brown					Grey					Black				Undiff.	CPX	Olivine	Total juvenile			Quartz	Mudstone	Siltstone	Sandstone	Total lithic	
		0-20	20-40	40-60	60-80	Total brown	0-20	20-40	40-60	60-80	Total grey	0-20	20-40	40-60	60-80												Total black
Vesicularity* (%)	0-20	20-40	40-60	60-80	Total brown	0-20	20-40	40-60	60-80	Total grey	0-20	20-40	40-60	60-80	Total black	-	-	-	Total juvenile	-	-	-	-	Total lithic	-	-	
<i>South peak</i>																											
2	TPS-04	6.2	6.5	4.2	0.0	16.9	10.2	14.6	13.2	1.2	39.0	1.9	0.9	0.0	0.0	2.8	2.1	4.9	0.2	65.8	0.0	3.5	0.2	0.0	3.7	28.9	1.6
2	TPS-06	11.7	2.8	11.0	0.0	25.5	14.5	6.9	11.2	9.2	41.7	0.7	0.2	0.0	0.0	0.9	1.4	4.4	0.0	73.9	0.0	0.7	0.9	0.0	1.6	22.7	1.8
Mean	-	9.0	4.6	7.6	0.0	21.2	12.3	10.7	12.2	5.2	40.4	1.3	0.6	0.0	0.0	1.8	1.7	4.6	0.1	69.8	0.0	2.1	0.6	0.0	2.7	25.8	1.7
1	TPS-07	15.3	5.0	4.1	2.1	26.6	14.4	5.3	14.6	4.1	38.4	1.8	2.8	0.0	0.0	4.6	3.4	1.8	0.0	74.8	0.0	0.5	0.2	1.8	2.5	16.9	5.7
<i>North peak</i>																											
1	TPN-04	23.9	9.3	5.7	0.9	39.7	6.8	4.7	5.0	0.0	16.5	0.5	0.0	0.0	0.0	0.5	2.0	1.4	0.0	60.1	1.6	3.4	0.9	1.1	7.0	33.0	0.0
1	TPN-07	4.4	0.2	0.0	0.0	4.7	9.1	12.9	5.8	8.0	35.8	0.9	0.0	0.0	0.0	0.9	2.2	4.9	3.1	51.6	4.9	1.8	0.7	0.7	8.0	40.4	0.0
1	TPN-13	21.2	5.7	8.2	3.2	38.3	7.8	1.1	0.5	0.9	10.3	1.4	0.0	0.0	0.0	1.4	1.4	1.1	0.2	52.6	0.7	5.2	0.2	0.5	6.6	40.8	0.0
Mean	-	16.5	5.1	4.6	1.4	27.6	7.9	6.3	3.7	3.0	20.8	0.9	0.0	0.0	0.0	0.9	1.9	2.5	1.1	54.7	2.4	3.5	0.6	0.8	7.2	38.1	0.0
2	TPN-05	9.6	3.1	2.9	1.4	17.1	8.7	2.7	13.3	4.3	28.9	11.8	0.2	0.2	0.0	12.3	3.6	3.9	0.2	66.0	0.0	4.6	3.1	1.4	9.2	24.8	0.0
2	TPN-15	6.5	3.0	5.8	1.6	17.1	7.2	4.9	19.6	0.5	32.2	12.2	3.7	0.9	0.0	16.8	4.9	2.1	1.4	74.5	0.0	1.2	0.0	0.0	1.2	18.5	5.8
Mean	-	8.1	3.1	4.4	1.5	17.1	8.0	3.8	16.4	2.4	30.6	12.0	2.0	0.6	0.0	14.6	4.3	3.0	0.8	70.3	0.0	2.9	1.6	0.7	5.2	21.6	2.9

*Vesicularity terms are from Houghton and Wilson (1989). 0-20% = non-vesicular to incipiently vesicular, 20-40% = poorly vesicular, 40-60 = moderately vesicular, 60-80% = highly vesicular

Table 4.3: Integration of point counts measurements in clast counts data to calculate the whole componentry of unit 1 and unit 2

Unit	Sample	Juvenile clasts					Total	Lithic	Interstitial material	Cement	
		Brown	Grey	Black	Undiff.	Free CPX/Olivine		Total lithic*			
<i>South peak</i>											
2	TPS-04	6.3	52.4	3.0	22.8	1.9	86.4	2.4	10.7	0.6	
2	TPS-06	10.9	74.0	1.4	0.6	1.9	88.8	0.7	9.7	0.8	
	Mean	-	8.6	63.2	2.2	11.7	1.9	87.6	1.5	10.2	0.7
<i>North peak</i>											
1	TPN-07	2.9	56.6	0.5	1.3	6.0	67.3	8.2	24.6	0.0	
1	TPN-13	22.1	29.3	6.6	5.6	2.5	66.1	16.8	17.1	0.0	
	Mean	-	12.5	43.0	3.6	3.5	4.3	66.7	12.5	20.9	0.0
2	TPN-05	5.6	55.9	4.1	20.8	1.4	87.8	4.0	8.2	0.0	
2	TPN-15	16.9	60.5	6.5	4.4	0.9	89.2	4.5	4.8	1.5	
	Mean	-	11.3	58.2	5.3	12.6	1.1	88.5	4.3	6.5	0.8

* Total lithic is calculated considering the total of lithic in clast counts and point counts

4.8 Origin of Twin Peaks volcanic rocks

4.8.1 Volcano type

The top of both peaks approximately corresponds to the pre-eruptive surface, based on measured elevations and regional sedimentary stratigraphy. The lowest volcanic exposures are 70 m lower, so the pyroclastic and jointed lavas exposed on the two peaks were emplaced 0 to 70 m below the pre-eruptive surface (Fig. 4.1). The volcanic rocks are surrounded by sedimentary country rocks, with steep to gently dipping contacts, indicating a funnel shape. Given these shapes for the volcanic rocks and the regional context of the HBVF (White 1991; Lefebvre et al. 2013, 2016; Latutrie and Ross 2019), our interpretation is that the two main peaks and the satellite diatreme each represent the remnant of a maar-diatreme volcano. More specifically, for the two main peaks, the exposed pyroclastic and jointed lavas were deposited in coalesced maar craters, with eruptive styles ranging from phreatomagmatic to effusive and correspond to a Type II upper diatreme infill according to White and Ross (2011).

4.8.2 Provenance of lithic clasts

Units 1 and 2 contain 12-25% and 1-5% lithics, respectively (Table 4.3). Lithic clasts with recognizable provenances are derived mainly from the Bidahochi and Moenave Formations. This shows that excavation of country rocks during the eruption was largely constrained to the

first ~170 m below the pre-eruptive surface (Fig. 4.1). Some lithics have a deeper origin (probably the Chinle Formation), indicating limited excavation at greater depths.

4.8.3 Interpretation of juvenile clasts

Juvenile fragments in unit 1-3 have the same phenocrysts and almost the same geochemical signature than basanite lava samples of unit 4, suggesting that they were derived from the same parental magma, although there is evidence for limited compositional variation over time (Online Resource 4.1). The variation in color in the juvenile fragments from units 1 and 2 is related to their groundmass: altered sideromelane for brown juvenile clasts and tachylite for grey and black juvenile clasts. Formation of sideromelane is related to a high cooling rates whereas tachylite is formed by a slower cooling rate (e.g., Furnes 1975; Stroncik and Schmincke 2002; White and Valentine 2016). In the literature, sideromelane fragments are mostly associated with water/magma interaction (White and Ross 2011; Lefebvre et al. 2013, 2016; Bélanger and Ross 2018; Latutrie and Ross 2019) but sideromelane fragments can also form in magmatic explosions (e.g., Stromboli, Cannata et al. 2014 and Mt Etna, Taddeucci et al. 2004; Andronico et al. 2009). Amoeboid and spatter fragments were deposited while still hot.

4.8.4 Unit 1

Unit 1 pyroclastic rocks are poorly sorted, bedded, fine lapilli tuffs to tuff breccias that display a high proportion of interstitial (optically irresolvable) material (Table 4.3, average value of 21%), probably representing fine ash. The thickness of the multiple subhorizontal beds and lenses of unit 1 are centimeters to meters and vary from one facies to another (e.g., fLT-Ph to TB-Ph on Fig. 4.4). Rocks are variable in componentry but are generally rich in lithic clasts (5-25%, Table 4.3). This indicates abundant country rock fragmentation during the eruption. Several types of juvenile clasts occur in unit 1, but brown ones are more abundant than in other units. Finally, juvenile clasts have a variable vesicularity, ranging from 0% to over 60%, but about half are non-vesicular to incipiently vesicular (Table 4.2), showing that fragmentation occurred independently of magma vesiculation. All of this, plus the occurrence of this unit in a crater excavated into country rocks, points to phreatomagmatic activity for unit 1 (Valentine et al. 2017). Unit 1 is typical of phreatomagmatic deposits within upper diatremes in the HBVF and elsewhere (Lorenz 1986a; White 1991; White and Ross 2011; Lefebvre et al. 2013; Valentine et al. 2017; Latutrie and Ross 2019).

The bedded sequence of unit 1 is composed by multiple beds or lenses that were formed by numerous subterranean explosions located below the current levels of exposure in the diatreme structure. The strongest explosions were able to reach the surface (syn-eruptive crater floor) and form plumes in and above the crater (White and Ross 2011; Ross et al. 2013; Valentine et al. 2014). Coarse grained thick beds and lenses are inferred to have formed from fallback into the crater or from pyroclastic density currents (PDCs, White and Ross 2011; Ross et al. 2013; Latutrie and Ross 2019). Bedded deposits of unit 1 were likely emplaced where they are today, since no strong evidence of subsidence, like saucer shaped beds or faults, was found. This means that at some point during the eruption, the crater floor of the North Peak eruptive centre was deeper than the bottom part of unit 1 in the north cliff of the North Peak, i.e. ~70 m (Fig. 4.4).

4.8.5 Unit 2

Unit 2 is mainly formed by thick subhorizontal beds of poorly sorted coarse lapilli tuff to tuff breccia (Figs. 4.4, 4.5) and sometimes displays thinly bedded packets of better sorted medium lapilli tuff (Fig. 4.5). Interstitial material, brown juvenile lapilli and non-vesicular to incipiently vesicular clasts are less abundant than in unit 1 (Tables 4.2, 4.3). Unit 2 can be followed all around the two peaks, including a specific lithic-rich bed in the North Peak (Figs. 4.4, 4.5). Rocks from unit 2 are richer in moderately to highly vesicular clasts (scoria) than unit 1. Clasts like scoria are more typically formed in hawaiian and strombolian activity (Sumner et al. 2005; Cannata et al. 2014; Gurioli et al. 2014; Taddeucci et al. 2015). Yet unit 2 still has some phreatomagmatic characteristics such as a significant proportion of non-vesicular to incipiently vesicular juvenile clasts, brown juvenile clasts, and some beds with high lithic contents. The mix of strombolian and phreatomagmatic features within unit 2 can be called informally “phreato-strombolian” and can be explained in different ways. Two vents, one phreatomagmatic and one strombolian, may have been simultaneously active, as seen during the eruption of East Maar at Ukinrek (e.g., Self et al. 1980; Büchel and Lorenz 1993; Ort et al. 2018). These vents could have been located in the same crater, or in different craters (North Peak versus South Peak). An intriguing alternative is that a single vent, with an eruptive style transitional between strombolian and phreatomagmatic, produced unit 2 in each crater. The details of how this would work are unclear, but may involve sloppy strombolian bursts resulting from an entrainment of water saturated host sediments, peperite or pyroclastic deposits along with the magma, as proposed by Valentine and van Wyk de Vries (2014). Or else, ingestion of slurry or liquid water within the strombolian conduit at depth could trigger weakly explosive water-magma

interactions, as experimentally obtained by Sonder et al. (2018). The shift from purely phreatomagmatic activity for unit 1 to a more transitional one in unit 2 can be explained either by an increased magma flux or by a decreased water supply. The thick beds in unit 2 were mainly emplaced by fallback in the crater (White and Ross 2011; Latutrie and Ross 2019).

The small intrusive dikes and sills found in unit 2 formed after the end of the deposition of the pyroclastic deposits of unit 2 (Fig. 4.3). These intrusions display amoeboid edges implying an emplacement within unconsolidated pyroclastic deposits (Fig. 4.10e). We consider that these small intrusions derive from the feeder dike that nourished the following units 3 and 4. The feeder dike was able to form fingers that crosscut unit 2 and probably unit 1 deeper in the diatreme.

4.8.6 Unit 3

Unit 3 is composed by non-welded spatter (unit 3a, Fig. 4.9a) overlain by welded spatter (unit 3b, Figs. 4.9b, 4.9c). These deposits are juvenile-rich (<1% lithics) and mainly composed of flattened spatter clasts (bombs and coarse lapilli). The spatter clasts display a gradient in the vesicle size with larger vesicles in the core and small vesicles in the edges (Fig. 4.9f).

4.8.6.1 Unit 3a: non-welded spatter

Unit 3a is composed of non-welded spatter within a pyroclastic matrix (fine/medium lapilli tuff), which is not typical of classic lava fountain deposits (Wolff and Sumner 2000; Andronico et al. 2008; Taddeucci et al. 2015). The pyroclastic matrix and the spatter were emplaced simultaneously, so unit 3a is a “phreato-hawaiian” deposit (informal term). To form this mixed deposit, two vents might have been active at the same time: one phreatomagmatic (or phreato-strombolian), and one hawaiian (lava fountain). Water may have been still available for water-magma interactions at the phreatomagmatic or phreato-strombolian vent, while a lava fountain started at the other vent (Kósik et al. 2016). Again, these two vents could have been located in the same crater, or in separate craters. The accumulation rate of the spatter was probably low to accommodate mixing of the pyroclastic matrix and non-welded spatter. More speculatively, unit 3a could have formed from a single “phreato-hawaiian” vent. Slurry or liquid water may have been entrained within the hawaiian conduit, resulting in recycling of existing pyroclastic debris and/or additional water-related magma fragmentation. Or, if there was a steep slope around the vent, pyroclastic deposits could have slid to the lava fountain and have been recycled.

4.8.6.2 Unit 3b: welded spatter

Unit 3b is composed of welded spatter deposits and clastogenic lavas typical of lava fountain activity (Head and Wilson 1989; Sumner 1998; Sumner et al. 2005; Andronico et al. 2008). No hint of magma-water interaction is seen in unit 3b. Non-vesicular clasts found in clastogenic lava could come from the recycling of non-vesicular clasts from unit 1 or unit 2.

4.8.7 Unit 4

Unit 4, at the top of the two peaks, is a thick lava with well-developed columnar joints in some portions. The thick feeder dikes (1 to 9 m wide) that crosscut the three underlying pyroclastic units (Figs. 4.4, 4.5, 4.6, 4.10b) are not typical of the HBVF, where most dikes are 0.4-1 m wide (Re et al. 2015, 2016; Muirhead et al. 2016). A large flux of basanite magma widened the feeder dikes within the diatremes, and the top of the dikes may have further widened due to the weight of the lava accumulation in the crater. Ongoing lava fountaining in the maar craters, with a high rate of spatter agglutination, could have nourished clastogenic lavas (Head and Wilson 1989; Sumner et al. 2005; Carracedo Sánchez et al. 2012) and formed a lava lake (Tazieff 1994; Lavine and Aalto 2002). Or else the magma within the dike was unable to fragment and the activity became effusive. Eventually the coalesced maar craters filled up with lava up to the pre-eruptive surface and may have overflowed. The lava lakes then cooled slowly over decades (Wright and Peck 1978; Cas and Wright 1988; Tazieff 1994), during which joints formed perpendicularly to the cooling surface (DeGraff and Aydin 1987). Joints patterns on both peaks are typical of lava lakes formed within a crater (Tietz et al. 2018).

4.8.8 Simultaneously active craters?

There is no evidence for any long pauses during the formation of the Twin Peaks volcanic complex. It seems likely that the formation of the two main peaks and the satellite diatreme are part of the same overall eruptive activity, along the same NW-SE feeder dike, although whether the craters were all active simultaneously is not clear. A first possibility is that activity migrated laterally over time to form separate volcanoes, like happened at Ukinrek (e.g., Self et al. 1980; Büchel and Lorenz 1993, Ort et al. 2018). This implies that the North and South Peaks had the same evolution in eruptive styles, but each formed completely separately, in succession. Because the two main craters (North and South Peaks) are close in space, and might have eventually coalesced, this seems unlikely. Also, the geochemical differences actually observed, for example the MgO variations, are between units 1-3 versus unit 4, *not* between the two peaks

(Online resource 4.1), suggesting that the unit 4 magma was the same at the two peaks, and was erupted after units 1-3 were emplaced at each peak.

So we hypothesize that the complex generally evolved from pyroclastic activity (units 1-3 in both peaks) to effusive and more Mg-rich magma (unit 4 in both peaks). However, the detailed timing of emplacement for units 1 to 3 in each of the main craters remains unclear. It is possible that a first crater was active, forming the succession from phreatomagmatic to magmatic pyroclastic deposits (units 1 to 3) before the feeder dike migrated and formed the second crater in exactly the same way. Alternatively, there could have been a simultaneous activity of the two main peaks evolving more or less in the same way. Or their evolution may have been similar, but not perfectly synchronous, so that one crater could still have been in the phreatomagmatic stage while the other had turned strombolian or phreato-strombolian. This would help to explain the 'mixed' or 'transitional' deposits in units 2 and 3a, by cross-contamination.

4.9 Twin Peaks evolution model

Since the North Peak and the South Peak show the same overall evolution, for simplicity our model shows only the activity of the North Peak (Fig. 4.11). The model has six steps and is presented as a cross-section through the interior of the peak (see section A-A' in Fig. 4.2). Features that are below the current erosion level are inferred from the literature and from other examples of maar-diatreme volcanoes in the HBVF.

4.9.1 Onset of activity

A basanite dike rose through the sedimentary rocks of the Colorado Plateau and interacted explosively with groundwater (Fig. 4.11a). Maar-diatreme volcanoes can be fed by plugs, sills or sheets (Re et al. 2015, 2016; Muirhead et al. 2016; Le Corvec et al. 2018) but because pyroclastic rocks of unit 1 to unit 3 are cross-cut by thick feeder dikes (Figs, 4.4, 4.5, 4.6, 4.10b) we chose to draw a dike as the feeder of the Twin Peaks volcanic complex. Initially, the dike is inferred to have a thickness close to the typical thickness of dikes in the HBVF (~0.4-1 m thick, Re et al. 2015, 2016; Muirhead et al. 2016). Phreatomagmatic explosions that occurred close to the pre-eruptive surface were able to excavate a small maar crater (Fig. 4.11a, Valentine et al. 2014). Pyroclastic surges and fallout started to form the ejecta ring while phreatomagmatic activity deepened the maar crater and progressively filled it with pyroclastic deposits of the proto-diatreme.

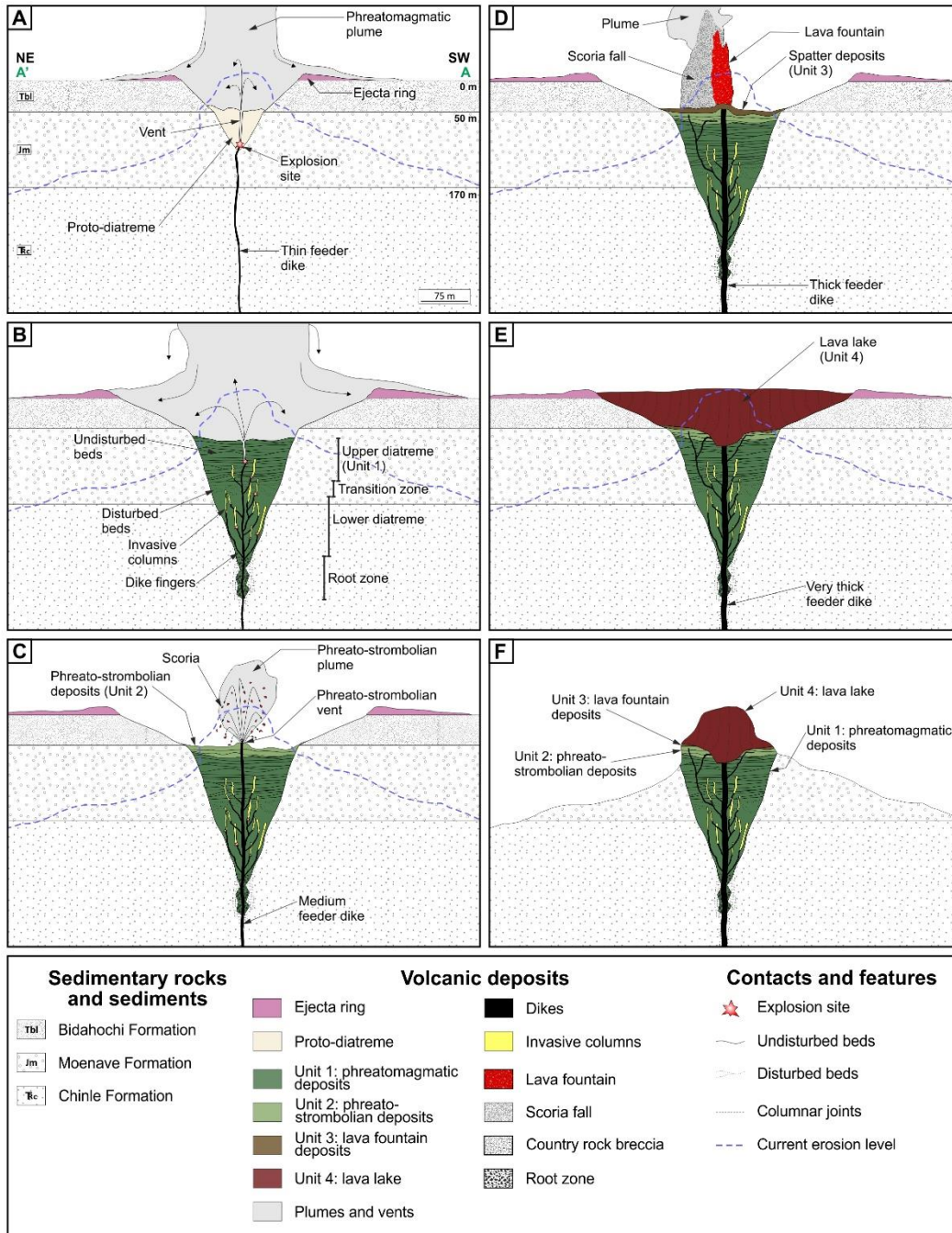


Figure 4.11: Twin Peaks evolution model built for the A-A' cross-section in the North Peak (Fig. 4.2). A) Onset of activity with the first crater and a small proto-diatreme, B) Phreatomagmatic phase building a relatively deep crater and a well-developed diatreme. The upper diatreme/unit 1 crops out at Twin Peaks whereas the transition zone, the lower diatreme with invasive columns and the root zone were not directly observed. These parts of the diatreme are drawn following the model of Latutrie and Ross (2019), C) Phreato-strombolian phase that formed deposits of unit 2, D) Lava fountain phase that formed spatter deposits of unit 3, E) Lava lake filling the crater, F) Current morphology of the North Peak after erosion of the surrounding country rocks. Note: events between step A and step B are unknown, hence the marked difference in the maturity of the diatreme.

4.9.2 Phreatomagmatic activity

With ongoing phreatomagmatic activity, country rocks were excavated and a relatively deep diatreme formed (Fig. 4.11b), with a crater that was likely at least 100 m deep. Bedded pyroclastic rocks of unit 1 are a typical example of phreatomagmatic upper diatreme bedded deposits in the HBVF, and were deposited at the bottom of this maar crater. In Fig. 4.11b, deposits below unit 1 are hypothetical and based on the model proposed by Latutrie and Ross (2019) for the nearby Round Butte diatreme. There, the diatreme is composed at the top by a well-bedded upper diatreme and at the bottom by a lower non-bedded diatreme, either homogeneous or displaying vertical structures called “invasive columns” (Fig. 4.11b). In between the upper and lower diatreme is a transition zone. At this stage, the feeder dike was still thin and nourished fingers within the lower diatreme deposits (and perhaps the upper diatreme as well) to allow phreatomagmatic explosions (Fig. 4.12a).

4.9.3 Phreato-strombolian activity

Unit 2 displays both phreatomagmatic and magmatic (strombolian) characteristics and its formation is discussed in detail above. To simplify the figure, we choose to draw one “phreato-strombolian” vent, but separate strombolian and phreatomagmatic vents could have been active. The change in eruptive regime, relative to that which prevailed earlier, could have resulted from an increased magma flux and/or a decreased water supply. At the end of this stage the feeder dike reached a shallower depth and thickened or widened, to feed the lava fountain and the lava lake (Fig. 4.12b).

4.9.4 Lava fountain activity

Unit 3a is transitional between phreatomagmatic and lava fountain deposits (see details on its origin above), whereas unit 3b consists of typical hawaiian lava fountain products. To simplify the figure, we choose to draw a typical lava fountain for the whole unit 3 (Fig. 4.11d). At the same time, the feeder dike formed fingers that cross-cut pyroclastic deposits of unit 1 and 2.

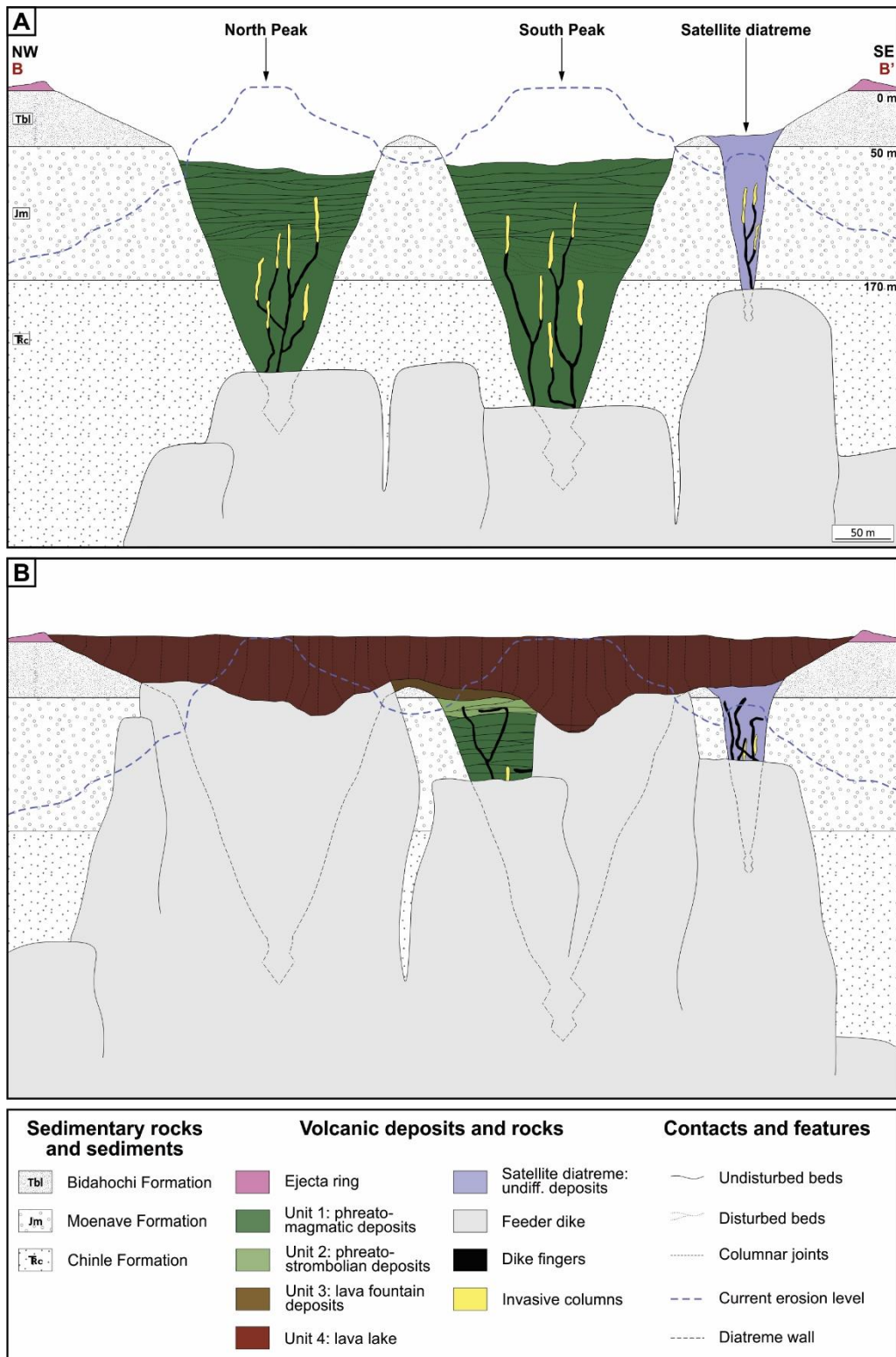


Figure 4.12: Longitudinal cross-section of the Twin Peaks volcanic complex parallel to the feeder dike orientation (B-B' in Fig. 4.2). A) Subterranean morphologies of the North, the South and the satellite diatremes at the end of the emplacement of unit 1, B) Subterranean morphologies of the volcanic complex at the end of the formation of unit 4.

4.9.5 Lava lake filling the crater

The final stage of the eruption formed a lava lake (unit 4) which likely finished filling up the maar crater (Fig. 4.11e). The lava lake may have overflowed to feed lava flows on the pre-eruptive surface. Concurrently, within the diatreme, the feeder dike probably continued to thicken and form more fingers. These fingers did not have water/magma interactions because the pyroclastic deposits of the diatreme had dried up. After the eruptive activity ended, the lava lake cooled slowly and joints started to form.

4.9.6 Post-eruptive erosion

After the end of the eruptive activity, erosion removed part of the surrounding country rocks (Fig. 4.11f). Sedimentary rocks from the Bidahochi Formation were completely eroded whereas those from the Moenave Formation are still present and form the steep to gentle slopes around the volcanic remnants. However, the thick jointed basanite masses of unit 4 protected the pyroclastic deposits of units 1 to 3.

4.10 Phreatomagmatic vs magmatic eruptive styles in ultramafic to mafic maar-diatreme settings

White and Valentine (2016) summarized the difficulties to find unambiguous criteria to distinguish phreatomagmatic vs magmatic fragmentation in pyroclastic deposits. They reviewed traditional criteria such as grain size, juvenile clast vesicularity and morphology, the nature of the volcanic glass, welding and agglutination, particle aggregation, and lithic contents. When all magma compositions (ultramafic to felsic) and eruption styles, including subaqueous ones, are taken into account, the traditional criteria tend to be ambiguous or have exceptions.

Fortunately, the phreatomagmatic versus magmatic distinction problem is much simpler if restricted to subaerial ultramafic to mafic monogenetic volcanoes, and maar-diatreme ones in particular (White and Ross 2011; Ross et al. 2018). Within this very restricted realm, the traditional criteria reviewed by White and Valentine (2016) still mostly work (Table 4.4). We present mainly field to macroscopic criteria, that can be applied to both historical eruptions and ancient deposits such as those at Twin Peaks, which are altered and cemented. This prevents examination of the 3D shapes and surface features of ash particles, which are therefore not included in Table 4.4.

Table 4.4 Traditional criteria used to distinguish phreatomagmatic from magmatic eruptive styles in basaltic maar-diatreme volcanoes

Eruptive style	Phreatomagmatic	Phreatomagmatic	Strombolian	Hawaiian
Maar-diatreme part	Upper diatreme	Ejecta ring	Upper diatreme/ejecta ring	Upper diatreme/ejecta ring
<u>Deposits</u>				
Color	Paler ¹	Paler ¹	Darker ¹	Darker# ¹
Thickness of beds	Millimeters to meters* ^{2, 3, 4, 5}	Millimeters to meters ^{2, 6, 7, 8, 9, 10, 11, 12, 13}	Tens of centimeters to meters ^{10, 13, 14, 15}	Meters where bedded# ^{1, 10, 13}
Morphology of beds	Sheets to lenses* ^{2, 3, 4, 5}	Sheets to lenses ^{2, 6, 7, 8, 9, 10, 11, 12, 13}	Sheets draping topography ^{10, 13, 14, 15}	Form ramparts ^{1, 10, 13}
Structures	Mostly plane-parallel bedding; rare crossbedding, dunes or bomb sags ^{2, 3, 4, 5}	Mostly plane-parallel bedding; common crossbedding, dunes and bomb sags ^{2, 6, 7, 8, 9, 10, 11, 12, 13}	Internally structureless to diffusely stratified beds ^{10, 13, 14, 15}	Internally structureless# ^{10, 13}
Mode of emplacement	PDCs, fallback* [^] , ballistic bombs ^{2, 3, 4, 5}	PDCs, mostly surges (rare pyroclastic flows), fallout, ballistic bombs ^{2, 6, 7, 8, 9, 10, 11, 12, 13}	Fallout from plume [^] , ballistic bombs ^{10, 13, 14, 15}	Fallout from fountain#, ballistic bombs ^{10, 13}
Degree of sorting	Generally poorly sorted* ^{^ 2, 3, 4, 5}	Variably sorted ^{2, 9, 10, 11, 12, 13}	Better sorted than phreatomagmatic deposits ^{^ 10, 13, 14, 15}	Better sorted than phreatomagmatic deposits# ^{10, 13}
Fine particle content	High ash content* ^{^ 2, 3, 4, 5, 16}	High ash content ^{2, 10, 11, 12, 13, 16}	Low ash content in proximal deposits ^{10, 13, 14, 15, 17, 18}	Low ash content in proximal deposits# ^{10, 13}
Size of particles	Extremely fine ash (<63 µm) to blocks and bombs (>64 mm)* ^{^ 3, 4, 5}	Extremely fine ash (<63 µm) to blocks and bombs (>64 mm) ^{2, 10, 11, 12, 13, 16}	Fine lapilli (>2 mm) to blocks and bombs (>64 mm) in proximal deposits ^{15, 17, 18}	Coarse lapilli (>2 mm) to blocks and bombs (>64 mm) in proximal deposits# ^{10, 13}
Lithic content	Low to high (few tens of % to over 80%)* ^{^ 1, 2, 3, 4, 5, 19}	Low to very high (few % to 90%) ^{1, 2, 10, 11, 12, 13, 19, 20}	Nil to low (5%) ^{^ 1, 10, 13, 14, 15, 18, 21}	Nil to low (5%)# ^{1, 10, 13, 21}
Accretionary lapilli	Possible but often absent ^{1, 21}	Possible but often absent ^{t1, 8, 21, 22}	No ^{1, 21}	No# ^{1, 21}
Cementation	Typically cemented* ^{^ 1, 2, 3, 4, 5}	Poorly to strongly cemented ^{1, 10, 11, 12, 13}	Usually poorly cemented ^{10, 13, 14, 15}	Non to poorly cemented# ^{10, 13}
Agglutination/welding	No* ^{^ 1, 3, 21}	No ^{1, 10, 12, 13}	Possible ^{1, 15, 18}	Non to strongly welded# ^{1, 23, 24}
<u>Juvenile clasts</u>				
Vesicularity	Typically non to moderately vesicular; rarely highly vesicular* ^{^ 1, 21, 25}	Typically non to moderately vesicular; rarely highly vesicular ^{1, 10, 21, 25}	Moderately to extremely vesicular ^{^ 1, 14, 15, 25}	Moderately to extremely vesicular ^{1, 24, 25, 26}
Size of vesicles	Typically small* ^{^ 1, 21, 25}	Typically small ^{1, 10, 21, 25}	Can be large and coalesced ^{^ 1, 18, 25}	Can be large and coalesced# ^{1, 18, 25, 26}
Morphology/shape	Angular/blocky to irregular/amoeboid* ^{^ 21, 27, 28, 29}	Angular/blocky to irregular/amoeboid ^{21, 27, 28, 29}	Mainly scoria [^] , shape is controlled by vesicles ^{^ 18, 24, 29}	Mainly scoria/spatter#, shape is controlled by vesicles# ^{18, 24, 26, 29}
Loaded/cored bombs	Frequent ^{11, 30}	Frequent ^{11, 30}	Rare	Absent

*Criteria found in unit 1 at Twin Peaks, ^ Criteria found in unit 2 at Twin Peaks, # Criteria mainly found in unit 3b at Twin Peaks

References: ¹Ross et al. (2018); ²White (1991); ³Bélanger and Ross (2018); ⁴Latutrie and Ross (2019); ⁵Delpit et al. (2014); ⁶Fisher and Waters (1970); ⁷Crowe and Fisher (1973); ⁸Lorenz (1974); ⁹Sohn (1996); ¹⁰Ross et al. (2011); ¹¹Lefebvre et al. (2013); ¹²Graettinger and Valentine (2017); ¹³Ort et al. (2018); ¹⁴Houghton and Schmincke (1989); ¹⁵Houghton et al. (1996); ¹⁶Zimanowski et al. (1997); ¹⁷Self et al. (1974); ¹⁸Cannata et al. (2014); ¹⁹Ollier (1967); ²⁰Womer et al. (1980); ²¹White and Ross (2011); ²²Moore et al. (1966); ²³Head and Wilson (1989); ²⁴Sumner et al. (2005); ²⁵Houghton and Wilson (1989); ²⁶Stovall et al. (2012); ²⁷Walker and Croasdale (1971); ²⁸Heiken (1972); ²⁹Heiken and Wohletz (1985); ³⁰Sottili et al. (2010)

As shown here for Twin Peaks and in previous studies elsewhere, phreatomagmatic bedded deposits in upper diatremes and maar ejecta rings are usually paler in color, more poorly sorted, poorly to strongly cemented, richer in ash, and richer in lithic clasts, compared to the rare magmatic pyroclastic deposits found in the same settings (Moore et al. 1966; Houghton and Schmincke 1989; White 1991; Houghton et al. 1996; Zimanowski et al. 1997; White and Ross 2011; Latutrie and Ross 2018; Ross et al. 2018). These bedded deposits display millimetric to metric subhorizontal to lensoid beds formed by PDCs, surges, fallback (upper diatreme), fallout (ejecta ring), and ballistic ejection (e.g., White and Ross 2011; Bélanger and Ross 2018; Latutrie and Ross 2019). Cross-bedding, dunes and bomb sags can be found in those deposits (e.g., Fisher and Waters 1970; Crowe and Fisher 1973; Ross et al. 2011; Delpit et al. 2014). Phreatomagmatic juvenile clasts are angular to irregular (and amoeboid) in shape and can display brittle to fluidal surface features (Walker and Croasdale 1971; Heiken and Wohletz 1985; Ross et al. 2018). Loaded and cored bombs are frequent in phreatomagmatic eruptions (Sottili et al. 2010; Lefebvre et al. 2013). They also exhibit a large range of vesicularities from non-vesicular to rarely highly vesicular (Houghton and Wilson 1989; White and Ross 2011; Ross et al. 2018).

On the other hand, strombolian deposits in maar-diatreme settings are darker in color, better sorted, generally poorly cemented, poorer in ash, and poorer in lithic clasts (Self et al. 1974; Houghton and Schmincke 1989; Houghton et al. 1996; Ross et al. 2011, 2018; Saucedo et al. 2017). Fallout from the small plume and ballistic ejection are the main processes responsible for the formation of strombolian beds (Houghton and Schmincke 1989; Houghton et al. 1996; Ross et al. 2011, 2018; Cannata et al. 2014). Beds are usually subhorizontal, structureless to diffusely stratified (Houghton and Schmincke 1989; Houghton et al. 1996; Ross et al. 2011). The juvenile clasts are more vesicular, with a smaller range of vesicularities and they are more irregular in shape, with their shapes controlled by vesicles (Walker and Croasdale 1971; Heiken and Wohletz 1985; Houghton and Wilson 1989; Cannata et al. 2014). Hawaiian deposits in maar-diatreme volcanoes are dark brown to black, diffusely bedded, non-welded to welded, better sorted than phreatomagmatic deposits, poor in ash and lithic clasts (Sumner et al. 2005; Andronico et al. 2008, 2009). Hawaiian juvenile clasts are mainly scoria and spatter, moderately vesicular to extremely vesicular (Stovall et al. 2011, 2012; Gurioli et al. 2014). These juvenile clasts are amoeboid fluidal clasts that flatten on landing and can agglutinate (Head and Wilson 1989; Sumner 1998; Andronico et al. 2008, 2009).

The texture of the groundmass of juvenile fragments seems to be an ambiguous criterion. Although the classic view is that sideromelane forms in contact with water whereas tachylite does not (e.g., White 1996b; White and Ross 2011; Latutrie and Ross 2019), there are now too many exceptions to keep this as a strong rule. For example, strombolian to hawaiian activity at Stromboli (Cannata et al. 2014) and Mt Etna (Taddeucci et al. 2004; Andronico et al. 2009) have formed sideromelane. Conversely, tachylitic juvenile clasts have been reported from phreatomagmatic deposits in maar-diatreme settings (e.g., Ross et al. 2011; Lefebvre et al. 2013; Bélanger et al. 2019; Latutrie and Ross 2019).

4.11 Conclusions

This study documents for the first time one of the 'plug'-dominated volcanic remnants which are common in the HBVF⁴ (Williams 1936). The Twin Peaks volcanic complex is an excellent site to discuss:

1. the nature of these 'plug'-dominated volcanic remnants;
2. the processes that produce a change in the eruptive regime from phreatomagmatic to magmatic;
3. the criteria used to distinguish phreatomagmatic from magmatic eruptive styles in ultramafic to mafic maar-diatremes.

The two main peaks (North and South) and the satellite diatreme that compose the Twin Peaks volcanic complex are preserved within Moenave Formation sedimentary rocks. The North and South Peaks are composed by pyroclastic rocks (unit 1 to 3) overlain by jointed lava (unit 4) and these volcanic rocks have gentle to steep contacts with the sedimentary rocks implying a funnel shape structure. Twin Peaks volcanic complex was probably formed by the simultaneous eruption of three maar-diatremes volcanoes along a southeast-northwest direction (Fig. 4.12a). All pyroclastic rocks and lavas exposed on the two main peaks were deposited within maar craters. These volcanoes were probably active for days to weeks (Self et al. 1980; Büchel and Lorenz 1993) whereas the small satellite diatreme was probably active during a few days at most.

In this paper we documented an eruptive sequence that starts with purely phreatomagmatic deposits (unit 1) overlain by phreato-strombolian deposits (unit 2), by phreato-hawaiian deposits

⁴ This chapter describes for the first time 'plug'-dominated volcanic remnants in the HBVF. Other examples have been described in Europe (Martin and Németh 2004; Lexa et al. 2010; Hencz et al. 2017)

(unit 3a), and by hawaiian lava fountain deposits (unit 3b). It ended with lava lakes filling the maar craters (unit 4, Fig. 4.12b). This sequence found in the North and South Peaks resulted from the progressive increase of the magma flux and/or the decrease of the water supply or availability.

We reviewed the traditional criteria to distinguish phreatomagmatic from magmatic explosive eruptive styles in ultramafic to mafic maar-diatreme settings and conclude that most of those criteria are still helpful. However, groundmass textures (tachylite vs sideromelane) in juvenile fragments appear to be an ambiguous criteria and more work seems needed to investigate these criteria carefully.

4.12 Acknowledgements

Twin Peaks was first visited by PSR during a field trip with James D.L. White, Greg A. Valentine, and Nathalie Lefebvre. These researchers have influenced our ideas through discussions and their papers. We thank Greg A. Valentine for reading the draft of the manuscript and Romain Jattiot for helping us during the field work in the steep slopes. We thank the Morris family for allowing us to work at Twin Peaks. Any persons wishing to conduct geological investigations on the Navajo Nation must first apply for, and receive, a permit from the Navajo Nation Minerals Department, P.O. Box 1910, Window Rock, Arizona 86515, USA, telephone 1-928-871-6587. We thank Alison H. Graettinger, Karoly Németh and editor Jacopo Taddeucci for their constructive reviews.

4.13 Online Resource 4.1: Geochemistry and petrography of coherent samples from Twin Peaks volcanic complex

4.13.1 Methods

At the Twin Peaks volcanic complex, 14 coherent samples were collected for geochemical and petrographic analyses:

- two samples from Unit 3 (welded spatter),
- four samples from Unit 4 (lava lake),
- three samples from coherent dikes (two from the North peak and one from the South peak),
- four samples from juvenile blocks and bombs (two in unit 1 and two in unit 2)
- one from a dike crossing the satellite diatreme.

Sample location is shown on Fig. 4.3 in the article. Weathered crusts were cut away with a diamond blade and discarded. Rare calcite amygdules and lithic xenoliths (mainly whitish to greenish sedimentary rocks) were avoided as much as possible. Then, fist size samples were sent to Activation Laboratories (ActLabs) in Ancaster, Ontario, Canada, to analyze major oxides and trace elements. The samples were coarsely crushed and then pulverized in a mild steel shutter box. The resulting powders were mixed with lithium metaborate and lithium tetraborate and fused by melting. The melts were dissolved in a 5% nitric acid solution and read on a ICP-OES for major oxides and some trace elements (Ba, Be, Sc, Sr, V and Zr) and on a ICP-MS for 39 trace elements.

4.13.2 Petrographic observations

All the 14 coherent samples of Twin Peaks volcanic complex display the same phenocrysts and microphenocrysts:

- 5-10%, 0.2-5 mm, slightly to extremely serpentinized olivine,
- 10-15%, 0.2-10 mm, euhedral clinopyroxene.

In the lava, dike and juvenile block samples, the groundmass is entirely crystalline (serpentinized olivine, euhedral clinopyroxene and euhedral oxides) whereas in juvenile bomb and welded spatter samples, this groundmass is partly glassy. No primary hydrous phases like amphibole or phlogopite were seen. The mineral assemblage of Twin Peaks samples is typical of basanite (Vazquez 1998; Hooten 1999).

4.13.3 Major element geochemistry

4.13.3.1 Geochemical data

Major elements are presented in Table 4.5.

Table 4.5: Major oxides (wt.%) for Twin Peaks volcanic complex rocks.

Sample name	TPS-01	TPS-02	TPS-03	TPS-08	TPS-09	TPS-11	TPS-13	TPN-01	TPN-02	TPN-03	TPN-06	TPN-09	TPN-10	TPN-11
Sample type	Lava lake	Lava lake	South dike	Bomb	Block	Spatter	Dike	Lava lake	South dike	North dike	Lava lake	Spatter	Bomb	Bomb
Location	South peak	Sat Diat ¹	North peak											
SiO ₂	41.84	40.97	41.49	40.51	40.74	40.42	41.48	41.19	41.20	41.49	41.51	40.22	39.66	41.46
TiO ₂	3.77	3.79	3.93	3.69	3.68	3.44	3.73	3.91	3.86	3.93	3.79	3.45	3.61	3.87
Al ₂ O ₃	10.07	9.85	9.94	9.48	9.43	8.85	9.79	9.76	10.09	10.13	9.65	9.07	9.45	9.80
Fe ₂ O ₃ ^(T)	13.30	13.11	13.55	11.76	12.15	11.94	13.36	13.20	13.33	13.73	13.21	12.24	12.35	13.44
MnO	0.17	0.17	0.17	0.16	0.15	0.15	0.17	0.16	0.17	0.17	0.16	0.15	0.15	0.16
MgO	11.63	11.37	11.63	8.21	10.01	9.67	11.49	12.27	11.64	11.90	11.59	9.61	10.78	11.52
CaO	11.28	11.41	11.33	14.23	12.24	13.18	11.34	11.11	11.44	11.17	11.31	13.27	12.67	11.24
Na ₂ O	3.66	3.09	3.70	3.89	3.37	2.93	3.81	2.51	3.78	3.35	3.48	2.74	2.80	3.22
K ₂ O	0.49	0.83	0.55	0.13	0.22	0.45	0.39	1.14	0.34	0.89	0.34	0.43	0.28	0.57
P ₂ O ₅	1.11	1.15	1.18	1.12	1.07	1.01	1.13	1.12	1.13	1.10	1.12	0.99	1.03	1.09
LOI ²	2.77	3.29	2.34	5.82	6.03	6.66	2.52	3.53	2.10	2.35	3.51	7.71	7.20	3.19
Sum	100.10	99.03	99.80	99.00	99.09	98.70	99.20	99.91	99.07	100.20	99.65	99.90	100.00	99.56

Notes: ¹Satellite diatreme, ²Loss on ignition

4.13.3.2 TAS diagram

On the total alkali-silica (TAS) diagram, all samples from the Twin peaks volcanic complex fall in the tephrite/basanite field (Fig. 4.13). According to the criteria set by Le Bas (1986), all the Twin Peaks samples are basanites, because they have more than 10% of normative olivine in the CIPW norm. Data from the literature also shows a dominance of tephrite/basanite in the HBVF, whereas foidites or thrachy-basalts are rarer (e.g., Vazquez 1998; Hooten 1999; Lefebvre 2013, Latutrie and Ross 2019). Lava lake and dike samples from the two peaks and the satellite diatreme form a cluster, with higher average values of total alkalis than the block, bomb and spatter samples from units 1-3, although this distinction is more convincing on other diagrams presented below.

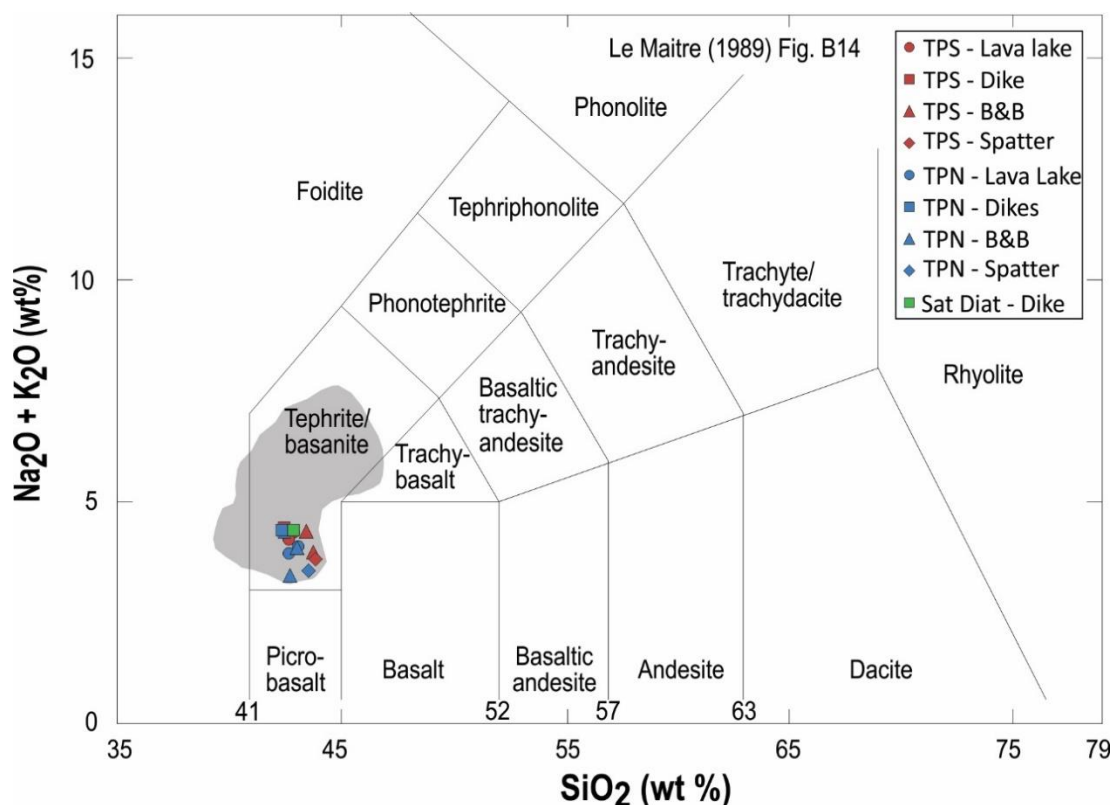


Figure 4.13: TAS diagram after Le Bas et al. (1986) and Le Maitre (1989). Twin Peaks coherent rocks are shown by symbols, and the grey shaded area corresponds to HBVF data from the literature (Vazquez 1998; Hooten 1999; Lefebvre 2013; Latutrie and Ross 2019). Notes: TPS = South peak, TPN = North peak, Sat Diat = Satellite Diatreme and B&B = Blocks and Bombs.

4.13.3.3 Harker diagram

Samples from Twin Peaks form a cloud of dots on all Harker diagrams, with only the CaO and Al₂O₃ versus SiO₂ diagram defining a trend (Fig. 4.14). This cloud largely overlaps regional

HBVF data. When the whole volcanic field is considered, the MgO, Fe₂O₃^(T) and CaO versus SiO₂ diagrams display weak negative trends. This must be related mostly to variable proportions of olivine and clinopyroxene in the rocks. The juvenile blocks and bombs and the welded-spatter from units 1-3 are generally less rich in Si, Fe, Ti and Mg than dike and lava (unit 4) samples. This shows a slight shift of magma composition over time, between units 1-3 versus the lava lake and its feeder dikes.

4.13.4 Trace element geochemistry

4.13.4.1 Geochemical data

Trace elements are presented in Table 4.6.

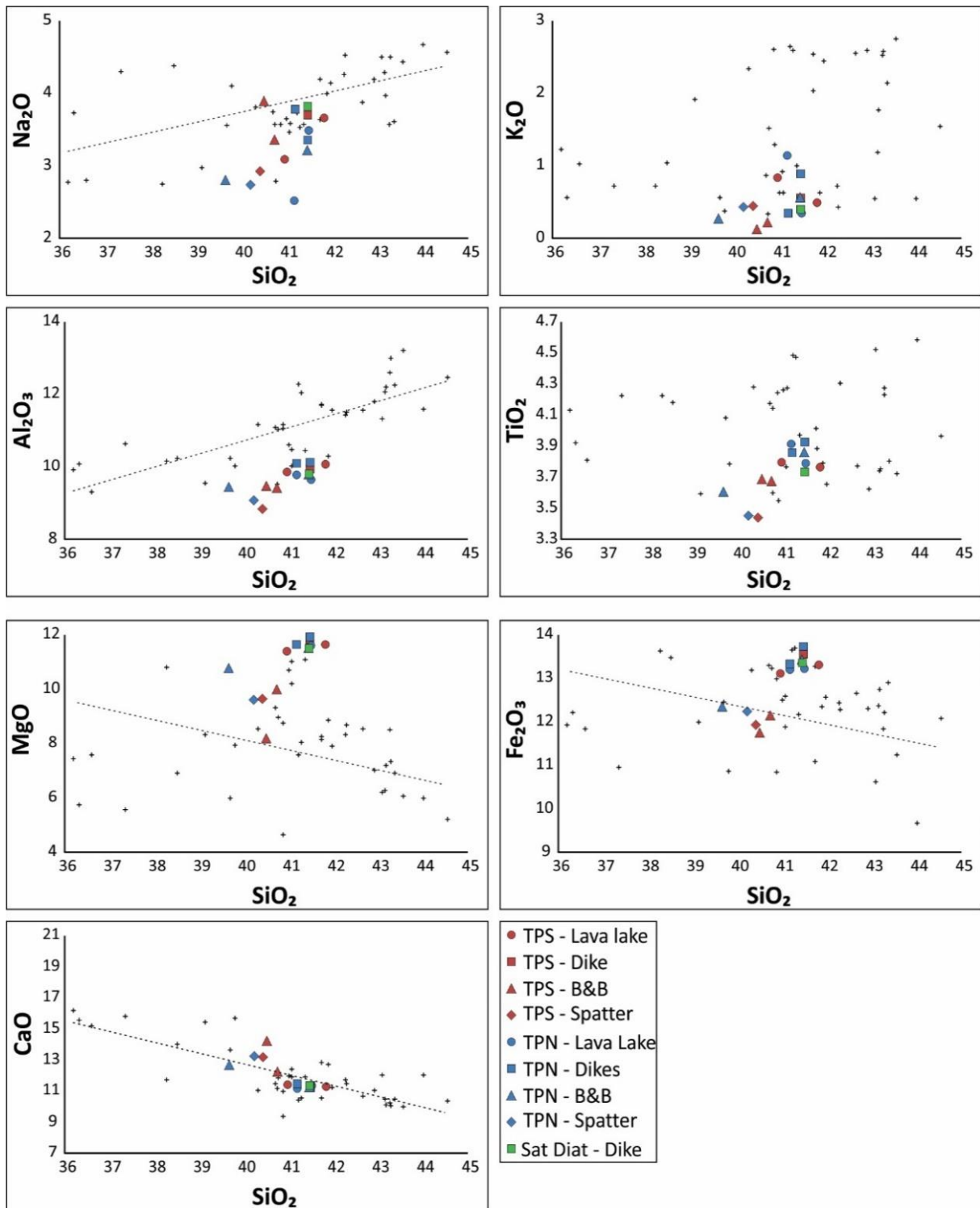


Figure 4.14: Harker diagrams. Twin Peaks coherent rocks generally fall within the HBVF literature field (crosses, Vazquez 1998; Hooten 1999; Lefebvre 2013; Latutrie and Ross 2019). Notes: TPS = South peak, TPN = North peak, Sat Diat = Satellite Diatreme and B&B = Blocks and Bombs.

Table 4.6: Trace elements (ppm) for Twin Peaks volcanic complex rocks.

Sample name	TPS-01	TPS-02	TPS-03	TPS-08	TPS-09	TPS-11	TPS-13	TPN-01	TPN-02	TPN-03	TPN-06	TPN-09	TPN-10	TPN-11
Sample type	Lava lake	Lava lake	South dike	Bomb	Block	Spatter	Dike	Lava lake	South dike	North dike	Lava lake	Spatter	Bomb	Bomb
Location	South peak	Sat diat ¹	North peak											
<i>LFSE</i>														
Cs	0.5	0.5	4.2	5.4	4.2	0.9	4.6	0.5	0.8	0.8	0.4	1.4	2.0	1.1
Rb	12	7	6	7	10	3	12	5	5	7	17	2	7	10
Ba	850	871	891	544	755	613	1867	898	902	895	893	777	778	843
Sr	1397	1370	1434	1461	1414	884	1234	1330	1538	1375	1319	1600	1331	1336
<i>HFSE</i>														
Th	8.49	8.91	8.66	8.47	8.29	8.15	8.55	8.45	8.77	8.50	8.86	7.74	8.21	8.49
U	2.68	2.36	2.56	2.21	2.71	4.27	2.64	2.53	2.52	2.52	2.39	2.48	2.19	2.56
Nb	71.4	74.9	74.6	74.5	72.0	67.0	75.2	76.4	76.8	80.8	78.1	71.6	73.6	75.8
Ta	5.00	5.12	5.02	4.88	4.83	4.53	5.11	5.09	5.14	5.18	5.11	4.60	4.82	5.03
Pb	5	6	5	< 5	< 5	< 5	5	< 5	5	5	5	< 5	< 5	< 5
Zr	436	441	441	428	423	398	428	444	449	457	456	402	423	445
Hf	9.4	10.2	9.4	9.6	9.1	8.7	9.5	9.5	9.5	10.1	10.0	8.6	9.2	9.7
Y	29.1	29.9	29.8	28.9	28.9	27.0	29.6	29.8	30.6	30.1	29.6	27.3	27.3	29.6
<i>REE</i>														
La	75.9	80.7	79.4	75.1	73.3	70.1	76.3	78.1	80.0	79.7	80.5	70.2	72.8	77.8
Ce	162	169	167	159	154	147	163	166	169	169	171	149	153	166
Pr	19.3	20.4	20.0	19.1	18.7	17.5	19.5	19.9	20.4	20.3	20.4	18.0	18.5	20.1
Nd	77.3	82.2	80.3	75.8	73.6	71.3	78.7	79.4	81.0	80.4	82.0	72.7	73.5	80.1
Sm	14.3	15.0	14.6	13.7	14.0	12.9	14.5	14.5	15.0	14.7	15.2	13.1	13.5	14.4
Eu	4.11	4.46	4.40	4.09	4.25	3.99	4.41	4.34	4.48	4.40	4.54	4.12	4.11	4.34
Gd	11.1	11.5	11.4	10.9	10.6	10.3	11.0	11.5	11.3	11.3	11.5	10.1	10.6	10.9
Tb	1.30	1.39	1.35	1.34	1.28	1.22	1.37	1.35	1.39	1.41	1.38	1.25	1.25	1.32
Dy	6.85	7.27	6.93	6.73	6.54	6.30	6.82	6.87	6.90	7.01	7.19	6.39	6.35	6.81
Ho	1.06	1.12	1.05	1.03	1.07	0.98	1.05	1.07	1.11	1.10	1.11	0.98	0.99	1.06
Er	2.51	2.83	2.62	2.59	2.46	2.45	2.60	2.52	2.68	2.61	2.67	2.40	2.45	2.66
Tm	0.305	0.340	0.297	0.314	0.293	0.284	0.327	0.311	0.317	0.327	0.299	0.281	0.292	0.316
Yb	1.65	1.82	1.69	1.69	1.71	1.71	1.74	1.73	1.81	1.78	1.78	1.59	1.53	1.86
Lu	0.241	0.243	0.253	0.217	0.208	0.208	0.220	0.224	0.241	0.229	0.242	0.195	0.216	0.233

Note: ¹Satellite diatreme

4.13.4.2 Zr/TiO₂ vs Nb/Y diagram

The classification diagram of Winchester and Floyd (1977) uses immobile element ratios. Twin Peaks coherent rocks fall in the alkali basalt field (Fig. 4.15), not far from the basanite field. In this diagram, the North and South peaks form two very narrow overlapping clusters of points whereas the sample from the Satellite diatreme plots in the middle of the clusters.

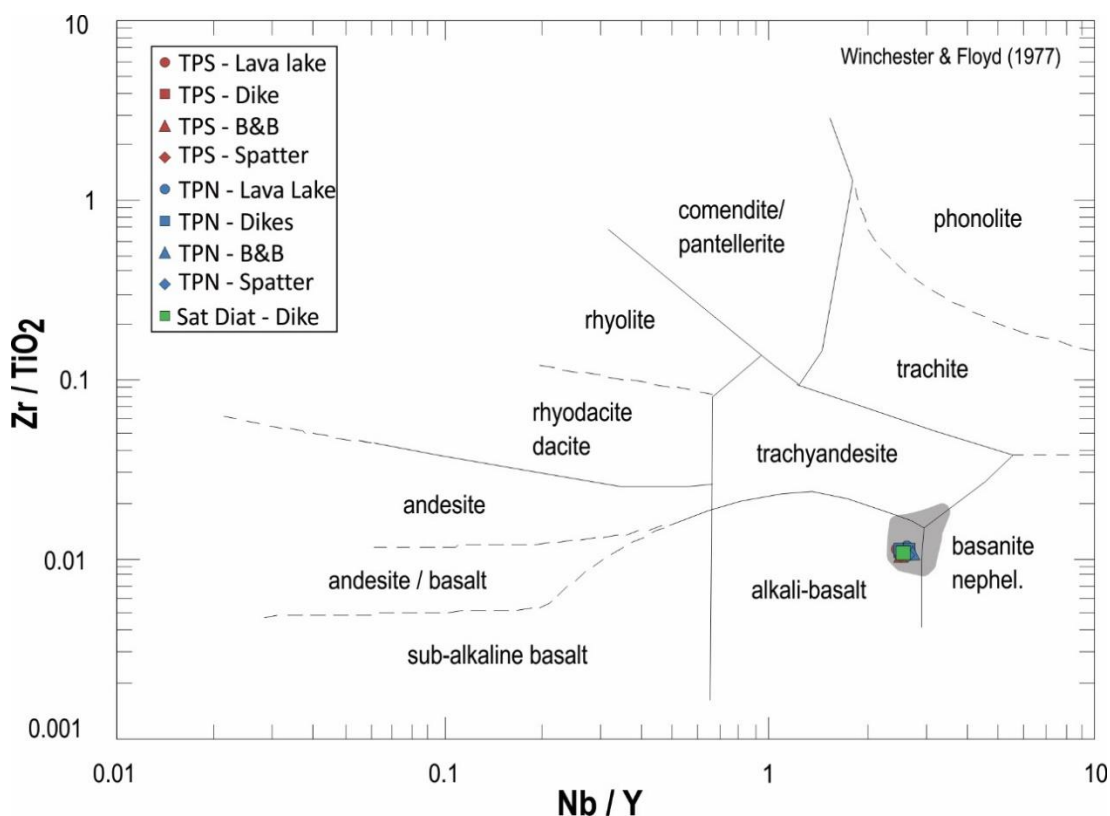


Figure 4.15: Immobility element diagram after Winchester and Floyd (1977) comparing Twin Peaks data (coloured symbols) with geochemical data from the literature (grey shaded area, Vazquez 1998; Hooten 1999; Lefebvre 2013; Latutrie and Ross 2019). Note: TPS = South peak, TPN = North peak, Sat Diat = Satellite Diatreme and B&B = Blocks and Bombs.

4.13.4.3 Spider diagram

Twin Peaks coherent rocks are enriched in incompatible elements in comparison to the primitive mantle of Sun and McDonough (1989), with negative slopes and smooth patterns (Fig. 4.16). Regional HBVF data shows small negative anomalies in Sm and Ti, whereas Twin peaks samples display only the Sm anomaly (Fig. 4.16). The general trend of the samples is close to the Ocean Island Basalt (OIB) end-member even if the actual setting is continental intraplate volcanism. The North peak, the South peak and the Satellite diatreme of the Twin peaks

volcanic complex display indistinguishable trends on the spider diagram. In detail, the concentrations of Th, Nb and La, for example, are slightly lower in juvenile fragments from units 1-3 than in unit 4 lavas and related dikes (Table 4.6).

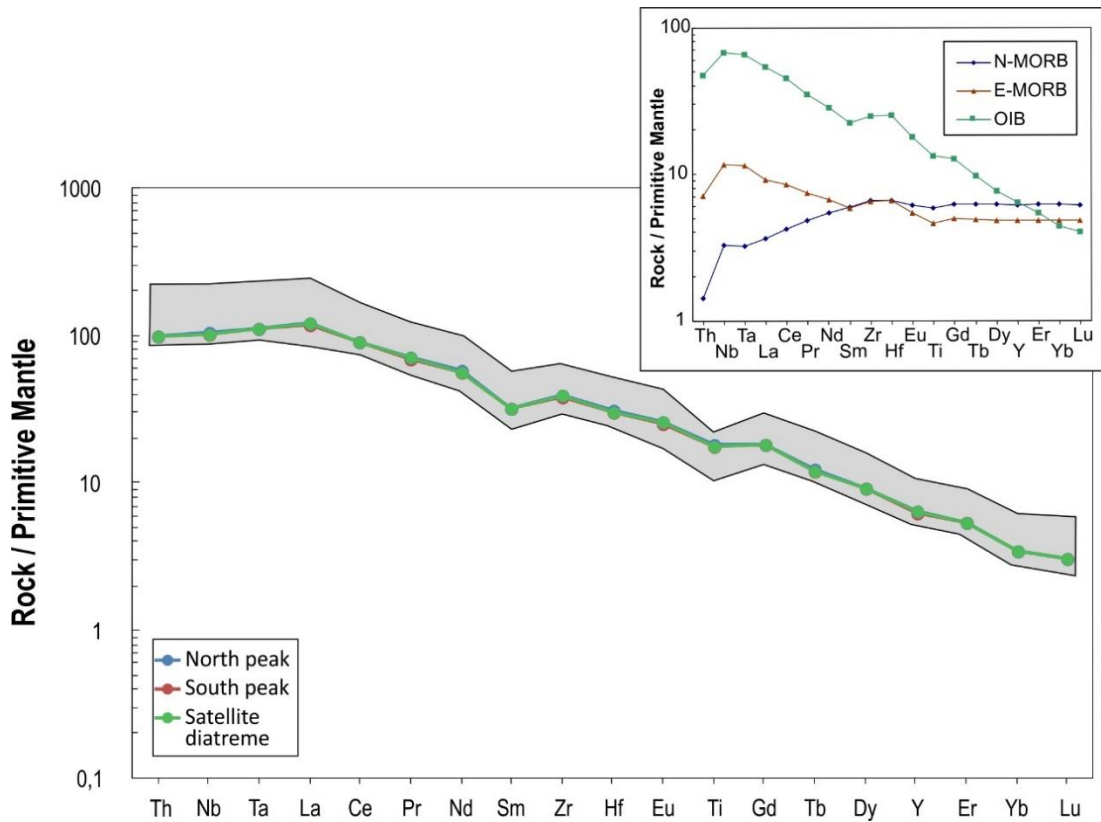


Figure 4.16: Extended trace elements normalized to the primitive mantle (Sun and McDonough 1989). Shaded area corresponds to geochemical data from the literature (Vazquez 1998; Hooten 1999; Lefebvre 2013; Latutrie and Ross 2019). Composition of N-MORB, E-MORB and OIB are from Sun and McDonough (1989).

5 Synthesis

5.1 Main conclusions and scientific contributions

Maar-diatreme volcanoes are hazardous to people and property, and they can also contain valuable diamond deposits, including in Canada. The internal workings of maar-diatreme volcanoes are not completely understood, especially for the underground portion, called the diatreme. A better understanding of eruptive processes in the diatreme therefore has socio-economic implications.

The HBVF, Navajo Nation, Arizona (Fig. 1.5) is a world-class location to study maar-diatreme volcanoes from the ejecta ring (White 1991; Vazquez and Ort 2006; Graettinger and Valentine 2017) to the lower diatreme (Lefebvre et al. 2013, 2016) and feeder intrusions (Re et al. 2015; 2016; Muirhead et al. 2016). This thesis has characterized and interpreted two diatreme sites in the southeastern part of the HBVF, Round Butte and Twin Peaks, to shed further light on their eruptive processes. In total, a month was spent on each locality in the field. The field methodology at both sites was similar, consisting of detailed facies mapping and detailed description of pyroclastic rocks and coherent lavas. Componentry was characterized with quantitative field methods. The laboratory follow-up was also similar at both sites, consisting of rock slab descriptions, petrography, point counting and geochemical analyses. This allowed the detailed characterisation of each volcano, interpretation of eruptive processes and styles, and construction of diatreme evolution models (Figs. 2.12, 4.11).

The relatively small Round Butte diatreme was the initial center of interest because of its surprising complexity and the presence of the transition zone between bedded pyroclastic rocks and non-bedded pyroclastic rocks. This diatreme has been known to be significant for several decades (White 1991; White and Ross 2011), but had never received detailed attention. The general volcanology of Round Butte is presented in [Chapter 2](#), published as an article in *Bulletin of Volcanology* in 2019. This presents the overall evolution of the volcano and focusses on the transition zone between the upper and lower diatreme. Since a large amount of data had been acquired at Round Butte, it could not fit in a single publication. Therefore, the lithic clasts and lithic-rich lithologies are presented separately in [Chapter 3](#), which is to be submitted to *Journal of Volcanology and Geothermal Research*. One interesting aspect of that work on lithic clasts is a country rock fragmentation model which was utilized to clarify where lithic clasts came from and how they are preserved within pyroclastic rocks of the diatreme (Fig. 3.8).

The nearby Twin Peaks was chosen as a second field site because of its progressive change of eruptive regime from phreatomagmatic to magmatic. The results of that investigation are presented in Chapter 4, which was published in Bulletin of Volcanology in early 2020. Twin Peaks is composed by two 'plug'-dominated (Williams 1936) main peaks and a small satellite diatreme. The main peaks each consist of a maar-diatreme volcano with a lava lake that filled the maar crater towards the end of the eruption.

5.1.1 Cycles of excavation and infilling

Chapter 2 describes how the Round Butte massif, forming the well-exposed central portion of the diatreme, is largely made of three facies groups. The undisturbed bedded pyroclastic group is located above an unconformity. Below this, the disturbed bedded pyroclastic group and the non-bedded pyroclastic group are found, and mostly form subvertical columns. One of the main conclusions of Chapter 2 is that this architecture results from at least two cycles of crater excavation and infilling. Although crater excavation and infilling can occur simultaneously, each cycle corresponds to an excavation-dominated phase followed by an infilling-dominated phase. During the first cycle, a deep crater was excavated and then filled by infill 1 that is now the disturbed bedded pyroclastic rocks (Figs. 2.12b, 2.12c). Phreatomagmatic explosions within the diatreme formed debris jets, which by propagating upwards, created invasive columns (non-bedded pyroclastic deposits) cross-cutting residual columns (disturbed pyroclastic deposits). The second cycle of crater excavation and infilling dug into infill 1 and left behind a crater floor that corresponds to the genetically important unconformity (Figs. 2.12d, 2.12e). Undisturbed bedded deposits (infill 2) were deposited above this unconformity and form the current upper diatreme. Based on historical maar-diatreme eruptions, Round Butte – which is a relatively small volcano – may have been formed in days to weeks. Each cycle of crater excavation and infilling would therefore have lasted hours to days, or at most a few weeks.

5.1.2 A transition zone between the upper and lower diatreme

The association of invasive columns and residual columns containing disturbed beds, below the unconformity at Round Butte, does not correspond to a classic definition of lower diatreme deposits (Fig. 2.12d). Those rocks are instead considered to form a transition zone between the typically well-bedded upper diatreme (above the unconformity) and the typically non-bedded lower diatreme (somewhere at depth below the current exposures). Chapter 2 integrates the transition zone into a generalized maar-diatreme model for the first time (Fig. 2.13), whereas

previous models (Fig. 1.1) showed the upper-lower diatreme contact as a line (or in 3D, a surface).

Here is how the transition zone is thought to have formed at Round Butte. During the first cycle of excavation and infilling, a relatively deep crater was formed and filled by bedded deposits of Infill 1 which was then part of the bedded upper diatreme (Figs. 2.12a, 2.12b). Meanwhile, subterranean phreatomagmatic explosions triggered disturbance of the bottom of Infill 1, mainly by injection of debris jets (Fig. 2.12c). This, perhaps along with some liquefaction, disturbed the bedding in infill 1. At the same time, the top of Infill 1 was excavated, forming a new crater floor which is preserved as the prominent unconformity. Infill 2 was then emplaced above this and formed the new bedded upper diatreme (Figs. 2.12d, 2.12e). The transition zone at Round Butte therefore consists of an intimate association of disturbed bedded deposits (residual columns) and non-bedded deposits (invasive columns). The transition zone is hypothesized to grade downward into the completely non-bedded lower diatreme.

5.1.3 Lower diatreme eruptive processes

Another contribution from the Round Butte study relates to eruptive processes in the lower diatreme, although these rocks are not directly exposed. Three general hypotheses were invoked for the lower diatreme in [Chapter 1](#): in vent-collapse of a plinian/subplinian column, whole-diatreme fluidization, and phreatomagmatism. The first two hypotheses often require disconnection between the lower diatreme which forms first, and the upper diatreme which forms later, perhaps with a different eruptive style. At Round Butte, the upper and lower diatreme are interpreted to have formed partly simultaneously, from the same phreatomagmatic activity. The initial infill of the upper diatreme (Infill 1) was progressively converted into disturbed beds in the transition zone, and perhaps deeper in the lower diatreme. Debris jets contributed to bedding disruption and also pushed material up, some of which was left behind to form invasive columns, and some of which rose to the atmosphere to create new beds on the floor of the syn-eruptive crater. This phreatomagmatic model is the most largely accepted hypothesis in the literature for non-kimberlitic maar-diatremes, and Round Butte further illustrates and strengthens this. Other possible causes of bedding disturbance in the transition zone and lower diatreme are liquefaction processes, which seem to have had some role at Round Butte or subsidence, which appears important elsewhere (e.g., Missouri River Breaks, Montana, Fig. 1.3a; Delpit et al. 2014).

5.1.4 Crater enlargement processes

Chapter 3 shows that Round Butte is also a good locality for the study of lithic clasts and lithic-rich lithologies preserved in diatremes. Many sedimentary megablocks (over 2 m in long axis) and debris avalanche deposits (DADs) are visible in the massif and some sedimentary megablocks also occur outside the massif, in the poorly exposed zone between the massif and the contact with the country rocks. A major DAD is preserved in the southwestern part of the massif, and smaller ones occur on the west side. Pyroclastic megablocks are also found and are interpreted as derived from the ejecta ring surrounding the syn-eruptive crater (but now eroded). During maar-diatreme eruptions, slumps that form DADs and individual sedimentary and pyroclastic megablocks are the main mechanism which enlarges the crater laterally.

5.1.5 Movement and preservation of lithic clasts

The country rock stratigraphy is well known in the HBVF, and many lithic clasts in the range of coarse lapilli to megablocks in the Round Butte diatreme can be assigned to a specific sedimentary formation. Therefore, studying lithic clasts in detail allows identification of their depth of origin. Building the country rock fragmentation model of Round Butte (Fig. 3.8) allows a comparison between 'theoretical' proportions of sedimentary rock formations fragmented and the actual proportions derived from line and clast counts. Depending on their origin, lithic clasts either moved down 0-190 m relative to their source, or moved up by 0-220 m relative to their source, to reach their current location about 190 m below the pre-eruptive surface.

Field componentry highlighted that no Paleozoic sedimentary rocks were found in the Round Butte diatreme. This means that Paleozoic sedimentary rocks were not fragmented, or did not move up as fragments to the current level of exposure, or are present in such a very low abundance so that they were not found. Instead, the deepest-sourced clasts found in a significant proportion are from the Moenkopi Formation, implying that the root zone of Round Butte is located around 440 m below the pre-eruptive surface.

Competent sedimentary formations (Moenave Formation, Owl Rock Member and Moenkopi Formation) are found in higher proportions in the diatreme than estimated from the country rock fragmentation model. This is because these formations are resistant to disaggregation so are readily preserved as recognizable lithic fragments. In contrast, less competent stratigraphic units (Bidahochi Formation, Petrified Forest Member and Shinarump Member) are under-represented in the field componentry data compared to the model, in part because they are easily disaggregated and hidden in the matrix of pyroclastic rocks. The depletion of Bidahochi

Formation in the diatreme is also due to preferential excavation and ejection during early crater development, since this formation sits at the top of the country rock stratigraphy.

At Round Butte, megablocks originate from the Bidahochi Formation, the Moenave Formation and Owl Rock Member but megablocks with a deeper origin may be preserved below the current level of exposure. No megablocks show a net upward movement from their origin. Debris jets are the main process allowing upward movements of material in the diatreme. Megablocks may be entrained within debris jets but because of their important mass and the low density of debris jets, they are probably not moved upwards permanently.

5.1.6 'Plug'-like remnants are maar-diatremes with lava-filled craters

Chapter 4 describes for the first time in the HBVF two 'plug'-like instances at the Twin Peaks volcanic complex. 'Plug'-like volcanic complexes are known elsewhere in the world, such as in Europe (Martin and Németh 2004; Lexa et al. 2010; Hencz et al. 2017; Tietz et al. 2018), but are rarely described and interpreted in detail. Williams (1936) considered that 'plug'-dominated volcanic remnants are typical of the Hopi Buttes, yet they had received no attention in the HBVF prior to this study. Detailed mapping of the main peaks (North and South) at Twin Peaks defined four stratigraphic units which consist of pyroclastic rocks (unit 1 to 3) overlain by jointed coherent lava (unit 4). Gentle to steep contacts between pyroclastic rocks and the country rocks, and the diatreme-like aspect of unit 1 in particular, support the presence of a diatreme under the coherent 'plugs'. The main peaks are interpreted as two initially phreatomagmatic maar-diatremes that eventually evolved to a lava lake filling the maar craters (Fig. 4.11). A third much smaller diatreme also occurs and forms a southeast-northwest alignment (Fig. 4.12). It seems likely that the three volcanoes formed simultaneously or in quick succession. Geochemistry shows a subtle change in magma composition from units 1-3 to unit 4, so that at the very least, the lava stage was simultaneous for the two main peaks. In terms of time of emplacement, based on its size and multiple craters, the Twin Peaks volcanic complex may have formed in a week to a couple of weeks, or months at most. At the end of the eruption, the two craters were probably filled by lava in a few days or weeks.

5.1.7 Magmatic versus phreatomagmatic fragmentation in maar-diatremes

The switch in eruptive regime was progressive for the two main peaks forming Twin Peaks. A phreatomagmatic first stage allowed maar craters to be excavated and unit 1 deposited (Figs. 4.11, 4.12). Subsequently the maar craters were progressively infilled, with the eruptive regime evolving from phreato-strombolian (unit 2), to phreato-hawaiian (unit 3a), then to a normal

hawaiian lava fountain (unit 3b) and ending with lava lakes (unit 4). This sequence is thought to have resulted from the progressive increase of the magma flux and/or the decrease of external water availability. Given this wide range of inferred eruptive styles, Chapter 4 was a good opportunity to review and discuss the criteria used to distinguish phreatomagmatic from magmatic explosive eruptive styles in ultramafic to mafic maar-diatremes (Table 4.4). Most of the traditional criteria are still helpful (general color, thickness and morphology of beds, sorting, content of fines, lithic content and morphology and vesicularity of juvenile clasts), but groundmass textures (tachylite vs sideromelane) in juvenile fragments now appear to be an ambiguous criterion.

5.2 An improved understanding of maar-diatreme volcanoes

This work introduced new insights on the eruptive processes and internal structure of maar-diatreme volcanoes. There are implications for hazard studies and kimberlite exploration and exploitation.

5.2.1 Phreatomagmatic activity in diatremes

A genetically important transition zone has been identified between the upper and lower diatreme. A revised generalized maar-diatreme model that incorporates the transition zone has been proposed (Fig. 2.13). This transition zone is the missing link between the upper clearly phreatomagmatic diatreme (at many sites including Round Butte) and the lower diatreme with more difficult to interpret emplacement processes. The work at Round Butte shows that the lack of bedding in the lower diatreme does not require an eruptive style fundamentally different from that of the bedded upper diatreme, since the two are connected and form at least partly at the same time. There is no evidence of a subplinian to plinian eruption, or whole-diatreme fluidization, at Round Butte. The non-bedded pyroclastic rocks typical of the lower diatreme are formed by debris jets forming invasive columns and by the progressive disturbance of previously bedded pyroclastic rocks.

Another, partly similar, example of a transition zone has been described at the Cathedral Cliff diatreme in the Navajo volcanic field, New Mexico (Bélanger and Ross 2018), although the authors did not specifically call it a “transition zone”. This diatreme is composed by bedded pyroclastic deposits in its upper part and non-bedded pyroclastic deposits in its lower part. The transition zone at Cathedral Cliff is composed of “broken beds” intruded at many places by sub-vertical invasive columns, which is equivalent to the association of disturbed beds (residual

columns) and non-bedded deposits (invasive columns) at Round Butte. The main difference between the two sites is the scale of the transition zone: Cathedral Cliff is a wider diatreme than Round Butte and the transition zone there is thicker. At Round Butte the transition zone could be tens of meters thick whereas at Cathedral Cliff it could be hundreds of meters thick. Transition zones should now be examined elsewhere.

Although there are eruptive phases dominated by excavation or by crater infilling in the life of maar-diatreme volcanoes, the two processes always occur simultaneously. Maar-diatreme volcanoes do not simply excavate a deep syn-eruptive crater and then fill it to form the diatreme. At Round Butte, several cycles of excavation-infilling are highlighted, and probably result from variations in the intensity of the phreatomagmatic activity or the location of phreatomagmatic explosions. Intense phases, probably with explosion loci at shallow levels, favour excavation and ejection of material toward the ejecta ring, although a portion falls back into the crater. Infilling-dominated phases may relate to less intense activity and/or explosion loci at deeper levels in the diatreme. Depositional processes in the crater include fallback (Ross et al. 2013) and pyroclastic surges (easier in big craters). At the same time, debris avalanche and megablock collapse can enlarge the crater laterally.

5.2.2 Magmatic activity

This work also clarifies that maar-diatremes are not exclusively phreatomagmatic volcanoes. They are mainly phreatomagmatic, otherwise the resulting landform would be different, but the activity can switch to become magmatic (explosive to effusive). At Twin Peaks, this change is related to the progressive increase of the magma flux and/or the decrease of the water supply or availability. The nearby Hoskietso Claim diatreme displays several spatter units and a lava cap possibly corresponding to a lava lake at its top (White 1991; White and Ross 2011). The spatter layers there are intercalated with phreatomagmatic deposits, so the eruptive style fluctuated towards the end of the eruption. At Triplets maar in the northern part of the HBVF, lava may have overflowed from the crater (Graettinger and Valentine 2017), and this might have occurred at Twin Peaks too, although the current outcrop exposure does not allow this to be verified (i.e. evidence has been eroded). Other examples of maar-diatreme volcanoes capped by lava lakes filling maar craters are known in other volcanic fields including in Europe (Martin and Németh 2004; Lexa et al. 2010; Hencz et al. 2017; Tietz et al. 2018). The change in the eruptive regime from phreatomagmatic to magmatic of maar-diatreme has implications for hazard assessment in active volcanic fields.

5.2.3 Implications for natural hazards

The main hazard associated with maar-diatreme volcanoes in the literature are the radial surges (Moore et al. 1966; Moore 1967; Vazquez and Ort 2006; Poppe et al. 2016). These are extremely destructive pyroclastic density currents that can travel 5 km laterally from the vent. Also documented is the fallout from eruption plumes, and the fall of ballistic blocks. Those hazards are taken into account in hazard maps such as those of Hayes et al. (2018; 2020) for the Auckland field in New Zealand, or Poppe et al. (2016) for Goma city in the Democratic Republic of Congo. But maar-diatreme volcanoes are not only phreatomagmatic: some of them can change their eruptive regime to magmatic, as described for Twin Peaks. Volcanic hazards related to magmatic activity in maar-diatreme eruptions are less taken into account because they are less known. Indeed, this work highlights the possible importance of lava flows. Lavas move much more slowly and are less immediately dangerous than surges, but could be destructive at great distances from the crater. An overflowing crater could nourish a lava flow or a lava plain around the maar. Ultramafic to mafic lava flows can channelize and can exceed over 10 km in length (Robert et al. 2014; Harris and Rowland 2015). This means that cities not directly impacted by surges during the phreatomagmatic activity could be hit later by lava flows. Lava flows should be added to prevention plans, even in monogenetic volcanic fields dominated by phreatomagmatic volcanoes. This will require modelling to predict lava flooding areas (Latutrie et al. 2015). A precise Digital Elevation Model (DEM) is needed to make good models of lava flows because most modeling software take the topography into account. The most accurate models use physical parameters such as lava crystallinity, viscosity, temperature at the vent or vesicularity. Acquisition of those physical parameters needs to be done quickly during new eruptions, but old volcanic remnants could be used as proxies to build preliminary evacuation maps. In summary, a large amount of work is needed to add magmatic hazards in relation with maar-diatreme prevention plans, and this should largely be done *before* the next eruption.

5.2.4 Implications for kimberlites

Kimberlites are small volcanoes such as tuff rings, tuff cones, scoria cones, maar-diatremes or lava flows, forming monogenetic volcanic fields (Lefebvre and Kurszlauskis 2008; McClintock et al. 2009; Brown et al. 2012; Brown and Valentine 2013). They were probably emplaced in the same fashion as other ultramafic to mafic monogenetic volcanoes (Kurszlauskis and Lorenz 2017).

However, many workers see kimberlitic pipes as fundamentally “different” from non-kimberlitic volcanoes because the magma displays a particular chemical composition, kimberlites *might* be exceptionally gas-rich, and they are sometimes diamond-bearing, indicating a deep mantle source (Kjarsgaard 2007). Also, many kimberlite workers have historically *not* been physical volcanologists, which has led to “alternative” nomenclatures and eruption models. Even among physical volcanologists who have looked at kimberlites, there has been a tendency to emphasize the differences over the common points, relative to non-kimberlitic volcanoes. This again has led to “alternative” eruption models (e.g., Sparks et al. 2006; Walters et al. 2006; Head and Wilson 2008; Porritt et al. 2008; Gernon et al. 2009). Difficulties with kimberlite volcanology include the typical lack of good natural outcrops (instead, drill cores and mine exposures are used) and variable alteration of the rock (Kurszlaukis and Lorenz 2008; Nowicki et al. 2008).

This thesis takes the view that kimberlites are *not* special and that they essentially formed by the same shallow eruptive processes as their non-kimberlitic, ultramafic to mafic cousins (Brown and Valentine 2013). A number of kimberlite ‘pipes’ are likely to represent maar-diatreme volcanoes, and therefore formed mostly by phreatomagmatic explosions (Kurszlaukis and Lorenz 2017). Since this thesis improved our understanding of how ultramafic maar-diatremes work in the HBVF, some of this knowledge could be useful in the comprehension of kimberlitic maar-diatremes. Two relevant themes are (i) the complexity of the transition zone; (ii) phreatomagmatic eruptive processes in the upper versus lower diatreme.

World-class outcrops and detailed field work at the Round Butte diatreme highlighted extreme complexities in the architecture of maar-diatremes over scales of meters to tens of meters, especially in the transition zone between the upper and lower diatreme. Contacts between pyroclastic facies range from subhorizontal to subvertical. Some of the subvertical non-bedded pyroclastic columns are only a few meters across, and have significantly different grain sizes and componentries relative to the neighbouring facies, which in a kimberlite pipe might lead to different diamond contents. Kimberlitic diatremes are mainly exposed in open pits or underground mines displaying dusty exposures and providing a partial view of the deposits. Drill cores are a useful tool to sample deposits preserved at a deeper level in pipes, but only give very local information. During the exploration stage of kimberlites, only relatively widely spaced, typically vertical, drill cores are available. The complex architecture of the Round Butte diatreme would have been very tricky to comprehend with only few vertical drill cores. It seems important to be careful when interpreting pyroclastic deposits in diatremes based on few drill cores,

especially if they are all oriented in the same direction. Angled holes designed to identify steep to vertical contacts might help.

There are several examples of kimberlitic diatremes which contain non-bedded pyroclastic rocks overlain by bedded ones, including the Mwadui kimberlite, Tanzania (Stiefenhofer and Darrell Farrow 2004), the Orapa Kimberlite, Botswana (Field et al. 1997) or the Yubileinaya kimberlite, Yakutia, Russia (Kurszlaukis et al. 2009). In many cases, these two portions of the 'pipe' have been interpreted very differently, and the origin of the non-bedded pyroclastic rocks has been especially strongly debated (Porrit et al. 2008, Gernon et al 2009, 2013). At Yubileinaya Kurszlaukis et al. (2009) observed well-bedded volcanoclastic (upper diatreme?) rocks above non-bedded pyroclastic (lower diatreme?) rocks, separated by a "xenolith belt". This lithic-rich 'belt' may be somewhat equivalent to the unconformity observed at Round Butte, where several debris avalanches are located. Yubileinaya pipe might have had excavation and infilling phases during its eruptive activity, and the xenolith belt may represent the bottom of a syn-eruptive crater. When Kurszlaukis et al. (2009) wrote their paper, they could only use one deep drill core to characterize the non-bedded pyroclastic rocks. It would be interesting to know if deeper mining has exposed transition zone-like deposits below the xenolith belt at Yubileinaya. More broadly, the conclusion that at Round Butte, the lower and upper diatreme form partly simultaneously, by the same chain of mostly phreatomagmatic processes, may be applicable to some kimberlitic diatremes as well (Kurszlaukis and Lorenz 2008).

In summary, ultramafic to mafic maar-diatremes and kimberlitic maar-diatremes are similar in many ways (White and Ross 2011; Kurszlaukis and Lorenz 2017) and it would be beneficial for the understanding of kimberlitic pipes to carefully consider the volcanology of non-kimberlitic maar-diatremes, which are often better preserved and exposed. This would help constrain the timing and mode of emplacement of different units/lithofacies preserved in the pipes, with implications on the distribution of diamonds.

5.3 Future work in the HBVF

The HBVF remains an excellent volcanic field for the study of maar-diatremes and numerous volcanic remnants deserve to be examined in detail. During the two months of field work done during this study, other locations have been visited and two of them captured attention because of their products: Bidahochi Butte and Mitten Peak.

Bidahochi Butte is located 6.5 km north of Twin Peaks (Fig. 1.5). It may have been formed by multiple maar-diatremes or by a multi-vent volcano. In the north of the massif, an interesting

ejecta ring is preserved. It is characterized by thinly bedded pyroclastic deposits displaying cross-beds, dunes and bomb sags. These deposits are found around a depression and seem to have an outward steep to subvertical dip that is abnormal for ejecta rings. At the top of the butte is coherent lava that may be filling a crater, the lava having been either internally erupted like at Twin Peaks or perhaps externally derived. The basal contact of the coherent lava with the loose sedimentary rocks of the Bidahochi Formation may be a peperite. Could post-eruptive crater-filling sediments be preserved at this contact?

The other location worth mentioning is Mitten Peak, 16 km south of Five Buttes. This site is not in the Navajo Nation and is not easy to access (4 km east of road 77, Fig. 1.5). This volcanic remnant is characterized by an elongated main body ending to the north with a dike turning to the east. Many thin to thick dikes crop out around the main body and pyroclastic rocks that crosscut the Petrified Forest Member of the Chinle Formation are also present around it. The main body is composed by an almost equal mix of pyroclastic rocks rich in lithic clasts and brown juvenile clasts, and coherent dikes. It would be interesting to document the relation between these dikes and the pyroclastic rocks in the main body and around it. Is this volcanic remnant a root zone? What was the movement of the magma in the surrounding dikes (toward the main body or away from it)?

Mitten Peak and Bidahochi Butte display elements of the maar-diatreme system that are not available at Round Butte or Twin Peaks, perhaps including a root zone and ejecta ring. More broadly, the HBVF has over 300 volcanic remnants, few of which have been studied yet and the volcanic field has not given up all of its secrets. It still has the potential to inform us on how maar-diatreme volcanoes work.

6 REFERENCES

- Akers JP, Shorty JC, Stevens PR (1971) Hydrogeology of the Cenozoic igneous rocks, Navajo and Hopi Indian Reservations, Arizona, New Mexico, and Utah. Geol Surv Profess Pap 521-D
- Alibert C, Michard A, Albarède F (1986) Isotope and trace element geochemistry of Colorado Plateau volcanics. *Geochim Cosmochim Acta* 50:2735-2750
- Andronico D, Cristaldi A, Scollo S (2008) The 4–5 September 2007 lava fountain at south-east crater of Mt Etna, Italy. *J Volcanol Geotherm Res* 173:325-328
- Andronico D, Cristaldi A, Del Carlo P, Taddeucci J (2009) Shifting styles of basaltic explosive activity during the 2002–03 eruption of Mt. Etna, Italy. *J Volcanol Geotherm Res* 180:110-122
- Atwater T (1970) Implications of plate tectonics for the Cenozoic tectonic evolution of western North America. *Geol Soc Am Bull* 81:3513-3536
- Auer A, Martin U, Nemeth K (2007) The Fekete-hegy (Balaton Highland Hungary) “soft-substrate” and “hard-substrate” maar volcanoes in an aligned volcanic complex—Implications for vent geometry, subsurface stratigraphy and the palaeoenvironmental setting. *J Volcanol Geotherm Res* 159:225-245
- Austin-Erickson A, Büttner R, Dellino P, Ort MH, Zimanowski B (2008) Phreatomagmatic explosions of rhyolitic magma: Experimental and field evidence. *J Geophys Res: Solid Earth* 113:B11201
- Austin-Erickson A, Ort MH, Carrasco-Núñez G (2011) Rhyolitic phreatomagmatism explored: Tepexitl tuff ring (Eastern Mexican Volcanic Belt). *J Volcanol Geotherm Res* 201:325-341
- Bélanger C, Ross P-S (2018) Origin of nonbedded pyroclastic rocks in the Cathedral Cliff diatreme, Navajo volcanic field, New Mexico. *Bull Volcanol* 80:article 61
- Bélanger C, White JDL, Fierstein J (2019) Pyroclast Characteristics of the Ubehebe Crater Cluster, Death Valley, California. In: IUGG Centennial. Montreal, Quebec, Canada
- Billingsley GH, Block D, Hiza-Redsteer M (2013) Geologic map of the Winslow 30'× 60' quadrangle, Coconino and Navajo Counties, northern Arizona. US Geol Surv Scientific Investigations, Map 3247, scale 1:50 000.

- Blaikie TN, Ailleres L, Cas RAF, Betts PG (2012) Three-dimensional potential field modelling of a multi-vent maar-diatreme—The Lake Coragulac maar, Newer Volcanics Province, south-eastern Australia. *J Volcanol Geotherm Res* 235:70-83
- Boivin P, Thouret J-C (2014) The volcanic Chaîne des Puys: a unique collection of simple and compound monogenetic edifices. In: *Landscapes and landforms of France*, Springer, pp 81-91
- Borrero C, Murcia H, Agustin-Flores J, Arboleda MT, Giraldo AM (2017) Pyroclastic deposits of San Diego maar, central Colombia: an example of a silicic magma-related monogenetic eruption in a hard substrate. *Geol Soc, London, Special Publication* 446:361-374
- Brown RJ, Valentine GA (2013) Physical characteristics of kimberlite and basaltic intraplate volcanism and implications of a biased kimberlite record. *Geol Soc Am Bull* 125:1224-1238
- Brown RJ, Gernon T, Stiefenhofer J, Field M (2008) Geological constraints on the eruption of the Jwaneng Centre kimberlite pipe, Botswana. *J Volcanol Geotherm Res* 174:195-208
- Brown RJ, Many S, Buisman I, Fontana G, Field M, Mac Niocaill C, Sparks RSJ, Stuart FM (2012) Eruption of kimberlite magmas: physical volcanology, geomorphology and age of the youngest kimberlitic volcanoes known on earth (the Upper Pleistocene/Holocene Igwisi Hills volcanoes, Tanzania). *Bull Volcanol* 74:1621-1643
- Büchel G, Lorenz V (1993) Syn-and post-eruptive mechanism of the Alaskan Ukinrek maars in 1977. In: *Paleolimnology of European Maar Lakes*, Springer, pp 15-60
- Büttner R, Zimanowski B (1998) Physics of thermohydraulic explosions. *Physical Review E* 57:5726
- Büttner R, Dellino P, La Volpe L, Lorenz V, Zimanowski B (2002) Thermohydraulic explosions in phreatomagmatic eruptions as evidenced by the comparison between pyroclasts and products from Molten Fuel Coolant Interaction experiments. *J Geophys Res: Solid Earth* 107:B11
- Cannata CB, De Rosa R, Donato P, Taddeucci J (2014) Ash features from ordinary activity at Stromboli volcano. *Int J Geosci* 5:1361
- Carracedo Sánchez M, Sarrionandia F, Arostegui J, Eguiluz L, Gil Ibarguchi JI (2012) The transition of spatter to lava-like body in lava fountain deposits: features and examples

from the Cabezo Segura volcano (Calatrava, Spain). *J Volcanol Geotherm Res* 227:1-14

Cas RAF, Wright JV (1987) *Volcanic successions modern and ancient: A geological approach to processes, products and successions*, Springer, 528 p.

Cas RAF, Van Otterloo J, Blaikie TN, Van Den Hove J (2017) The dynamics of a very large intra-plate continental basaltic volcanic province, the Newer Volcanics Province, SE Australia, and implications for other provinces. *Geol Soc, London, Special Publication* 446:123-172

Cho DH, Fauske HK, Grolmes MA (1976) Some aspects of mixing in large-mass, energetic fuel-coolant interactions. *Int Meet Fast React Saf Phys*, pp 1852-186

Clement CR (1982) A comparative geological study of some major kimberlite pipes in the Northern Cape and Orange Free State. PhD thesis, University of Cape Town, South Africa.

Cooley ME, Harshbarger JW, Akers JP, Hardt WF (1969) Regional hydrogeology of the Navajo and Hopi Indian Reservations, Arizona, New Mexico, and Utah. *US Geol Surv Prof Paper* 521-A

Cronenberg AW (1980) Recent developments in the understanding of energetic molten fuel-coolant interactions. *Nuclear Safety* 21:319-336

Crowe BM, Fisher RV (1973) Sedimentary structures in base-surge deposits with special reference to cross-bedding, Ubehebe Craters, Death Valley, California. *Geol Soc Am Bull* 84:663-682

Dallegge TA, Ort MH, McIntosh WC (2003) Mio-Pliocene chronostratigraphy, basin morphology and paleodrainage relations derived from the Bidahochi Formation, Hopi and Navajo Nations, northeastern Arizona. *The Mountain Geologist* 40:55-82

Davis GH (1978) Monoclinic fold patterns of the Colorado Plateau, in Matthews, V., ed., *Laramide folding associated with basement block faulting in the western United States*. *Geol Soc Am Mem* 151:215-233

Davis GH, Bump AP (2009) Structural geologic evolution of the Colorado Plateau, *in* Kay SM, Ramos VA, Dickinson WR eds. *Backbone of the Americas: Shallow subduction, Plateau Uplift, and Ridge and Terrane Collision*, Volume 204, *Geol Soc Am Memoirs*, p. 99-124.

- Davis JC (2002) *Statistics and Data Analysis in Geology - Third Edition*. John Wiley & Sons, New York, 638 p
- DeGraff JM, Aydin A (1987) Surface morphology of columnar joints and its significance to mechanics and direction of joint growth. *Geol Soc Am Bull* 99:605-617
- Delaney PT (1987) Ship Rock, New Mexico: the vent of a violent volcanic eruption. *Geol Soc Am Centennial Field Guide, Rocky Mountain Section* 2:411-415
- Delaney PT, Gartner AE (1997) Physical processes of shallow mafic dike emplacement near the San Rafael Swell, Utah. *Geol Soc Am Bull* 109:1177-1192
- Delpit S, Ross P-S, Hearn BC (2014) Deep-bedded ultramafic diatremes in the Missouri River Breaks volcanic field, Montana, USA: 1 km of syn-eruptive subsidence. *Bull Volcanol* 76:article 832
- Field M, Gibson JG, Wilkes TA, Gababotse J, Khujwe P (1997) The geology of the Orapa A/K1 kimberlite, Botswana: further insight into the emplacement of kimberlite pipes. *International Kimberlite Conference: Extended Abstracts*.
- Fisher RV (1961) Proposed classification of volcanoclastic sediments and rocks. *Geol Soc Am Bull* 72:1409-1414
- Fisher RV, Waters AC (1970) Base surge bed forms in maar volcanoes. *Am J Sci* 268:157-180
- Fisher RV, Schmincke H-U (1984) *Pyroclastic rocks*, Springer
- Fitton JG, James D, Leeman WP (1991) Basic magmatism associated with late Cenozoic extension in the western United States: Compositional variations in space and time. *J Geophys Res: Solid Earth* 96:B8 13693-13711
- Frassetto A, Gilbert H, Zandt G, Beck S, Fouch MJ (2006) Support of high elevation in the southern Basin and Range based on the composition and architecture of the crust in the Basin and Range and Colorado Plateau. *Earth Planet Sci Lett* 249:62-73
- Furnes H (1975) Experimental palagonitization of basaltic glasses of varied composition. *Contrib Mineral Petrol* 50:105-113
- Gernon TM, Gilbertson MA, Sparks RSJ, Field M (2008) Gas-fluidisation in an experimental tapered bed: insights into processes in diverging volcanic conduits. *J Volcanol Geotherm Res* 174:49-56

- Gernon TM, Gilbertson MA, Sparks RSJ, Field M (2009) The role of gas-fluidisation in the formation of massive volcanoclastic kimberlite. *Lithos* 112:439-451
- Gernon TM, Upton BGJ, Hincks TK (2013) Eruptive history of an alkali basaltic diatreme from Elie Ness, Fife, Scotland. *Bull Volcanol* 75:article 704
- Geshi N, Németh K, Oikawa T (2011) Growth of phreatomagmatic explosion craters: a model inferred from Suoana crater in Miyakejima Volcano, Japan. *J Volcanol Geotherm Res* 201:30-38
- Geshi N, Németh K, Noguchi R, Oikawa T (2019) Shift from magmatic to phreatomagmatic explosions controlled by the lateral evolution of a feeder dike in the Suoana-Kazahaya eruption, Miyakejima Volcano, Japan. *Earth Planet Sci Lett* 511:177-189
- Giaccio B, Sposato A, Gaeta M, Marra F, Palladino DM, Taddeucci J, Barbieri M, Messina P, Rolfo MF (2007) Mid-distal occurrences of the Albano Maar pyroclastic deposits and their relevance for reassessing the eruptive scenarios of the most recent activity at the Colli Albani Volcanic District, Central Italy. *Quaternary International* 171:160-178
- Gilbert H, Velasco AA, Zandt G (2007) Preservation of Proterozoic terrane boundaries within the Colorado Plateau and implications for its tectonic evolution. *Earth Planet Sci Lett* 258:237-248
- Graettinger AH (2018) Trends in maar crater size and shape using the global Maar Volcano Location and Shape (MaarVLS) database. *J Volcanol Geotherm Res* 357:1-13
- Graettinger AH, Valentine GA (2017) Evidence for the relative depths and energies of phreatomagmatic explosions recorded in tephra rings. *Bull Volcanol* 79:article 88
- Graettinger AH, Valentine GA, Sonder I, Ross PS, White JDL, Taddeucci J (2014) Maar-diatreme geometry and deposits: Subsurface blast experiments with variable explosion depth. *Geochemistry, Geophysics, Geosystems* 15:740-764
- Graettinger AH, Valentine GA, Sonder I, Ross P-S, White JDL (2015) Facies distribution of ejecta in analog tephra rings from experiments with single and multiple subsurface explosions. *Bull Volcanol* 77:66
- Gregory HE (1917) *Geology of the Navajo Country* US Geol Surv Profess Paper 93

- Gurioli L, Colo' L, Bollasina AJ, Harris AJL, Whittington A, Ripepe M (2014) Dynamics of Strombolian explosions: Inferences from field and laboratory studies of erupted bombs from Stromboli volcano. *J Geophys Res: Solid Earth* 119:319-345
- Hack JT (1942) Sedimentation and volcanism in the Hopi Buttes, Arizona. *Geol Soc Am Bull* 53:335-372
- Haller MJ, Ross P-S, White JDL, Lefebvre NS (2017) Overview of the Cerro Chivo volcanic field (CCVF), Chubut province, Argentina: Basalt sheets, root zones, diatremes and 'plugs'. In: XX Congreso Geologico Argentino. San Miguel de Tucumàn, Argentina
- Harris AJL, Rowland SK (2015) Lava flows and rheology. In: *Encyclopedia of volcanoes*, second edition, Elsevier, pp 321-342
- Hart RJ, Ward JJ, Bills DJ, Flynn ME (2002) Generalized hydrogeology and ground-water budget for the C aquifer, Little Colorado River Basin and parts of the Verde and Salt River Basins, Arizona and New Mexico. *US Geol Surv Water-Resources Investigations Report:02-4026*
- Hayes J, Tsang S, Fitzgerald RH, Blake DM, Deligne NI, Doherty A, Hopkins JL, Hurst AW, Le Corvec N, Leonard GS (2018) The DEVORA scenarios: multi-hazard eruption scenarios for the Auckland Volcanic Field. *GNS Science*
- Hayes JL, Wilson TM, Deligne NI, Lindsay JM, Leonard GS, Tsang SWR, Fitzgerald RH (2020) Developing a suite of multi-hazard volcanic eruption scenarios using an interdisciplinary approach. *J Volcanol Geotherm Res* 392:106763
- Head JW, Wilson L (1989) Basaltic pyroclastic eruptions: influence of gas-release patterns and volume fluxes on fountain structure, and the formation of cinder cones, spatter cones, rootless flows, lava ponds and lava flows. *J Volcanol Geotherm Res* 37:261-271
- Head JW, Wilson L (2008) Integrated model for kimberlite ascent and eruption. *International Kimberlite Conference: Extended Abstracts*.
- Heiken G (1972) Morphology and petrography of volcanic ashes. *Geol Soc Am Bull* 83:1961-1988
- Heiken G, Wohletz K (1985) *Volcanic ash*. University Presses of California, Chicago, Harvard & MIT

- Hencz M, Karátson D, Németh K, Biró T (2017) A Badacsony freatomagmás piroklasztit-sorozata: következtetések a monogenetikus bazaltvulkáni működés folyamataira és formáira. *Földtani Közlöny* 147:297-310
- Hooten JA (1999) Phreatomagmatic diatremes of the western Hopi Buttes volcanic field, Navajo Nation, Arizona. MSc thesis, University of Northern Arizona, USA
- Hooten JA, Ort MH (2002) Peperite as a record of early-stage phreatomagmatic fragmentation processes: an example from the Hopi Buttes volcanic field, Navajo Nation, Arizona, USA. *J Volcanol Geotherm Res* 114:95-106
- Houghton BF, Schmincke H-U (1986) Mixed deposits of simultaneous strombolian and phreatomagmatic volcanism: Rothenberg volcano, east Eifel volcanic field. *J Volcanol Geotherm Res* 30:117-130
- Houghton BF, Schmincke H-U (1989) Rothenberg scoria cone, East Eifel: a complex Strombolian and phreatomagmatic volcano. *Bull Volcanol* 52:28-48
- Houghton BF, Wilson CJN (1989) A vesicularity index for pyroclastic deposits. *Bull Volcanol* 51:451-462
- Houghton BF, Wilson CJN, Rosenberg MD, Smith IEM, Parker RJ (1996) Mixed deposits of complex magmatic and phreatomagmatic volcanism: an example from Crater Hill, Auckland, New Zealand. *Bull Volcanol* 58:59-66
- Hubbard F (1986) The diamond-source kimberlite paradox of Sierra Leone: an alternative kimberlite emplacement mode. *J Afric Earth Sci* 5:599-605
- Karlstrom KE, Bowring SA (1988) Early Proterozoic assembly of tectonostratigraphic terranes in southwestern North America. *J Geol* 96:561-576
- Karlstrom KE, Humphreys ED (1998) Persistent influence of Proterozoic accretionary boundaries in the tectonic evolution of southwestern North America. *Rocky Mountain Geology* 33:161-179
- Keller GR, Snelson CM, Sheehan AF, Dueker KG (1998) Geophysical studies of crustal structure in the Rocky Mountain region. *Rocky Mountain Geology* 33:217-228
- Kempton PD, Fitton JG, Hawkesworth CJ, Ormerod DS (1991) Isotopic and trace element constraints on the composition and evolution of the lithosphere beneath the southwestern United States. *J Geophys Res: Solid Earth* 96:B8 13713-13735

- Kereszturi G, Németh K (2011) Shallow-seated controls on the evolution of the Upper Pliocene Kopasz-hegy nested monogenetic volcanic chain in the Western Pannonian Basin (Hungary). *Geologica Carpathica* 62:535-546
- Kereszturi G, Németh K (2012) Monogenetic basaltic volcanoes: genetic classification, growth, geomorphology and degradation. In: *Updates in volcanology-new advances in understanding volcanic systems*, IntechOpen
- Kereszturi G, Németh K, Cronin SJ, Procter J, Agustín-Flores J (2014) Influences on the variability of eruption sequences and style transitions in the Auckland Volcanic Field, New Zealand. *J Volcanol Geotherm Res* 286:101-115
- Kienle J, Kyle PR, Self S, Motyka RJ, Lorenz V (1980) Ukinrek Maars, Alaska, I. April 1977 eruption sequence, petrology and tectonic setting. *J Volcanol Geotherm Res* 7:11-37
- Kjarsgaard BA (2007) Kimberlite diamond deposits. Geological Association of Canada, Mineral Deposits Division 5:245-272
- Kósik S, Németh K, Kereszturi G, Procter JN, Zellmer GF, Geshi N (2016) Phreatomagmatic and water-influenced Strombolian eruptions of a small-volume parasitic cone complex on the southern ringplain of Mt. Ruapehu, New Zealand: facies architecture and eruption mechanisms of the Ohakune Volcanic Complex controlled by an unstable fissure eruption. *J Volcanol Geotherm Res* 327:99-115
- Kurszlaukis S, Lorenz V (2008) Formation of “Tuffisitic Kimberlites” by phreatomagmatic processes. *J Volcanol Geotherm Res* 174(1-3):68-80
- Kurszlaukis S, Lorenz V (2017) Differences and similarities between emplacement models of kimberlite and basaltic maar-diatreme volcanoes. *Geol Soc, London, Special Publications* 446:101-122
- Kurszlaukis S, Büttner R, Zimanowski B, Lorenz V (1998) On the first experimental phreatomagmatic explosion of a kimberlite melt. *J Volcanol Geotherm Res* 80:323-326
- Kurszlaukis S, Mahotkin I, Rotman AY, Kolesnikov GV, Makovchuk IV (2009) Syn-and post-eruptive volcanic processes in the Yubileinaya kimberlite pipe, Yakutia, Russia, and implications for the emplacement of South African-style kimberlite pipes. *Lithos* 112:579-591

- Latutrie B, Ross P-S (2018) Lava lakes filling phreatomagmatic craters at Twin Peaks, Hopi Buttes volcanic field, Navajo Nation, Arizona. In: Seventh International Maar Conference, Olot, Spain
- Latutrie B, Ross P-S (2019) Transition zone between the upper diatreme and lower diatreme: origin and significance at Round Butte, Hopi Buttes volcanic field, Navajo Nation, Arizona. *Bull Volcanol* 81: article 26
- Latutrie B, Ross P-S (2020) Phreatomagmatic vs magmatic eruptive styles in maar-diatremes: a case study at Twin Peaks, Hopi Buttes volcanic field, Navajo Nation, Arizona. *Bull Volcanol* 82: article 28
- Latutrie B, Andredakis I, De Groeve T, Harris AJL, Langlois E, de Vries BvW, Saubin E, Bilotta G, Cappello A, Crisci GM (2015) Testing a geographical information system for damage and evacuation assessment during an effusive volcanic crisis. *Geol Soc, London, Special Publications* 426:649-672
- Lavine A, Aalto KR (2002) Morphology of a crater-filling lava lake margin, The Peninsula tuff cone, Tule Lake National Wildlife Refuge, California: implications for formation of peperite textures. *J Volcanol Geotherm Res* 114:147-163
- Le Bas MJ, Le Maitre RW, Streckeisen A, Zanettin B (1986) A chemical classification of volcanic rocks based on the total alkali-silica diagram. *J Petrol* 27:745-750
- Le Corvec N, Muirhead JD, White JDL (2018) Shallow magma diversions during explosive diatreme-forming eruptions. *Nat Commun* 9:1459
- Le Maitre RW, Streckeisen A, Zanettin B, Le Bas MJ, Bonin B, Bateman P, Bellieni G, Dudek A, Efremova S, Keller J, Lameyre J, Sabine PA, Schmid R, Sorensen H, Woolley AR (1989) *Igneous rocks: A classification and glossary of terms. Recommendations of the international union of geological sciences subcommission on the systematics of igneous rocks.* Cambridge University Press
- Lefebvre NS (2013) *Volcanology of maar-diatreme volcanic vent complexes, Hopi Buttes Volcanic Field, Navajo Nation, Arizona, USA.* PhD thesis, University of Otago, New Zealand
- Lefebvre N, Kurszlaukis S (2008) Contrasting eruption styles of the 147 Kimberlite, Fort à la Corne, Saskatchewan, Canada. *J Volcanol Geotherm Res* 174:171-185

- Lefebvre NS, White JDL, Kjarsgaard BA (2012) Spatter-dike reveals subterranean magma diversions: Consequences for small multivert basaltic eruptions. *Geology* 40:423-426
- Lefebvre NS, White JDL, Kjarsgaard BA (2013) Unbedded diatreme deposits reveal maar-diatreme-forming eruptive processes: Standing Rocks West, Hopi Buttes, Navajo Nation, USA. *Bull Volcanol* 75:1-17
- Lefebvre NS, White JDL, Kjarsgaard BA (2016) Arrested diatreme development: Standing Rocks East, Hopi Buttes, Navajo Nation, USA. *J Volcanol Geotherm Res* 310:186-208
- Lexa J, Seghedi I, Németh K, Szakács A, Konečný V, Pécskay Z, Fülöp A, Kovacs M (2010) Neogene-Quaternary volcanic forms in the Carpathian-Pannonian Region: a review. *Open Geosci* 2:207-270
- Leyrit H, Zylberman W, Lutz P, Jaillard A, Lavina P (2016) Characterization of phreatomagmatic deposits from the eruption of the Pavin maar (France). In: *Lake Pavin*, Springer, pp 105-128
- Lipman PW, Prostka HJ, Christiansen RL (1972) Cenozoic volcanism and plate-tectonic evolution of the Western United States. I. Early and Middle Cenozoic. *Philosophical Transactions of the Royal Society of London A: Mathematical, Physical and Engineering Sciences* 271:217-248
- Lorenz V (1973) On the formation of maars. *Bull Volcanol* 37:183-204
- Lorenz V (1974) Vesiculated tuffs and associated features. *Sedimentology* 21:273-291
- Lorenz V (1975) Formation of phreatomagmatic maar-diatreme volcanoes and its relevance to kimberlite diatremes. *Physics and Chemistry of the Earth* 9:17-27
- Lorenz V (1986a) On the growth of maars and diatremes and its relevance to the formation of tuff rings. *Bull Volcanol* 48:265-274
- Lorenz V (1986b) Phreatomagmatism and its relevance. *Chem Geol* 62:149-156
- Lorenz V (2003) Maar-diatreme volcanoes, their formation, and their setting in hard-rock or soft-rock environments. *Geolines* 15:72-83
- Lorenz V (2007) Syn-and posteruptive hazards of maar-diatreme volcanoes. *J Volcanol Geotherm Res* 159:285-312

- Lorenz V (2008) Explosive maar-diatreme volcanism in unconsolidated water-saturated sediments and its relevance for diamondiferous pipes. *Zeitschrift der Deutschen Gemmologischen Gesellschaft* 57:41-60
- Lorenz V, Kurszlaukis S (1997) On the last explosions of carbonatite pipe G3b, Gross Brukkaros, Namibia. *Bull Volcanol* 59:1-9
- Lorenz V, Kurszlaukis S (2003) Kimberlite pipes: growth models and resulting implications for diamond exploration. *International Kimberlite Conference: Extended Abstracts*.
- Lorenz V, Kurszlaukis S (2007) Root zone processes in the phreatomagmatic pipe emplacement model and consequences for the evolution of maar–diatreme volcanoes. *J Volcanol Geotherm Res* 159:4-32
- Lorenz V, Zimanowski B (2008) Volcanology of the West Eifel Maars and its relevance to the understanding of kimberlite pipes. In: 9th International Kimberlite Conference, field trip guidebook.
- Lorenz V, Suhr P, Suhr S (2017) Phreatomagmatic maar-diatreme volcanoes and their incremental growth: a model. *Geol Soc, London, Special Publications* 446:29-59
- Marshak S, Karlstrom K, Timmons JM (2000) Inversion of Proterozoic extensional faults: An explanation for the pattern of Laramide and Ancestral Rockies intracratonic deformation, United States. *Geology* 28:735-738
- Martin U, Nemeth K (2002) Interaction between lava lakes and pyroclastic sequences in phreatomagmatic volcanoes: Haláp and Badacsony, Western Hungary. *CBGA Conference*.
- McClintock M, White JDL (2006) Large phreatomagmatic vent complex at Coombs Hills, Antarctica: wet, explosive initiation of flood basalt volcanism in the Ferrar-Karoo LIP. *Bull Volcanol* 68:215-239
- McClintock M, Ross P-S, White JDL (2009) The importance of the transport system in shaping the growth and form of kimberlite volcanoes. *Lithos* 112:465-472
- McKee ED (1954) Stratigraphy and history of the Moenkopi Formation of Triassic age. *Geol Soc Am Memoir* 61
- Moore JG (1967) Base surge in recent volcanic eruptions. *Bull Volcanol* 30:337-363
- Moore JG, Nakamura K, Alcaraz A (1966) The 1965 eruption of Taal volcano. *Sci* 151:955-960

- Muirhead JD, Van Eaton AR, Re G, White JDL, Ort MH (2016) Monogenetic volcanoes fed by interconnected dikes and sills in the Hopi Buttes volcanic field, Navajo Nation, USA. *Bull Volcanol* 78:1-16
- Muller G, Veyl G (1957) The birth of Nilahue, a new maar type volcano at Rininahua. Chile. 20th International Geological Congress, Mexico, pp. 375–396.
- Nairn IA (1979) Rotomahana—Waimangu eruption, 1886: base surge and basalt magma. *New Zealand J Geol Geophys* 22:363-378
- Németh K, Kereszturi G (2013) On the variety of Mio-Pleistocene root zones of monogenetic volcanoes of the Pannonian Basin. In: Buechner J, Rappich V, Tietz O (eds) *Basalt 2013 - Cenozoic Magmatism in Central Europe, Abstract Book & Excursion Guides*
- Németh K, Kereszturi G (2015) Monogenetic volcanism: personal views and discussion. *Int J Earth Sci* 104:2131-2146
- Nemeth K, Martin U, Harangi S (2000) On the calculation of the geometry of the diatreme pipe from a deposits of an "accidental lithic clast rich" maar, Tihany East Maar, (Hungary). *Terra Nostra* 2000/6:383-390
- Németh K, Goth K, Martin U, Csillag G, Suhr P (2008) Reconstructing paleoenvironment, eruption mechanism and paleomorphology of the Pliocene Pula maar (Hungary). *J Volcanol Geotherm Res* 177:441-456
- Németh K, Cronin SJ, Smith IEM, Augustin Flores J (2012) Amplified hazard of small-volume monogenetic eruptions due to environmental controls, Orakei Basin, Auckland Volcanic Field, New Zealand. *Bull Volcanol* 74:2121-2137
- Nowicki T, Porritt L, Crawford B, Kjarsgaard B (2008) Geochemical trends in kimberlites of the Ekati property, Northwest Territories, Canada: insights on volcanic and resedimentation processes. *J Volcanol Geotherm Res* 174:117-127
- Nunns AG, Hochstein MP (2019) Geophysical constraints on the structure and formation of Onepoto, Orakei, Pupuke and Tank Farm maar volcanoes, Auckland Volcanic Field. *New Zealand J Geol Geophys* 62:1-16
- Nybo JP, McIntosh WC, Semken SC (2011) Ar-Ar phlogopite geochronology of the Navajo Volcanic Field and the Ship Rock diatreme of Northwest New Mexico define a 1.4 Ma pulse of potassic magmatism. American Geophysical Union Conference, San Francisco, CA, December 2011, abstract V23A2566

- Ollier CD (1967) Maars their characteristics, varieties and definition. *Bull Volcanol* 31:45-73
- Ort MH, Carrasco-Núñez G (2009) Lateral vent migration during phreatomagmatic and magmatic eruptions at Tecuitlapa Maar, east-central Mexico. *J Volcanol Geotherm Res* 181:67-77
- Ort MH, Lefebvre NS, Neal CA, McConnell VS, Wohletz KH (2018) Linking the Ukinrek 1977 maar-eruption observations to the tephra deposits: New insights into maar depositional processes. *J Volcanol Geotherm Res* 360:36-60
- Pirrung M, Büchel G, Lorenz V, Treutler HC (2008) Post-eruptive development of the Ukinrek East Maar since its eruption in 1977 AD in the periglacial area of south-west Alaska. *Sedimentology* 55:305-334
- Poppe S, Smets B, Fontijn K, Rukeza MB, Migabo ADMF, Milungu AK, Namogo DB, Kervyn F, Kervyn M (2016) Holocene phreatomagmatic eruptions alongside the densely populated northern shoreline of Lake Kivu, East African Rift: timing and hazard implications. *Bull Volcanol* 78: article 82
- Porritt LA, Cas RAF, Crawford BB (2008) In-vent column collapse as an alternative model for massive volcanoclastic kimberlite emplacement: an example from the Fox kimberlite, Ekati Diamond Mine, NWT, Canada. *J Volcanol Geotherm Res* 174:90-102
- Raue H (2004) A new model for the fracture energy budget of phreatomagmatic explosions. *J Volcanol Geotherm Res* 129:99-108
- Re G, White JDL, Ort MH (2015) Dikes, sills, and stress-regime evolution during emplacement of the Jagged Rocks complex, Hopi Buttes Volcanic field, Navajo Nation, USA. *J Volcanol Geotherm Res* 295:65-79
- Re G, White JDL, Muirhead JD, Ort MH (2016) Subterranean fragmentation of magma during conduit initiation and evolution in the shallow plumbing system of the small-volume Jagged Rocks volcanoes (Hopi Buttes Volcanic Field, Arizona, USA). *Bull Volcanol* 78: article 55
- Reagan AB (1924) Stratigraphy of the Hopi Buttes volcanic field, Arizona. *Pan-American Geologist* 41:355-366
- Reagan AB (1932) The Tertiary-Pleistocene of the Navajo Country in Arizona, with a description of some of its included fossils. *Transact Kansas Acad Sci* 35:253-259

- Repenning CA, Irwin JH (1954) Bidahochi Formation of Arizona and New Mexico. AAPG Bull 38:1821-1826
- Repenning CA, Cooley ME, Akers JP (1969) Stratigraphy of the Chinle and Moenkopi formations, Navajo and Hopi Indian reservations; Arizona, New Mexico, and Utah. U.S. Geological Professional Paper 521-B
- Riggs N, Ort M, Connor C, Alfano F, Conway M (2019) Volcanology and associated hazards of the San Francisco volcanic field. Geological Excursions in Southwestern North America 55:127-146
- Ripepe M, Donne DD, Harris AJL, Marchetti E, Olivieri G (2008) Dynamics of Strombolian activity. The Stromboli Volcano: An Integrated Study of the 2002–2003 Eruption:39-48
- Robert B, Harris A, Gurioli L, Médard E, Sehlke A, Whittington A (2014) Textural and rheological evolution of basalt flowing down a lava channel. Bull Volcanol 76:824
- Rock NMS (1991) Lamprophyres. Blackie, Glasgow
- Roduit N (2007) JMicroVision: un logiciel d'analyse d'images pétrographiques polyvalent. PhD thesis, University of Geneva
- Ross P-S, White JDL (2006) Debris jets in continental phreatomagmatic volcanoes: a field study of their subterranean deposits in the Coombs Hills vent complex, Antarctica. J Volcanol Geotherm Res 149:62-84
- Ross P-S, White JDL (2012) Quantification of vesicle characteristics in some diatreme-filling deposits, and the explosivity levels of magma–water interactions within diatremes. J Volcanol Geotherm Res 245:55-67
- Ross P-S, White JDL, McClintock M (2008a) Geological evolution of the Coombs–Allan Hills area, Ferrar large igneous province, Antarctica: Debris avalanches, mafic pyroclastic density currents, phreatocauldrons. J Volcanol Geotherm Res 172:38-60
- Ross P-S, White JDL, Zimanowski B, Büttner R (2008b) Multiphase flow above explosion sites in debris-filled volcanic vents: Insights from analogue experiments. J Volcanol Geotherm Res 178:104-112
- Ross P-S, White JDL, Zimanowski B, Büttner R (2008c) Rapid injection of particles and gas into non-fluidized granular material, and some volcanological implications. Bull Volcanol 70:1151-1168

- Ross P-S, Delpit S, Haller MJ, Németh K, Corbella H (2011) Influence of the substrate on maar–diatreme volcanoes—an example of a mixed setting from the Pali Aike volcanic field, Argentina. *J Volcanol Geotherm Res* 201:253-271
- Ross P-S, White JDL, Valentine GA, Taddeucci J, Sonder I, Andrews RG (2013) Experimental birth of a maar–diatreme volcano. *J Volcanol Geotherm Res* 260:1-12
- Ross P-S, White JDL, Valentine GA, Latutrie B (2018) Distinguishing magmatic from phreatomagmatic pyroclastic deposits at prehistoric mafic maar volcanoes. In: *Cities on volcanoes, Naples, Italy*
- Ross P-S, Carrasco-Núñez G, Hayman P (2017) Felsic maar-diatreme volcanoes: a review. *Bull Volcanol* 79: article 20
- Saucedo R, Macías JL, Ocampo-Díaz YZE, Gómez-Villa W, Rivera-Olguín E, Castro-Govea R, Sánchez-Núñez JM, Layer PW, Torres Hernández JR, Carrasco-Núñez G (2017) Mixed magmatic–phreatomagmatic explosions during the formation of the Joya Honda maar, San Luis Potosí, Mexico. *Geol Soc Special Pub* 446:255-279
- Self S, Sparks RSJ, Booth B, Walker GPL (1974) The 1973 Heimaey strombolian scoria deposit, Iceland. *Geol Mag* 111:539-548
- Self S, Kienle J, Huot J-P (1980) Ukinrek Maars, Alaska, II. Deposits and formation of the 1977 craters. *J Volcanol Geotherm Res* 7:39-65
- Semken S (2003) Black rocks protruding up: the Navajo volcanic field. *Geology of the Zuni Plateau. New Mexico Geol Soc Guidebook* 54:397-412
- Sheridan MF, Updike RG (1975) Sugarloaf Mountain Tephra—A Pleistocene rhyolitic deposit of base-surge origin in northern Arizona. *Geol Soc Am Bull* 86:571-581
- Shoemaker EM, Roach CH, Byers FMJ (1962) Diatremes and uranium deposits in the Hopi Buttes, Arizona. *Petrologic Studies—A Volume in Honor of AF Buddington: Boulder, Colorado, Geol Soc Am*:327-355
- Snyder WS, Dickinson WR, Silberman ML (1976) Tectonic implications of space-time patterns of Cenozoic magmatism in the western United States. *Earth Planet Sci Lett* 32:91-106
- Sohn YK (1996) Hydrovolcanic processes forming basaltic tuff rings and cones on Cheju Island, Korea. *Geol Soc Am Bull* 108:1199-1211

- Sohn YK, Chough SK (1989) Depositional processes of the Suwolbong tuff ring, Cheju Island (Korea). *Sedimentology* 36:837-855
- Sonder I, Harp AG, Graettinger AH, Moitra P, Valentine GA, Büttner R, Zimanowski B (2018) Meter-Scale Experiments on Magma-Water Interaction. *J Geophys Res: Solid Earth* 123:10,597-510,615
- Sottili G, Taddeucci J, Palladino DM (2010) Constraints on magma–wall rock thermal interaction during explosive eruptions from textural analysis of cored bombs. *J Volcanol Geotherm Res* 192:27-34
- Sparks RSJ, Baker L, Brown RJ, Field M, Schumacher J, Stripp G, Walters A (2006) Dynamical constraints on kimberlite volcanism. *J Volcanol Geotherm Res* 155:18-48
- Spera FJ (2000) Physical properties of magma. In: *Encyclopedia of volcanoes*, First edition, Academic Press, pp 171-190
- Stiefenhofer J, Farrow DJ (2004) Crater deposits of the Mwadui kimberlite. *International Kimberlite Conference: Extended Abstracts*.
- Stoppa F (1996) The San Venanzo maar and tuff ring, Umbria, Italy: eruptive behaviour of a carbonatite-melilitite volcano. *Bull Volcanol* 57:563-577
- Stovall WK, Houghton BF, Gonnermann H, Fagents SA, Swanson DA (2011) Eruption dynamics of Hawaiian-style fountains: the case study of episode 1 of the Kīlauea Iki 1959 eruption. *Bull Volcanol* 73:511-529
- Stovall WK, Houghton BF, Hammer JE, Fagents SA, Swanson DA (2012) Vesiculation of high fountaining Hawaiian eruptions: episodes 15 and 16 of 1959 Kīlauea Iki. *Bull Volcanol* 74:441-455
- Stroncik NA, Schmincke H-U (2002) Palagonite—a review. *Int J Earth Sci* 91:680-697
- Sumner JM (1998) Formation of clastogenic lava flows during fissure eruption and scoria cone collapse: the 1986 eruption of Izu-Oshima Volcano, eastern Japan. *Bull Volcanol* 60:195-212
- Sumner JM, Blake S, Matela RJ, Wolff JA (2005) Spatter. *J Volcanol Geotherm Res* 142:49-65
- Sun S-S, McDonough WF (1989) Chemical and isotopic systematics of oceanic basalts: implications for mantle composition and processes. *Geol Soc Special Pub* 42:313-345

- Sweeney MR, Valentine GA (2015) Transport and mixing dynamics from explosions in debris-filled volcanic conduits: numerical results and implications for maar-diatreme volcanoes. *Earth Planet Sci Lett* 425:64-76
- Taddeucci J, Pompilio M, Scarlato P (2004) Conduit processes during the July–August 2001 explosive activity of Mt. Etna (Italy): inferences from glass chemistry and crystal size distribution of ash particles. *J Volcanol Geotherm Res* 137:33-54
- Taddeucci J, Valentine GA, Sonder I, White JDL, Ross P-S, Scarlato P (2013) The effect of pre-existing craters on the initial development of explosive volcanic eruptions: An experimental investigation. *Geophys Res Lett* 40:507-510
- Taddeucci J, Alatorre-Ibarguengoitia MA, Palladino DM, Scarlato P, Camaldo C (2015) High-speed imaging of Strombolian eruptions: Gas-pyroclast dynamics in initial volcanic jets. *Geophys Res Lett* 42:6253-6260
- Tazieff H (1994) Permanent lava lakes: observed facts and induced mechanisms. *J Volcanol Geotherm Res* 63:3-11
- Thomas APW (1888) Report on the Eruption of Tarawera and Rotomahana, NZ [With Maps and Plates], Wellington NZ
- Thompson GA, Zoback ML (1979) Regional geophysics of the Colorado Plateau. *Tectonophysics* 61:149-181
- Tietz O, Buchner J, Lapp M, Scholle T (2018) The Stolpen Volcano in the Lausitz Volcanic Field (East Germany) - volcanological, petrographic and geochemical investigations at the type locality of basalt. *J Geosci* 63:299-315
- Tingey DG, Christiansen EH, Best MG, Ruiz J, Lux DR (1991) Tertiary minette and melanephelinite dikes, Wasatch Plateau, Utah: Records of mantle heterogeneities and changing tectonics. *J Geophys Res: Solid Earth* 96:13529-13544
- Ulrich GE (1987) SP Mountain cinder cone and lava flow, northern Arizona. *Centennial Field Guide* 2:385-388
- Ulrich GE, Billingsley GH, Hereford R, Wolfe EW, Nealey LD, Sutton RL (1984) Map showing geology, structure, and uranium deposits of the Flagstaff 1 degree by 2 degrees Quadrangle, Arizona. Map 1-1446, scale 1:250 000
- Underwood EE (1970) Quantitative stereology. Addison-Wesley, Reading, Mass

- Valentine GA (2012) Shallow plumbing systems for small-volume basaltic volcanoes, 2: Evidence from crustal xenoliths at scoria cones and maars. *J Volcanol Geotherm Res* 223:47-63
- Valentine GA, White JDL (2012) Revised conceptual model for maar-diatremes: Subsurface processes, energetics, and eruptive products. *Geology* 40:1111-1114
- Valentine GA, Cortés JA (2013) Time and space variations in magmatic and phreatomagmatic eruptive processes at Easy Chair (Lunar Crater Volcanic Field, Nevada, USA). *Bull Volcanol* 75: article 752
- Valentine GA, van Wyk de Vries B (2014) Unconventional maar diatreme and associated intrusions in the soft sediment-hosted Mardoux structure (Gergovie, France). *Bull Volcanol* 76: article 807
- Valentine GA, White JDL, Ross P-S, Amin J, Taddeucci J, Sonder I, Johnson PJ (2012) Experimental craters formed by single and multiple buried explosions and implications for volcanic craters with emphasis on maars. *Geophys Res Lett* 39, L20301
- Valentine GA, Graettinger AH, Sonder I (2014) Explosion depths for phreatomagmatic eruptions. *Geophys Res Lett* 41:3045-3051
- Valentine GA, Sottili G, Palladino DM, Taddeucci J (2015) Tephra ring interpretation in light of evolving maar–diatreme concepts: Stracciacappa maar (central Italy). *J Volcanol Geotherm Res* 308:19-29
- Valentine GA, White JDL, Ross P-S, Graettinger AH, Sonder I (2017) Updates to concepts on phreatomagmatic maar-diatremes and their pyroclastic deposits. *Frontiers Earth Sci* 5:68
- Van der Plas L, Tobi AC (1965) A chart for judging the reliability of point counting results. *Am J Sci* 263:87-90
- van Otterloo J, Ort MH, Cruden AR (2018) Unique occurrence of a folded in-vent dike: New insights on magma-water mixing. *Geology* 46:379-382
- Vazquez JA (1998) Maar volcanism in the Wood Chop Mesa area, Hopi Buttes volcanic field, Navajo Nation, Arizona. MSc thesis, University of Northern Arizona, USA

- Vazquez JA, Ort MH (2006) Facies variation of eruption units produced by the passage of single pyroclastic surge currents, Hopi Buttes volcanic field, USA. *J Volcanol Geotherm Res* 154:222-236
- Vespermann D, Schmincke H-U (2000) Scoria cones and tuff rings. In: *Encyclopedia of volcanoes*, First edition, Academic Press, pp 683-694
- Walker GPL, Croasdale R (1971) Characteristics of some basaltic pyroclastics. *Bull Volcanol* 35:303-317
- Walters AL, Phillips JC, Brown RJ, Field M, Gernon T, Stripp G, Sparks RSJ (2006) The role of fluidisation in the formation of volcanoclastic kimberlite: grain size observations and experimental investigation. *J Volcanol Geotherm Res* 155:119-137
- White JDL (1989) Basic elements of maar-crater deposits in the Hopi Buttes volcanic field, northeastern Arizona, USA. *J Geol* 97:117-125
- White JDL (1990) Depositional architecture of a maar-pitted playa: sedimentation in the Hopi Buttes volcanic field, northeastern Arizona, USA. *Sediment Geol* 67:55-84
- White JDL (1991) Maar-diatreme phreatomagmatism at Hopi Buttes, Navajo Nation (Arizona), USA. *Bull Volcanol* 53:239-258
- White JDL (1992) Pliocene subaqueous fans and Gilbert-type deltas in maar crater lakes, Hopi Buttes, Navajo Nation (Arizona), USA. *Sedimentology* 39:931-946
- White JDL (1996a) Impure coolants and interaction dynamics of phreatomagmatic eruptions. *J Volcanol Geotherm Res* 74:155-170
- White JDL (1996b) Pre-emergent construction of a lacustrine basaltic volcano, Pahvant Butte, Utah (USA). *Bull Volcanol* 58:249-262
- White JDL, McClintock M (2001) Immense vent complex marks flood-basalt eruption in a wet, failed rift: Coombs Hills, Antarctica. *Geology* 29:935-938
- White JDL, Houghton BF (2006) Primary volcanoclastic rocks. *Geology* 34:677-680
- White JDL, Ross P-S (2011) Maar-diatreme volcanoes: a review. *J Volcanol Geotherm Res* 201:1-29
- White JDL, Houghton BF (2015) Surtseyan and related phreatomagmatic eruptions. In: *Encyclopedia of volcanoes*, Decond edition, Elsevier, pp 495-511

- White JDL, Valentine GA (2016) Magmatic versus phreatomagmatic fragmentation: absence of evidence is not evidence of absence. *Geosphere* 12:1478-1488
- White JDL, Lefebvre NS, Ort MH (2008) Maar Rims, Crater Deposits, Diatremes and Root Zones: Hopi Buttes, Navajo Nation, Arizona. In: Commission on Volcanogenic Sediments Workshop. Flagstaff, Arizona, p 48
- White JD, Lefebvre N, Ort M, Kjarsgaard BA, Vazquez J, Valentine G (2012a) Hopi Buttes Volcanic Field Workshop: Maar-Diatreme Volcanism. In: Field Trip Guide – Part 1. p 47
- White JD, Lefebvre N, Ort M, Kjarsgaard BA, Vazquez J, Valentine G (2012b) Hopi Buttes Volcanic Field Workshop: Interpreting Maar-Diatreme Volcanism using base to top exposures, syn-eruptive surface deposits and country-rock strata. Field Trip Guide – Part 2
- White JDL, Dürig T, Murch AP, Zimanowski B, Büttner R, Mele D, Dellino P, Carey R (2019) Induced Fuel Coolant Interaction—making ash from viscous magma and seawater in the 2012 Havre eruption. AGU Fall Meeting
- Williams H (1936) Pliocene volcanoes of the Navajo-Hopi country. *Geol Soc Am Bull* 47:111-172
- Winchester JA, Floyd PA (1977) Geochemical discrimination of different magma series and their differentiation products using immobile elements. *Chem geol* 20:325-343
- Wolff JA, Sumner JM (2000) Lava fountains and their products. In: *Encyclopedia of volcanoes*, First edition, Elsevier, pp 321-330
- Womer MB, Greely R, King JS (1980) The geology of Split Butte—a maar of the south-central Snake River Plain, Idaho. *Bull Volcanol* 43:453-471
- Wright TL, Peck DL (1978) Crystallization and differentiation of the Alae Lava Lake, Hawaii. *U.S. Geol Surv Prof Pap* 935-C:1-20
- Zimanowski B (1998) Phreatomagmatic explosions. In Freundt A, Rosi M, *From magma to tephra*. Amsterdam, Elsevier v 4, pp 25-53
- Zimanowski B, Fröhlich G, Lorenz V (1991) Quantitative experiments on phreatomagmatic explosions. *J Volcanol Geotherm Res* 48:341-358
- Zimanowski B, Büttner R, Lorenz V, Häfele HG (1997) Fragmentation of basaltic melt in the course of explosive volcanism. *J Geophys Res: Solid Earth* 102:B1 803-814

7 Appendix 1: Conference abstracts

7.1 Poster session at IAVCEI⁵ (2017), Portland, USA

Bedded to non-bedded transition at Round Butte diatreme, Hopi Buttes volcanic field, Arizona

Benjamin Latutrie¹, Pierre-Simon Ross¹, James D.L White²

¹Institut National de la Recherche Scientifique, Centre Eau Terre Environnement, 490 Rue de la Couronne, Québec (QC), G1K 9A9, Canada

²Department of Geology, University of Otago, P.O. Box 56, Dunedin 9054, New Zealand

The Hopi Buttes volcanic field (HBVF) in the Navajo Nation (Arizona, USA) provides excellent exposures of maar-diatreme volcanoes at different erosion depths, from the maar ejecta ring and crater infill (White 1991) to the deep diatreme (Lefebvre et al. 2013). This makes it an ideal locality to better understand eruptive processes for this type of volcano. We are currently investigating the Round Butte diatreme in the eastern portion of the HBVF. The current exposure lies at the top of the Owl Rock member of the Chinle formation (Upper Triassic) near the contact with the bottom of the Moenave Formation (Lower Jurassic), at ~190 m below the eruptive paleosurface. At this depth, Round Butte is 130 m in diameter and the exposure consists of 30 m high cliffs. It displays the transition between the lower (non-bedded) and the upper (bedded) portions of the diatreme. This contact is irregular, varying in apparent angle from subhorizontal to subvertical.

In order to constrain the morphologies of this contact and the processes that created Round Butte we carried out one month of field work. We mapped the cliffs of Round Butte, described and sampled all the units defined during the mapping and we did componentry measurements using the line count method proposed by Lefebvre (2013). Our preliminary observations highlighted that at Round Butte the upper part of the diatreme is composed of diffuse to well defined bedding with some accumulation levels of juvenile and lithic blocks, while the lower part is massive and non-bedded. A relatively large debris avalanche in the southwest of the outcrop seems to arrive early in the growth of Round Butte and shows a succession of Moenave and Bidahochi blocks intercalated by tuffs from the ejecta ring. In the south face, the transition seems to be linked to an intense activity of a “main vent”.

Our preliminary model has four steps. (1) The first phase of crater excavation was deep and directly followed by (2) infilling with bedded units and a debris avalanche. The crater level must

⁵ International Association of Volcanology and Chemistry of the Earth's Interior

have been higher than the current top of the outcrop at this stage. (3) The “main vent” starts another phase of excavation that created the current upper-lower transition at Round Butte and that (4) deposited the last phase of crater infill.

Keyword: maar-diatreme, transition, bedded deposits, non-bedded deposits

7.2 Oral session at 7IMC⁶ (2018), Olot, Spain

How the early syn-eruptive crater infill progressively becomes the lower diatreme: Round Butte, Hopi Buttes volcanic field, Navajo Nation, Arizona

Benjamin Latutrie¹, Pierre-Simon Ross¹

¹ Institut National de la Recherche Scientifique, Centre Eau Terre Environnement, 490 Rue de la Couronne, Québec (QC), G1K 9A9, Canada: Benjamin.Latutrie@ete.inrs.ca

Keywords: diatreme, crater, eruptive processes.

The Miocene Hopi Buttes volcanic field (HBVF) in the Navajo Nation (Arizona, USA) provides excellent exposures of maar-diatreme volcanoes (White and Ross 2011) at different erosion depths, from the maar ejecta ring and crater infill (White 1991) to the deep diatreme (Lefebvre et al. 2013). The base of the current exposure at Round Butte, in the eastern part of the HBVF, lies ~190 m below the pre-eruptive surface. At this depth, the Round Butte diatreme is ~130 m in diameter and the exposure consists of 30 m high cliffs. The diatreme displays an intriguingly complex history, given its relatively small size. We carried out one month of field work there as part of the first author's PhD project. Geological contacts were mapped on high resolution pictures of the cliffs (Fig. 1). We described and sampled all the units defined during the mapping and then did componentry measurements using the line count method proposed by Lefebvre et al. (2013).

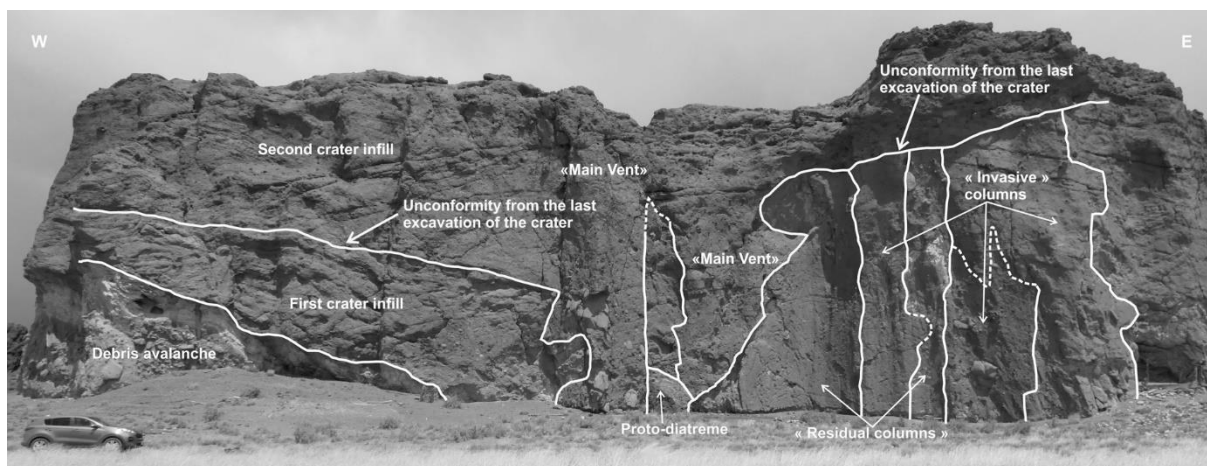


Fig. 1 – South face of Round Butte diatreme in the Hopi Buttes volcanic field. The cliff displays a complex history with two phases of crater infill and the transition between upper and lower diatreme.

⁶ IAVCEI - 7th International Maar Conference

The upper part of the diatreme (syn-eruptive crater infill) is composed of two main bedded pyroclastic units. The **older bedded unit** is coarse grained (lapilli tuff), diffusively to well bedded, and heterolithic (mixture of juvenile fragments and lithics in sub-equal proportions). It contains a number of megablocks of Bidahochi Formation, the youngest formation in the country rock stratigraphy (Billingsley et al., 2013). The older bedded unit has locally suffered liquefaction and has been invaded by debris jets in many places. The debris jets created “invasive” columns of non-bedded material, between which domains of early diffusely bedded crater infill are left; we call these “residual columns” (Fig. 1).

The **younger bedded unit**, mostly consisting of thick, lenticular to planar, lapilli tuff to tuff breccia beds, represents the late syn-eruptive crater infill. The composition mostly ranges from heterolithic to juvenile-rich. The younger bedded unit does *not* have the disturbed aspect of the older one and is not clearly cut by invasive columns. It was deposited on top of an unconformity where subvertical columns are truncated (Fig. 1). At least on the South face, the late bedded unit was fed by a vent which we informally call the “main vent” (Fig. 1, middle). The upper bedded unit is generally poor in Bidahochi megablocks.

Non-bedded pyroclastic rocks are also found at Round Butte. They range in grain size from fine lapilli tuff to tuff breccia and vary in composition from juvenile-rich to heterolithic, with a great diversity of lithics clasts, including some sourced from the Moenkopi Formation ~440 m below the pre-eruptive surface. The non-bedded rocks form invasive columns into the older bedded unit, and sometimes invasive columns emplaced into other invasive columns, a feature typical of lower diatremes (Lefebvre et al. 2013).

In the southwest part of the diatreme, a relatively large **debris avalanche** crops out (Fig. 1, lower left). This deposit shows a succession of Moenave Formation breccias and liquefied Bidahochi Formation, intercalated by a pyroclastic level.

Our preliminary model has six steps (Fig. 2).

- (a) A dike rises and interacts explosively with a wet substrate. This creates the initial crater and a proto-diatreme, now found preserved locally as a megablock of Bidahochi-rich bedded pyroclastic rock cut by a coherent dike on the South face (Fig. 1, middle).
- (b) A phase of intensely explosive activity leads to deep excavation of the country rock, creating a crater deeper than the current lower level of exposure, and probably a significant ejecta ring on top of the initial paleo-surface.

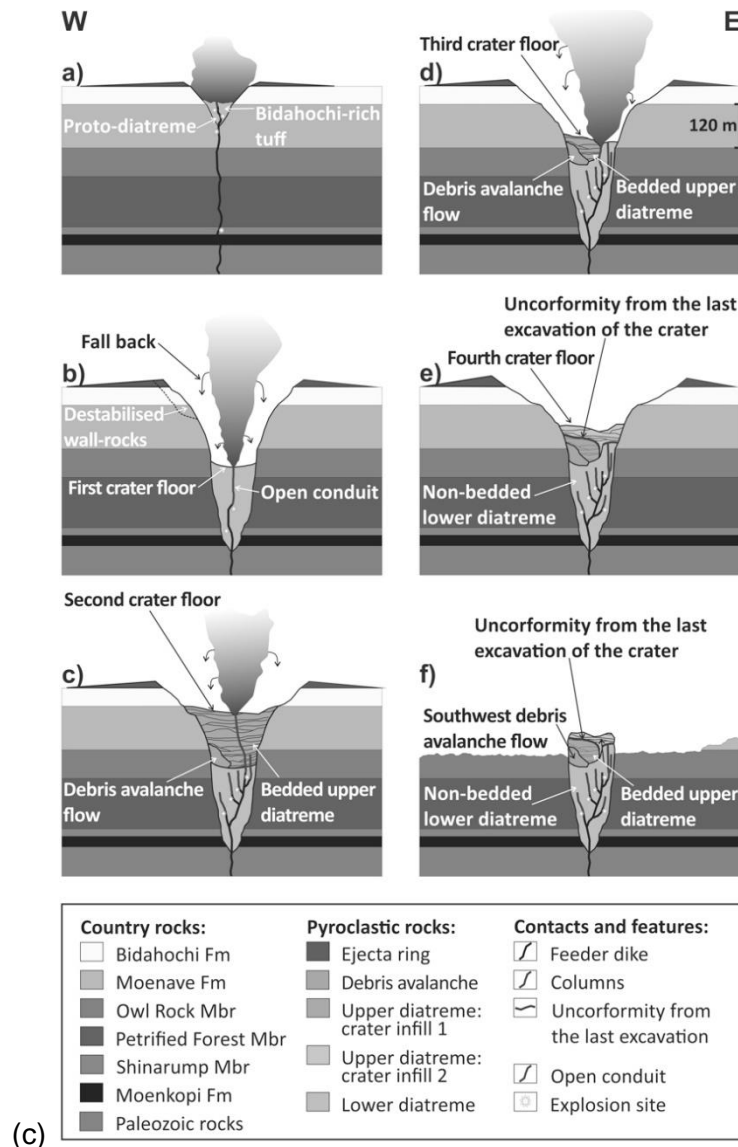


Fig. 2 – Preliminary model displaying the formation of the different units at Round Butte diatreme.

(d) Crater excavation triggers the debris avalanche, emplaced in several stages during which explosive activity continued. The older crater infill is deposited. Megablocks of the Bidahochi Formation are falling repeatedly, leading to lateral enlargement of the crater. The early ejecta ring is also partly recycled, and is now found as lapilli- to megablock-sized fragments of bedded tuff and lapilli tuff in the early crater infill. Continued infilling by pyroclastic material leads to the crater level being higher than the top of the current outcrop. This early crater infill becomes locally liquefied, blurring some of the bedding. Elsewhere it is invaded by debris jets (White and Ross 2011), the passage of which also disturbs bedding, and creates non-bedded invasive columns. Residual columns, with mostly destroyed bedding, are left

between the invasive columns. This is how the (bedded) early syn-eruptive crater infill progressively evolves into the (non-bedded) lower diatreme.

- (e) Another period of intensely explosive activity leads to the second major excavation phase. This digs into the early bedded pyroclastic rocks and locally exposes the non-bedded pyroclastic rocks at the bottom of the new crater, creating the “unconformity”.
- (f) The younger bedded pyroclastic unit is deposited on top of the unconformity and explosive activity ends. Post-eruptive crater infilling might have taken place but is not preserved.
- (g) Erosion leads to the current outcrop with typical inverted topography.

Acknowledgements

James D.L. White did the early work on Round Butte and introduced PSR to this fascinating volcano. Pier-Paolo Comida helped us in the field. We thank the Morris family for allowing us to work at Round Butte. Any persons wishing to conduct geological investigations on the Navajo Nation must first apply for, and receive, a permit from the Navajo Nation Minerals Department, P.O. Box 1910, Window Rock, Arizona 86515, USA, telephone 1-928-871-6587.

References

- Billingsley, G.H., Block, D., Hiza-Redsteer, M. 2013. Geologic map of the Winslow 30'× 60' quadrangle, Coconino and Navajo Counties, northern Arizona. US Geological Survey Scientific Investigations, Map 3247, Scale 1:50000.
- Lefebvre, N.S., White, J.D., Kjarsgaard, B. 2013. Unbedded diatreme deposits reveal maar-diatreme-forming eruptive processes: Standing Rocks West, Hopi Buttes, Navajo Nation, USA. *Bulletin of Volcanology* 75:739.
- White, J.D. 1991 Maar-diatreme phreatomagmatism at Hopi Buttes, Navajo Nation (Arizona), USA. *Bulletin of Volcanology* 53:239-258.
- White, J.D., Ross, P-S. 2011 Maar-diatreme volcanoes: a review. *Journal of Volcanology and Geothermal Research* 201:1-29.

7.3 Poster session at 7IMC (2018), Olot, Spain

Lava lakes filling phreatomagmatic craters at Twin Peaks, Hopi Buttes volcanic field, Navajo Nation, Arizona

Benjamin Latutrie¹, Pierre-Simon Ross¹

¹ *Institut National de la Recherche Scientifique, Centre Eau Terre Environnement, 490 Rue de la Couronne, Québec (QC), G1K 9A9, Canada: Benjamin.Latutrie@ete.inrs.ca*

Keywords: diatreme, crater, eruptive regimes.

The Hopi Buttes volcanic field (HBVF) is located on the Colorado Plateau in Arizona (USA). This Miocene volcanic field provides excellent exposures of maar-diatreme volcanoes (White and Ross 2011). In the HBVF, the variable erosion level allows the study of maar-diatremes from top to bottom. Williams (1936) defined the typical HBVF volcanic necks as “plug”-dominated (i.e. mostly filled by coherent rocks) and those of the older Navajo volcanic field (NVF) further north as a tuff-breccia “shafts” (i.e. mostly pyroclastic). Yet the plug-dominated necks of the HBVF have received little scientific attention so far, with almost all recent studies addressing diatremes filled by pyroclastic rocks.

Twin Peaks is a complex of two adjacent “plug”-dominated necks in the eastern HBVF, called informally the north peak and south peak. Our overall interpretation is that each peak represents a maar-diatreme volcano which evolved into a lava lake filling the crater, possibly all the way to the pre-eruptive surface. The base of the lava lakes lie about 60 m below the current summits and corresponds to the bottom of the craters at the end of the explosive phase of the eruptions. This elevation is also inferred to correspond approximately to the contact between the Jurassic Moenave Fm and the Miocene Bidahochi Fm (Billingsley et al. 2013).

One month of field work was carried out at Twin Peaks. We mapped four main volcanic units, the first three being pyroclastic and the final one coherent. Those units occur in stratigraphic order from bottom to top; for simplicity in this abstract we give them numbers (Fig. 1) and a description of each unit is presented below. Unit 1 is only visible in the north peak but the others occur on both peaks. We described and sampled all these units and then did componentry measurements using the line count method proposed by Lefebvre (2013).

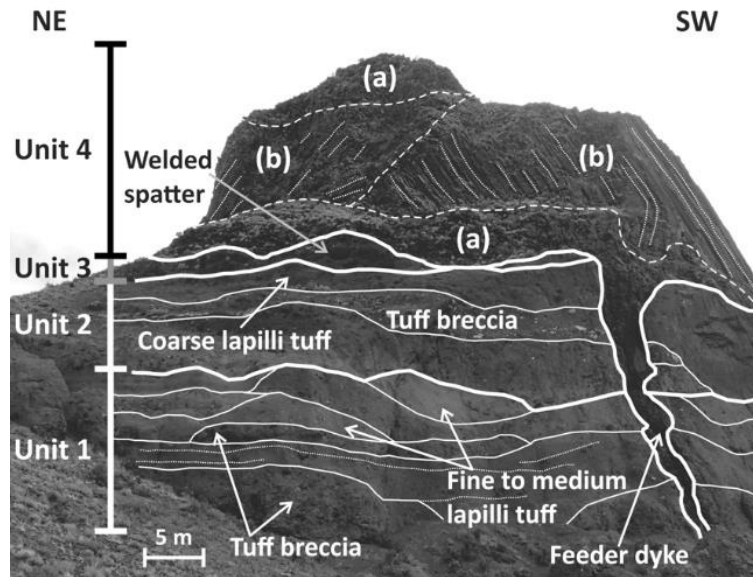


Fig. 1 – The four main units present on the northwest cliff of the north peak at Twin Peaks.

Unit 1 is brown and typically bedded, with layers tens of centimeters to several meters thick. Some layers are lensoid in appearance and cross-bedding occurs locally. The rocks range from fine lapilli tuff to tuff breccia and are poorly sorted, with particles from ash to block in size. Beds are relatively juvenile-rich in composition (65-80%). Juvenile clasts are light grey to black and often brown (10-75%) due to palagonite alteration. They are dense to vesicular (10 to 60% vesicles) and blocky to amoeboid in shape. The lithics are mainly from the Bidahochi and Moenave Fms but some are from the Chinle Fm and the Moenkopi Fm, 200-400 m below their current location. We think that this unit is phreatomagmatic in origin.

The overlying **unit 2** is darker brown and composed of three beds several meters in thickness. The beds are poorly sorted with a high proportion of ash matrix (up to 30%) and range from medium lapilli tuff to tuff breccia. Juvenile fragments constitute 70-80% of the rock and are mainly sub-round to amoeboid and sometime flat like spatter, with a vesicularity ranging from 10 to 70%. Dense clasts and spindle bombs are present in this unit but they are rare. The lithics are mainly white in color (Bidahochi Fm, or cooked Moenave Fm clasts, or greyish Moenkopi Fm). We interpret the eruptive style as phreato-strombolian.

The ~3-10 m-thick **unit 3** consists of black coarse lapilli tuff to tuff breccia. These rocks are extremely spatter-rich with just a few randomly scattered lithics. At the bottom of this unit the spatter clasts are non-welded in a matrix of fine lapilli to ash and at the top the spatter is tack-welded to strongly welded, grading locally into small lenses of clastogenic lava. Spatter

fragments are generally flat and extremely vesicular (up to 80%) with bigger vesicles in the middle. This unit corresponds to a hawaiian explosive phase.

Finally **unit 4** forms the lava lakes. The coherent samples from this unit are porphyritic with about 15% olivine, 7% euhedral clinopyroxene and 0-1% vesicles. On the south peak the lava lake is entirely jointed but in the north peak a portion of the unit lacks well-developed columnar joints (zones “a” versus “b” on Fig. 1).

Our preliminary model for Twin Peaks has six steps and it can be applied to the two peaks (Fig. 2).

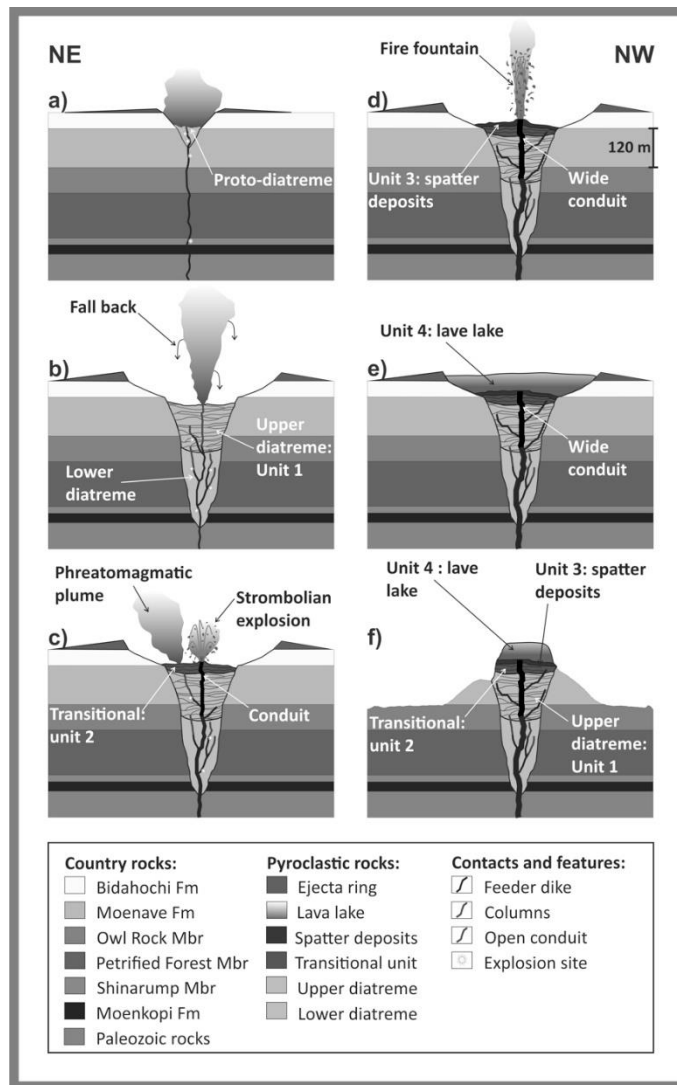


Fig. 2 – Preliminary model representing the steps leading to the current outcrop at Twin Peaks, for one of the peaks only.

- (a) Onset of the activity at Twin Peaks when a dyke rises and generates phreatomagmatic explosions by interaction with a wet substrate.
- (b) Ongoing phreatomagmatic activity until a well-developed maar-diatreme is formed. The lower part of the diatreme is composed of massive deposits (not exposed) while the upper part is composed of the bedded phreatomagmatic facies (**unit 1**) that crops out in the north peak. At this stage the craters may have been 400-500 m in diameter and 60 m deep.
- (c) The eruptive regime switches to a transitional phreato-strombolian style (**unit 2**). This can be due to the formation of a better-sealed conduit linked to the increase in the magmatic flux in the dyke (Valentine and White 2012) or perhaps to external water becoming depleted, or to simultaneously active strombolian and phreatomagmatic vents (e.g., Ukinrek 1977).
- (d) The magmatic flux increases again, or water runs out completely. A large dike/conduit is now able to transport relatively large quantities of magma up to the surface. Fire fountains form spatters deposits of **unit 3**.
- (e) This evolves into a lava lake (**unit 4**), which mostly or complete fills the crater and may have fed a lava flow beyond the crater (not shown).
- (f) Erosion leads to the current outcrop at Twin Peaks.

Acknowledgements

Twin Peaks was first visited by PSR during a field trip with James White, Greg Valentine, and Nathalie Lefebvre. These researchers have influenced our ideas through discussions and their papers. Romain Jattiot helped us during the field work in the steep slopes. We thank the Morris family for allowing us to work at Twin Peaks. Any persons wishing to conduct geological investigations on the Navajo Nation must first apply for, and receive, a permit from the Navajo Nation Minerals Department, P.O. Box 1910, Window Rock, Arizona 86515, USA, telephone 1-928-871-6587.

References

- Billingsley, G.H., Block, D., Hiza-Redsteer, M., 2013. Geologic map of the Winslow 30'× 60' quadrangle, Coconino and Navajo Counties, northern Arizona. US Geological Survey Scientific Investigations, Map 3247, Scale 1:50000.
- Lefebvre, N.S., 2013. Volcanology of maar-diatreme volcanic vent complexes, Hopi Buttes Volcanic Field, Navajo Nation, Arizona, USA. PhD thesis, University of Otago, 282 p.

Valentine, G.A., White, J.D., 2012. Revised conceptual model for maar-diatremes: Subsurface processes, energetics, and eruptive products. *Geology* 40(12): 1111-1114

White, J.D., Ross, P-S., 2011. Maar-diatreme volcanoes: a review. *Journal of Volcanology and Geothermal Research* 201: 1-29.

Williams, H., 1936. Pliocene volcanoes of the Navajo-Hopi country. *Geological Society of America Bulletin* 47(1): 111-172

7.4 Oral session at GAC-MAC-IAH⁷ (2019), Quebec City, Canada

Miocene eruptive activity of the Round Butte maar-diatreme volcano, Hopi Buttes volcanic field, Arizona

Benjamin Latutrie*, Pierre-Simon Ross

Institut national de la recherche scientifique, Centre Eau Terre Environnement, 490 rue de la Couronne, Québec (QC), G1K 9A9, Canada

The Miocene Hopi Buttes volcanic field (HBVF) in the Navajo Nation (Arizona, USA) provides excellent exposures of maar-diatreme volcanoes at different erosion depths, from the maar ejecta ring and crater infill to the deep diatreme. Round Butte diatreme crops out ~190 m below the pre-eruptive surface, in the southeastern part of the volcanic field. It consists of a small but complex phreatomagmatic diatreme 170-190 m in diameter, of which the central 130-150 m is well-exposed in a massif featuring 20-30 m high subvertical cliffs. A 50 cm-thick basanite dike is also exposed outside the diatreme. Field mapping allowed us to define three main groups of pyroclastic rocks in the diatreme: undisturbed beds, disturbed beds and non-bedded rocks. Pyroclastic rocks range in grain size from coarse tuff to tuff breccia and in componentry from juvenile-rich to lithic-rich, with a dominance of heterolithic lapilli tuffs. Two minor facies groups were also documented: pyroclastic to sedimentary megablocks, and debris avalanche deposits. Rocks from the undisturbed bedded pyroclastic group are present above an unconformity found all around the massif, whereas the disturbed bedded and the non-bedded pyroclastic groups are always found below it. This unconformity was previously understood as the contact between the upper and the lower diatreme. The undisturbed beds above the unconformity indeed compose the upper diatreme, but the assemblage of non-bedded rocks (invasive columns) and disturbed beds (residual columns) below it are not typical of the lower diatreme. Instead, they represent a transition zone between the upper and lower diatreme. Such a transition zone also occurs in other diatremes, it is important genetically, and we propose to add it to the general model of maar-diatreme volcanoes.

Keywords: maar-diatreme, crater, upper diatreme, lower diatreme, transition zone

⁷ Geological Association of Canada - Mineralogical Association of Canada - International Association of Hydrogeologists

7.5 Oral session at IUGG⁸ (2019), Montreal, Canada

Maar craters filled by lava lakes: Twin Peaks volcanic complex, Hopi Buttes volcanic field, Navajo Nation, Arizona

Benjamin Latutrie*, Pierre-Simon Ross

Institut national de la recherche scientifique, Centre Eau Terre Environnement, 490 rue de la Couronne, Québec (QC), G1K 9A9, Canada

The Miocene Hopi Buttes volcanic field (HBVF) is located on the Colorado Plateau in Arizona (USA). In this volcanic field, the variable erosion level allows the study of maar-diatremes from top to bottom. The Twin Peaks volcanic complex consists of two hills with thick coherent rocks at their summits, informally called the north peak and south peak. In the HBVF, such features have received little scientific attention so far. Our field observations allowed us to interpret the complex as two maar-diatreme volcanoes that each evolved into a lava lake filling the maar crater. The bottom of the lava lakes lies about 60 m below the current summits and corresponds to the contact between the Jurassic Moenave Formation and the Miocene Bidahochi Formation. One month of field mapping allowed us to distinguish four volcanic units, the first three being pyroclastic and the final one coherent. We named these units according to their stratigraphic order, Unit 1 being at the bottom and Unit 4 at the top. Unit 1 is only visible in the north peak but the others occur on both peaks. Componentry measurements and field descriptions suggest that Unit 1 is phreatomagmatic, Unit 2 is transitional with a phreato-strombolian style, Unit 3 is spatter-rich and Unit 4 is effusive, forming the lava lakes. We propose a six steps model to illustrate the change in eruptive regime from phreatomagmatic to magmatic at Twin peaks.

Keywords: Hopi Buttes, maar-diatremes, lava lakes, phreatomagmatic, magmatic

⁸ 27th International Union of Geodesy and Geophysics – General Assembly

7.6 Poster session at IUGG (2019), Montreal, Canada

Architecture of the subterranean phreatomagmatic deposits at Round Butte diatreme, Hopi Buttes volcanic field, Navajo Nation, Arizona

Benjamin Latutrie*, Pierre-Simon Ross

Institut national de la recherche scientifique, Centre Eau Terre Environnement, 490 rue de la Couronne, Québec (QC), G1K 9A9, Canada

The Hopi Buttes volcanic field (HBVF) in Arizona is principally composed of maar-diatreme volcanoes. This Miocene volcanic field provides excellent exposures from the maar ejecta ring to the deep diatreme. The small but surprisingly complex Round Butte diatreme is located in the southeastern part of the HBVF and crops out ~190 m below the pre-eruptive surface. The diatreme is 170-190 m in diameter, the central 130-150 m of which is a well-exposed massif featuring 20-30 m high subvertical cliffs. One month of field mapping allowed us to define three main groups of pyroclastic rocks in the diatreme: undisturbed beds, disturbed beds and non-bedded rocks. Pyroclastic rocks range from coarse tuff to tuff breccia, with the componentry mainly heterolithic. Mapping highlighted two other minor groups: megablocks (pyroclastic and sedimentary), and debris avalanche deposits. An important unconformity is observable all around the diatreme separating the undisturbed bedded rocks above it from the disturbed bedded rocks and the non-bedded rocks below it. This unconformity was previously understood as the contact between the upper and the lower diatreme. The undisturbed beds correspond to the upper diatreme, but the assemblage of non-bedded rocks and disturbed beds are not typical of the lower diatreme. Instead, they represent a transition zone between the upper and lower diatreme. Such a transition zone also occurs in other diatremes, it is important genetically, and we propose to add it to the general model of maar-diatreme volcanoes.

Keywords: maar-diatreme, crater, upper diatreme, lower diatreme, transition zone

7.7 Oral session planned for COV11⁹ (2020), Heraklion, Greece

Lithics, megablocks and debris avalanches within the small Round Butte diatreme, Hopi Buttes volcanic field, Navajo Nation, Arizona

Benjamin Latutrie, Pierre-Simon Ross

Institut national de la recherche scientifique, Centre Eau Terre Environnement, 490 rue de la Couronne, Québec (QC), G1K 9A9, Canada

The Miocene Hopi Buttes volcanic field in northern Arizona comprises many maar-diatreme volcanoes, and provides excellent exposures of diatremes filled by phreatomagmatic deposits. In the southeastern part of the HBVF, the Round Butte diatreme crops out ~190 m below the pre-eruptive surface and is 170-190 m in diameter. Its central part is 130-150 m in diameter, forming a massif with 20-30 m high subvertical cliffs. One month of field mapping, componentry measurements and facies descriptions allowed us to define three main groups of pyroclastic rocks: undisturbed beds, disturbed beds and non-bedded columns. Two minor facies groups were also identified: pyroclastic and sedimentary megablocks (blocks over 2 m in long axis), and debris avalanche deposits. Round Butte had a complex eruptive history with phases dominated by excavation processes followed by phases dominated by crater infilling processes. To better constrain the stratigraphic origin of lithic clasts and megablocks, we developed a method based on portable X-ray fluorescence (pXRF) geochemical analyses. We sampled all the regional sedimentary formations to create discriminant diagrams which allowed us to identify the origin of specific lithic clasts and megablocks within the pyroclastic rocks of Round Butte diatreme. We find that lithic megablocks originate either from above, or from the same level, relative to their current location, i.e. no megablock has a net upward displacement. Smaller lithic clasts, in contrast, come from various stratigraphic levels, including up to 220 m below their current locations. Units displaying the richest content of lithic clasts with a deep origin are typically the non-bedded ones and these units were formed by debris jets.

Keywords: maar-diatreme, crater, upper diatreme, lower diatreme, transition zone

⁹ Cities on Volcanoes 11